7-2013

A. Catalysis of CO-PROX by Water-Soluble Rhodium Fluorinated Porphyrins B. Studies toward Fluorination of Electron Rich Aromatics by Nucleophilic Fluoride

Shri Harsha Uppaluri
University of Nebraska-Lincoln, usharsha@huskers.unl.edu

A. CATALYSIS OF CO-PROX BY WATER-SOLUBLE RHODIUM

FLUORINATED PORPHYRINS

B. STUDIES TOWARD FLUORINATION OF ELECTRON RICH AROMATICS

BY NUCLEOPHILIC FLUORIDE

by

Shri Harsha Uppaluri

A DISSERTATION

Presented to the Faculty of

The Graduate College at the University of Nebraska

In Partial Fulfillment of Requirements

For the Degree of Doctor of Philosophy

Major: Chemistry

Under the Supervision of Professor Stephen G. DiMagno

Lincoln, Nebraska

July, 2013

A. CATALYSIS OF CO-PROX BY WATER-SOLUBLE RHODIUM

FLUORINATED PORPHYRINS

B. STUDIES TOWARD FLUORINATION OF ELECTRON RICH AROMATICS

BY NUCLEOPHILIC FLUORIDE

Shri Harsha Uppaluri, Ph.D.

University of Nebraska, 2013

Adviser: Stephen G. DiMagno

The rhodium(III) derivative of a water soluble, heavily fluorinated porphyrin is shown to catalyze the low temperature, low pressure selective oxidation of carbon monoxide in hydrogen gas streams for use in fuel cell applications. The catalytic activity is a direct result of the removal of electron density from the metal center. Selectivity for CO oxidation is a direct consequence of fluorination of the porphyrin periphery, since these substituents enhance the rate of the reaction and prevent the formation of Rh(II)-Rh(II) dimmers. Significantly, the dramatic increase in rhodium hydride acidity caused by fluorination precludes hydrogen activation and generation, thereby permitting preferential oxidation (PROX) of carbon monoxide in the presence of hydrogen. Addition of the redox mediator dye indigo carmine scavenges deleterious active oxygen species and hence permits air or dioxygen to be used as a terminal oxidant for this process.

An improved arene fluorination methodology via the reductive elimination of diaryliodonium fluoride salts is applied to the synthesis of 2-fluoroestradiol, whose

fluorine-18 analog is a radiotracer used in positron emission tomography (PET). The use of nonpolar solvents suppresses disproportionation and other deleterious reactions and leads to significant improvements in the fluorination yields. The method is conducive to the rapid synthesis of fluorine-18 labeled radiotracers using nucleophilic fluoride sources for PET applications.

Attempts at accomplishing fluorination of an electron rich aromatic using nucleophilic fluoride via the reductive elimination of arylfluoropalladium(II) complexes are described.

To

My Dear Parents and Loving Family

Fabulous Friends

And Revered Teachers

TABLE OF CONTENTS

LIST OF CHARTS

LIST OF FIGURES

LIST OF SCHEMES

LIST OF TABLES

CHAPTER 1

HEAVILY FLUORINATED WATER-SOLUBLE RHODIUM PORPHYRINS: APPLICATION TO LOW TEMPERATURE PREFERENTIAL OXIDATION OF CARBON MONOXIDE
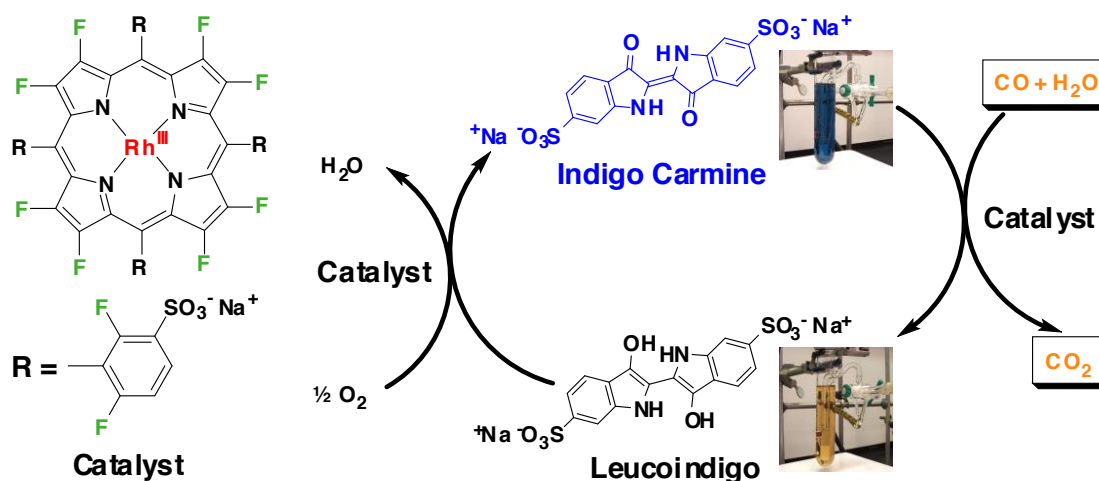
Graphic reproduced from reference 144.

Portions of the text and certain graphics in this chapter have been reprinted (adapted) with permission from "Biffinger, J. C.; Uppaluri, S.; Sun, H.; DiMagno, S. G., "Ligand fluorination to optimize preferential oxidation of carbon monoxide by water soluble rhodium porphyrins", *ACS Catalysis* **2011**, 1, 764-771" (Reference 144). Copyright 2011 American Chemical Society (ACS). http://dx.doi.org/10.1021/cs2001187. These items are appropriately cited in the body of the chapter.

1.1 Introduction

1.1.1 Alternative Energy and Hydrogen Economy

Current estimates state that the carbon-energy economy based on conventional and non-conventional fossil fuels can sustain current energy use for another century.[1-3] However, current levels of fuel production fail to keep pace with an ever-increasing global energy demand.[4] Additionally, carbon dioxide emissions associated with fossil fuel combustion lead to greenhouse warming and climate change.[1,2,5-7] The looming crisis has triggered research aimed at enhancing the efficiency of current energy technologies, accomplishing carbon capture, and harvesting alternative sources of energy such as solar, nuclear fusion, wind, geothermal and tidal, to meet the energy demands of the future in a sustainable and clean fashion.[1,6-8] It has been predicted that a transition to a new energy paradigm, propelled by a combination of current and emerging technology alternatives, will be made in the next fifty years.[6,9] There is also a vision for an ultimate transition to a "hydrogen economy" that uses hydrogen as a fuel/energy carrier to usher in an era of sustainable and environmentally benign energy.[2,10,11] Iceland is a leader in alternative energy use. Currently geothermal and hydroelectric sources are supplying almost all of its heat and electricity, and it is poised to achieve energy self-sufficiency. It has also set up a prototype hydrogen infrastructure for transportation and has committed itself to a full-fledged hydrogen economy by 2050.[12]

Hydrogen is a tempting, yet hard-to-tap fuel. Its energy density, by mass, is about three times that of liquid hydrocarbons. When reacted with oxygen, either by combustion or by passing it through a fuel cell to generate electricity, the lone product is environmentally innocuous water – a particularly attractive feature for transportation

applications.[2,10-15] However there is a downside. Although it is the most abundant element in the universe, on earth the amount of free dihydrogen is vanishingly small. Hydrogen is mostly bound up in water, fossil fuel hydrocarbons and biomass, and energy is needed to strip it free for use.[2,10-15] Hence it has been argued that hydrogen is not a fuel in itself, like coal and oil are. Like electricity, it is an energy carrier that must be generated by expending another source of energy.[2,11] There are scientific and technological challenges that must be surmounted before a large scale, economically viable hydrogen economy can be established. Creation of a massive infrastructure that is capable of producing, storing and delivering hydrogen in a sustainable, efficient and safe manner is a daunting barrier to the hydrogen economy.[2,10,13,16-19]

1.1.2 Fuel Cells

Although hydrogen can be burned to release energy, a more efficient and cleaner way to harness its energy, particularly for transport/automobile applications, is to use it in a fuel cell. A hydrogen fuel cell is an electrochemical device that combines hydrogen and
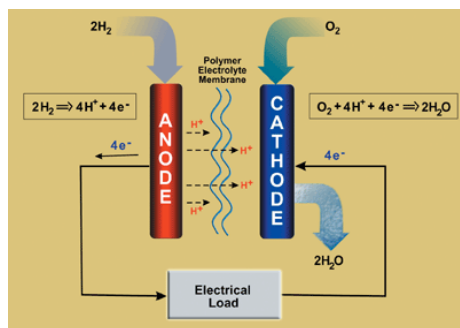
Figure 1.1. Schematic for a PEM Fuel Cell

Image source: www.epa.gov

oxygen to generate electricity.[21-23] Fuel cells are more than twice as efficient as conventional internal combustion engines (ICE).[2,20,24] Current generation hydrogen fuel

cells are proton exchange membrane or polymer electrolyte membrane fuel cells (PEMFC). A schematic is shown in Figure 1.1. Hydrogen gas is oxidized at a platinum anode to generate protons. The protons travel across a proton selective membrane (such as Nafion®) to the cathode. The electrons from the anodic oxidation travel across the external circuit (generating an electric current in the process) to the anode, where they (along with the protons) reduce oxygen to water. Nafion® (DuPont) is a perfluorosulfonic acid resin that is selectively permeable to the protons from anodic oxidation, but not to the feed gases (H_2 or O_2).[25,26] Various types of fuel cells are commercially available. Each type is characterized by the electrochemical reaction it uses to generate power. However, the PEMFC has clear advantages in terms of operating temperature and generality of application, especially in automobiles. [21-23,27,28]

Notwithstanding the promise that PEM fuel cell technology holds for the future, there are severe limitations that are impediments to immediate large scale commercialization. These limitations pertain to design, cost, durability and performance of materials and components in current generation fuel cells.[20,27,28] One significant problem is that the platinum anodes are intolerant to trace levels of carbon monoxide in the hydrogen gas stream.[28,29] A potential solution to this problem is the focus of this chapter. The U.S. Department of Energy (DOE) Hydrogen Program funds research and development for solving the current problems associated with hydrogen techonology.[30] The long term objective of the program is to refine fuel cell technology so that it is ready to be deployed for vehicular use. The short term goals are three fold; (i) to make hydrogen fuel cell vehicles practical, affordable, and competitive with other entrenched technologies (like gasoline-ICE and hybrids) by the year 2020, (ii) to reduce dependence

on foreign oil, and (iii) to achieve short term reduction targets in CO_2 emissions. The research has already paid rich dividends. State-of-the-art fuel cell technology is approaching the DOE's 2015 benchmarks for commercialization. [20,31] The automotive industry has also spent billions of dollars on hydrogen fuel cell vehicle R&D. As a result, there is already a host of experimental prototype fuel cell cars and other light and heavy vehicles (including buses and trucks) from all major auto manufacturers on the market.[2] A representative example is the GM Chevy Equinox FC SUV. GM has committed itself to the sale of one million hydrogen fuel cell cars by 2015.[2] Energy companies have also installed a hydrogen fueling infrastructure in California, thanks to a partially successful initiative by that state's government.[32]

1.1.3 Production of Hydrogen for Fuel Cell Applications

For a truly sustainable hydrogen economy, hydrogen production would have to be accomplished by the electrolysis of water powered by the conversion of solar (photobiological[33] and photoelectrochemical[34-38] methods), nuclear, wind, tidal or geothermal energies.[3,39-41] These technologies are still in their infancy and daunting challenges must be overcome before they can be deployed on a wide scale.[2] Ironically, carbon-based fossil fuels will provide the initial foray into a hydrogen economy. In what has been termed the 'carbon conundrum', a transition would have to be made first from hydrocarbons to carbon-based hydrogen, and finally to hydrogen.[7] Currently hydrogen can be produced by the catalytic steam reforming[42-46] of fossil fuel hydrocarbons[47-49] like natural gas (methane) and gasoline, alcohols,[45,50,51] biomass[52-67] and coal gasification.[3] Of these, the cheapest, most efficient and cleanest (least carbon emissions) source is natural gas.[2,20,68] Catalytic steam reforming of methane is about 85% efficient.[2,69] The principal

steam reforming reactions of methane are shown in Scheme 1.1. A mix of hydrogen, carbon dioxide and carbon monoxide is generated. The steam reforming reaction is endothermic with temperatures of up to 700 °C being required. The accompanying mildly exothermic water gas shift (WGS) reaction that enhances the hydrogen yield is also shown.

$$CH_4 + H_2O \longrightarrow CO + 3\,H_2 \qquad \text{eqn 1.1}$$

$$C_xH_y + x\,H_2O \longrightarrow x\,CO + (y/2 + x)\,H_2 \qquad \text{eqn 1.2}$$

$$CO + H_2O \rightleftharpoons CO_2 + H_2 \qquad \text{WGS}$$
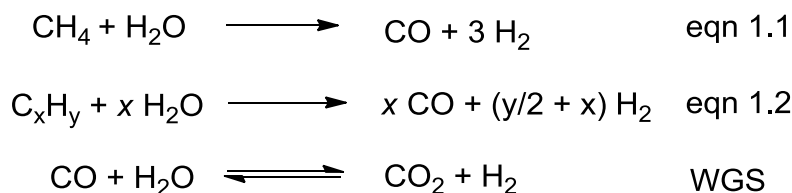
Scheme 1.1. Steam Reforming of Hydrocarbons[49,58]

1.1.4 Carbon Monoxide Removal from Hydrogen Gas Streams for Fuel Cell Applications[144]

The work described in the chapter has been published as a journal article on which I am a coauthor. This section is drawn from the same publication – Biffinger, J. C.; Uppaluri, S.; Sun, H.; DiMagno, S. G., "Ligand fluorination to optimize preferential oxidation of carbon monoxide by water soluble rhodium porphyrins", *ACS Catalysis* **2011**, 1, 764-771 (reference 144) – and is shown in quotes. "Ultrapure hydrogen is the essential fuel for today's PEM (proton exchange membrane) fuel cells. While H_2 generated by electrolysis of water is generally pristine, hydrogen fuel streams produced by hydrocarbon, alcohol, or biomass steam reforming are invariably contaminated with carbon monoxide (Scheme 1.1). Subsequent high temperature water gas shift (WGS) catalysis can reduce CO concentrations to the thermodynamic limit (20-50 ppm) in such H_2 gas streams.[54,70-74] However, the platinum anodes common in PEM fuel cells are poisoned by CO at concentrations as low as 10 ppm.[28,29] One solution to this problem is

to develop catalytic methods to oxidize CO selectively, preferably below the PEM fuel cell operating temperature (353 K). Such a catalyst would enable CO removal without compromising the overall fuel cell efficiency. Design requirements for such catalysts are severe, since selective CO oxidation must be performed in the presence of H_2, CO_2, and water prior to entry of the gas into the fuel cell."[75-81]

"Preferential oxidation (PROX) of CO can be performed either indirectly or directly. The advantage of the indirect approach[82-88] is that the reducing equivalents of CO can be captured at a fuel cell anode; such energy recovery is appropriate when the gas stream contains a high CO concentration. Direct oxidation[89] of CO with air or O_2 is an attractive option for scrubbing the relatively low concentrations of CO present, for example, in H_2 streams produced by WGS catalysis. Previous work has shown that supported noble metal and metal oxide catalysts perform direct CO PROX; though these catalysts generally function efficiently only at or well above the PEM fuel cell operating temperature.[90-110] Noble metal clusters (Rh, Ru, Pt, Au) supported on alumina, zeolites or mesoporous materials display good reactivity for CO PROX,[111-113] and excellent selectivity has been reported when Ru-Pt nanoparticles are used as the active catalysts.[114] PROX catalysts comprising less expensive metal oxides, such as CeO_2/CuO nanoparticle composites, show good specificity for CO (at 350 ºK) with comparable activity to alumina supported noble metals.[115-118] Though gold clusters and nanotubes have been explored for low temperature (0 ºC) oxidation of CO, these catalysts have not proven to be as robust as mesoporous supported catalysts."[119]

"Instead of eradicating CO from alkane reformate H_2 gas streams, utilization of the CO contaminant as a fuel for power generation has also been explored. In the early

1980s, Kubiak and co-workers constructed a PEM-CO/O_2 cell that utilized [Rh(CO)$_2$Br]$^-$ as a homogeneous CO oxidation catalyst, a graphite anode and an oxygen reduction cathode.[120] Yamazaki and coworkers reported a CO-PEM/O_2 fuel cell system that featured immobilized rhodium octaethylporphyrins on carbon anodes.[121] Dumesic and coworkers fabricated fuel cells featuring aqueous phosphomolybdic acid (a polyoxometallate, POM) and gold nanoparticle catalysts to oxidize CO and hydrogen simultaneously, thereby decreasing the gas purity requirements in their PEM fuel cell.[82,122] Phosphomolybdic acid (**PA**) functions as a multielectron-accepting terminal oxidant in this system, and it permits the use of untreated carbonaceous electrode materials to collect the reducing equivalents from the oxidation of hydrogen."

1.1.5   Rationale for the Work Presented[144]

This section is drawn from reference 144 (Biffinger, J. C.; Uppaluri, S.; Sun, H.; DiMagno, S. G., "Ligand fluorination to optimize preferential oxidation of carbon monoxide by water soluble rhodium porphyrins", *ACS Catalysis* **2011**, 1, 764-771), on which I am a coauthor, and is shown in quotes. "The study of discrete homogeneous transition metal complexes provides mechanistic insight useful for the design of selective CO oxidation catalysts. The porphyrin ligand offers a controlled environment for coordination of metal ions that bind carbon monoxide, with the flexibility of tuning electron density on coordinated metal centers through peripheral substitution.   Group IX transition metal metalloporphyrins are known to be good catalysts for diverse organic transformations such as alkane activation[123] and functionalization.[124] Cobalt and rhodium porphyrins in particular have been shown to catalyze carbon monoxide electro-oxidation[125-129] and the insertion of CO into organometallic hydrides.[130] Anson[129] used

Co^{II} octaethylporphyrin adsorbed on graphite as an efficient electrochemical catalyst for aqueous CO oxidation. Rhodium and iridium porphyrins immobilized on Norit BRX support are active catalysts for CO oxidation.[128] Coordination of CO to transition metal complexes is a well-documented phenomenon.[131] It was posited that nucleophilic attack by water on the metal-coordinated CO molecule, an established reaction for Rh^{III} porphyrins first reported by Eisenberg in 1976[132], was the key step, and possibly, the rate limiting step[129] in this process. While construction of CO oxidation catalysts based upon rhodium porphyrins has ample precedent, application of these compounds for removal of CO from H_2 gas streams is compromised by their hydrogenase activity (hydride transfer, hydrogen activation and evolution, proton reduction).[124,133-139] We hypothesized that strong electron-withdrawing groups on the porphryin periphery could lead to more active CO oxidation catalysts while simultaneously reducing or eliminating hydrogen activation or proton reduction."

"The rationale for our design of electron-deficient metalloporphyrin PROX catalysts is threefold: 1) removal of metal electron density by ligand substituents should increase the thermodynamic driving force and reduce the activation barrier for nucleophilic attack of water on CO, thereby enhancing activity, 2) the use of polar coordinating solvents should destabilize the Rh(II) state and enhance disproportionation,[140] thereby precluding direct hydrogen activation, and 3) the substituents should increase the acidity of rhodium hydrides and increase the stability of Rh(I) to such an extent that proton reduction will not occur. *β*-fluorination of porphyrins is an effective approach to reduce the electron density of coordinated ligands without drastically changing the coordination sphere of the metal center."[141]

"The impact of β-fluorination on porphyrin ring and chelated metal redox potentials has been studied extensively.[142] DiMagno and coworkers have shown that fluorination of the porphyrin ring can shift the formal potential for the rhodium(II)/rhodium(I)$^-$ reversible redox couple by 540 mV in nonaqueous solutions[140] making these complexes excellent oxidants for a wide variety of reductants. Cyclic voltammetry experiments conducted in aqueous solutions showed that the water-soluble rhodium porphyrins exhibit significant redox potential shifts caused by β-fluorination, though the magnitudes of the shifts were slightly smaller than those measured for the nonionic derivatives in CH_2Cl_2."[143]

"Here" I "report that a heavily fluorinated water-soluble rhodium porphyrin is able to perform direct and indirect preferential CO oxidation catalysis under exceptionally mild conditions.[144] Fluorination of the porphyrin periphery leads to enhancement of the rate of CO oxidation while simultaneously increasing selectivity. Fluorinated water-soluble rhodium porphyrins are able to selectively oxidize CO in H_2 streams at 308 °K using sacrificial electron acceptors (e.g. indigo carmine) and oxygen as the terminal oxidant. Direct oxidation[89] of CO with air or O_2 is an attractive option for scrubbing trace CO from H_2 streams produced by WGS catalysis, since energy loss by direct oxidation is minimal under these conditions."

There were three coworkers on this project, with the principal investigator being Dr. Stephen DiMagno. The work was published as a journal article – Biffinger, J. C.; Uppaluri, S.; Sun, H.; DiMagno, S. G., "Ligand fluorination to optimize preferential oxidation of carbon monoxide by water soluble rhodium porphyrins", *ACS Catalysis* **2011**, 1, 764-771 (reference 144). For the purpose of completeness, I have included the

23

contributions of all coworkers in the "Results & Discussion" section that ensues. However, I have clearly delineated each coworker's contributions. My key contributions to the work include: a) investigation of the reactivity of the most optimal catalyst (designated as **2[Rh(III)]**) with CO by NMR and GC, b) optimization of reaction conditions that afford the highest catalytic rate and enhance catalyst stability, c) accurate and reproducible determination of the reaction kinetics under multiple turnover conditions, and d) establishing the selectivity of the catalyst for CO in the presence of H_2 under the conditions of catalysis. These contributions were critical for the completeness of the work in order to merit publication as a peer-reviewed journal article.[144]

1.2   Results and Discussion

1.2.1 Synthesis of Water Soluble Free Base *β*-Octafluoro-*meso*-tetraarylporphyrins[144,148]

I prepared the precursor free base fluorinated macrocycles via the modified Lindsey condensation of 3,4-difluoropyrrole[146] and the requisite aromatic aldehyde using (Scheme 1.2)[147] using procedures developed by other members of our group. [143,145]
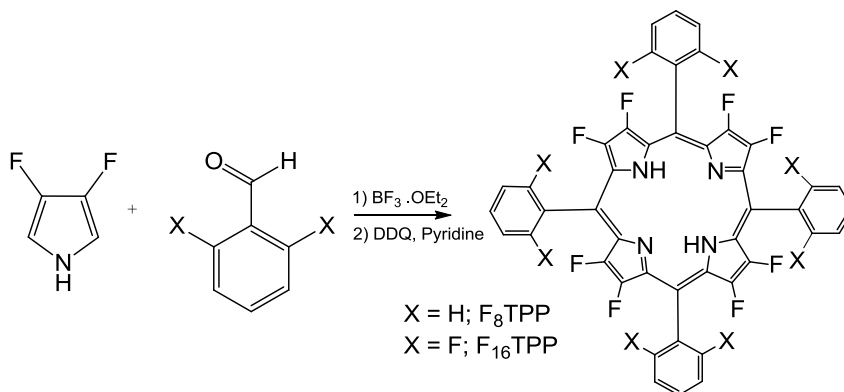
Scheme 1.2. Synthesis of *β*-Fluorinated Porphyrins

I prepared 3,4-difluoropyrrole via a multistep synthetic procedure that was originally developed[146] by Eric Woller and Valeriy Smirnov of our group, and was able to reproduce the reported yields. The synthetic procedures that I used for the free base porphyrins 2,3,7,8,12,13,17,18-octafluoro-5,10,15,20-tetraphenylporphyrin[143] [**F₈TPP**] and 2,3,7,8,12,13,17,18-octafluoro-5,10,15,20-tetrakis(2,6-difluorophenyl)porphyrin [**F₁₆TPP**][145] were originally developed by Eric Woller and Andrew Nelson of our group; I was able to reproduce the reported yields.

Table 1.1. Synthesis of β-Fluorinated Water-Soluble Porphyrins

(1) R = H Su₁ = H Su₂ = SO₃Na
(2) R = F Su₁ = SO₃Na Su₂ = H
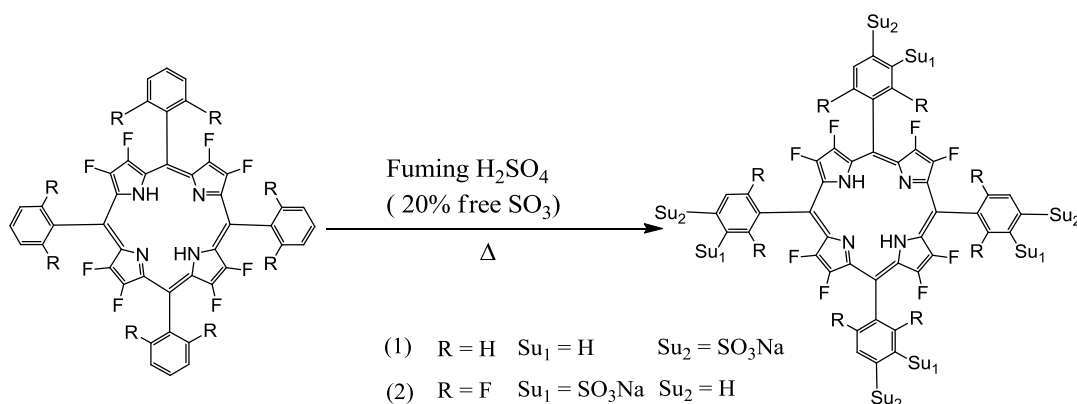
Compound	
F₈TSTPP (1)	Prepared by Biffinger for use in this work
F₁₆TSTPP (2)	Prepared by Uppaluri using Biffinger procedure[148] for use in this work

Sulfonation of the *meso*-aryl rings of **F₈TPP** and **F₁₆TPP** was used to impart water solubility to these fluorinated porphyrins. I sulfonated **F₁₆TPP** using a procedure that was originally developed by Justin Biffinger of our group.[145,148] Sulfonation was carried out by heating the fluorinated free base porphyrin in fuming sulfuric acid containing 18-20% free SO_3. Neutralization of the acidic reaction mixture with aqueous NaOH followed by salt removal afforded the exclusively tetrasulfonated porphyrin in a

yield (85%) that equaled the reported yield. The product of sulfonation of **F$_{16}$TPP** is

5,10,15,20-tetrakis(2,6-difluoro-3-sulfonatophenyl)-2,3,7,8,12,13,17,18-

octafluoroporphyrin, designated as **F$_{16}$TSTPP** (Table 1.1). Sulfonation of **F$_8$TPP** yields

5,10,15,20-tetrakis(4-sulfonatophenyl)-2,3,7,8,12,13,17,18-octafluoroporphyrin,

F$_8$TSTPP (Table 1.1). The **F$_8$TSTPP** used in the studies presented here was prepared by

Justin Biffinger.[144] The sulfonate groups were added to the *para* positions of the *meso*-

aryl rings in **F$_8$TPP** following the classical regioselectivity of electrophilic aromatic

substitution. In contrast, sulfonation occurred at the *meta* positions of the *meso*-aryls in

the case of **F$_{16}$TPP** since fluorine is an *ortho*, *para*-directing group. According to Justin

Biffinger[148], unlike the sulfonation of nonhalogenated porphyrins,[149,150] which results in

partially sulfonated derivatives, the sulfonation of **F$_8$TPP** and **F$_{16}$TPP** afforded no

detectable amounts of partially sulfonated porphyrins. Biffinger, who investigated this

aspect, surmised that the highly electron-deficient nature of these porphyrins so stabilizes

the porphyrin core that electrophilic aromatic substitution using the harsh sulfonating

reagent can be run to completion. The sulfonated water-soluble porphyrins prepared are

highly hygroscopic and need to be stored in vacuum desiccators. When stored under these

conditions, they are stable indefinitely.

1.2.2 Synthesis of Water Soluble Rhodium(III) *β*-Octafluoro-*meso*-tetraarylporphyrins[144.148]

The metalation procedure used to insert rhodium into **F$_8$TSTPP** and **F$_{16}$TSTPP**

was first developed by Justin Biffinger of our group.[144,148] Biffinger adapted procedures

previously reported by Krishnamurthy[151] and Ashley[152,153] to prepare diaquo[5,10,15,20-

tetrakis-(4-sulfonatophenyl)-porphyrinato]rhodium(III) tetrasodium salt, [RhTSTPP or

3[Rh(III)]], which was prepared by Krishnamurthy.[151] Krishnamurthy also studied the acid-base and lability characteristics of the water molecules axially ligated to the rhodium center **3[Rh(III)].** Metalation did not occur when Biffinger[148] attempted rhodium insertion on the sodium or potassium salts of **F₈TSTPP** and **F₁₆TSTPP**. However, the corresponding ammonium salts could be metalated successfully.[148]

I prepared the ammonium salt of **F₁₆TSTPP** by using the procedure reported by Justin Biffinger.[148] The solvent was removed *in vacuo* from the sulfuric acid containing reaction mixture in the synthesis of **F₁₆TSTPP.** This was followed by addition of dry methanol and neutralization by bubbling anhydrous ammonia gas. The ammonium sulfate that precipitated was removed by passing through a membrane filter, and the methanol was removed *in vacuo*. The solid residue was dried under high vacuum in a drying pistol containing anhydrous P_2O_5.
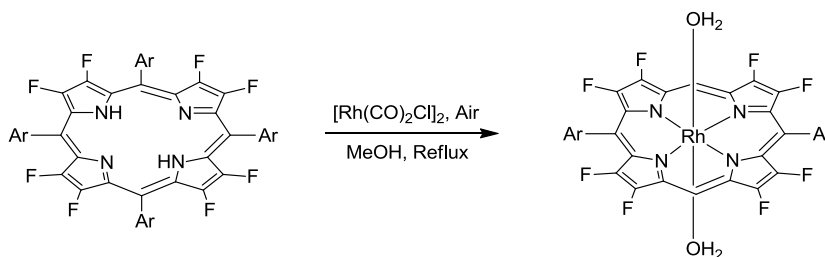
Scheme 1.3. Rhodium Insertion into β-Fluorinated Water-Soluble Porphyrins

I carried out rhodium insertion on the isolated ammonium salt of **F₁₆TSTPP** using the procedure reported by Justin Biffinger.[148] As is described later in this section, I slightly modified one of the last steps in the workup procedure to increase the purity of the product. The ammonium salt of **F₁₆TSTPP** was treated with $[Rh(CO)_2Cl]_2$ in refluxing methanol (Scheme 1.3). Since the reaction was carried out in the presence of air, the Rh(I) precursor in the $[Rh(CO)_2Cl]_2$ was oxidized *in situ* and inserted as Rh(III).

When the Soret band of the free base porphyrin disappeared (monitored by UV-vis spectroscopy), the refluxing was stopped, and the methanol was removed *in vacuo*. When the residual solid was re-dissolved in water, a black precipitate formed (rhodium black) and the supernatant solution was orange in color.[154] This crude mixture of the ammonium salt of the rhodium porphyrin was syringe-filtered and ion-exchanged to the sodium salt on a DOWEX50WX8-100 resin, Na^+ salt. The sodium salt of the rhodium porphyrin that eluted as an orange band was directly loaded onto a water-washed neutral aluminum oxide column and eluted with deionized water. The orange rhodium porphyrin fraction was collected and the water evaporated *in vacuo*. The resulting residue was dissolved in methanol, syringe filtered (0.2 μm PTFE), and diethyl ether was added until an orangish-brown precipitate formed. Thus the rhodium-porphyrin – aquohydroxy[5,10,15,20-tetrakis(3-sulfonato-2,6-difluorophenyl)-2,3,7,8,12,13,17,18-octafluoroporphyrinato]rhodium(III) tetrasodium salt, designated as **2[Rh(III)]** or $RhF_{16}TSTPP$ – was obtained in a 90% yield, which equaled the reported yield.

As mentioned earlier, the orange rhodium-porphyrin band was eluted off the neutral alumina column with deionized water. This is slightly different from Justin Biffinger's original procedure[148] that used 0.05 M sodium hydroxide solution for eluting the rhodium-porphyrin. As pointed earlier, the Rh(I) in the $[Rh(CO)_2Cl]_2$ precursor is oxidized by aerial oxygen *in situ* and inserted as Rh(III) into the porphyrin macrocycle. As a consequence, oxygen is reduced. A possible product is hydrogen peroxide (H_2O_2), which results from the 2-electron reduction of dioxygen. **2[Rh(III)]** is unstable in the presence of H_2O_2, and undergoes decomposition, especially under basic conditions. The decomposition is slowed at lower, neutral to acidic pH. More details about this

phenomenon and the experimental detection of H_2O_2 are presented later in section 1.2.10.

The other rhodium-porphyrins – aquohydroxy[5,10,15,20-tetrakis(4-sulfonatophenyl)-2,3,7,8,12,13,17,18-octafluoroporphyrinato]rhodium(III) tetrasodium salt, designated as **1[Rh(III)]** or RhF$_8$TSTPP, and **3[Rh(III)]** or RhTSTPP – used in the studies reported here were prepared by Justin Biffinger.[148]

1[Rh(III)]	**2[Rh(III)]**	**3[Rh(III)]**
RhTSF$_8$TPP	RhTSF$_{16}$TPP	RhTSTPP
Prepared by Biffinger	Prepared by Uppaluri via Biffinger procedure	Prepared by Biffinger
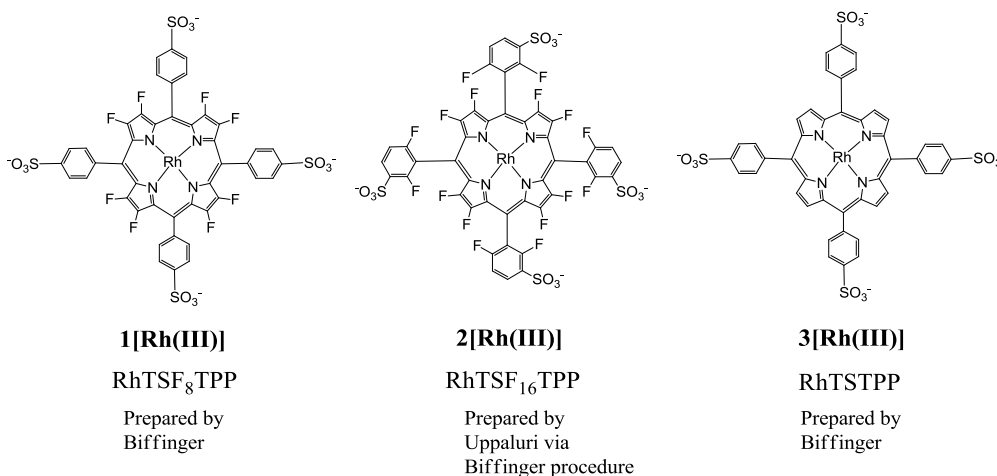
Axial ligands not shown for clarity

Chart 1.1. Rhodium(III) β-Fluorinated Water-Soluble Porphyrin Complexes Studied

1.2.3 Acid Dissociation Constants of Water-Soluble Aquo Rhodium(III) β-octafluoro-*meso*-tetraaryl Porphyrin Complexes[144,148]
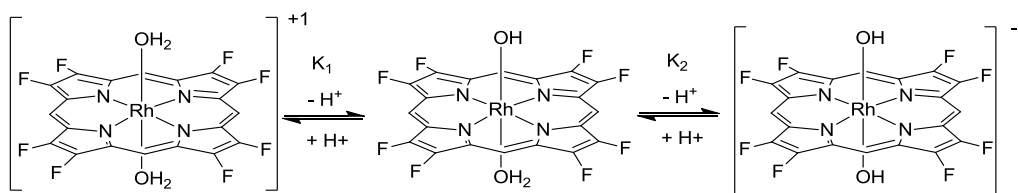
Scheme 1.4. Acid Dissociation Equilibria for Rhodium(III) Water-Soluble Porphyrins
Figure from reference 144. Copyright 2011 ACS.

Major portions of this section are drawn from reference 144 (Biffinger, J. C.; Uppaluri, S.; Sun, H.; DiMagno, S. G., "Ligand fluorination to optimize preferential oxidation of carbon monoxide by water soluble rhodium porphyrins", *ACS Catalysis*

2011, 1, 764-771), on which I am a coauthor, and are shown in quotes. "Ashley,[152] and more recently Wayland,[137,155] reported that [5,10,15,20-tetrakis(4-sulfonatophenyl)porphyrinato]rhodium(III) (**3[Rh(III)]**) forms six-coordinate complexes in aqueous solution; the diaquo, aquohydroxo, or dihydroxo species predominates depending on the pH of the solution" (Scheme 1.4). "In aqueous solution, binding of CO by six-coordinate Rh(III) porphyrins is gated by deligation of axial ligands/water molecules." The lability of the axial aquo and hydroxo ligands will determine the rate of CO ligation/deligation. Also, since CO is a σ-basic and π-acidic ligand, the strength of CO coordination will depend upon the amount of electron density on the rhodium center, which is in turn determined by the pH-dependent ionization state (aquo or hydroxo) of the axially ligated water molecules. Thus, Justin Biffinger "investigated[144,148] the general coordination properties[145,149,157] of **1[Rh(III)]** and **2[Rh(III)]**."

Table 1.2. Acid Dissociation Constants for Rhodium(III) Water-Soluble Porphyrins[148]

Entry	Compd.	pK_1	pK_2	Method	Ref.
1	RhTSTPP(H$_2$O)$_2$	7.01±0.12	9.80±0.24	UV-vis	152
2	RhTSTPP(H$_2$O)$_2$	7.9±0.2	11.5±0.2	NMR	137
3	RhTSF$_8$TPP(H$_2$O)$_2$	5.9±0.1	9.7±0.2	UV-vis	Biffinger[148]
4	RhTSF$_{16}$TPP(H$_2$O)$_2$	5.7±0.1	10.0±0.1	UV-vis	Biffinger[148]

Table from Biffinger.[148]

Biffinger's "spectrochemical titration with aqueous sodium hydroxide [0.01 - 1 M] over the pH range 1 – 12 revealed three successive optical absorption spectra with clean isosbestic points."[144,148] His "analyses[156] of the spectral changes in the Soret region sufficed to determine the relative concentrations of the diaquo, aquohydroxo, and dihydroxo at each pH." "Equilibrium constants obtained from these analyses are listed in" Table 1.2, "along with literature data from comparable experiments conducted upon **3[Rh(III)]**." "These data show that porphyrin fluorination reduces the first acidity

constant (pK_1) by more than one unit, but that pK_2 is surprisingly insensitive to fluorine substitution at the porphyrin β-positions. Such behavior is consistent with a leveling effect arising from significant additional donation of electron density from the axial aquo ligand once it is deprotonated. It is reasonable to expect that the bound hydroxide would contribute more electron-density into the more electron-deficient rhodium centers found in the fluorinated porphyrins."

1.2.4 Electrochemistry of Water-Soluble Rhodium(III) β-Fluorinated Porphyrins[144,148]

Major portions of this section are drawn from reference 144 (Biffinger, J. C.; Uppaluri, S.; Sun, H.; DiMagno, S. G., "Ligand fluorination to optimize preferential oxidation of carbon monoxide by water soluble rhodium porphyrins", *ACS Catalysis* **2011**, 1, 764-771), on which I am a coauthor, and are shown in quotes. "While Rh(III) porphyrins are typically axially ligated in aqueous solution,[137,151-153,155] a two-electron reduction fills the metal d$_z^2$ orbital, and is expected to result in deligation for Rh(I) porphyrin complexes. If relatively strongly coordinating ligands and/or anions are present in solution, an irreversible, apparently 2-electron reduction (a typical ECE process in which the first reduction is followed by rapid deligation and a second reduction)[134,139,140] is observed for rhodium(III) porphyrins. Complexes **1[Rh(III)]**, **2[Rh(III)]**, and **3[Rh(III)]** show an ECE reduction in alkaline aqueous solution. The role coordinating ligands play in bringing about this disproportionation event has been thoroughly investigated."[134,139,140,158] Electrochemical investigations on **1[Rh(III)]** and **2[Rh(III)]** were performed by Haoran Sun.[144] "Despite the relatively complex electrochemical behavior of these species, it is apparent from the cyclic voltammetry (CV) results in"

Table 1.3 "that porphyrin fluorination shifts the Rh(III)/Rh(I) redox potential to more positive values under alkaline conditions." The results are in line with our findings on other β-fluorinated metalloporphyrins prepared in our lab. They were

Table 1.3. Irreversible Reduction Potentials for Rhodium Water Soluble Porphyrins

Compound	$E_{pc}{}^a$	$E_{pa}{}^b$	Ref.
1[Rh(III)]	-1.39	-0.30	this work
2[Rh(III)]	-1.17	-0.20	this work
3[Rh(III)]	-1.59^c	-0.34^c	[152]

a: irreversible reduction reaction in 0.5 M $NaPF_6$, 0.1 M NaOH, pH = 12.7, vs. NHE. b: E_{pa} irreversible oxidation reaction in 0.5 M $NaPF_6$, 0.1M NaOH, pH 12.7 vs. NHE. Table from Biffinger.[148]

determined to have more positive redox potentials compared to their non-fluorinated congeners.[140,142,143] Hence the fluorinated metalloporphyrins should act as stronger oxidants. "The CV experiments on **1[Rh(III)]** and **2[Rh(III)]** were performed at basic pH to assure that only the dihydroxo species was present, thereby allowing a direct comparison of metal centers with identically charged coordination spheres. Because the axial ligands are contributing the greatest electron density to the rhodium center at this pH, the potentials reported in Table 1.3 should be an indication of the minimum impact of fluorination on the Rh(III) metal centers; at lower pH the impact of fluorination should be significantly larger." The results shown in Table 1.4 bear out this hypothesis.

Table 1.4. Electrochemical Behavior of **1[Rh(III)]** and **2[Rh(III)]** at Different pH Values

1[Rh(III)]		**2[Rh(III)]**	
pH	$\mathbf{E_{pc}{}^a}$	**pH**	$\mathbf{E_{pc}{}^a}$
7.4	-0.78	6.7	-0.64
8.1	-0.87	9.9	-0.87
12.7	-1.39	12.7	-1.17

a: irreversible reduction reaction in 0.5 M $NaPF_6$, 0.1 M NaOH, vs. NHE. Table from Biffinger[148]

1.2.5   Water-Soluble Rhodium(I) *β*-Fluorinated Porphyrins[144,148]

The Rh(I) porphyrins described in this section were prepared and characterized by Justin Biffinger.[144,148] This section has been drawn from reference 144 (Biffinger, J. C.; Uppaluri, S.; Sun, H.; DiMagno, S. G., "Ligand fluorination to optimize preferential oxidation of carbon monoxide by water soluble rhodium porphyrins", *ACS Catalysis* **2011**, 1, 764-771), on which I am a coauthor, and is shown in quotes. "Rh(I) porphyrins were prepared by electrochemical or chemical (alkaline sodium borohydride)[135] reduction, and these air-sensitive compounds were characterized by optical and NMR spectroscopies. In the optical absorption spectrum, the Soret band shifted from 403 nm to 383 nm upon reduction of **2[Rh(III)]** under alkaline conditions" (Figure 1.3).
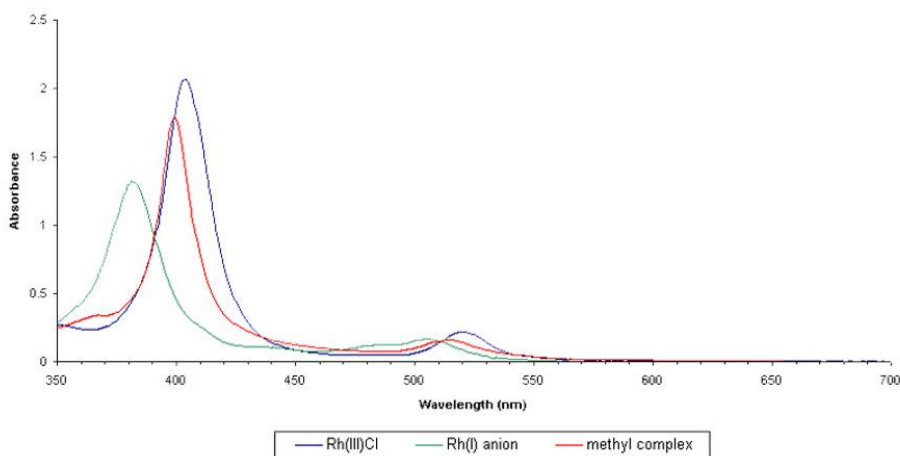
Figure 1.2. Representative UV-vis Spectral Changes for **2[Rh(III)]** going
from **2[Rh(III)]** → **2[Rh(I)]** → **2[Rh-CH₃]**
Figure from Biffinger.[148]

"Hypsochromism upon reduction is diagnostic for formation of Rh(I) β-fluorinated porphyrins, such as cobaltacenium [2,3,7,8,12,13,17,18-octafluoro-5,10,15,20-tetrakis(pentafluorophenyl)porphyrinato] rhodate in tetrahydrofuran.[124] The diamagnetic **2[Rh(I)]** complex generated a signal in the ^{19}F NMR spectrum (δ = -151

ppm) for the *β*-fluorines that was significantly upfield of that for **2[Rh(III)]** (δ = -144

ppm). This relatively large shift of the *β*-fluorine signal stems from the sensitivity of the

^{19}F NMR resonance frequency to changes in the metal ion electron density. The ^{19}F NMR

spectrum of **1[Rh(III)]** showed the same general chemical shift changes upon reduction

to **1[Rh(I)]**" (Table 1.5).

Table 1.5. ^{19}F NMR Shifts for *β*-Fluorines on
1[Rh] and **2[Rh]** at Different Oxidation States

Compound	Rh(III) shift (ppm)	Rh(I) shift (ppm)
1[Rh(III)]	-142	-148
2[Rh(III)]	-144	-151

Table from Biffinger.[144,148]

"Characteristically for nucleophilic Rh(I) porphyrins,[162-164] both rhodium(I)

porphyrins were alkylated with methyl iodide under standard conditions.[137] The

methylated complexes were identified by the chemical shift of the shielded Rh-CH$_3$

methyl group signal (δ = -6.61 and -6.31 ppm for **1[Rh-CH$_3$]** and **2[Rh-CH$_3$]**,

respectively) in the ^{1}H NMR spectrum, and also by changes in the optical absorption

spectra relative to the starting Rh(I) porphyrins" (Figure 1.3). "Solutions of **1[Rh(I)]** and

2[Rh(I)] are oxidized rapidly (<10 s as monitored by UV-vis) to regenerate **1[Rh(III)]**

and **2[Rh(III)]** quantitatively upon exposure to air or purified dioxygen."

1.2.6 Acid Dissociation Constants for Rh(III) Deuteride Porphyrin

Complexes[144,148]

The M-H acidity work on the water-soluble, fluorinated, rhodium-porphyrins

described here was done by Justin Biffinger.[144,148] This section is drawn from reference

144 (Biffinger, J. C.; Uppaluri, S.; Sun, H.; DiMagno, S. G., "Ligand fluorination to

optimize preferential oxidation of carbon monoxide by water soluble rhodium

porphyrins", *ACS Catalysis* **2011**, 1, 764-771), on which I am a coauthor, and is shown in quotes. "The M-H acidity of deuterido[5,10,15,20-tetrakis(4-sulfonatophenyl)porphyrinato]rhodium(III) (**3[Rh-D]**) was reported by Wayland and co-workers;[137,155] the pK_a of this species was calculated to be 7.1 ± 0.4" (Table 1.6). "Since fluorination of the porphyrin periphery acidifies pendant aquo ligands and has a substantial effect on the Rh(I)/Rh(III) redox potential, it was expected that the pK_a of the metal hydride **2[Rh-D]** would be significantly lower than 7.1." Biffinger determined the pK_a of **2[Rh-D]** to be 2.2 ± 0.2 using a ^{19}F NMR spectroscopic titration method. [144,148]

Table 1.6. Determination of the pK_a of **2[Rh-D]** by NMR spectroscopic titration

Compound	pK_a	Reference
2[Rh-D]	2.2 ± 0.2	Biffinger[144,148]
3[Rh-D]	7.1 ± 0.4	[137]

Data from Biffinger.[144,148]

"The increased acidity of **2[Rh-H]** assures that only the clean, two electron reduction of **2[Rh(III)]** will be observed upon exposure to CO under mildly acidic to alkaline conditions. Unfortunately, **1[Rh(I)]** is sufficiently basic to form the metal hydride **1[Rh-H]**, which collapses to a dimeric, unreactive Rh(II) species under neutral to acidic conditions" (Appendix A, Figure A1).[148] "Hence the pK_a of **1[Rh-D]** could not be determined using the procedure above. The mechanism for **1[Rh(II)]** formation was unexplored, but presumably this occurs by proton reduction; discrete monomeric Rh(II) intermediates were not observed.[134] Dimerization of Rh(II) porphyrins is well documented for complexes not containing bulky *ortho*-substituents on the *meso*-aryl rings.[130] Apparently, the Rh-Rh bond is sufficiently strong to frustrate disproportionation for **1[Rh(II)]**, and this complex is trapped in its low energy dimer. In contrast, under

alkaline conditions, chemical or electrochemical reduction of **1[Rh(III)]** yielded **1[Rh(I)]** as the only species observed by ^{19}F NMR spectroscopy. The anaerobic one-electron oxidation of **1[Rh(I)]** to **1[Rh(II)]**, and subsequent dimerization contrasts with the behavior of **2[Rh(I)]**, which is monomeric under acidic and basic conditions. While electronic tuning of the metal center and coordinating solvent preclude easy formation of stable Rh(II) intermediates for this compound, it has also been shown previously that four *meso*-2,6-difluoroaryl substituents provide sufficient steric bulk to thwart dimer formation in the event that any Rh(II) porphyrin would form."[130]

"DiMagno and coworkers have demonstrated previously that *β*-fluorination has a significant impact upon porphyrin ring and chelated metal ion electronic properties.[124,143,165,166] In keeping with these observations, the rhodium center of the water-soluble derivative **2[Rh(III)]** has a more positive reduction potential (-1.17 V, pH = 12.7, 0.5 M NaPF$_6$) in aqueous solution than that of **1[Rh(III)]** (-1.39 V) under identical conditions (Table 1.3). Similarly, the pK_a of the Rh(III) deuteride **2[Rh-D]** (pK_a = 2.2 ± 0.2) is considerably lower than that measured by Wayland for **3[Rh-D]** (pK_a = 7.1 ± 0.4)" (Table 1.6). "The dramatic increase in the hydride acidity caused by fluorination precludes hydrogen activation near neutral pH, potentially permitting PROX of CO in the presence of H$_2$."

1.2.7 Reactivity of Water-Soluble Rh(III) *β*-fluorinated Porphyrins with Carbon Monoxide[144,148]

The preliminary CO reactivity studies described in this section were done in collaboration with Justin Biffinger[148]. While Biffinger worked on **3[Rh(III)]** and

1[Rh(III)], I worked on **2[Rh(III)]**. At pH = 13, all three Rh(III) water-soluble porphyrins exist in the dihyroxo axial ligated state. CO oxidation was initially examined at this basic pH to ensure complete and clean reduction of the Rh(III) porphyrins to the Rh(I) porphyrins, and thereby preclude complications arising out of Rh(III) hydride porphyrins. Also, it was postulated that attack of the stronger nucleophile – hydroxide – at this pH (as opposed to that of water) on the Rh(III)-coordinated CO molecule should afford a rate enhancement, assuming that nucleophilic attack at the rhodium carbonyl is the rate limiting step.[127]
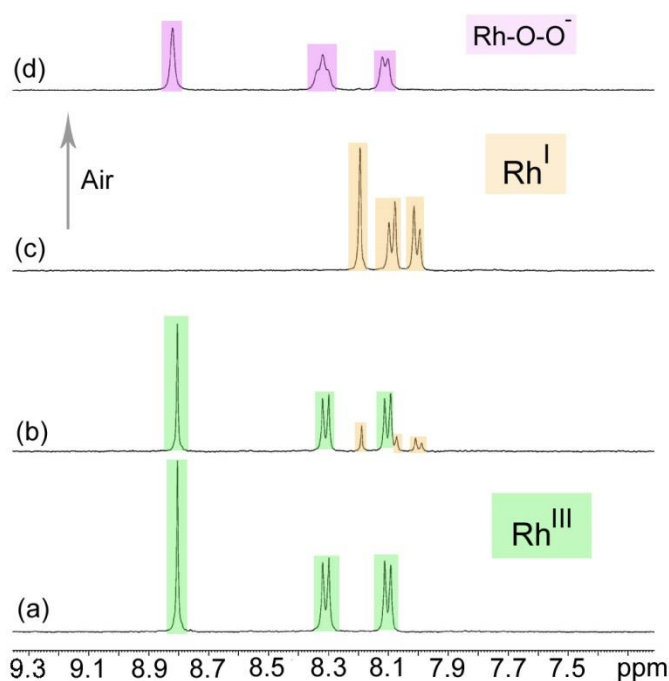
Figure 1.3. Changes in the ^{1}H NMR during the Reaction of **3[Rh(III)]** with CO in D_2O at pH = 13 a: initial, b: 20 minutes, c: 120 minutes, d: 1 min after exposure to air. Figure from Biffinger.[148]

A basic (100 mM NaOH, pH = 13) degassed D_2O solution of **3[Rh(III)]** at room temperature was charged with CO (1 atm), and the reaction was monitored by ^{1}H NMR.

Over the course of about 120 min, **3[Rh(III)]** was cleanly converted to **3[Rh(I)]** (Figure 1.4), thereby indicating reduction of the former complex to the latter, with concomitant oxidation of CO. The marked upfield shift of the porphyrin β-proton and *meso*-aryl proton signals indicates formation of the Rh(I) complex (spectrum c).[137] Complex **3[Rh(III)]** provides a benchmark against which the rates of reduction of **1[Rh(III)]** and **2[Rh(III)]** can be compared.

Similar reactions of **1[Rh(III)]** (Biffinger[148]) and **2[Rh(III)]** (Uppaluri) with carbon monoxide were monitored by ^{1}H and ^{19}F NMR spectroscopy. The porphyrin complexes underwent reduction from Rh(III) to Rh(I) indicating CO oxidation; ^{19}F NMR and ^{1}H spectra showed the telltale upfield shifts in the β-fluorine and *meso*-aryl fluorine/proton resonances upon reduction similar to **3[Rh(I)]**. Figure 1.5 shows changes in the ^{19}F NMR during the reaction of **2[Rh(III)]** with carbon monoxide (1 atm) in 100 mM NaOH/D$_2$O at 298 K, and Figure 1.6 corresponds to a similar reaction using **1[Rh(III)]**. The peak at δ = -151 ppm in Figure 1.5 is indicative of the Rh(I) oxidation state, which is also observed in the reduction of Rh(III) porphyrins with alkaline sodium borohydride. In a 100 mM sodium hydroxide solution, **1[Rh(III)]** was reduced cleanly to **1[Rh(I)]** (δ = -148 ppm). Because of the relatively low pK_a values (2.2 – 7.1) for the hydride complexes of these rhodium(III) water soluble porphyrins, only the Rh(I) anion complex will be formed under these basic reaction conditions.
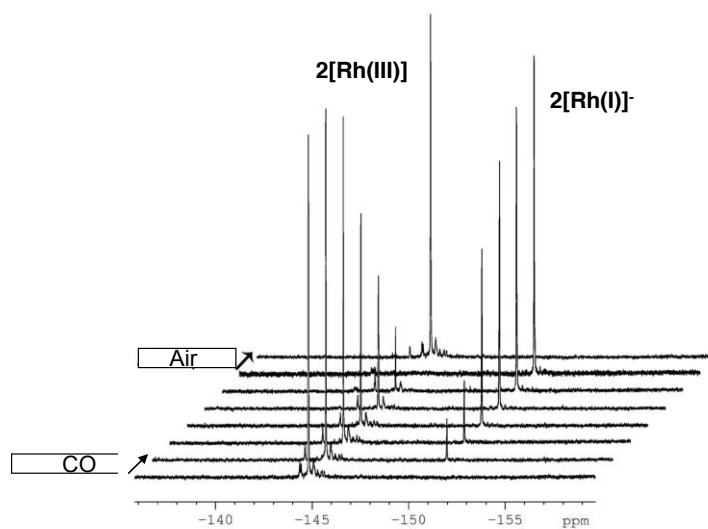
Figure 1.4. Changes in the ^{19}F NMR during the Reaction
of **2[Rh(III)]** with CO in D$_2$O at pH = 13
Figure from reference 144. Copyright 2011 ACS.
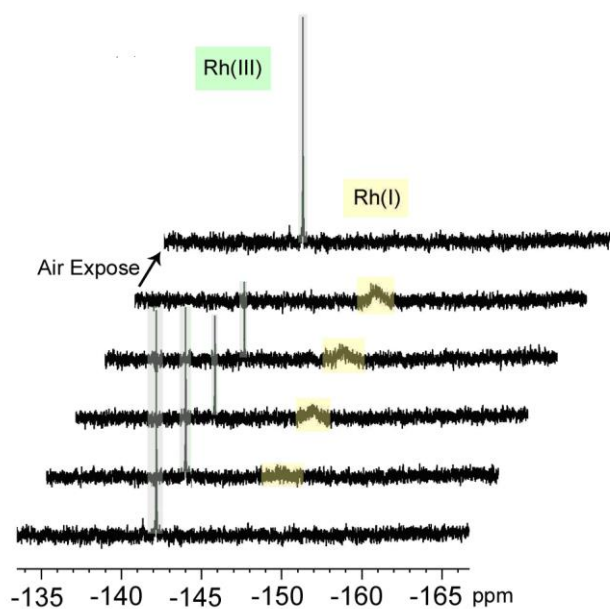
Figure 1.5. Changes in the ^{19}F NMR during the
Reaction of **1[Rh(III)]** with CO in D$_2$O at pH = 13
Figure from Biffinger.[148]

"The increased acidity of **2[Rh-H]** ensures that only the clean two electron reduction of **2[Rh(III)]** to **2[Rh(I)]** is observed under mildly acidic to alkaline conditions (pH = 4 – 13)." However, as mentioned previously, "**1[Rh(I)]** is sufficiently basic to form **1[Rh-H],** which collapses to a dimeric, unreactive Rh(II) species under neutral to acidic conditions (pH = 4 – 8)" (Appendix A, Figure A1).[148] "The mechanism for **1[Rh(II)]** formation was unexplored, but presumably this occurs by proton reduction; discrete monomeric Rh(II) intermediates were not observed.[134] Dimerization of Rh(II) porphyrins is well documented for complexes not containing bulky *ortho*-substituents on the *meso*-aryl rings.[130,137,167] Apparently, the Rh-Rh bond is sufficiently strong to frustrate disproportionation for **1[Rh(II)]**, and thereby, this complex is trapped in its low energy dimer. Nevertheless, complex **1[Rh(I)]** was the only species observed upon reduction of **1[Rh(III)]** by CO under basic conditions. The anaerobic oxidation of **1[Rh(I)]** and subsequent dimerization of **1[Rh(II)]** contrasts with the behavior of **2[Rh(I)]**, which is monomeric under acidic and basic conditions. Electronic tuning of the metal center and presence of coordinating solvent preclude easy formation of stable Rh(II) intermediates for **2[Rh(III)]**. Also, it has been shown previously that the four *meso*-2,6-difluoroaryl substituents in **2[Rh(III)]** provide sufficient steric bulk to thwart Rh-Rh dimer formation in the event that any Rh(II) porphyrin would form."[130]

2[Rh(III)] and **1[Rh(III)]** were regenerated immediately upon venting the NMR tubes containing aqueous solutions of **2[Rh(I)]** and **1[Rh(I)]** to air, suggesting that the fluorinated porphyrin complexes might be able to use air or dioxygen as the terminal oxidant for CO oxidation. In contrast, **3[Rh(III)]** was not regenerated upon exposure of the solution of **3[Rh(I)]** to air. Spectrum d in Figure 1.4 shows the air oxidation of

3[Rh(I)]. The slightly broadened peaks and change in multiplicities indicate an inequivalence between the two faces of the porphyrin thereby making one *ortho*-proton chemically inequivalent from the other *ortho*-proton on the *meso*-aryl rings. The same applies to the *meta*-protons.[168] Wayland reported a rhodium-peroxo complex that would fit with the observed complex.[169] This new complex is not capable of reducing CO. From
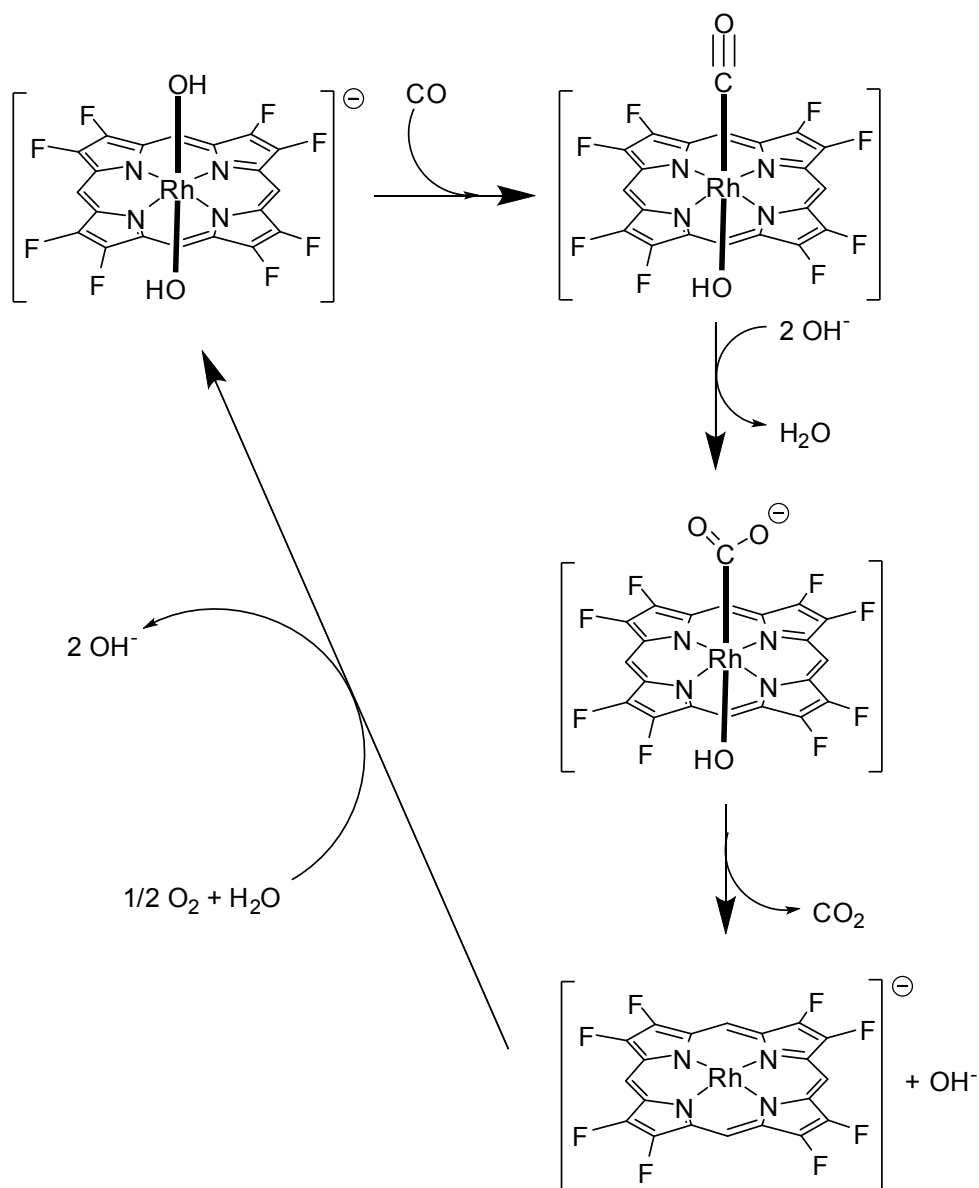
Scheme 1.5. General Reaction Pathway for CO Oxidation by **2[Rh(III)]** & **1[Rh(III)]** under Basic Conditions. Figure adapted from reference 144. Copyright 2011 ACS.

the above observations regarding the reactivity of the water-soluble rhodium β-fluorinated porphyrin complexes with CO and air/O$_2$, a general catalytic pathway for CO oxidation as shown on the previous page (Scheme 1.5) can be put together for basic conditions (pH = 11 – 13).

1.2.8 Evaluation of the Rate of Reduction of Rhodium(III) Water-Soluble Porphyrins by CO at Basic pH[148] and Associated Problems

The preliminary kinetic studies described in this section were done by Justin Biffinger.[148] The rates of reduction of **1[Rh(III)]**, **2[Rh(III)]**, and **3[Rh(III)]** by CO were followed by monitoring the disappearance of Rh(III) complexes by UV-vis spectroscopy. Upon sealing Schlenk-style cuvettes containing **1[Rh(III)]**, **2[Rh(III)]**, or **3[Rh(III)]** in degassed aqueous 100 mM sodium hydroxide solutions at 30 °C with CO (1 atm), clean isosbestic conversion to the corresponding Rh(I) complexes was observed.

Biffinger used a second order kinetic model[148] to fit[172] the kinetic data obtained for the reduction of **1[Rh(III)]**, **2[Rh(III)]**, and **3[Rh(III)]** by CO. A second order fit requires the initial solution concentration of CO and the concentrations of CO at various time points along the kinetic run. He used an approximation and treated CO concentration as a "fitted variable parameter."[148] His results are presented in Table 1.7.

Table 1.7. Second Order Rate Constants for the Reduction
of Rhodium-Porphyrins by CO[148]

Compound	[NaOH] (mM)	[Porphyrin] [mM]	k' ($M^{-1}s^{-1}$)
1[Rh(III)]	100	0.5	2.4 ± 0.3
2[Rh(III)]	100	0.05	140 ± 13
3[Rh(III)]	100	0.5	2.0 ± 0.2
2[Rh(III)]	10	0.5	3.8 ± 0.3

Data from Biffinger.[148]

The highest rate of reduction was observed for **2[Rh(III)]** with a second order rate constant of 140 ± 13 M^{-1} s^{-1} (Table 1.7). This rate was about 70 times greater than the rates for **1[Rh(III)]** and **3[Rh(III)]** under identical conditions. These observations are consistent with the hypothesis that the most electron deficient porphyrin would enhance the rate of nucleophilic attack on the bound carbonyl. The rate of reduction of **1[Rh(III)]** and **[3[Rh(III)]]** are (within experimental error) identical.

The reaction of Lewis basic nucleophiles on metal carbonyl complexes has been well documented.[174,175] Since attack of the nucleophile on the metal carbonyl is posited to be the rate determining step[127] for CO oxidation, Biffinger probed the effect of varying the hydroxide concentration on the rate. The rate varied as a function of hydroxide concentration. With **2[Rh(III)]**, there was a drop in the reaction rate upon decreasing the hydroxide concentration from 100 mM to 10 mM (Table 1.7). Since the preceding preliminary studies established **2[Rh(III)]** as the most effective catalyst for CO oxidation, further studies and optimization were done using only this complex.

After Biffinger reported[148] the above kinetic studies, it came to light that the results were fraught with instrumental errors, and the kinetics had to be re-determined accurately using our newly acquired Varian Cary 5000 spectrophotometer. When I attempted kinetic runs on **2[Rh(III)]** at pH = 13 using the above Biffinger procedure, I ran into problems that were two-fold. Firstly, I observed that an induction period preceded the reduction of **2[Rh(III)]** by CO. During the induction period, there was no change in the concentration of **2[Rh(III)]**. This was attributed to residual O_2 left in solution and/or the head space of the Schlenk-style cuvette even after meticulous degassing (7 freeze-pump-thaw cycles). Multiple turnovers were facilitated by the trace

O_2 as the catalyst regenerating agent. Secondly, once it initiated, the reduction of **2[Rh(III)]** to **2[Rh(I)]** did not go to completion (Appendix A, Figure A2). It was hypothesized that the solution ran out of dissolved CO due to the oxygen-scavenging induction period, and that diffusion of the sparingly soluble CO from the head space into solution was rate-limiting. When the cuvette was shaken vigorously to introduce fresh CO into solution, the concentration of **2[Rh(III)]** was diminished significantly relative to the initial concentration with which the kinetic run was begun. It is surmised that the reduction in **2[Rh(III)]** concentration upon shaking resulted from a partial decomposition of **2[Rh(III)]** caused by hydrogen peroxide (H_2O_2) that can form under the reaction conditions from the 2-electron reduction of dioxygen. **2[Rh(III)]** is unstable in the presence of hydrogen peroxide, and undergoes decomposition, especially under basic conditions. More details about this phenomenon are presented later in section 1.2.10. Furthermore, a second induction period was observed, which can be attributed to fresh trace O_2 being introduced into solution from the head space when the cuvette was shaken. Due to the above complications arising from lagging mass transfer between the gas phase and solution phase, and catalyst decomposition, the above strategy to determine the kinetics was abandoned. I came up with a new method that surmounts the above problems to determine the kinetics under multiple turnover conditions. Results obtained using this method are presented in section 1.2.11. The rate constant obtained was significantly lower than the value determined by Biffinger.[148]

1.2.9 Oxidation of 2[Rh(I)] with Terminal Oxidants or Air[144,148]

As was discussed in section 1.2.7, **2[Rh(I)]** can be oxidized rapidly by air or dioxygen to regenerate **2[Rh(III)]** thereby completing a catalytic cycle for CO oxidation

(Scheme 1.5). However, I observed rapid catalyst decomposition when air was used as the terminal oxidant. From reference 144, on which I am a coauthor: "For example, if a buffered D_2O solution of **2[Rh(III)]** was cycled repeatedly through a three step (degassing/CO/air) sequence, the formation of free fluoride (detected at about δ = -123 ppm by ^{19}F NMR spectroscopy) and bleaching of the **2[Rh(III)]** optical signature were apparent after fewer than 10 turnovers. This decomposition was the fastest at pH = 13 and the slowest at pH = 4." The cause of such catalyst decomposition will be discussed later in section 1.2.10. An inorganic terminal oxidant (phosphomolybdic acid, a polyoxometallate) and a host of organic terminal oxidants were explored as catalyst regeneration agents to abate the problem of catalyst decomposition. The experiments were done in collaboration with Justin Biffinger.
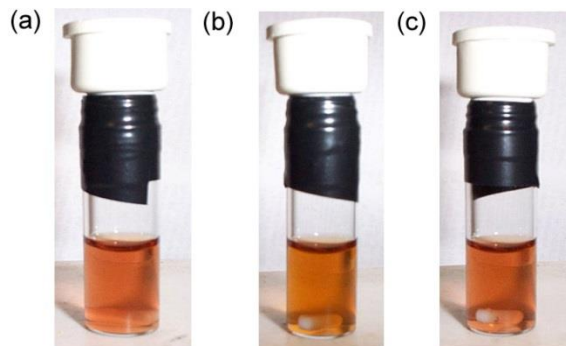
Figure 1.6. Color Changes for **2[Rh(III)]** at pH = 7
(a) initial, (b) after reaction with CO, (c) after
exposure to air
Figure from Biffinger.[148]

Figure 1.7 shows the color changes observed for a pH = 7 (200 mM sodium phosphate buffer) solution of **2[Rh(III)]** at room temperature: (a) initial solution, (b) upon reduction to **2[Rh(I)]** by passing a stream of research grade CO through the solution, and (c) regeneration of **2[Rh(III)]** upon exposure to air. These color changes

are not very pronounced and are in line with observations on the optical signatures of the complexes; reduction of the Rh(III) complex to the Rh(I) complex is characterized by a hypsochromic shift for the Soret band and a decrease in the molar absorptivity.

Figure 1.8 shows the color changes for a pH = 7 (200 mM sodium phosphate buffer) solution of **2[Rh(III)]** and 100 equivalents of phosphomolybdic acid (**PA**) at room temperature: (a) initial solution, (b) during the course of passing a stream of CO, and (c) after passing CO for 10 minutes. A striking color change from orange-brown to
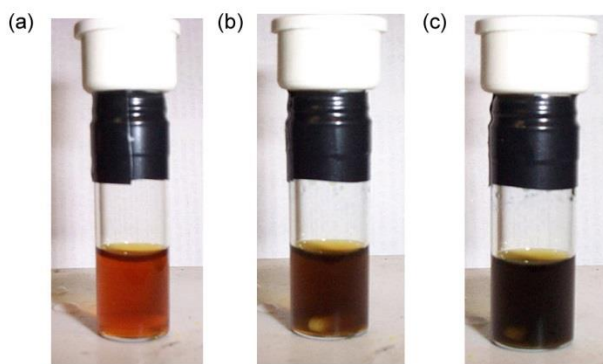
Figure 1.7. Reaction of **2[Rh(III)]** with
Phosphomolybdic Acid Under a CO Atmosphere
Figure from Biffinger.[148]

 blue was observed. An aqueous solution of phosphomolybdic acid is yellow in color, but upon reduction it takes a characteristic blue color which is generated by charge transfer between the Mo^V and Mo^{VI} states.[176,177] These color changes do not occur in the absence of **2[Rh(III)]** indicating that **2[Rh(III)]** is catalyzing the reduction of **PA** by CO. In other words, **2[Rh(I)]**, formed by the reduction of **2[Rh(III)]** by CO, is being oxidized by **PA** to regenerate the Rh(III) complex.   The overall reaction for the anaerobic oxidation of CO by **PA** is shown in equation 1.3.

$$H_2O + CO + PMo_{12}O_{40}^{3-} \rightarrow CO_2 + 2\,H^+ + PMo_{12}O_{40}^{5-} \qquad \text{Eq. 1.3}$$
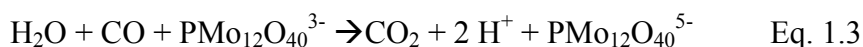
The applicability of several organic terminal oxidants was explored (Appendix A, Table A1). None of the mediators in Table A1 was stable under basic conditions. At neutral to acidic pH, indigo carmine turned out to be the most efficient and robust oxidant of all the candidates tested.
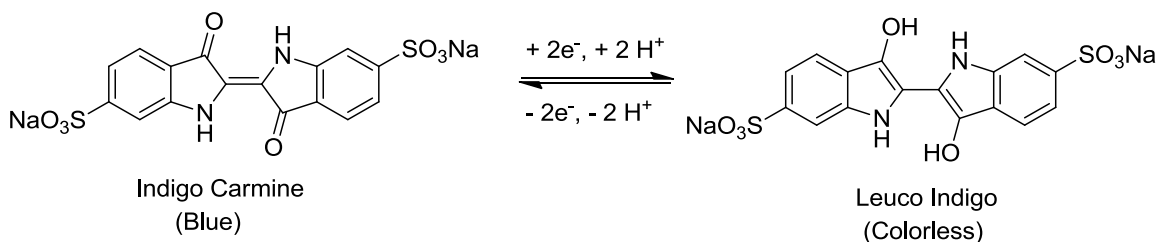
Scheme 1.6 Redox Equilibrium of Indigo Carmine and Leucoindigo

The structures of indigo carmine and its reduced state are shown in Scheme 1.6.[178] The color change involved in the redox equilibrium is suitable for the visual monitoring of the reaction. Figure 1.8 shows the color changes (in a reactor that I designed) for a pH = 7 (200 mM sodium phosphate buffer) solution of **2[Rh(III)]** and 100 equivalents of indigo carmine at room temperature: (a) immediately after mixing with blue due to the indigo carmine, (b) 25 minutes after passing a stream of CO and then sealing the reaction under a CO atmosphere causes the blue color to fade, (c) 1 minute later - the orange-brown color corresponds to the hitherto masked rhodium porphyrin indicating formation of the colorless leucoindigo. These color changes do not occur in the absence of **2[Rh(III)]** indicating that **2[Rh(III)]** is catalyzing the reduction of indigo carmine by CO. In other words, **2[Rh(I)]** (formed by the reduction of **2[Rh(III)]** by CO) is being oxidized by indigo carmine to regenerate the Rh(III) complex, with concomitant reduction of indigo carmine to leucoindigo. Thus the anaerobic oxidation of CO by indigo carmine is catalyzed by **2[Rh(III)].** When the solution in Figure 1.8 c is exposed

to air, the color instantly returns to the original blue (Figure 1.8 d) indicating that indigo carmine and **2[Rh(III)]** are regenerated. This suggests that air can be potentially used as a terminal oxidant. The above reaction sequence was accomplished at other acidic pH values of 4, 5 and 6 also.
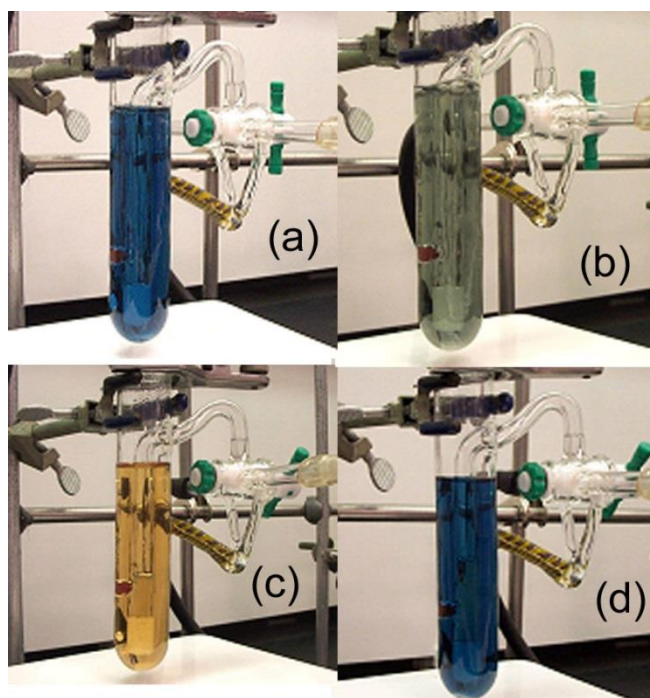
Figure 1.8. Reaction of CO with Indigo Carmine in the presence of **2[Rh(III)]** at pH = 7 and room temperature
Figure from reference 144. Copyright 2011 ACS.

Since it is known that aerobic oxidation of leucoindigo is relatively slow,[179,180] it was suspected that **2[Rh(III)]** was catalyzing the air oxidation of leucoindigo upon exposure of the solution in Figure 1.8 c to air. A pH = 7 (200 mM sodium phosphate buffer) degassed solution of indigo carmine was treated with sodium dithionite[181] under a nitrogen atmosphere. The blue color disappeared rapidly to give a clear, colorless solution indicating the reduction of indigo carmine to leucoindigo. When air was introduced into this sample, there was a gradual (about 30 minutes) color change back to

the original blue, indicating regeneration of indigo carmine. However, when a catalytic amount of **2[Rh(III)]** was added to the leucoindigo followed by injection of air, the reappearance of the blue color was very rapid (~ 10 s). This suggests that **2[Rh(III)]** is catalyzing the air oxidation of the leucoindigo.

I followed the reaction sequence in Figure 1.8 by ^{19}F NMR and UV-vis spectroscopies, and gas chromatography (GC). The formation of **2[Rh(I)]** and regeneration of **2[Rh(III)]** were observed by both ^{19}F NMR (Appendix A, Figure A5) and UV-vis spectroscopies. The disappearance/reduction of indigo carmine was observed by UV-vis spectroscopy (Figure 1.9). Clean isosbestic behavior was observed in the UV-vis spectra. Head gas analysis by GC showed that the amount of CO_2 generated corresponded to the amount of CO consumed (Appendix A, Figure A6). Quantitation of the amounts of CO and CO_2 was done using a calibration curve that I built for a set of standards of gas mixes (Appendix A, Figure A13).
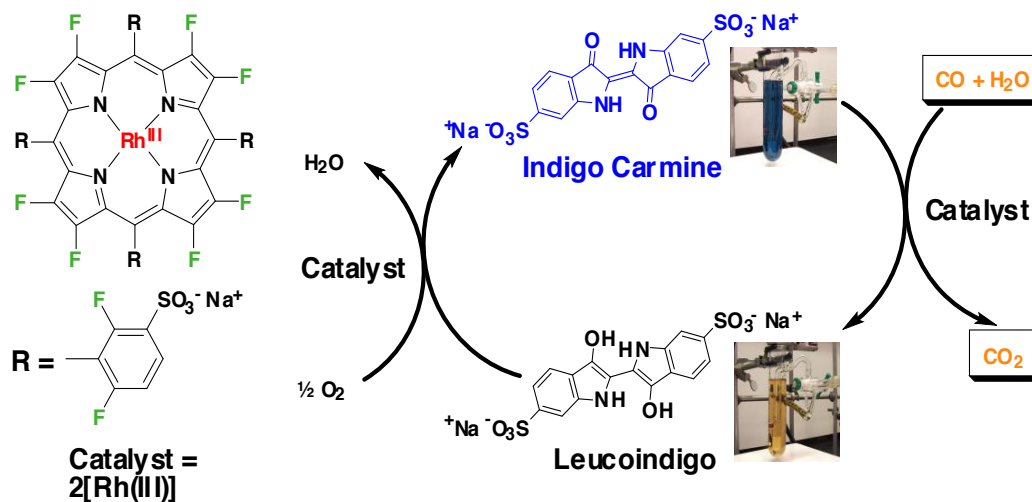
Scheme 1.7. General Reaction Cycle for the **2[Rh(III)]** Catalyzed CO Oxidation by Indigo Carmine at pH = 4 − 7. Taken from reference 144. Copyright 2011 ACS.

Based on the above observations, the general catalytic cycle shown in Scheme 1.7 can be put together for the **2[Rh(III)]** catalyzed oxidation of CO at pH = 4 – 7.

The Rh^{III}/Rh^{I} reduction potential for **2[Rh(III)]** was determined by Haoran Sun of our group by titration with hydroxymethyl ferrocene to be -0.057 V vs. NHE.[148,159-161] Hence, redox compounds suitable as oxidants for this chemistry require reversible redox potentials more positive than -0.06 V vs. NHE.[148] Based on the electrochemical analysis (Appendix A, Figure A3) of all of the redox compounds (Appendix A, Table A1)[148] done under identical conditions, indigo carmine was the only dye that showed reversible redox behavior in the desired potential range.[148]

1.2.10 Role of the Redox Dye Indigo Carmine[144]
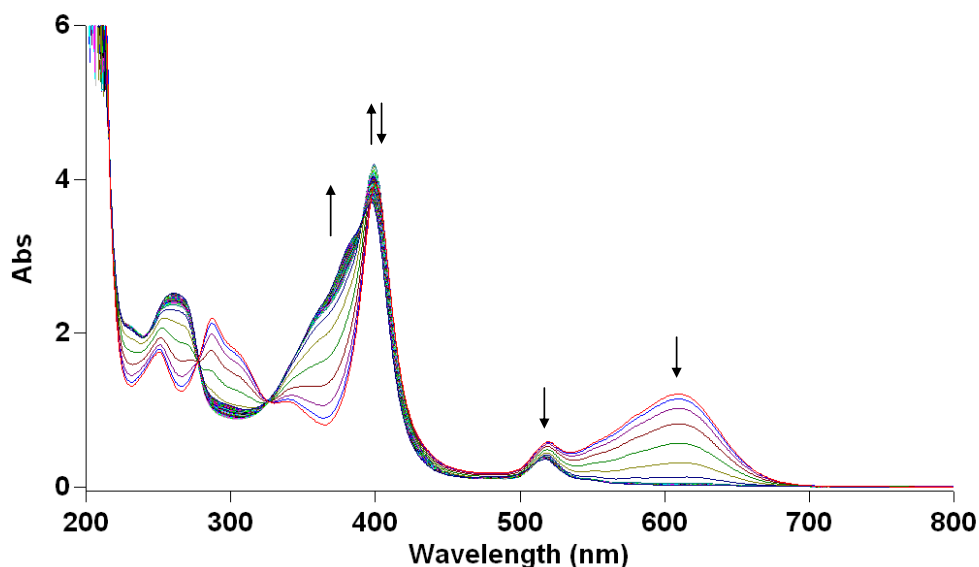
Figure 1.9. UV-vis Spectra of the **2[Rh(III)]** Catalyzed Oxidation of CO by Indigo Carmine at pH 4 and 35 °C. Figure from reference 144. Copyright 2011 ACS.
Initial concentrations: 0.032 mM **2[Rh(III)]** and 0.064 mM indigo carmine. The progressive decrease in absorbance at 520 nm (which is the λ_{max} for the Q-band of **2[Rh(III)]**) corresponds only to a decrease in absorbance of indigo carmine (See Appendix A, Figure A4).

The discussion in this section is based on my work, and the section is drawn from reference 144 (Biffinger, J. C.; Uppaluri, S.; Sun, H.; DiMagno, S. G., "Ligand

fluorination to optimize preferential oxidation of carbon monoxide by water soluble rhodium porphyrins", *ACS Catalysis* **2011**, 1, 764-771), on which I am a coauthor, and is shown in quotes. "The redox dye indigo carmine (IC) plays two important roles in the rhodium porphyrin-catalyzed CO oxidation. First, it is a very efficient oxidant for **2[Rh(I)]**." "UV-vis spectra" that I "gathered under turnover conditions showed that **2[Rh(III)]** was the only porphyrin species present as long as oxidized IC remained in solution, indicating that dye-mediated oxidation of **2[Rh(I)]** is extremely fast and that re-oxidation of the catalyst was not rate limiting" (Figure 1.9). I also observed that a blue solution of IC (aqueous, buffered) was instantly decolorized by a solution of **2[Rh(I)]** obtained by reducing **2[Rh(III)]** (aqueous, buffered) with CO.

"A second, equally important role for the leuco form of IC is as a redox buffer that is capable of scavenging strong oxidants in the presence of **2[Rh(III)]**. In the absence of indigo carmine, rapid catalyst decomposition was observed. For example, if a buffered (pH = 4) D_2O solution of **2[Rh(III)]** (1 mM) was cycled repeatedly through a three step (degassing/CO/air) sequence, the formation of free fluoride (detected at about -123 ppm by ^{19}F-NMR spectroscopy) and bleaching of the **2[Rh(III)]** optical signature were apparent after fewer than 10 turnovers. In contrast, when IC was present in 10-fold excess compared to **2[Rh(III)]**, 10 degassing/CO/air cycles could be performed to oxidize more than 100 equivalents of CO without measurable loss in catalytic activity. Given that **2[Rh(III)]** is unstable in the presence of hydrogen peroxide, we suspected that H_2O_2 generated by dioxygen reduction was responsible for porphyrin decomposition" (Appendix A, Figures A9 – A12). "Rotating ring-disk voltammetry" performed by Haoran Sun of our group "confirmed that **2[Rh(I)]** reduces dioxygen by two- and four-

electron processes at approximately equal rates at pH = 4; so H_2O_2 was confirmed as a significant byproduct of CO oxidation when dioxygen was the terminal oxidant" (Experimental Section). "Finally, we confirmed that the reduced dye is rapidly oxidized by H_2O_2 in the presence of **2[Rh(III)]**. These observations indicate that IC is acting as a catalyst preservative by scavenging active oxygen species. As long as the reduced form of the dye is present, air can be used as the terminal oxidant for **2[Rh(III)]** catalyzed oxidation of carbon monoxide." Also, when a **2[Rh(III)]** solution in the presence of 10-fold excess dye was reacted with a gas mixture containing CO (1 atm) and O_2 (0.2 atm), only 80 turnovers could be achieved before complete loss of catalytic activity. Hence the presence of O_2 in the feed gas is detrimental to catalyst stability.

1.2.11 Optimization of the Rate of 2[Rh(III)] Catalyzed Oxidation of Carbon Monoxide in the Presence of the Redox Dye Indigo Carmine at Acidic pH[144]

The discussion in this section is based on my work, and major portions of the section are drawn from reference 144 (Biffinger, J. C.; Uppaluri, S.; Sun, H.; DiMagno, S. G., "Ligand fluorination to optimize preferential oxidation of carbon monoxide by water soluble rhodium porphyrins", *ACS Catalysis* **2011**, 1, 764-771), on which I am a coauthor, and is shown in quotes. "In phosphate buffer, **2[Rh(III)]** exists as the diaquo complex at pH = 4, and as the aquohydroxo complex at pH = 7. As discussed in section 1.2.4, the redox potentials of **2[Rh(III)]** become more positive at lower pH, thus making this complex a stronger oxidant at lower pH. Hence we investigated the reaction rates at pH = 4 and pH = 7 (200 mM sodium phosphate buffers). The following technique was used to measure CO oxidation kinetics under multiple turnover conditions. The sacrificial oxidant, indigo carmine (IC), was used as an indicator dye; the oxidized, dark blue form

of the dye is reduced rapidly by **2[Rh(I)]** to generate the colorless leuco derivative"

(Figure 1.8). "Thus, the bleaching of a measured amount of dye served as a convenient

(and sharp) end point indicating generation of a known quantity of **2[Rh(I)]**."

"In a typical experiment, an aqueous solution of **2[Rh(III)]** varying in

concentration from 0.025 mM – 0.25 mM and a measured amount of IC (1-100 equiv.)

was degassed under dynamic vacuum. The vigorously agitated solution was placed under

CO (1 atm) and the time to the endpoint (dye bleaching) was measured." The agitation

was done by various methods – magnetic stirring, manual shaking, or bubbling of CO.

"The turnover frequency (TOF) at pH = 4 and 35 °C remained constant (1.8 – 2.0 TO

min^{-1}) over this porphyrin concentration range. When the CO concentration was diluted

to 0.5 atm with either 50% N_2 or 50% H_2 carrier, the TOF was also halved. The measured

TOF at pH = 4 corresponds to a bimolecular rate constant of 35 ± 3 $M^{-1}s^{-1}$ for CO

oxidation at 35 °C." The solution concentration of CO,[173] which is needed to calculate the

bimolecular rate constant, was derived based on Henry's Law and using the IUPAC

solubility data series (volume 43) that lists the mole fraction of carbon monoxide in water

at various temperatures.[170] Values reported in the CRC Handbook[171] (based on Henry's

Law) were used to calculate the solution concentration of CO in water. The mole fraction

at 303 K corresponds to a solution concentration of CO of 8.7×10^{-4} M.

"Also, it is notable that the TOF for CO oxidation was unaltered by the presence

of hydrogen; TOF values depended only on the partial pressure of CO. There was also no

observable formation of **2[Rh(I)]** from **2[Rh(III)]** with pure H_2 (1 atm) under the

turnover conditions of the CO oxidation experiments (as determined by examination of

the UV-vis and ^{19}F-NMR spectroscopy)." Detailed results of the kinetics at pH = 4 are

presented in Table 1.8 and Table 1.9. The TOF at pH = 7 is 0.50 TO min^{-1}(Appendix A,

Table A3). The difference in the TOF at pH = 4 and pH = 7 can be ascribed to the

difference in the axial ligation states of **2[Rh(III)]** at these two pH values. The kinetic

model used is based on the reaction steps in Scheme 1.8.

2[Rh(III)] + CO + H_2O $\longrightarrow$ **2[Rh(I)]** + CO_2 + 2H$^+$ (slow)

2[Rh(I)] + 2H$^+$ + IC $\longrightarrow$ **2[Rh(III)]** + IC-H_2 (fast)

CO + H_2O + IC $\longrightarrow$ CO_2 + IC-H_2 (overall)

                            blue   colorless
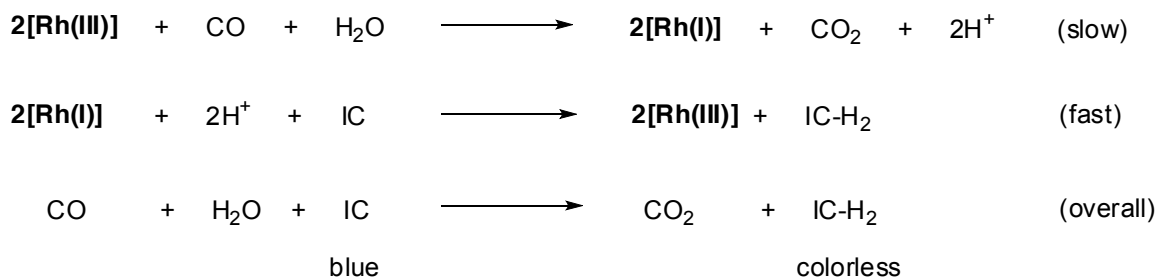
Scheme 1.8. Reaction Steps Considered in the Kinetic Model for the **2[Rh(III)]**
Catalyzed Oxidation of CO by Indigo Carmine

"UV-vis spectra gathered under turnover conditions showed that **2[Rh(III)]** was

the only porphyrin species detectable as long as oxidized IC remained in solution,

indicating that dye-mediated oxidation of **2[Rh(I)]** is extremely fast and that re-oxidation

of the catalyst is not rate limiting" (Figure 1.9).

Rate = -d[CO] / dt = d[CO_2] / dt = -d[IC] / dt = k [CO] [**2[Rh(III)]**]

When the concentrations of CO & **2[Rh(III)]** remain constant, the rate is a constant.

Turnover Frequency, TOF = Rate / [**2[Rh(III)]**] = k [CO] = k'

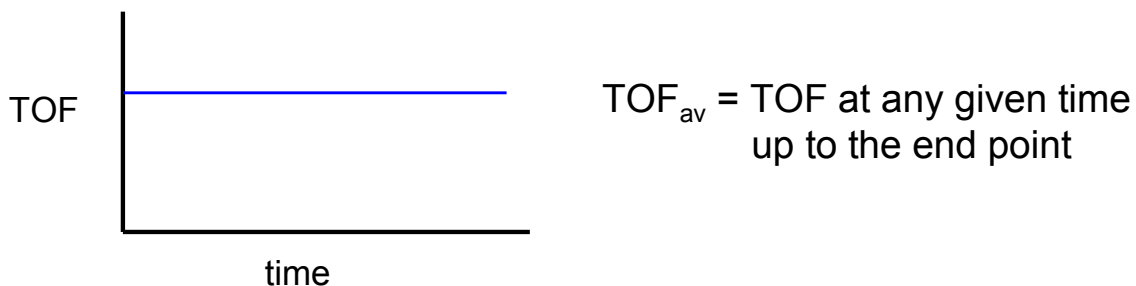TOF_{av} = TOF at any given time
up to the end point

Table 1.8. TOF at pH = 4 for **2[Rh(III)]** Catalyzed CO Oxidation by IC at 1 atm Pressure, 35 °C (intermediate concentration range of **2[Rh(III)]**). Table from reference 144. Copyright 2011 ACS.

Run	2[Rh(III)] (mM)	IC (mM)	Turnover No. TON	End point (min)	TOF$_{av}$ (TO min^{-1})	Corrected[a] TOF$_{av}$ (TO min^{-1})
1	0.25	1.0	4.0	5.0	0.80	
2	0.25	5.0	20.0	13.5	1.48	1.88
3	0.25	10.0	40.0	24.5	1.63	1.85
4	0.10	1.0	10.0	9.5	1.0	
5	0.10	2.0	20.0	15.0	1.33	1.82
6	0.10	5.0	50.0	31.0	1.61	1.86
7	0.050	0.50	10.0	11.5	0.87	
8	0.050	1.0	20.0	17.5	1.14	1.67
9	0.050	2.0	40.0	27.0	1.48	1.93
10	0.025	0.25	10.0	21.0	0.48	
11	0.025	0.50	20.0	26.0	0.77	2.0

a. The corrected TOF$_{av}$ is obtained by calculating the difference in TON ($\Box$TON/$\Box$time) for consecutive table entries run under the same conditions. This approach corrects for an initial induction period that arises from scrubbing of residual dissolved O$_2$. For example, the corrected TOF$_{av}$ for run 5 was calculated by using the difference in TON and the difference in end points between run 5 and run 4 [(20-10) / (15.0-9.5)].

"Several potential sources of error in the rate constant measurements were probed by varying the concentration of **2[Rh(III)]** in the kinetic runs" (Appendix A, Table A2). "At low **2[Rh(III)]** concentration and in experiments run at low turnover numbers, an induction period was required to scrub the residual oxygen contaminant remaining after sample preparation. At high porphyrin concentration (> 0.5 mM), mass transfer of the sparingly soluble CO (8.7 x 10^{-4} M at 1 atm and 308 K)[170] resulted in reduced measured TOFs. Nevertheless, consistent and reproducible turnover numbers were achieved at intermediate catalyst concentrations (0.025 mM – 0.25 mM) at 1 atm CO pressure" (Table 1.8). Thus I successfully surmounted the problems encountered in the UV-vis method described in section 1.2.8.

Table 1.9. TOF at pH = 4 for **2[Rh(III)]** Catalyzed CO Oxidation by IC at 35 °C Using 50% CO (in N_2 or H_2); Total Pressure = 1 atm. Table from reference 144. Copyright 2011 ACS.

Run	2[Rh(III)] (mM)	IC (mM)	Turnover No. TON	End pt (min)	TOF_{av} (TO min^{-1})	Corrected[a] TOF_{av} (TO min^{-1})
1	0.10	1.0	10.0	16.0	0.62	
2	0.10	2.0	20.0	27.0	0.74	0.91
3	0.025	0.25	10.0	46.0	0.22	
4	0.025	0.50	20.0	57.5	0.35	0.87

a. Defined and calculated in the same way as for the data in Table 1.8

In view of the optimal rate of **2[Rh(III)]** catalyzed CO oxidation at pH = 4 in the presence of indigo carmine, the following general reaction cycle can be put together at this pH (Scheme 1.9).
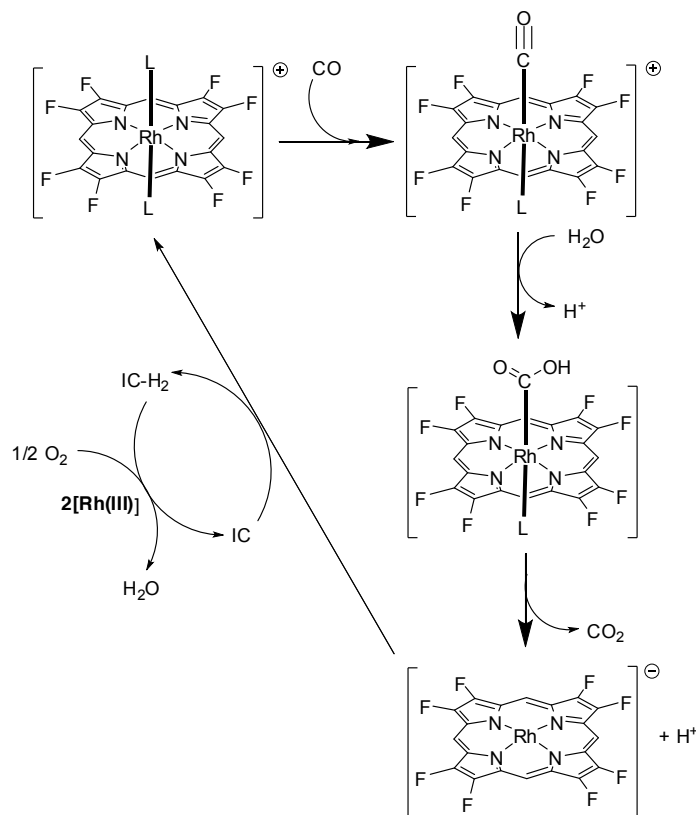
Scheme 1.9. General Reaction Cycle for CO Oxidation at pH 4. Adapted from reference 144. Copyright 2011 ACS.

Justin Biffinger reported enhancement in the rate of reduction of **2[Rh(III)]** by CO upon the addition of halide nucleophiles (Br⁻ and I⁻) at pH = 7. However, I did not see any such rate enhancement at pH = 4 or pH = 7 in the catalytic reaction carried out under multiple turnover conditions with the addition of Br⁻ (1 – 1000 mM range). I also determined that there was no effect of varying the buffer concentration (50 – 1000 mM range) at both pH = 4 and 7.

Based on the kinetic analysis at pH = 4, the observed rate law for CO oxidation is first order in **2[Rh(III)]** and CO. The only observable (by NMR) solution species is **2[Rh(III)]**. Kinetic measurements (Figure 1.10) conducted at temperatures ranging from 35 – 80 °C gave activation parameters for CO oxidation ($\Delta H^{\ddagger}$ = 7.5 kcal/mol, $\Delta S^{\ddagger}$ = -27 eu). This is consistent with a bimolecular rate determining step.
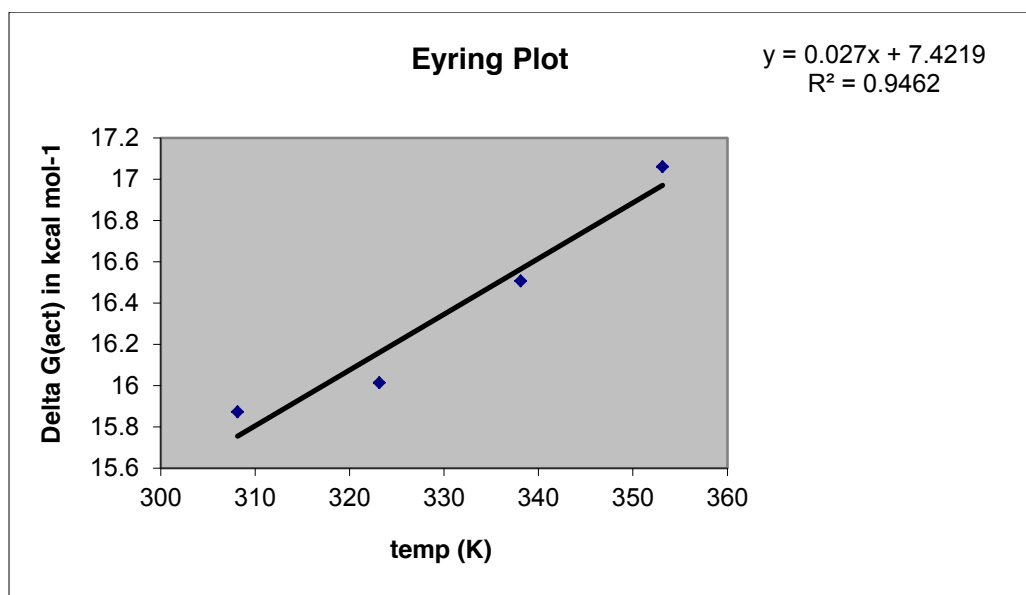

Figure 1.10. Eyring Plot of Variable Temperature Kinetic Measurements at pH = 4 for the **2[Rh(III)]** Catalyzed Oxidation of CO by Indigo Carmine

1.2.12 Evaluation of 2[Rh(III)] as a PROX Catalyst for CO in Hydrogen[144]

Drawn from reference 144, on which I am a coauthor: "To show the general applicability of these compounds as PROX catalysts", Justin Biffinger "placed the most active catalyst (**2[(Rh(III)]**) under an atmosphere of hydrogen or carbon monoxide in a sealed cuvette in 100 mM sodium hydroxide solution and the reduction of **2[Rh(III)]** to **2[Rh(I)]** was followed by UV-vis spectroscopy at 50 °C and 30 °C, respectively" (Figure 1.11). "Under these conditions, only the reaction of **2[(Rh(III)]** with carbon monoxide was observed." I made similar observations at pH = 4, where the experiments were done in the presence of indigo carmine.
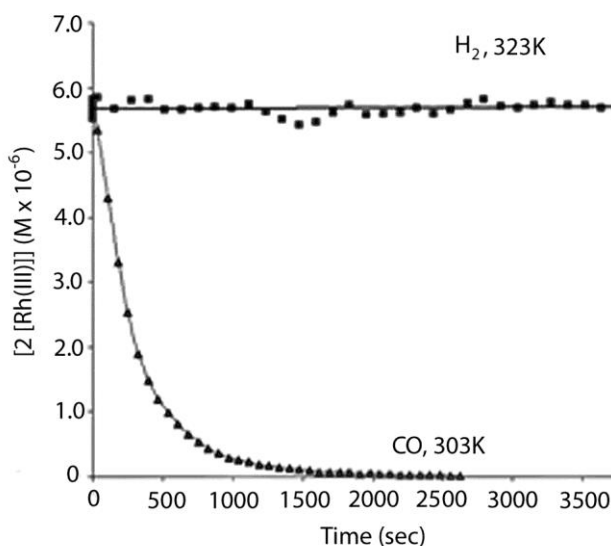
Figure 1.11. Comparison of the Reaction of **2[Rh(III)]** with Carbon Monoxide or Hydrogen.[144,148] Figure from reference 144. Copyright 2011 ACS.

My work drawn from reference 147: "The oxidation of CO catalyzed by **2[Rh(III)]** was also monitored by head gas analysis in a mixture of CO balanced with H_2 and N_2. In a typical experiment a degassed buffered aqueous solution of **2[Rh(III)]** (0.6 mM) and IC (6.0 mM) was charged with 1 atm of a gas mixture containing CO and H_2." "Head gas analysis by gas chromatography" (Figure 1.12) "confirmed that CO was

consumed, that CO_2 was generated during the course of the reaction, and that H_2 was not oxidized simultaneously, even when residual dioxygen was present. Head gas analysis demonstrated conclusively that CO can be scrubbed from hydrogen gas streams by **2[Rh(III)]** to generate CO_2. A calibration curve generated by using standard gas mixes was used to quantitate CO and CO_2."
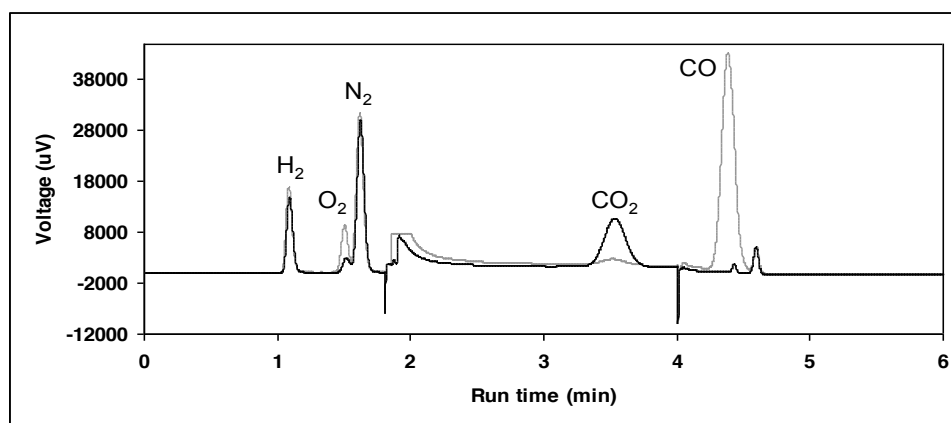
Figure 1.12. Scrubbing of CO from a mixture of 10% CO in H_2 (total pressure of 1 atm) by a pH 4 solution of 0.6 mM **2[Rh(III)]** and 6.0 mM indigo carmine at 35 °C. Initial head gas sample – grey line; final head gas sample – black line. The two small peaks at 4.4 and 4.6 minutes were also observed in control (blank) gas injections. The peaks at ~ 2 min and ~ 4 min are artifacts generated during the valve switching associated with multiple column GC operation (Figure 1.13). Figure from reference 144. Copyright 2011 ACS.
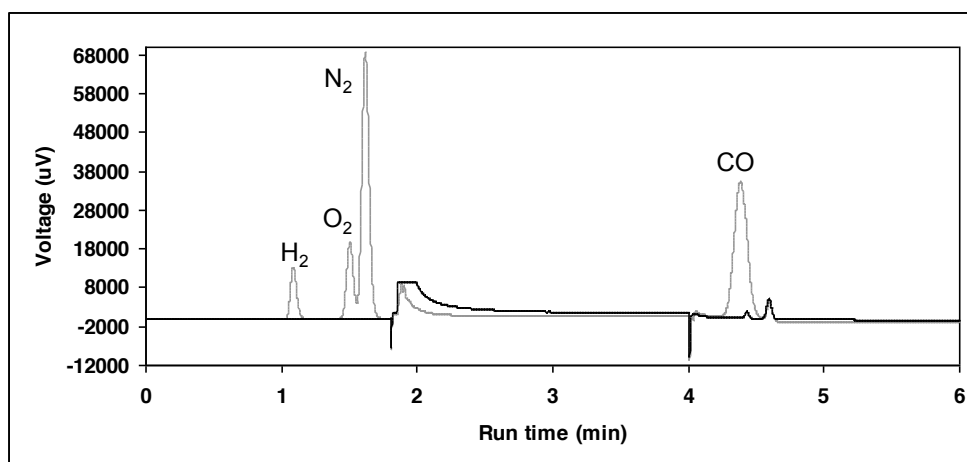
Figure 1.13. Reference GC traces. Grey trace – 10% CO/H_2 balance. Black trace – helium blank. Figure from reference 144. Copyright 2011 ACS.

1.3   Summary

Drawn from reference 144, on which I am a coauthor: "The introduction of fluorine substituents into water-soluble rhodium porphyrins permits these complexes to act as effective low-temperature, low pressure homogenous PROX catalysts for CO. The indicator dye indigo carmine serves as a redox reservoir providing reducing equivalents that effectively scavenge active oxygen species. The combination of **2[Rh(III)]** and IC under both acidic and neutral conditions comprises a robust catalyst system capable of selectively oxidizing CO in H_2 streams using air as the terminal oxidant. Although the maximum turnover frequency obtained with the rhodium porphyrin catalytic system is modest, the strategy of using ligand substituent effects to tune metal hydride acidity, control proton reduction, and preclude hydrogen activation provides a rational framework for optimizing more robust and active Rh-based PROX catalysts."

1.4   Experimental Section

1.4.1   Materials and Instruments

Reagents were used as received from Aldrich, Sigma, Fisher, Fluka, or Cambridge Isotope Laboratories unless otherwise indicated. ^{1}H NMR spectra were obtained in D_2O, methanol-d_4 or DMSO-d_6 using the 400, 500, and 600 MHz spectrometers at the University of Nebraska-Lincoln. ^{19}F NMR spectra were collected at 376 MHz or 470 MHz in the same solvents using hexafluorobenzene as a chemical shift reference (δ = -164.9 ppm). Research grade gases and gas mixes were used as received from Linweld, Lincoln, NE. Absorption spectra were obtained using modified (OLIS-14) Cary-14 UV-Vis-NIR or Varian Cary 5000 spectrophotometers equipped with a variable-

temperature cell holder and a circulating bath (Laude RC3). Analyses of gaseous reaction components were performed on a Varian CP-3800 equipped with HayeSep Q 80/100 mesh and Supelco 13X molecular sieve 45/60mesh columns with valved systems, and a thermal conductivity detector (TCD). A Fisher Scientific Accumet meter with a combination pH electrode (Ag/AgCl reference, gel-filled) was used for pH determinations. Mass spectra were collected at the University of Nebraska Center for Mass Spectrometry. Elemental analyses were conducted by QTI, Whitehouse, NJ. All electrochemical experiments were performed with a computer controlled EG&G M273A Potentiostat/Galvanostat with M270 electrochemical software. A single compartment cell consisting of a glassy carbon working electrode (either from Cypress (0.018 cm^2) or EG&G (0.031 cm^2)), a homemade Ag/AgCl (sat. aqueous KCl) reference electrode, and a platinum wire counter electrode was used for cyclic voltammetry. The working electrode was polished using an EG&G polishing kit and cleaned by ultrasound prior to each use. Filtered, deionized water (>18 MΩ) was used to prepare the electrolyte solutions (0.5 M $NaPF_6$, supporting electrolyte, 0.1 M phosphate buffer) and 0.1 M NaOH was used to adjust the solution pH. All electrochemical experiments were performed under nitrogen at room temperature. All potentials are referenced to the Ag/AgCl electrode.

1.4.2   Free Base Porphyrins

2,3,7,8,12,13,17,18-Octafluoro-5,10,15,20-tetrakis(4-sulfonatophenyl)porphyrin tetrasodium salt, [F₈TSTPP or 1].[145] Prepared by Biffinger.[145] F₈TPP[143] (50 mg, 0.066 mmol) was dissolved in fuming H_2SO_4 (18-20% free SO_3, 0.5 mL) and heated to 80°C for 45 minutes in a vessel was capped with a $CaSO_4$ drying tube. The mixture was

cooled to room temperature prior to careful addition of H_2O (20 mL). Upon neutralization with 1 M aqueous NaOH, the solution color changed from green to red. The solvent was removed *in vacuo* and the remaining solid was taken up in CH_3OH and filtered to remove Na_2SO_4. This desalting step was repeated twice. The desalted compound was precipitated from CH_3OH by layering dry diethyl ether on top of the solution. The precipitate was filtered and dried in vacuo. Yield (65 mg, 87%): (Found: C, 38.64; H, 2.38; N, 4.10. Calc. for $C_{44}H_{18}F_8N_4Na_4O_{12}S_4 \cdot 11\ H_2O$: C, 38.72; H, 2.90; N, 4.10%); λ_{max} (CH_3OH)/nm 408 (ε/dm^3 mol^{-1} cm^{-1}190000), 500 (13000), 531 (5500), 581 (4100), 638 (3400); ^{19}F NMR (470 MHz; CD$_3$OD): δ = -142.11 (4F, s, β-F); -147.70 (4F, s, β-F); ^{1}H NMR (500 MHz, CD$_3$OD): δ = 8.21 (8H, d, *J* 8, *m*-H); 8.17 (8H, d, *J* 8, *o*-H); *m/z* (FAB neg. ion) 1099 (calc. [M-2H+Na$^+$]$^-$ 1099), 1121 (calcd [M-3H+2Na$^+$]$^-$ 1121).

2,3,7,8,12,13,17,18-Octafluoro-5,10,15,20-tetrakis(3-sulfonato-2,6-difluorophenyl)porphyrin tetrasodium salt, [F$_{16}$TSTPP or 2].[145] Prepared by me using Biffinger's procedure.[145] A solution of F$_{16}$TPP[145] (52mg, 0.058 mmol) in fuming H_2SO_4 (18-20% free SO$_3$, 0.5mL) was heated at 90°C for 4 h. The remaining steps in the experimental procedure were identical to those described for 1. Yield (66 mg, 86%); (Found: C, 34.47; H, 1.19; N, 3.51. Calc. for $C_{44}H_{10}F_{16}N_4Na_6O_{16}S_5 \cdot 5\ H_2O$: C, 34.66; H, 1.19; N, 3.67%); λ_{max} (CH_3OH)/nm 409 (ε/dm^3 mol^{-1} cm^{-1}160000), 496 (1400), 530 (2700), 580 (3600), 635 (1000); ^{19}F NMR (470 MHz; CD$_3$OD): δ = -108.1 (4F, broad s, *o*-F adjacent to -SO$_3^-$), -108.9 (4F, m, *o*-F), -145.98 (4F, s, β-F), -151.1 (4F, s, β-F); ^{1}H NMR (500 MHz; CD$_3$OD): δ = 8.37 (4H, dd, *J* 15 and 9, *p*-H), 7.49 (4H, m, *m*-H); *m/z* (high res. FAB) 1310.8569 (Calc. $C_{44}H_{11}N_4O_{12}F_{16}S_4Na_4^+$ 1310.8592).

1.4.3 Rhodium(III) Water-Soluble Porphyrins

[2,3,7,8,12,13,17,18-Octafluoro-5,10,15,20-tetrakis(4-sulfonatophenyl)

porphyrinato]rhodium(III) tetrasodium salt, [Rh(III)F$_8$TSTPP or 1[Rh(III)]].[144,148]

Prepared by Biffinger.[144,148] 2,3,7,8,12,13,17,18-octafluoro-5,10,15,20-tetrakis(4-sulfonatophenyl)porphyrin[145] tetraammonium salt (65 mg, 0.057 mmol) was dissolved in methanol. [Rh(CO)$_2$Cl]$_2$ (22 mg, 0.057 mmol) was added as a solid to the porphyrin solution. The reaction was heated gently for 15 h. with reaction progress monitored by the disappearance of free-base by UV-vis spectroscopy. The solvent was evaporated and the crude material was re-dissolved in de-ionized water and loaded onto a column containing DOWEX®50WX8-100 ion exchange resin (Na$^+$ salt), and eluted with H$_2$O until the column discharge was colorless. The collected fractions were loaded directly onto a water-washed neutral aluminum oxide column. The porphyrin was eluted with a 0.02 M NaOH solution. After the solvent was evaporated to dryness the compound was re-dissolved in methanol. The methanol solution was filtered through a 0.20 μm HPLC syringe filter (Fisherbrand, PTFE) prior to precipitation with diethyl ether. After three precipitations, the solid was collected using an Osmonics/MSI Magna Nylon Membrane filter (0.45μm) and the solid was dried *in vacuo*. The yield of **1** was 69 mg (94%). The NMR spectra indicate several different axially ligated species in buffered water; only the major species is described: ^{19}F NMR (470 MHz, D$_2$O, 20 mM phosphate buffer, pH 7): δ = −141.24 (s, 8F); ^{1}H NMR (500 MHz, D$_2$O, 20 mM phosphate buffer, pH 7): δ = 8.15 (d, 4H, J = 10 Hz), 8.03 (d, 4H, J = 10 Hz); UV-vis (water) [λ$_{max}$ (ε x 10^3), pH 7, 20 mM phosphate] 398 (150), 515 (18), 549 (6.0); MS (low res FAB pos. ion) *m/z* 1178.8 (calcd

$C_{44}H_{16}F_8N_4Na_4O_{12}S_4Rh^+$ 1179); Anal calcd for $C_{45}H_{20}F_8N_4Na_6O_{16}S_5RhCl\cdot4\ H_2O$: C, 35.25; H, 1.84; N, 3.65. Found: C, 35.48; H, 1.42; N, 3.64.

[2,3,7,8,12,13,17,18-Octafluoro-5,10,15,20-tetrakis(3-sulfonato-2,6-difluorophenyl) porphyrinato]rhodium(III) tetrasodium salt, [Rh(III)F$_{16}$TSTPP or 2[Rh(III)]].[144,148] Prepared by me using Biffinger's procedure.[144,148] A similar procedure as for [2,3,7,8,12,13,17,18-Octafluoro-5,10,15,20-tetrakis(4-sulfonatophenyl) porphyrinato]rhodium chloride tetrasodium salt was used. Yield (92%): ^{19}F NMR (470 MHz, D_2O, 20 mM phosphate buffer, pH 7): $\delta = -107.05$ (s, 8F), -110.76 (s, 8F), -144.92 (s, 8F); ^{1}H NMR (500 MHz, D_2O, 20 mM phosphate buffer, pH 7): $\delta = 8.28$ (q, 4H, J = 8 Hz), 7.53 (t, 4H, J = 8 Hz); UV-vis (water) [λ_{max} (ϵ x 10^3), pH 7, 20 mM phosphate] 399 (140), 518 (14), 550 (4.3); MS (high res FAB pos. ion) *m/z* 1390.776 (calcd $C_{44}H_{11}F_{16}N_4Na_3O_{12}S_4Rh^+$ 1390.774); Anal calcd for $C_{44}H_8F_{16}N_4Na_4O_{12}S_4RhCl\cdot5\ H_2O$: C, 33.98; H, 1.30; N, 3.60. Found: C, 34.16; H, 0.82; N, 3.45.

[Meso-tetrakis(*p*-sulfonatophenyl)porphyrinato]rhodium(III),   [Rh(III)TSTPP   or 3[Rh(III)]]. Prepared by Biffinger. 5,10,15,20-tetrakis(4-sulfonatophenyl)porphyrin, tetrasodium salt was purchased from Aldrich and used as received. The rhodium insertion was modified from previous work[182] to the insertion conditions used for **1[Rh(III)]** and **2[Rh(III)]**. The analytical data were identical to published work.[137,182]

1.4.4 Rhodium(I), and Rhodium-methyl Water-Soluble Porphyrins – Prepared and Characterized by Justin Biffinger[144,148]

In Situ **Generation of [2,3,7,8,12,13,17,18-Octafluoro-5,10,15,20-tetrakis(3-sulfonato-2,6-difluorophenyl) porphyrinato]rhodium(I) tetrasodium salt, 2[Rh(I)].[144,148]** A 1 mM solution of **2[Rh(III)]** (0.5 mL in D_2O was degassed with a stream of nitrogen in a NMR tube sealed with a septum. A 0.1 mL aliquot of a 20 mM solution of sodium borohydride in degassed 0.5 M sodium hydroxide (diluted with deuterium oxide) was added via syringe. The color changed from dark brown to light orange immediately. Upon reduction, only one species is evident in the NMR spectrum due to ligand loss: ^{19}F NMR (376 MHz, D_2O/NaOH, pH 10): $\delta = -107.10$ (m, 4F), -109.76 (m, 4F), -151.09 (s, 8F); ^{1}H NMR (400 MHz, D_2O/NaOH, pH 10): $\delta = 8.07$ (q, 4H, $J = 8$ Hz), 7.53 (t, 4H, $J = 8$ Hz); UV-vis (20 mM phosphate buffer, pH 7): λ_{max} (ε) = 383 (140000), 484 (2700), 508 nm (3700).

In Situ **Generation of [2,3,7,8,12,13,17,18-Octafluoro-5,10,15,20-tetrakis(4-sulfonatophenyl) porphyrinato]diaquo rhodium tetrasodium salt, 1[Rh(I)].[144,148]** The procedure used to generate **2[Rh(I)]** was also used for this complex. ^{19}F NMR (376 MHz, D_2O/NaOH, pH 10): $\delta = -148.04$ (s, 8F); ^{1}H NMR (400 MHz, D_2O/NaOH, pH 10): $\delta = 7.95$ (m, 8H), 7.67 (m, 8H); UV-vis (D_2O/NaOH, pH 9): λ_{max} (ε) = 390 (110000), 488 (13000), 480 nm (7800).

Methyl [2,3,7,8,12,13,17,18-octafluoro-5,10,15,20-tetrakis(4-sulfonatophenyl) porphyrinato]rhodium tetrasodium salt, 1[Rh-CH₃].[144,148] Excess CH_3I (1.0 mL) was added to an ethanol solution (20 mL) of 1[Rh(I)] (25 mg, 0.019 mmol) under a nitrogen atmosphere. The reaction was stirred under nitrogen in the absence of light for 12 hours. The solution was dried over sodium sulfate prior to precipitation of 1[Rh-CH₃] with diethyl ether. After the third precipitation, this complex was sufficiently pure for analysis. Yield: 20 mg (82 %). ^{19}F NMR (376 MHz, D_2O, pH 8): δ = -142.64 (s, 8F); ^1H NMR (400 MHz, D_2O, pH 8): δ = 8.15 (broad d, 8H, J = 8 Hz), 8.05 (m, 8H), -6.61 (broad s, 3H); ^{19}F NMR (470 MHz, DMSO-d_6): δ = -144.16 (s, 8F); ^1H NMR (500 MHz, DMSO-d_6): δ = 8.02 – 7.87 (m, 16H), -6.33 (broad s, 3H) UV-vis (20 mM phosphate buffer, pH 7): λ_{max} (ε) = 403 (150000), 520 nm (12000).

Methyl [2,3,7,8,12,13,17,18-octafluoro-5,10,15,20-tetrakis(3-sulfonato-2,6-difluorophenyl) porphyrinato]rhodium tetrasodium salt,2[Rh-CH₃].[144,148] A procedure identical to that used to prepare **1[Rh-CH₃]** was employed. ^{19}F NMR (376 MHz, 20 mM phosphate buffer, pH 7): δ = −105.05 (m, 4F), -109.34 (m, 4F), −146.24 (s, 8F); ^1H NMR (400 MHz, 20 mM phosphate buffer, pH 7): δ = 8.21 (m, 4H), 7.49 (m, 4H), -6.31 (d, 3H, J = 18 Hz); UV-vis (20 mM phosphate buffer, pH 7): λ_{max} (ε) = 399 (180000), 516 (13000), 544 nm (4500).

1.4.5 Determination of the pK_a of D-RhTSF₁₆TPP (2[Rh-D)])[144,148]

Work of Justin Biffinger.[144,148] Samples of **2[Rh(III)]** loaded into J. Young NMR tubes (in deuterium oxide, 20mM phosphate, acetate, or oxalate buffers) were degassed

via Schlenk techniques. The evacuated tubes were pressurized with H_2 (1.0 atm) and ^{19}F NMR were collected to determine the acid dissociation constant (298 K, C_6F_6 internal standard). The observed ^{19}F chemical shift of the β-signal was independent of buffer composition, but strongly dependent on pH. The pH was monitored with a properly calibrated combination pH electrode before and after the NMR experiment. The data were linearized using the Henderson-Hasselbalch equation[156] using the observed NMR shifts and fit with the standard linear regression package in Mathematica 5.0.[172] The limiting chemical shift values used were **2[Rh-D]** = -146 ppm and **2[Rh(I)]** = -151 ppm.

1.4.6   Rotating ring-disk voltammetry[144]

Work of Haoran Sun.[144] Reduction of O_2 was performed using a rotating platinum ring-graphite disk electrode. The activated platinum disk electrode was calibrated using quantitative oxygen reduction and hydrogen oxidation measurements in sulfuric acid, as was previously described.[183,184] The graphite disk was coated with the cationic condensation polymer poly(1,4-diazoniabicyclo[2.2.2]octane-1,4-phenylene methylene dibromide), and **2[Rh(III)]** was immobilized on the disk by ion exchange with the resin. The supporting electrolyte was 0.1M phosphate buffer saturated with oxygen. The platinum ring electrode was held at + 0.8 V to oxidize the H_2O_2 that was generated at the disc electrode. Proton reduction was observed at potentials negative of − 0.6 V versus (Ag/AgCl). Rotating ring/disk voltammograms (S = 10 μA and 2 μA for the disk and the ring currents respectively, scan rate = 2 mV s^{-1}, rotation rate = 100 rpm) show that a substantial fraction (50% for **2[Rh(III)]**) of the dioxygen reduction product is H_2O_2. Representative output is shown in Figure A8 (Appendix A).

1.4.7 UV-vis and NMR Monitoring of Reaction Mixtures under Air Free Conditions[144]

My work. A quartz cuvette modified for Schlenk work was charged with 3 mL of a buffered aqueous solution with the required reactants. The solution was degassed by freeze-pump-thawing three times directly on the Schlenk line. The cuvette was then pressurized (1 atm) with the required gas/gas mix through a mercury bubbler. The cuvette was shaken vigorously for 30 seconds to ensure introduction of the gas into solution phase at a uniform concentration, and it was placed in the temperature controlled (35 °C) cuvette holder. UV-Vis spectra were collected at regular time intervals. A similar method using J Young tubes was employed for NMR monitoring.

1.4.8 Kinetic Measurements for the Determination of TOF_{av} of the 2[Rh(III)] catalyzed oxidation of CO by Indigo Carmine[144]

My work. A 5 mm NMR tube equipped with a resealable PTFE valve was charged with 1 mL of an aqueous solution (buffered at pH 4 with a 200 mM phosphate buffer) of **2[Rh(III)]** and IC at the required concentrations. The blue solution was degassed by cool (0 °C)-pump-warming (35 °C) ten times directly on a Schlenk line. The tube was then pressurized (1 atm) with pure CO or 50% CO in (N_2 or H_2) through a mercury bubbler. The solution was shaken vigorously for 30 seconds to ensure quick introduction of a uniform concentration of CO into solution and subsequently placed in a 35 °C water bath. The tube was removed from the heating bath every 1.5 min and the solution agitated as for 15 seconds, and was then returned to the heating bath. This procedure was repeated until the blue color of the solution disappeared leaving behind a

faintly brown solution characteristic of the color of **2[Rh(III)].** The time taken to reach this end point after the introduction of CO was noted.

1.4.9 Analysis of Head Gas from Reactions by GC[144]

My work. A Schlenk flask (total volume 12 mL) was charged with 8.5 mL of an aqueous solution (buffered at pH 4 with a 200 mM phosphate buffer) of **2[Rh(III)]** (0.6 mM) and IC (6.0 mM). A magnetic stir bar was dropped in and the flask was sealed. The solution was degassed by freeze-pump-thawing three times on the Schlenk line. The flask was then pressurized (1 atm) with the required gas or gas mix (CO, 10% CO in H_2 or 1% CO in H_2) through a mercury bubbler, transferred to an oil bath maintained at 35 °C, and the solution was set to vigorous stirring. 25 µL aliquots of the head gas were withdrawn using a gas-tight syringe, initially, and from time to time through the progress of the reaction, and analyzed by GC. Changes in gas partial pressures were determined by using standard calibration curves that were built for each gas.

1.5 References

1. Dresselhaus, M. S.; Thomas, L. L., "Alternative energy technologies", *Nature*, **2001**, *414*, 332-337.

2. Service, R. F., "The hydrogen backlash", *Science (Washington, DC)*, **2004**, *305*, 958-961.

3. Turner, J. A., "Sustainable hydrogen production", *Science (Washington, DC)* **2004**, *305*, 972-974.

4. http://www.eia.gov/oiaf/ieo/ (U.S. Energy Information Administration).

5. Kerr, R. A., "Three degrees of consensus", *Science (Washington, DC)* **2004**, *305*, 932-934.

6. Pacala, S.; Socolow, R., "Stabilization wedges: Solving the climate problem for the next 50 years with current technologies", *Science (Washington, DC)* **2004**, *305*, 968-971.

7. Service, R. F., "The carbon conundrum", *Science (Washington, DC)* **2004**, *305*, 962-963.

8. Berinstein, P., *Alternative Energy: Facts, Statistics, and Issues*, 1st Ed., Greenwood Publishing Group, Westport, **2001**.

9. Whitesides, G. M.; Crabtree, G. W., "Don't forget long-term fundamental research in energy", *Science (Washington, DC)* **2007**, *315*, 796-7986.

10. Penner, S. S., "Steps toward the hydrogen economy", *Energy (Amsterdam, Netherlands)* **2006**, *31*, 33-43.

11. Winter, C-J., "Hydrogen energy – abundant, efficient, clean: A debate over the energy system of change", *Int. J. of Hydrogen Energy* **2009**, *34*(14), Suppl. 1, S1-S52.

12. Vogel, G., "Will the future dawn in the north?" *Science (Washington, DC)* **2004**, *305*, 966-967.

13. Ward, M. D., "Materials Science: Molecular fuel tanks", *Science (Washington, DC)* **2003**, *300*, 1104-1105.

14. Service, R. F., "New routes toward practical hydrogen?", *Science (Washington, DC)* **2005**, *309*, 1811.

15. Service, R. F., "Hydrogen economy? Let sunlight do the work", *Science (Washington, DC)* **2007**, *315*, 789.

16. Cumalioglu, I.; Ertas, A.; Ma, Y.; Maxwell, T., "State of the art: Hydrogen Storage", *J. Fuel Cell Sci. Tech.* **2008**, *5*, 034001/1-034001/10.

17. Makowski, P.; Thomas, A.; Kuhn, P.; Goettmann, F., "Organic materials for hydrogen storage applications: From physisorption on organic solids to chemisorption in organic molecules" *Energy Environ. Sci.* **2009**, *2*, 480-490.

18. Fakioglu, E.; Yurum, Y.; Veziroglu, T. N., "A review of hydrogen storage systems based on boron and its compounds", *Int. J. Hydrogen Energy* **2004**, *29*, 1371-1376.

19. Sherif, S. A.; Barbir, F.; Veziroglu, T. N.; "Principles of hydrogen energy production, storage and utilization", *J. Sci. Ind. Res.* **2003**, *62*, 46-63.

20. Martin, K. E.; Kopasz, J. P.; McMurphy, K. W., "Status of fuel cells and the challenges facing fuel cell technology today", *ACS Symposium Series* **2010**, Volume 1040, Fuel Cell Chemistry and Operation, Chapter 1, 1-13.

21. Winter, M., Brodd, R. J., "What are batteries, fuel cells, and supercapacitors?" *Chem. Rev.* **2004**, *104*, 4245-4269.

22. Laboratory, N. E. T., Energy, U. D. O., *Fuel Cell Handbook*, University Press of the Pacific, San Francisco, **2005**.

23. Larminie, J.; Dicks, A., *Fuel Cell Systems Explained*, 2nd Ed., John Wiley and Sons, West Sussex, **2003**.

24. Vogel, J., *U.S. DOE Hydrogen Program Annual Progress Report* 2008, http://www.hydrogen.energy.gov/pdfs/progress08/v_d_4_vogel.pdf

25. Banerjee, S.; Curtin, D. E., "Nafion perfluorinated membranes in fuel cells", *J. Fluorine Chem*. **2004**, *125*, 1211-1216.

26. Kaneko, M., "Charge transport in solid polymer matrixes with redox centers", *Progress in Polymer Science* **2001**, *26*, 1101-1137.

27. de Bruijn, F., "The current status of fuel cell technology for mobile and stationary applications", *Green Chemistry* **2005**, *7*, 132-150.

28. Steele, B. C. H.; Heinzel, A., "Materials for fuel cell technologies", *Nature (London, United Kingdom)* **2001**, *414*, 345-352.

29. Stonehart, P.; Kohlmayr, G., "Effect of poisons on kinetic parameters for platinum electrocatalyst sites", *Electrochim. Acta* **1972**, *17*, 369-82.

30. http://www.hydrogen.energy.gov/index.html

31. Service, R. F., "Hydrogen cars: Fad or the future?", *Science (Washington, DC)* **2009**, *324*, 1257-1259.

32. Cho, A., "Fire and ICE: Revving up for H_2", *Science (Washington, DC)* **2004**, *305*, 964-965.

33. Melis, A., "Green alga hydrogen production: Progress, challenges and prospects", *Int. J. Hydrogen Energy* **2002**, *27*, 1217-1228.

34. Walter, M. G.; Warren, E. L.; McKone, J. R.; Boettcher, S. W.; Mi, Q.; Santori, E. A.; Lewis, N. S., "Solar water splitting cells", *Chem. Rev*. **2010**, *110*, 6443-6476.

35. Minggu, L. J.; Daud, W. R. W.; Kassim, M. B., "An overview of photocells and photoreactors for photoelectrochemical water splitting", *Int. J. Hydrogen Energy* **2010**, *35*, 5233-5244.

36. Khaselev, O.; Turner, J. A., "A monolithic photovoltaic-electrochemical device for hydrogen production via water splitting", *Science (Washington DC)* **1998**, *280*, 425-427.

37. Graetzel, M., "Photoelectrochemical cells", *Nature (London)* **2001**, *414*, 338-344.

38. Lewis, N., "Photochemistry: Light work with water", *Nature (London)* **2001**, *414*, 589-590.

39. Steinfeld, A., "Solar hydrogen production via a two-step water-splitting thermochemical cycle based on Zn/ZnO redox reactions", *Int*. *J*. *Hydrogen Energy* **2002**, *27*, 611-619.

40. Turner, J. A,, "A realizable renewable energy future", *Science (Washington DC)* **1999**, *285*, 687-689.

41. Khaselev, O.; Bansal, A.; Turner, J. A., "High efficiency integrated multijunction photovoltaic/electrolysis systems for hydrogen production", *Int*. *J*. *Hydrogen Energy* **2001**, *26*, 127-132.

42. Gehrke, H.; Ruthardt, K.; Mathiak, J.; Roosen, C., "Hydrogen: A small molecule with a large impact", *DGMK Tagungsbericht* **2010**, *2010-3*, 7-16.

43. Holladay, J. D.; Hu, J.; King, D. L.; Wang, Y., "An overview of hydrogen production technologies", *Catalysis Today* **2009**, *139*, 244-260.

44. Gray, P.; Jaffray, C., "An introduction to fuel processing and some advances in fuel processing catalysts", *Fuel Cells for Automotive Applications*, Edited by Thring, R. H., p 61-73, Professional Engineering Publishing Ltd., Bury St. Edmunds, U.K., **2004**.

45. Joensen, F.; Rostrup-Nielsen, J. R., "Conversion of hydrocarbons and alcohols for fuel cells", *J. Power Sources* **2002**, *105*, 195-201.

46. Rostrup-Nielsen, J. R.; Rostrup-Nielsen, T., "Large-scale hydrogen production", *CATTECH* **2002**, *6*, 150-159.

47. Ming, Q.; Healy, T.; Allen, L.; Irving, P., "Steam reforming of hydrocarbon fuels", *Catal. Today* **2002**, *77*, 51-64.

48. Sasaki, K.; Teraoka, Y., "Equilibria in fuel cell gases", *Proc. Electrochem. Soc.* **2003**, *2003-7*, 1225-1239.

49. Rostrup-Nielsen, J. R., "Steam reforming of hydrocarbons. A historical perspective", *Stud. Surf. Sci. Catal.* **2004**, *147*, 121-126.

50. Deluga, G. A.; Salge, J. R.; Schmidt, L. D.; Verykios, X. E., "Renewable hydrogen from ethanol by autothermal reforming", *Science (Washington DC)* **2004**, *303*, 993-997.

51. Davda, R. R.; Shabaker, J. W.; Huber, G. W.; Cortright, R. D.; Dumesic, J. A., "A review of catalytic issues and process conditions for renewable hydrogen and alkanes by aqueous-phase reforming of oxygenated hydrocarbons over supported metal catalysts", *Applied Catalysis, B: Environmental* **2005**, *56*, 171-186.

52. Cortright, R, D.; Davda, R. R.; Dumesic, J. A., "Hydrogen from catalytic reforming of biomass-derived hydrocarbons in liquid water", *Nature (London)* **2002**, *418*, 964-967.

53. Huber, G. W.; Shabaker, J. W.; Dumesic, J. A., "Raney Ni-Sn catalyst for H_2 production from biomass-derived hydrocarbons", *Science (Washington DC)* **2003**, *300*, 2075-2078.

54. Davda, R. R.; Dumesic, J. A., "Catalytic reforming of oxygenated hydrocarbons for hydrogen with low levels of carbon monoxide", *Angewandte Chemie, International Edition* **2003**, *42*, 4068-4071.

55. Jacobsen, H., ""Heterogreeneous" chemistry: Catalysts for hydrogen production from biomass", *Angewandte Chemie, International Edition* **2004**, *43*, 1912-1914.

56. Woodward, J.; Orr, M.; Cordray, K.; Greenbaum, E., "Biotechnology: Enzymatic production of biohydrogen", *Nature (London)* **2000**, *405*, 1014-1015.

57. Balt, H.; Kirtay, E., "Hydrogen from biomass – Present scenario and future prospects", *Int. J. Hydrogen Energy* **2010**, *35*, 7416-7426.

58. Lucas, C.; Szewczyk, D.; Blasiak, W.; Mochida, S., "High-temperature air and steam gasification of densified biofuels", *Biomass and Bioenergy* **2004**, *27*, 563-575.

59. Keenan, J. D., "Biomass as alternative energy source", *Journal of the Energy Division (American Society of Civil Engineers)* **1982**, *108*, 11-22.

60. Chum, H. L.; Overend, R. P., "Biomass and renewable fuels", *Fuel Processing Technology* **2001**, *71*, 187-195.

61. McKinley, K. R.; Browne, S. H.; Neill, D. R.; Seki, A.; Takahashi, P. K., "Hydrogen fuel from renewable resources", *Energy Sources* **1990**, *12*, 105-10.

62. Klass, D. L., *Biomass for Renewable Energy, Fuels, and Chemicals*, **1998**.

63. Demirbas, A.; Demirbas, M. F., "Biomass and wastes: Upgrading alternative fuels", *Energy Sources* **2003**, *25*, 317-329.

64. Furness, D. T.; Hoggett, L. A.; Judd, S. J., "Thermochemical treatment of sewage sludge", *Water and Environmental Management* **2000**, *14*, 57-65.

65. Midilli, A.; Dogru, M.; Akay, G.; Howarth, C. R., "Hydrogen production from sewage sludge via a fixed bed gasifier product gas", *Int. J. Hydrogen Energy* **2002**, *27*, 1035-1041.

66. Marquevich, M.; Czernik, S.; Chornet, E.; Montane, D., "Hydrogen from biomass: Steam reforming of model compounds of fast-pyrolysis oil", *Energy Fuels* **1999**, *13*, 1160-1166.

67. Wang, D.; Czernik, S.; Chornet, E., "Production of hydrogen from biomass by catalytic steam reforming of fast pyrolysis oil", *Energy Fuels* **1998**, *12*, 19-24.

68. Learning Demonstration Vehicle Green House Gas Emissions. http://www.nrel.gov/hydrogen/docs/cdp/cdp_62.ppt#494,1,CDP#62.

69. Rase, H. F., *Handbook of Commerical Catalysts: Heterogeneous Catalysts*, CRC Press, Boca Raton, **2000**.

70. Fu, Q.; Saltsburg, H.; Flytzani-Stephanopoulos, M., "Active nonmetallic Au and Pt species on ceria-based water-gas shift catalysts", *Science (Washington, DC)* **2003**, *301*, 935-938.

71. Koryabkina, N. A.; Phatak, A. A.; Ruettinger, W. F.; Farrauto, R. J.; Ribeiro, F. H., "Determination of kinetic parameters for the water-gas shift reaction on copper catalysts under realistic conditions for fuel cell applications", *J. Catal.* **2003**, *217*, 233-239.

72. Wang, X.; Gorte, R. J.; Wagner, J. P., "Deactivation mechanisms for Pd/ceria during the water-gas-shift reaction", *J. Catal.* **2002**, *212*, 225-230.

73. Ovesen, C. V.; Stolze, P.; Norskov, J. K.; Campbell, C. T., "A kinetic model of the water gas shift reaction", *J. Catal.* **1992**, *134*, 445-468.

74. Mendes, D.; Mendes, A.; Madeira, L. M.; Iulianelli, A.; Sousa, J. M.; Basile, A. "The water-gas shift reaction: From conventional catalytic systems to Pd-based membrane reactors − A review", *Asia-Pacific Journal of Chemical Engineering* **2010**, *5*, 111-137.

75. Kolb, G., *Fuel Processing for Fuel Cells*, Wiley-VCH Verlag: Weinheim, Germany, **2008**.

76. Marino, F.; Descorme, C.; Duprez, D., "Noble metal catalysts for the preferential oxidation of carbon monoxide in the presence of hydrogen (PROX)"*, Applied Catalysis, B: Environmental* **2004**, *54*, 59-66.

77. Bai, H. H.; Winston, W. H., "Recent developments in fuel processing and proton exchange membranes for fuel cells", *Polym. Int.* **2011**, *60*, 26-41.

78. Gallucci, F.; Basile, A., "Pd-based membranes synthesis and their application in membrane reactors", *Handbook of Membrane Research*, Nova Science Publishers, Inc., Hauppauge, N. Y., **2010**.

79. Basile, A.; Gallucci, F., "Ultra-pure hydrogen production in membrane reactors", *Handbook of Energy, Hydrogen Energy and Hydropower Research*, Edited by Pelissier, G.; Calvet, A., p 99-123, Nova Science Publishers, Inc., Hauppauge, N. Y., **2009**.

80. Jacobs, G.; Davis, B. H., "Low temperature water gas shift catalysts", *Catalysis* **2007**, *20*, 122-285.

81. Burch, R., "Gold catalysts for hydrogen production in the water gas shift reaction: Activity, structure and reaction mechanism", *Phys. Chem. Chem. Phys.* **2006**, *8*, 5483-5500.

82. Kim, W. B.; Voitl, T.; Rodriguez-Rivera, G. J.; Evans, S. T.; Dumesic, J. A., "Preferential oxidation of CO in H_2 by aqueous polyoxometalates over metal catalysts", *Angewandte Chemie, International Edition* **2005**, *44*, 778-782.

83. Paulus, U. A.; Endruschat, U.; Feldmeyer, G. J.; Schmidt, T. J.; Bonnemann, H.; Behm, R. J., "New PtRu Alloy Colloids as Precursors for Fuel Cell Catalysts", *J. Catal.* **2000**, *195*, 383-393.

84. Hayden Brian, E.; Rendall Michael, E.; South, O., "Electro-oxidation of carbon monoxide on well-ordered Pt(111)/Sn surface alloys", *J. Am. Chem. Soc.* **2003**, *125*, 7738-42.

85. Kalinkin, A. V.; Pashis, A. V.; Bukhtiyarov, V. I., "CO oxidation over the Pt-Rh system. 2. Reaction on an alloy", *React. Kinet. Catal. Lett.* **2003**, *78*, 107-112.

86. Uchida, H.; Ozuka, H.; Watanabe, M., "Electrochemical quartz crystal microbalance analysis of CO-tolerance at Pt-Fe alloy electrodes", *Electrochim. Acta* **2002**, *47*, 3629-3636.

87. Gasteiger, H. A.; Markovic, N.; Ross, P. N., Jr.; Cairns, E. J., "Carbon monoxide electrooxidation on well-characterized platinum-ruthenium alloys", *J. Phys. Chem.* **1994**, *98*, 617-25.

88. Gasteiger, H. A.; Markovic, N. M.; Ross, P. N., Jr., "H_2 and CO electrooxidation on well-characterized Pt, Ru, and Pt-Ru. 2. Rotating disk electrode studies of CO/H_2 mixtures at 62 degC", *J. Phys. Chem.* **1995**, *99*, 16757-67.

89. Fukuoka, A.; Kimura, J-I.; Oshio, T.; Sakamoto, Y.; Ichikawa, M., "Preferential oxidation of carbon monoxide catalyzed by platinum nanoparticles in mesoporous silica", *J. Am. Chem. Soc.* **2007**, *129*, 10120-10125.

90. Xu, L.; Ma, Y.; Zhang, Y.; Jiang, Z.; Huang, W., "Direct evidence for the interfacial oxidation of CO with hydroxyls catalyzed by Pt/oxide nanocatalysts", *J. Am. Chem. Soc.* **2009**, *131*, 16366-16367.

91. Rico, V. J.; Hueso, J. L.; Cotrino, J.; Gallardo, V.; Sarmiento, B.; Brey, J. J.; Gonzalez-Elipe, A. R., "Hybrid catalytic-DBD plasma reactor for the production of hydrogen and preferential CO oxidation (CO-PROX) at reduced temperatures", *Chem. Commun.* **2009**, 6192-6194.

92. Deng, W.; Flytzani-Stephanopoulos, M., "On the issue of deactivation of Au-ceria and Pt-ceria water gas shift catalysis in practical fuel cell applications", *Angew. Chem., Int. Ed.* **2006**, *45*, 2285-2289.

93. Pozdnyakova, O.; Teschner, D.; Wootsch, A.; Kröhnert, J.; Steinhauer, B.; Sauer, H.; Toth, L.; Jentoft, F. C.; Knop-Gericke, A.; Paál, Z.; Schlögl, R., "Preferential CO oxidation in hydrogen (PROX) on ceria supported catalyst, part I: Oxidation state and surface species on Pt/CeO$_2$ under reaction conditions", *J. Catal.* **2006**, *237*, 1-16.

94. Minemura, Y.; Ito, S.; Miyao, T.; Naito, S.; Tomishige, K.; Kunimori, K., "Preferential CO oxidation promoted by the presence of H$_2$ over K-Pt/Al$_2$O$_3$", *Chem. Commun.* **2005**, 1429-1431.

95. Pedrero, C.; Waku, T.; Iglesia, E., "Oxidation of CO in H$_2$-CO mixtures catalyzed by platinum: Alkali effects on rates and selectivity", *J. Catal.* **2005**, *233*, 242-255.

96. Landon, P.; Ferguson, J.; Solosna, B. E.; Garcia, T.; Carley, A. F.; Herzing, A. A.; Kiely, C. J.; Golunski, S. E.; Hutcnings, G. J., "Selective oxidation of CO in the

presence of H_2, H_2O and CO_2 via gold for use in fuel cells", *Chem. Commun.* **2005**, 3385-3387.

97. Sirijaruphan, A.; Goodwin, J. G.; Jr., Rice, R. W.; Wei, D.; Butcher, K. R.; Roberts, G. W.; Spivey, J. J., "Effect of metal foam supports on the selective oxidation of CO on Fe-promoted Pt/γ-Al_2O_3", *Applied Catalysis, A: General* **2005**, *281*, 11-18.

98. Tanaka, K.; Moro-oka, Y.; Ishigure, K.; Yajima, T.; Okabe, Y.; Kato, Y.; Hamano, H.; Sekiya, S.; Tanaka, H.; Matsumoto, Y.; Koinuma, H.; He, H.; Zhang, C.; Feng, Q., "A new catalyst for selective oxidation of CO in H2: Part 1, Activation by depositing a large amount of FeO_x on Pt/Al_2O_3 and Pt/CeO_2 catalysts", *Catal. Lett.* **2004**, *92*, 115-121.

99. Echigo, M.; Tabata, T., "A study of CO removal on an activated Ru catalyst for polymer electrolyte fuel cell applications", *Applied Catalysis, A: General* **2003**, *251*, 157-166.

100. Chilukuri, S.; Joseph, T.; Malwadkar, S.; Damle, C.; Halligudi, S. B.; Rao, B. S.; Sastry, M.; Ratnasamy, P., "Au and Au-Pt bimetallic nanoparticles in MCM-41 materials: Applications in CO preferential oxidation", *Stud. Surf. Sci. Catal.* **2003**, *146*, 573-576.

101. Watanabe, M.; Uchida, H.; Ohkubo, K.; Igarashi, H., "Hydrogen purification for fuel cells: Selective oxidation of carbon monoxide on Pt-Fe/zeolite catalysts", *Applied Catalysis B: Environmental* **2003**, *46*, 595-600.

102. Han, Y-F.; Kahlich, M. J.; Kinne, M.; Behm, R. J., "Kinetic study of selective CO oxidation in H$_2$-rich gas on a Ru/γ-Al$_2$O$_3$ catalyst", *Phys. Chem. Chem. Phys.* **2002**, *4*, 389-397.

103. Sotowa, K.-I.; Hasegawa, Y.; Kusakabe, K.; Morooka, S., "Enhancement of CO oxidation by use of H$_2$-selective membranes impregnated with noble-metal catalysts", *Int. J. Hydrogen Energy* **2002**, *27*, 339-346.

104. Kim, D. H.; Lim, M. S., "Kinetics of selective CO oxidation in hydrogen-rich mixtures on Pt/alumina catalysts", *Applied Catalysis, A: General* **2002**, *224*, 27-38.

105. Kahlich, M. J.; Gasteiger, H. A.; Behm, R. J., "Kinetics of the selective CO oxidation in H$_2$-rich gas on Pt/Al$_2$O$_3$", *J. Catal.* **1997**, *171*, 93-105.

106. Anderson, J. A., "Infrared study of carbon monoxide oxidation over platinum-rhodium/alumina catalysts", *J. Catal.* **1993**, *142*, 153-65.

107. Oh, S. H.; Sinkevitch, R. M., "Carbon monoxide removal from hydrogen-rich fuel cell feed streams by selective catalytic oxidation", *J. Catal.* **1993**, *142*, 254-262.

108. Ko, E-Y.; Park, E. D.; Lee, H. C.; Lee, D.; Kim. S., "Supported Pt-Co catalysts for selective CO oxidation in a hydrogen-rich stream", *Angew. Chem., Int. Ed.* **2006**, *45*, 1-5.

109. Bion, N.; Epron, F.; Moreno, M.; Marino, F.; Duprez, D., "Preferential oxidation of carbon monoxide in the presence of hydrogen (PROX) over noble metals and transition metal oxides: Advantages and drawbacks", *Top. Catal.* **2008**, *51*, 76-88.

110. Trimm, D. L., "Minimisation of carbon monoxide in a hydrogen stream for fuel cell application", *Applied Catalysis, A; General* **2005**, *296*, 1-11.

111. Faur Ghenciu, A., "Review of fuel processing catalysts for hydrogen production in PEM fuel cell systems", *Curr. Opin. Solid State Meter. Sci.* **2002**, *6*, 389-399.

112. Kim, Y. H.; Park, E. D.; Lee, H. C.; Lee, D.; Lee, K. H., "Preferential CO oxidation over supproted noble metal catalysts", *Catal. Today* **2009**, *146*, 253-259.

113. Ishida, Y.; Ebashi, T.; Ito, S.-i.; Kubota, T.; Kunimori, K.; Tomishige, K., "Preferential CO oxidation in a H_2-rich stream promoted by ReO_x species attached to Pt metal particles", *Chem. Commun.* **2009**, 5308-5310.

114. Alayoglu, S.; Nilekar, A. U.; Mavrikakis, M.; Eichhorn, B., "Ru-Pt core shell nanoparticles for preferential oxidation of carbon monoxide in hydrogen", *Nat. Mater.* **2008**, *7*, 333-338.

115. Liu, W.; Flytzani-Stephanopoulos, M. F., "Total oxidation of carbon monoxide and methane over transition metal-fluorite oxide composite catalyst. I. Catalyst composition and activity", *J. Catal.* **1995**, *153*, 304-316.

116. Liu, Y.; Fu, Q.; Stephanopoulos, M. F., "Preferential oxidation of CO in H_2 over CuO-CeO_2 catalysts", *Catal. Today* **2004**, *93-95*, 241-246.

117. Hornes, A.; Hungira, A. B.; Bera, P.; Lopez Camara, A.; Fernandez-Garcia, M.; Marinez-Arias, A.; Barrio, L.; Estrella, M.; Zhou, G.; Fonseca, J. J.; Hanson, J. C.; Rodiguez, J. A., "Inverse CeO_2/CuO catalyst as an alternative to classical direct configurations for preferential oxidation of CO in hydrogen-rich streams", *J. Am. Chem. Soc.* **2010**, *132*, 34-35.

118. Wootsch, A.; Descorme, C.; Duprez, D., "Preferential oxidation of carbon monoxide in the presence of hydrogen (PROX) over ceria-zirconia and alumina supported Pt catalysts", *J. Catal.* **2004**, *225*, 259-266.

119. Rossignol, C.; Arrii, S.; Morfin, F.; Piccolo, L.; Caps, V.; Rousset, J.-L., "Selective oxidation of CO over model gold-based catalysts in the presence of H_2", *J. Catal.* **2005**, *230*, 476-483.

120. Wu, J.; Kubiak, C. P., "Electrocatalytic oxidation of carbon monoxide in a carbon monoxide/oxygen fuel cell", *J. Am. Chem. Soc.* **1983**, *105*, 7456-7457.

121. Yamazaki, S-I.; Ioroi, T.; Yamada, Y.; Yasuda, K.; Kobayashi, T., "A direct polymer electrolyte membrane fuel cell", *Angewandte Chemie, International Edition* **2006**, *45*, 3120-3122.

122. Kim, W. B.; Voitl, T.; Rodriguez-Rivera, G. J.; Dumesic, J. A., "Powering fuel cells with CO via aqueous polyoxometalates and gold catalysts", *Science (Washington, DC)* **2004**, *305*, 1280-1283.

123. Sherry, A. E.; Wayland, B. B., "Metalloradical activation of methane", *J. Am. Chem. Soc.* **1990**, *112*, 1259-1261.

124. Nelson, A. P.; DiMagno, S. G., "Umpolung of a metal-carbon bond: A potential route to porphyrin-based methane functionalization catalysts", *J. Am. Chem. Soc.* **2000**, *122*, 8569-8570.

125. Kadish, K. M.; Li, J.; Van Caemelbecke, E.; Ou, Z.; Guo, N.; Autret, M.; D'Souza, F.; Tagliatesta, P., "Electrooxidation of cobalt(II) β-brominated-pyrrole tetraphenylporphyrins in CH_2Cl_2 under an N_2 or a CO atmosphere", *Inorg. Chem.* **1997**, *36*, 6292-6298.

126. Mu, X. H.; Kadish, K. M., "Oxidative electrochemistry of cobalt tetraphenylporphyrin under a CO atmosphere. Interaction between carbon monoxide and electrogenerated [(TPP)Co]$^+$ in nonbonding media", *Inorg. Chem.* **1989**, *28*, 3743-3747.

127. Shi, C.; Anson, F. C., "Catalysis of the electro-oxidation of carbon monoxide by cobalt octaethylporphyrin", *Inorg. Chem.* **2001**, *40*, 5829-5833.

128. Van Baar, J. F.; Van Veen, J. A. R.; De Wit, N., "Selective electrooxidation of carbon monoxide with carbon-supported rhodium and iridium porphyrins at low potentials in acid electrolyte", *Electrochim. Acta* **1982**, *27*, 57-59.

129. Zhang, X.-X.; Parks, G. F.; Wayland, B. B., "One-electron activation of CO by a rhodium(II) porphyrin bimetalloradical complex and concerted reactions of two (RhCO).bul. units", *J. Am. Chem. Soc.* **1997**, *119*, 7938-7944.

130. Fu, X.; Li, S. L.; Wayland, B. B., "Reactivity and equilibrium thermodynamic studies of rhodium tetrakis(3,5-disulfonatomesityl)porphyrin species with H_2, CO and olefins in water", *Inorg. Chem.* **2006**, *45*, 9884-9889.

131. Crabtree, R. H., *The Organometallic Chemistry of the Transition Metals*, 3rd ed., John Wiley & Sons, Inc., New York, **2001**.

132. Hendriksen, D. E.; Eisenberg, R., "The role of water in the rhodium(I) catalyzed reduction of nitric oxide by carbon monoxide. An isotope labeling study", *J. Am. Chem. Soc.* **1976**, *98*, 4662-4664.

133. Collman, J. P.; Wagenknecht, P. S.; Lewis, N. S., "Hydride transfer and dihydrogen elimination from osmium and ruthenium metalloporphyrin hydrides:

Model processes for hydrogenase enzymes and the hydrogen electrode reaction", *J. Am. Chem. Soc.* **1992**, *114*, 5665-5673.

134. Grass, V.; Lexa, D.; Saveant, J.-M., "Electrochemical generation of rhodium porphyrin hydrides. Catalysis of hydrogen evolution", *J. Am. Chem. Soc.*, **1997**, *119*, 7526-7532.

135. Aoyama, Y.; Tanaka, Y.; Fujisawa, T.; Watanabe, T.; Toi, H.; Ogoshi, H., "Catalytic reactions of metalloporphyrins. 3. Catalytic modification of hydroboration-oxidation of olefins with rhodium(III) porphyrin as catalyst", *J. Org. Chem.* **1987**, *52*, 2555-9.

136. Aoyama, Y.; Midorikawa, K.; Toi, H.; Ogoshi, H., "Photosensitized hydride transfer. Highly regioselective 1,4-photoreduction of $NAD(P)^+$ models under visible light with an organometallic rhodium(III) porphyrin as sensitizer", *Chem. Lett.* **1987**, 1651-1654.

137. Fu, X.; Wayland, B. B., "Equilibrium thermodynamic studies in water: Reactions of dihydrogen with rhodium(III) porphyrins relevant to Rh-Rh, Rh-H, and Rh-OH bond energetics", *J. Am. Chem. Soc.* **2004**, *126*, 2623-2631.

138. Wayland, B. B.; Ba, S.; Sherry, A. E., "Activation of methane and toluene by rhodium(II) porphyrin complexes", *J. Am. Chem. Soc.* **1991**, *113*, 5305-5311.

139. Grass, V.; Lexa, D.; Momenteau, M.; Saveant, J-M., "Reductive electrochemistry of rhodium porphyrins. Disproportionation of intermediary oxidation states", *J. Am. Chem. Soc.* **1997**, *119*, 3536-3542.

140. Sun, H.; Xue, F.; Nelson, A. P.; Redepenning, J.; DiMagno, S. G., "Reversible electrochemical generation of a rhodium(II) porphyrin: Thwarting

disproportionation with weakly coordinating anions", *Inorg. Chem.* **2003**, *42*, 4507-4509.

141. Dolphin, D.; Traylor, T. G.; Xie, L. Y., "Polyhaloporphyrins: Unusual ligands for metals and metal-catalyzed oxidations", *Acc. Chem. Res.* **1997**, *30*, 251-259.

142. *The Porphyrin Handbook*; Kadish, K. M.; Smith, K. M.; Guilard, R., Eds.; Academic Press: New York, **1999**; Vol. 1.

143. Woller, E. K.; DiMagno, S. G., "2,3,7,8,12,13,17,18-Octafluoro-5,10,15,20-tetraarylporphyrins and their zinc complexes: First spectroscopic, electrochemical, and structural characterization of a perfluorinated tetraarylmetalloporphyrin", *J. Org. Chem.* **1997**, *62*, 1588-1593.

144. Biffinger, J. C.; Uppaluri, S.; Sun, H.; DiMagno, S. G., "Ligand fluorination to optimize preferential oxidation of carbon monoxide by water soluble rhodium porphyrins", *ACS Catalysis* **2011**, 1, 764-771.

145. Biffinger, J. C.; Sun, H.; Nelson, A. P.; DiMagno, S. G., "Differential substituent effects on beta-halogens in water-soluble porphyrins", *Org. Biomol. Chem.* **2003**, *1*, 733-736.

146. Woller, E. K.; Smirnov, V. V.; DiMagno, S. G., "A straightforward synthesis of 3,4-difluoropyrrole", *J. Org. Chem.* **1998**, *63*, 5706-5707.

147. Lindsey, J. S.; Schreiman, I. C.; Hsu, H. C.; Kearney, P. C.; Marguerettaz, A. M., "Rothemund and Adler-Longo reactions revisited: Synthesis of tetraphenylporphyrins under equilibrium conditions", *J. Org. Chem.* **1987**, *52*, 827-836.

148. Biffinger, J. C., "Late transition metal organometallic porphyrin complexes as catalysts for the activation of organic and biological substrates", Ph.D. Thesis **2005**, University of Nebraska.

149. Hambright, P. In *The Porphyrin Handbook*; Guilard, R., Ed.; Academic Press: San Diego, **2000**; Vol. 3, p 129-210.

150. Sutter, T. P. G.; Rahimi, R.; Hambright, P.; Bommer, J. C.; Kumar, M.; Neta, P., "Steric and inductive effects on the basicity of porphyrins and on the site of protonation of porphyrin dianions: radiolytic reduction of porphyrins and metalloporphyrins to chlorins or phlorins", *J. Chem. Soc., Faraday Trans.* **1993**, *89*, 495-502.

151. Krishnamurthy, M., "Kinetics of anation reactions of a water-soluble rhodium(III)-porphyrin", *Inorg. Chim. Acta* **1977**, *25*, 215-218.

152. Ashley, K. R.; Shyu, S-B.; Leipoldt, J. G., "Kinetic and equilibrium study of the reaction of (meso-tetrakis(p-sulfonatophenyl)porphinato)diaquorhodate(III) with chloride, bromide, iodide, and thiocyanate ions in aqueous solution", *Inorg. Chem.* **1980**, *19*, 1613-1616.

153. Collman, J. P.; Kang, J. W., "Acetylene Complexes of Iridium and Rhodium", *J. Am. Chem. Soc.* **1967**, *89*, 844-851.

154. Cotton, F. A.; Wilkinson, G.; Murillo, C. A.; Bochmann, M., *Advanced Inorganic Chemistry*, 6th ed., John Wiley & Sons, Inc., New York, **1999**.

155. Fu, X.; Basickes, L.; Wayland, B. B., "Aqueous organometallic reactions of rhodium porphyrins: equilibrium thermodynamics", *Chem. Commun. (Cambridge, United Kingdom)* **2003**, 520-521.

156. Polster, J.; Lachmann, H., *Spectrometric Titrations: Analysis of Chemical Equilibria*, VCH Publishers, New York,NY, **1989**.

157. White, W. I. In *The Porphyrins*; Dolphin, D., Ed.; Academic Press: New York, **1978**, Vol. 5, p 303-339.

158. Collman, J. P.; Boulatov, R., "Synthesis and reactivity of porphyrinatorhodium(II)-triethylphosphine adducts: The role of PEt_3 in stabilizing a formal Rh(II) state", *J. Am. Chem. Soc.* **2000**, *122*, 11812-11821.

159. Koelle, U., "Transition metal-catalyzed proton reduction", *New J. Chem.* **1992**, *16*, 157-169.

160. Collman, J. P.; Ha, Y.; Wagenknecht, P. S.; Lopez, M. A.; Guilard, R., "Cofacial bisorganometallic diporphyrins: Synthetic control in proton reduction catalysis", *J. Am. Chem. Soc.* **1993**, *115*, 9080-9088.

161. Yang, X.; Hall, S. B.; Tan, S. N., "Electrochemical reduction of a conjugated cinnamic acid diazonium salt as an immobilization matrix for glucose biosensor", *Electroanalysis* **2003**, *15*, 885-891.

162. Lexa, D.; Grass, V.; Saveant, J.-M., "Metal alkylation of electrochemically generated low-valent metalloporphyrins. Is there something special with rhodium?" *Organometallics* **1998**, *17*, 2673-2676.

163. Collman, J. P., Murphy, D. W.; Dolcetti, G., "Reactive new d_8 metal center for oxidative addition reactions", *J. Am. Chem. Soc.* **1973**, *95*, 2687-2689.

164. Collman, J. P.; Boulatov, R., "Unexpected reactivity of Rh(TPP)I(CO) toward an alkoxide in CH_2Cl_2: Synthesis and crystal structure of $Rh(TPP)(CH_2Cl_2)$", *Inorg. Chem.* **2001**, *40*, 560-563.

165. Sun, H.; Smirnov, V. V.; DiMagno, S. G., "Slow electron transfer rates for fluorinated cobalt porphyrins: Electronic and conformational factors modulating metalloporphyrin ET", *Inorg. Chem.* **2003**, *42*, 6032-6040.

166. Smirnov, V. V.; Woller, E. K.; DiMagno, S. G., "^{19}F NMR and structural evidence for spin-state modulation of six-coordinate cobalt(II) in a weak field porphyrin ligand", *Inorg. Chem.* **1998**, *37*, 4971-4978.

167. Ogoshi, H.; Setsune, J.; Yoshida, Z., "Hydridorhodium(III) porphyrin and porphyrin rhodium(II) dimmer", *J. Am. Chem. Soc.* **1977**, *99*, 3869-3870.

168. Wayland, B. B.; Newman, A. R., "Dioxygen and nitric oxide complexes of rhodium porphyrins", *Inorg. Chem.* **1981**, *20*, 3093-3097.

169. Wayland, B. B.; Newman, A. R., "Dioxygen complexes of rhodium porphyrins", *J. Am. Chem. Soc.* **1979**, *101*, 6472-6473.

170. *IUPAC Solubility Data Series*; Cargill, R. W., Ed.; Pergammon Press: Oxford, **1990**, Vol. 43.

171. *CRC Handbook of Chemistry and Physics*; 76th ed.; Lide, D. R., Ed.; CRC Press: Boca Raton, **1995-1996**.

172. WolframResearch; Mathematica For Students 5.0 ed., **1988-2003**.

173. Anthony, J. L.; Anderson, J. L.; Maginn, E. J.; Brennecke, J. F., "Anion effects on gas solubility in ionic liquids", *Journal of Physical Chemistry B* **2005**, *109*, 6366-6374.

174. Ford, P. C.; Rokicki, A., "Nucleophilic activation of carbon monoxide: applications to homogeneous catalysis by metal carbonyls of the water gas shift and related reactions", *Adv. Organomet. Chem.* **1988**, *28*, 139-217.

175. Yamamoto, A., "Fundamentals of molecular catalysis: General introduction", *Current Methods in Inorganic Chemistry* **2003**, *3*, 1-63.

176. Gomez-Romero, P.; Casan-Pastor, N., "Photoredox chemistry in oxide clusters. Photochromic and redox properties of polyoxometalates in connection with analog solid state colloidal systems", *J. Phys. Chem.* **1996**, *100*, 12448-12454.

177. Guo, Y-R.; Pan, Q-J.; Wei, Y-D.; Li, Z-H.; Li, X., "Theoretical studies on the electronic and spectroscopic properties of Keggin-structure polyoxometalates a/b-[XM12O40]$_n$- (X = Si, P; M = Mo, W)", *THEOCHEM* **2004**, *676*, 55-64.

178. Castano-Alvarez, M.; Fernandez-Abedul, M. T.; Costa-Garcia, A., "Gold electrodes for detection of enzyme assays with 3-indoxylphosphate as substrate", *Electroanalysis* **2004**, *16*, 1487-1496.

179. Fernelius, W. C.; Renfrew, E. E., "Indigo", *J. Chem. Educ.* **1983**, *60*, 633-634.

180. Schatz, P. F., "Ncw 2", *J. Chem. Educ.* **2001**, *78*, 1442-1443.

181. Srividya, N.; Paramasivan, G.; Seetharaman, K.; Ramamurthy, P., "Two-step reduction of indigo carmine by dithionite: a stopped-flow study", *J. Chem. Soc., Faraday Trans.* **1994**, *90*, 2525-2530.

182. Ashley, K. R.; Shyu, S-B.; Leipoldt, J. G., "Kinetic and equilibrium study of the reaction of [meso-tetrakis(p-sulfonatophenyl)porphinato]diaquorhodate(III) with chloride, bromide, iodide, and thiocyanate ions in aqueous solution", *Inorg. Chem.* **1980**, *19*, 1613-1616.

183. Feltham, A. M.; Spiro, M., "Platinized platinum electrodes", *Chem. Rev.* **1971**, *71*, 177-193.

184. Sawyer, D. T.; Roberts, J. L., Jr., *Experimental Electrochemistry for Chemists*, **1974**.

CHAPTER 2

IMPROVED FLUORINATION METHODOLOGY FOR ELECTRON-RICH AROMATICS VIA DIARYLIODONIUM SALTS: APPLICATION TO THE SYNTHESIS OF 2-FLUOROESTRADIOL
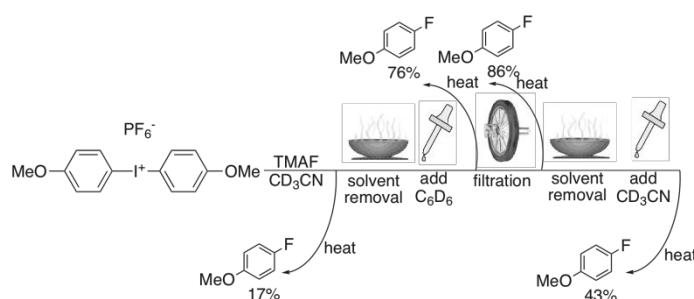
Above figure reproduced from reference 46.
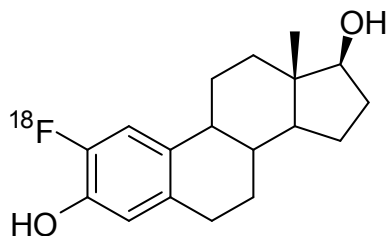
Portions of the text and certain graphics in this chapter have been reprinted (adapted) with permission from "Wang, B.; Qin, L.; Neumann, K, D.; Uppaluri, S.; Cerny, R. L.; DiMagno, S. G., "Improved arene fluorination methodology for I(III) salts", *Org. Lett.* **2010**, *12*, 3352-3355" (Reference 46). Copyright 2010 American Chemical Society (ACS). http://dx.doi.org/10.1021/ol101145h. These items are appropriately cited in the body of the chapter.

2.1   Introduction

2.1.1   Positron Emission Tomography

Positron Emission Tomography (PET)[1] is a potent *in vivo* molecular imaging technique that provides anatomic as well as functional information in biological systems. It has found valuable application in (a) non-invasive clinical diagnosis (early detection, characterization and real time monitoring) of disease, (b) basic biomedical research for the understanding of physiological/biochemical processes, and (c) pharmaceutical discovery and development to aid in evaluating the distribution, pharmacokinetics, mechanism of action and metabolism of drugs. The process of obtaining a PET scan begins with administering a molecular probe called a radiotracer/radiopharmaceutical to the subject. A radiotracer is a molecule appropriately labeled with a positron (β^+) emitting radionuclide. After the radiotracer has localized inside the body, the positrons emitted from the imaging agent aid in the detection process.
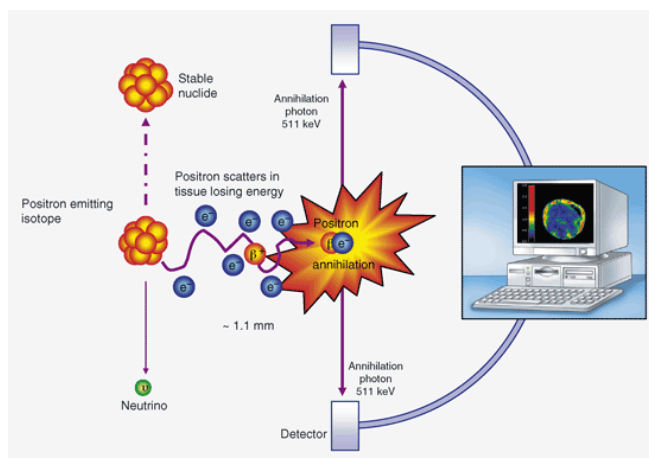
Figure 2.1. Physical Basis of Positron Emission Tomography (PET)

From http://vefir.mh.is/emjul/efni/nemverk/nemverkv09/SPG/eldsneyti.htm

After it is emitted from the radionuclide, the positron traverses a short distance before colliding with an electron in the surrounding matrix or tissue in an annihilation event that produces two 511 keV γ-rays, which correspond to the rest masses ($e = mc^2$) of the positron and electron. These two γ-rays are ejected simultaneously in opposite directions and are detected by an array of scintillation detectors positioned around the subject (Figure 2.1). A detector pair generates a line along which positron annihilation must have occurred. The exact site of annihilation is unknown, but the acquisition of a large number of coincidence events along all the lines can help reconstruct the numerous annihilation events that have been registered into an image that provides information on the spatial distribution of radioactivity as a function of time. The distance traveled by the positron before annihilation is known as the positron range, which is dependent on the positron kinetic energy (KE). Low KE positron emitters provide higher resolution images since the root mean squared (rms) distance traveled by the positron after being emitted from the nucleus is shorter. The positron is captured proximal to the decay site.

2.1.2   Fluorine-18 for PET Imaging

Table 2.1. Common Positron (β⁺) Emitters Used in PET

Isotope	Half life	Decay Mode	Avg. Positron KE $E_{\beta^+ avg}$ [keV]	Max. (Avg.) Range in Tissue [mm]	Max. Specific Activity [GBq μmol^{-1}]
^{11}C	20.39 min	β⁺ (99.8%) EC (0.24%)	385	3.8 (1)	3.4×10^5
^{13}N	9.965 min	β⁺ (99.8%) EC (0.2%)	491	5 (1.5)	7.0×10^5
^{15}O	122.24 s	β⁺ (99.8%) EC (0.01%)	735	7.6 (2.7)	3.4×10^6
^{18}F	109.77 min	β⁺ (99.8%) EC (3.3%)	242	2.2 (0.3)	6.3×10^4

Nuclear properties of commonly used positron emitting radionuclides used in PET. Data taken from Brown and Firestone 1986 and from Brookhaven National Laboratory internet database, BNL 2003

Table 2.1 shows some positron emitting radionuclides commonly employed in PET. Of all of these, fluorine-18 [^{18}F] has the most favorable physical properties for imaging.[1,2] First, its relatively low positron KE ensures a short positron range in tissue; thus the annihilation event occurs very close to the decay event thereby affording a relatively high spatial resolution. Second, its half-life of about 2 h makes ^{18}F optimal and amenable to relatively extended imaging protocols and relatively complex and elaborate radiotracer synthesis; radioactivity in the subject attenuates soon after the clinical procedure. Also, commercial distribution of ^{18}F-radiotracers to "satellite" clinical PET centers (lacking an on-site cyclotron) from a central production facility in a timely manner becomes possible. Third, the intrinsically high yielding nuclear reaction, ^{18}O(p,n)^{18}F with ^{18}O-enriched water (H$_2$^{18}O) as the bombardment target, can afford several Curie (Ci) amounts of ^{18}F from a single cyclotron run, whereas only $5 - 15$ mCi of radiotracer need to be injected to a human subject for a single PET scan. Fourth, certain labeling procedures can afford ^{18}F-radiotracers in high radiochemical yield (RCY). And last, the decay of ^{18}F gives innocuous ^{18}O as the product atom.

In addition to these inherent merits of ^{18}F as a radiolabel on tracer molecules, fluorine substitution of drugs often leads to enhanced pharmacological profiles.[3,4] Although organofluorine compounds are rare in nature,[5] the unique physical characteristics of the fluorine atom make fluorination of biologically active molecules a powerful strategy in medicinal chemistry.[6-8] Approximately 30% of all currently prescribed pharmaceuticals contain at least one fluorine atom. The high electronegativity and small atomic radius of the fluorine atom coupled with the short C-F bond length mean that its incorporation induces relatively small structural perturbations, but

drastically alters the electronic properties and bioavailability of the compounds.[9,10] C-F substitution is an attractive bioisosteric replacement for a number of functional groups including C-OH, C-H and C=O. Fluorine incorporation can alter drug metabolism[11-13] and enzyme substrate recognition.[14-16] Improved bioavailability is seen in some systems where fluorine substitution leads to enhanced hydrolytic stability.[17] The hydrophobic nature of fluorinated compounds (attributed to a reduced overall molecular polarizability that is in turn caused by the relatively nonpolarizable C-F bond) is cited for a general increase in lipophilicity.[18,19] Furthermore, replacement of sensitive or reactive groups with fluorinated substituents has led to mechanism-based inhibitors for a wide variety of diseases and to chemotherapeutic drugs.[20-22] Fluorine substitution is a particularly effective strategy for stabilizing oxidatively sensitive aromatic groups to prolong drug lifetime. This stems from the fact that the electron-withdrawing nature of the fluorine atom makes the aryl ring less susceptible to cytochrome P-450 catalyzed hydroxylation, a common step in drug catabolism.[23] The C-F dipole in fluoroaromatic moieties can also lead to an increase in molecular recognition through favorable, though generally weak, electrostatic interactions.[3,6] Apart from a negligible isotopic effect, the radiolabeled ("hot") [^{18}F]-pharmaceutical possesses the same physicochemical and biochemical properties as its nonlabeled ("cold") [^{19}F]-counterpart.[1]

2.1.3 Generation of the ^{18}F Radionuclide and Radiolabeling Strategies

^{18}F is generated in a particle accelerator/cyclotron. Both radionuclide generation and its subsequent incorporation into a radiotracer are done in lead-shielded automated systems to ensure radiation safety (Figure 2.2).[2] Table 2.2 shows the most common production methods for ^{18}F. It is evident that both the nuclear reactions that generate

elemental ^{18}F-labeled fluorine (^{18}F^{19}F) designated [^{18}F]F$_2$, yield the product in low specific activity (radioactivity per unit mass, 0.02 – 4 GBq µmol^{-1}). [^{18}F]F$_2$ and secondary reagents derived from it are used for electrophilic labeling reactions of electron rich tracer precursors. Such reactions are usually employed to access radiotracers that are not available via nucleophilic labeling.[1]

Cyclotron	Radiosynthesis/labeling
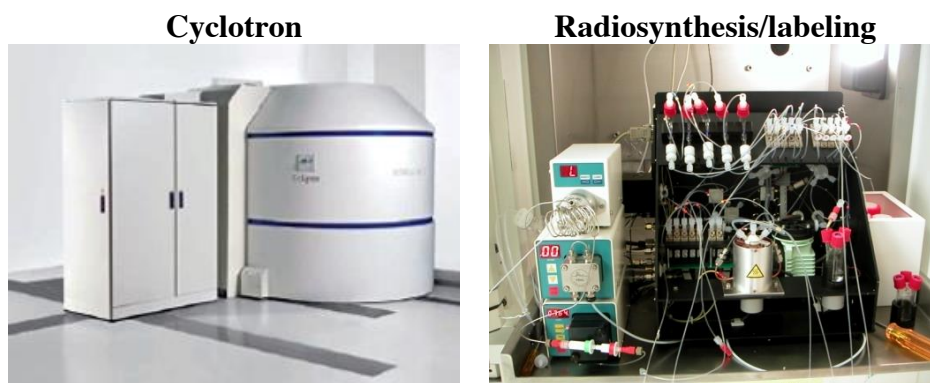
Figure 2.2. ^{18}F-Radionuclide Generation and Radiochemical Synthesis
From http://healthcare.siemens.com/molecular-imaging/

Table 2.2. Production Routes for Fluorine-18.[59,60,61,62] Table from reference 63.

Nuclear Reaction	^{18}O(p,n)^{18}F	^{16}O(^{3}He,p)^{18}F	^{20}Ne(d,α)^{18}F	^{18}O(p,n)^{18}F
Target	H$_2$^{18}O	H$_2$O	Ne (0.1 – 0.2% F$_2$)	^{18}O$_2$, Kr (1% F$_2$)
Particle Energy [MeV]	16 → 3	36 → 0	14 → 0	10 → 0
Product Chemical Form	[^{18}F]F$^-_{aq}$	[^{18}F]F$^-_{aq}$	[^{18}F]F$_2$	[^{18}F]F$_2$
Yield [GBq µAh^{-1}]	2.22	0.26	0.37-0.44	~ 0.37
Specific Activity [GBq µmol^{-1}]	4 x 10^4	4 x 10^4	0.04 – 0.4	0.04 – 2

For radiolabeling reactions involving [^{18}F]F$_2$, the maximum theoretical radiochemical yield (RCY) can only be 50%.[1] This is due to the fact that only one of the fluorine atoms in [^{18}F]F$_2$ carries the ^{18}F label (i.e. ^{18}F^{19}F). Another shortcoming of the electrophilic labeling method is the low specific radioactivity of the final ^{18}F-labeled product (i.e., the amount of ^{18}F-radioactivity per unit mass of radiotracer). The low

specific activity values stem from carrier (i.e., unlabeled $^{19}F_2$ or $^{19}F^{19}F$ gas) addition, which is required for the recovery of $[^{18}F]F_2$ from the surface of the target wall. Electrophilic labeling routes are hence restricted to PET imaging applications where high specific radioactivity tracers are not imperative. $[^{18}F]F_2$ is generally converted into less reactive and more selective ^{18}F-labeled fluorination agents such as acetyl hypofluorite $(AcO^{18}F)$, xenon difluoride $(Xe^{18}F_2)$ and N-fluorosulfonamides.

In contrast to $[^{18}F]F_2$, $[^{18}F]$fluoride ion or $[^{18}F]F^-$ can be generated without added carrier ("no carrier added" or nca). This means the $[^{18}F]F^-$ has a very high specific activity (4×10^4 GBq μmol^{-1}). High specific radioactivity is mandatory especially for radiotracers that are targeted at brain receptors.[1] For these receptors, the low concentration of binding sites requires radiotracers with high binding affinities (in the subnanomolar range). Low specific activity tracers saturate the target receptors with non-radioactive ligand thereby drastically attenuating signal generation for imaging. High specific radioactivity also enables radiotracers to be administered to human subjects in low doses (typically about 50 pmol), thereby minimizing toxic side effects.[2] These attractive features make nucleophilic labeling using nca $[^{18}F]F^-$ the method of choice for accessing radiotracers with high radiochemical purity.

Following cyclotron bombardment, nca $[^{18}F]F^-$ is obtained as $H^{18}F$ in aqueous solution.[2] It is extensively hydrated in this form, and hence extremely unreactive. To transform it into a potent nucleophile for labeling reactions, it must be dehydrated and solublilized in a polar, aprotic organic solvent. This is typically accomplished by capturing the $H^{18}F$ on an ion exchange resin, recovering the unreacted $H_2^{18}O$ target, and liberating the $[^{18}F]F^-$ by eluting with aqueous solutions of alkali metal (K^+, Rb^+, Cs^+) or

quaternary ammonium (TMA, tetramethylammonium; TBA, tetrabutylammonium) salts of weakly nucleophilic bases such as carbonate, bicarbonate, oxalate or hydroxide. Residual water is removed by multiple azeotropic evaporations with acetonitrile. Alkali metal salts are used in conjunction with a cryptand such as polyaminoether 2.2.2., Kryptofix 2.2.2., to enable ion separation and solubilization of $[^{18}F]F^-$ in polar aprotic organic solvents. The degree of dehydration of the $[^{18}F]F^-$ that is obtained by this procedure is not known, but it is highly likely that it is never completely anhydrous.[2]
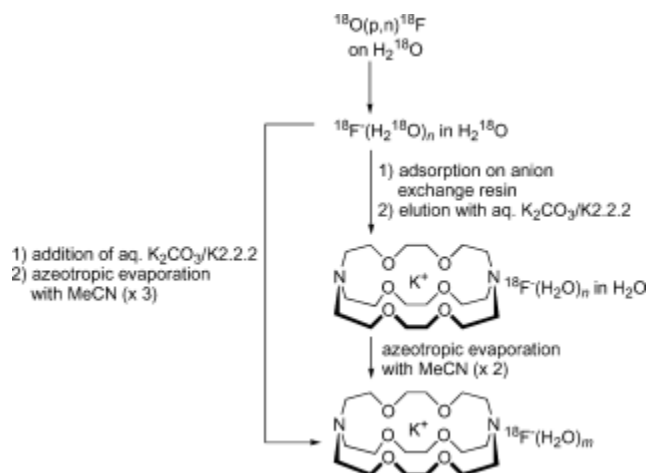
Scheme 2.1. Method for $[^{18}F]F^-_{aq}$ Isolation from Cyclotron Target. Figure from reference 2.

However access to highly anhydrous and weakly coordinated fluoride would enable labeling reactions that are otherwise recalcitrant. DiMagno and Sun reported the direct synthesis of highly anhydrous tetrabutylammonium fluoride (TBAF) from ultra-dry starting materials (Scheme 2.2).[24] The resulting fluoride showed exceptional reactivity towards a variety of substrates in aliphatic and aromatic nucleophilic substitution. The reactions proceeded under mild conditions and in high yield.[25]
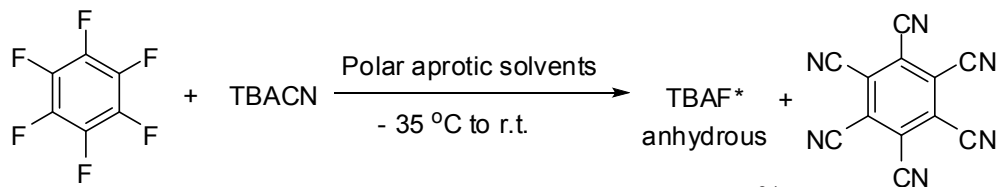
Scheme 2.2. Anhydrous TBAF Synthesis[24]

Subsequently they demonstrated a conceptual "fluoride relay" strategy (using aqueous ^{19}F-fluoride) to make the above methodology amenable to [^{18}F]F$^-$ synthesis on a time scale commensurate with radiotracer synthesis (Scheme 2.3).[26]
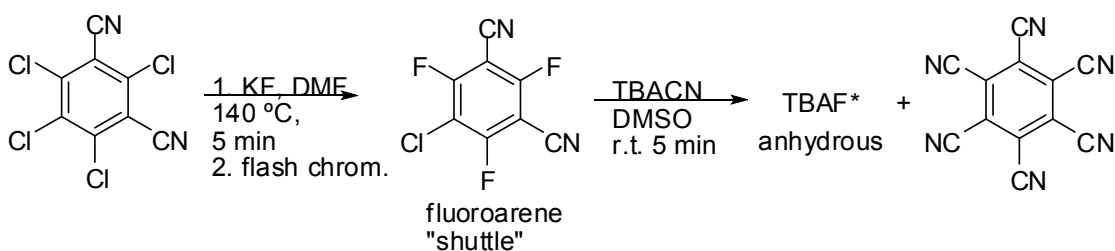
Scheme 2.3. "Fluoride Relay"[26]

Aqueous ^{19}F$^-$ was first incorporated efficiently into a fluoroarene "shuttle", which was then purified and dehydrated before being treated with TBACN to release anhydrous ^{19}F$^-$ as TBA^{19}F. Further optimization of the procedure and testing of the feasibility of "[^{18}F]fluoride relay" are needed.

Whether the source of the ^{18}F label is electrophilic or nucleophilic, there are some general considerations for successful radiotracer synthesis.[1] The relatively short half-life of ^{18}F imposes constraints on the synthesis time for a PET radiotracer. Ideally, the radiosynthesis and purification period should be accomplished within 2 to 3 times the physical half-life of the radionuclide in use, and radiosynthetic methodologies that facilitate late-stage radiolabel installation are highly desirable. Multistep syntheses can be employed for complex molecules that require labeling via prosthetic groups or contain sensitive functional groups that need to be protected prior to radiolabeling and then

deprotected. A highly superstoichiometric amount of the unlabeled precursor, typically about 10^3 to 10^4-fold excess of the radiolabeling reagent, is employed to drive the radiolabeling reaction to completion. The high superstoichiometric ratio also causes pseudo-first-order reaction kinetics, which leads to enhanced reaction rates. High purity of the radiotracer, usually achieved by radio HPLC, is required to minimize toxicity effects when administered to human subjects for PET. Image quality can be deteriorated by the presence of unlabeled analogs of the tracer that can also bind to the target receptors.
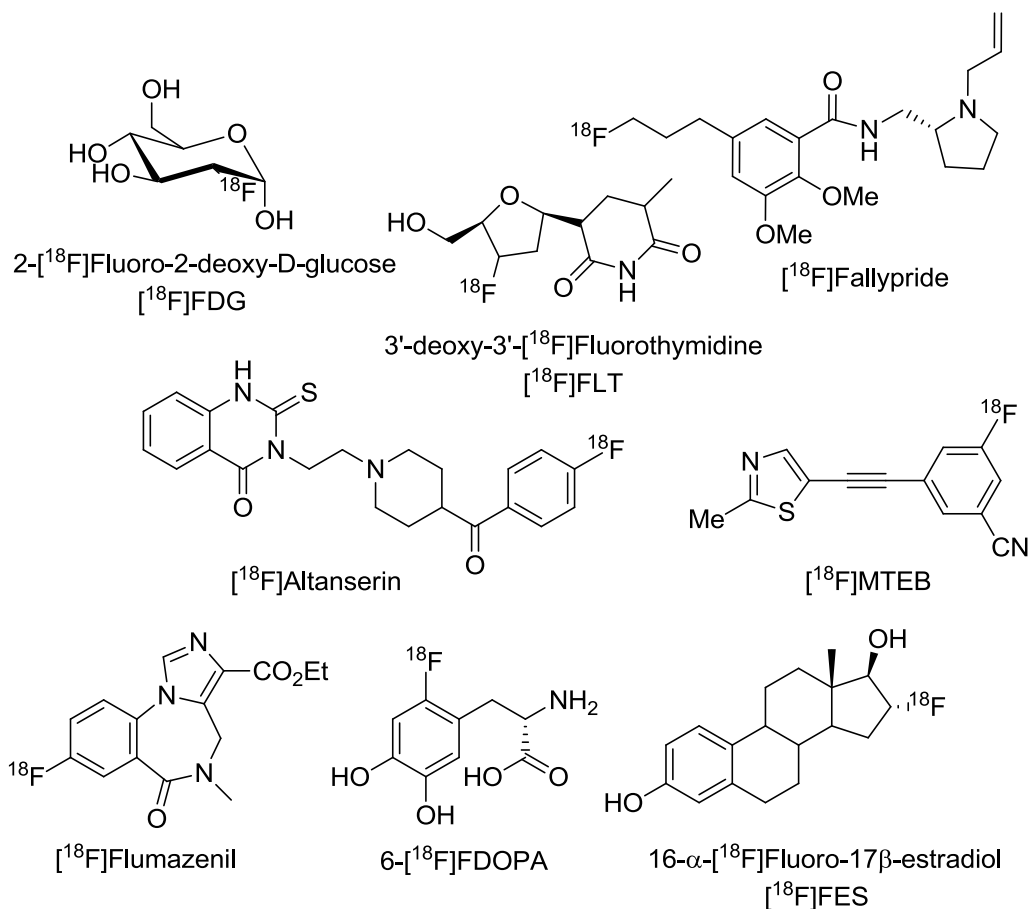
Chart 2.1. Some Significant ^{18}F-labeled Radiotracers[2,2a]

Chart 2.1 shows the structures of some significant ^{18}F-radiotracers that are currently in clinical use or undergoing preclinical studies.[2,2a] [^{18}F]2-fluoro-2-deoxy-D-

glucose ([^{18}F]FDG) is a radiotracer based on glucose metabolism. [^{18}F]FDG is very widely used as a clinical research tool and as a diagnostic agent in oncology and neurology, and can be prepared easily by the nucleophilic fluorination of peracetylated mannose triflate. A limitation of [^{18}F]FDG is that it is rather widely distributed in the body and lacks target specificity. To surmount this problem, a variety of target specific radiotracers have been developed. Some of these radiotracers can be accessed by aliphatic nucleophilic fluorination of suitable sulfonated derivative of alcohol precursors. Some of the promising radiotracers feature an aromatic fluorine label. Radiotracers with electron deficient aromatic groups can be obtained facilely via classical S$_N$Ar reactions (halex, fluorodenitration etc)[25] from suitable precursors. Those with electron rich aromatic groups (like 6-[^{18}F]FDOPA) can be prepared, in principle, via electrophilic fluorination using [^{18}F]F$_2$ or other ^{18}F-labeled electrophilic fluorinating agents mentioned previously. In addition to the innate limitation of achieving low specific activity with these reagents, there are other drawbacks associated with electrophilic fluorination. Direct fluorination of electron rich aromatics with the highly reactive [^{18}F]F$_2$ generally affords poor regioselectivity. Fluorodestannylation with [^{18}F]F$_2$ or the tamer [^{18}F]AcOF can improve regioselectivity, but metal toxicity is a concern. Nucleophilic fluorination (S$_N$Ar) of electron rich aromatics is difficult because these substrates are unactivated. S$_N$Ar of electron rich aromatics can be accomplished by introducing an accessory activating group that will facilitate S$_N$Ar. The accessory can be removed later or suitably elaborated. However these multistep transformations are sometimes ineffective for PET chemistry. The inability to fluorinate electron rich aromatics with nca [^{18}F]F$^-$ limits the substrate scope of direct radiolabeling with nca [^{18}F]F$^-$ and hinders the commercial

affordability of highly sought ^{18}F PET radiotracers featuring electron rich aromatic rings. Research in our group is aimed at addressing this issue.

2.1.4 Methods for Nucleophilic Fluorination of Unactivated Aromatics

A traditional method for fluorinating aromatics (including unactivated aromatics) using nucleophilic fluoride is the Balz-Schiemann reaction (Scheme 2.4). The reaction converts an aryl amine to an aryl fluoride via an intermediate aryl diazonium salt. Nucleophilic displacement of the diazonium group by fluoride affords the fluoroarene.[2]
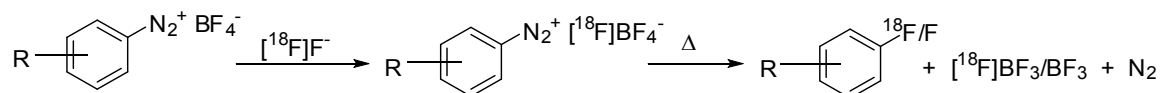
Scheme 2.4. The Balz-Schiemann Reaction for the Preparation of [^{18}F]fluoroarenes[2]

The reaction has been employed for the preparation of many [^{18}F]fluoroarenes, including electron rich arenes, such as ^{18}F-labeled amino acids[27] (e.g., the 5-fluoro isomer of [^{18}F]FDOPA). Generally, the incorporation of ^{18}F is low (2-15%). Use of BF_4^- or other labile fluoride anions leads to low specific activity. In addition, the use of BF_4^- would lower the maximum theoretical RCY to 25%. Counterions without a labile fluoride source, such as BCl_4^- have been used to preclude dilution of specific radioactivity but with only limited success. Additionally, diazotization typically requires acidic conditions that may be incompatible with certain polyfunctional aromatics, which are frequently encountered on tracer precursors. Side reactions of the diazonium salt with residual water or other adventitious species also limit the utility of the reaction. A slight variation of the Balz-Schiemann reaction is the Wallach reaction that uses aryl triazene precursors instead of aryl amines. It is fraught with many of the same limitations as the Balz-Schiemann reaction.[2]

Late transition metal catalyzed/mediated fluorination (Scheme 2.5)[28] of electron

rich aromatics using a nucleophilic fluoride source had been a holy grail in

organofluorine chemistry until it was finally accomplished by Buchwald and colleagues[32]

in 2009. Access to the methodology was hitherto hindered by the inability to effect C-F

reductive elimination to generate Ar-F. The first reports of attempted Ar-F reductive

elimination from late transition metal complexes were from Grushin's laboratory.[28-30]

[$L_nPd(II)Ar(F)$] complexes (L = simple monodentate and bidentate phosphines and
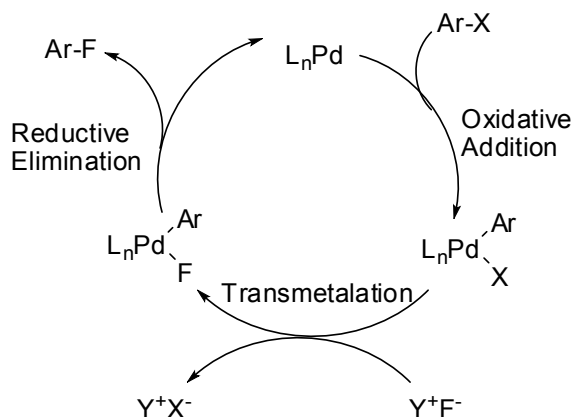
Scheme 2.5. Transition Metal Catalyzed/Mediated Fluorination of Aromatics Using
Nucleophilic Fluoride. From reference 28.

N-heterocyclic carbenes, F = fluoro) were prepared from the corresponding

[$L_nPd(II)Ar(I)$] complexes (I = iodo) by halide exchange using excess AgF and a 6 h

sonication. Thermal decomposition of the isolated [$L_nPd(II)Ar(F)$] complexes was

selective for the unproductive P-F and C-F reductive eliminations involving the

supporting ligands. The desired Ar-F reductive elimination was not observed.

Independent studies from our laboratory confirmed these results. However the I/F

exchange to generate [$L_nPd(II)Ar(F)$] complexes from the corresponding [$L_nPd(II)Ar(I)$]

complexes using our truly anhydrous tetraalkylammonium fluoride salts (1 eq.)

proceeded very rapidly (< 5 min) at room temp. In order to preclude the undesired ligand-

fluorine reductive elimination pathway we prepared the complex [LPd(II)Ar(F)] (L = the bidentate nitrogenous ligand TMEDA – tetramethylethylenediamine, Ar = *p*-methoxyphenyl). When a benzene solution of this complex was heated, ligand-fluorine reductive elimination was blocked. However, no *p*-fluoroanisole was formed and *p*-methoxybiphenyl was the only observed organic product. These results are discussed elaborately in chapter three of this thesis. Sanford and coworkers[31] reported the successful reductive elimination of Ar-F from a Pd^{IV} trifluoride complex, [LPd(IV)Ar(F)$_3$] (L = the bidentate nitrogenous ligand *t*Bu-bpy – 4,4'-di-*tert*-butyl-2,2'-bipyridine). Ar-F was formed in 45-60% yields after 1 h of reaction, and biaryls were formed in trace quantities. The complex [LPd(IV)Ar(F)$_3$] was prepared by treating the corresponding Pd^{II} complex [LPd(II)Ar(F)] with 3 eq. of XeF$_2$. Although [LPd(II)Ar(F)] was prepared by I/F exchange from the corresponding iodo complex using a nucleophilic fluoride source (3.9 eq. AgF) under sonication (1.5 – 4 h at room temperature), XeF$_2$ is only available from electrophilic fluorine sources. The presence of three fluorines in the precursor to Ar-F is a severe limitation for the applicability of this methodology for PET chemistry. The limitation pertains to a dilution of specific radioactivity of the final radiotracer. If ^{18}F-labeled XeF$_2$ is used, it will lead to an unproductive loss of radionuclide.

Buchwald and coworkers[32] posited that dimer formation from arylfluoro-palladium complexes hampers Ar-F reductive elimination. Hence they prepared the complex LPd(II)Ar(F), which was monomeric in solution, and underwent the coveted reductive elimination and afforded ArF as the product. L = *t*BuBrettPhos (Scheme 2.6) functions as an effective supporting ligand in the Pd-catalyzed fluorination of aryl

triflates using simple inorganic salts like CsF or spray-dried KF as the fluoride source. The enormous steric bulk of *t*BuBrettPhos perhaps precludes reductive eliminations involving the supporting ligand and forces Ar-F reductive elimination by forcing the Ar and F groups closer together.
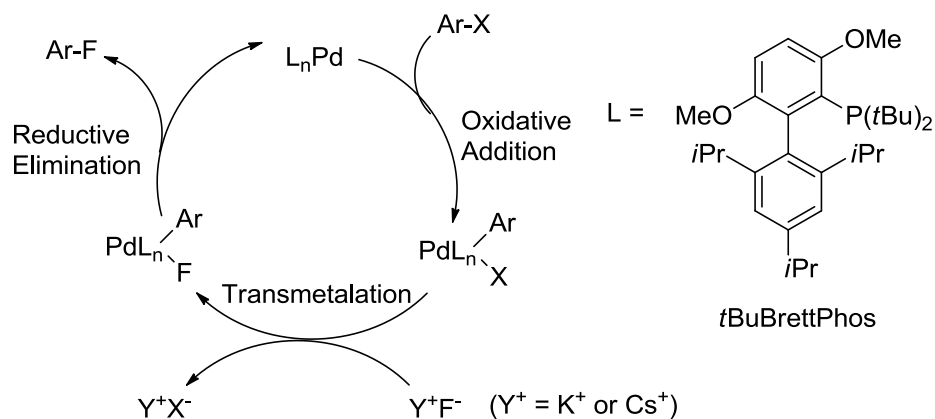
Scheme 2.6. Pd-catalyzed Aromatic Fluorination Using Buchwald's *t*BuBrettPhos as Ligand. From reference 32.

The Buchwald methodology was effective for the fluorination of aromatics with electron withdrawing substituents, affording single products. However, electron-rich aromatics required higher temperatures and/or longer reaction times. In some cases (e.g., anisole), regioisomeric aryl fluorides were formed, especially if toluene was the reaction solvent. *Ortho*-deprotonation of the aryl ring by dissociated F$^-$ to form a benzyne intermediate followed by capture of HF was put forth as a plausible mechanism, and it explains why the regioselectivity improved upon substituting toluene with the extremely nonpolar cyclohexane as the reaction solvent. Formation of reduced products (Ar-H) was another side reaction that reduced overall yields. Although the method is a breakthrough in metal catalyzed arene fluorination, it is still not optimized for ^{18}F PET radiotracer synthesis. The long reaction times (12 h) and requirement of excess fluoride source (6 eqs. of CsF) render the method incompatible with the demands of PET chemistry.

Nonetheless, optimization of this promising methodology should offer the advantage of broad functional group tolerance, which in turn could expand the substrate scope for the late stage fluorination of radiotracer precursors. More recent breakthroughs in this field are discussed in chapter three of this thesis.

The next three paragraphs are based on the literature review and introductory background in chapter 3 of the Ph.D. thesis of Bijia Wang[45] of our group. In contrast to the infancy of transition metal mediated fluorination, arene fluorination via the thermal decomposition of diaryliodonium salts is an older methodology[33-35] (Scheme 2.7). Reductive elimination at a metal center becomes more facile as the metal becomes more electronegative. Hence, higher valent transition metal complexes are more prone to reductive elimination. However, they have a propensity to bind more than one anionic ligand and more than one reductive elimination mode is possible. Therefore, we turned our attention to higher valent I(III)/diaryliodonium salts. With the approximation that iodine is a highly electronegative large transition metal, it was reasoned that the higher electronegativity of the I(III) state coupled with the enhanced stability of the Ar-I(I) complex should make reductive eliminations from I(III) centers more favorable. Therefore the conceptual framework used in the optimization of organometallic reactions should be applicable to I(III) chemistry. Stang and coworkers have stressed the similarities between iodonium ion and transition metal chemistries.[36]

Pike and colleagues[37] were the first to exploit diaryliodonium salts for ^{18}F-PET tracer synthesis. The two examples (E & F) shown in Scheme 2.7 illustrate the convenience of a one-step reaction to fluorinate unactivated aromatics in high RCY. The fluorination reactions were carried out in polar solvents such as acetonitrile and DMF

based on the assumption of a polar SNAr-type mechanism. Scheme 2.7 shows the studies

of Emert and coworkers[38] comparing various one-step nca radiosyntheses of 1-bromo-4-

[^{18}F]fluorobenzene. Their results illustrate that decomposition of the symmetrical bis(4-

bromophenyl)iodonium salt was the most effective method affording the highest RCY of

50-65%. The unsymmetrically substituted (4-bromophenyl)phenyliodonium salt afforded

a lower RCY of 32-37 % because it could react through an alternative regiochemical

pathway to afford [^{18}F]fluorobenzene (30 %) as a byproduct. It is evident that

Figure from B. Wang[45]
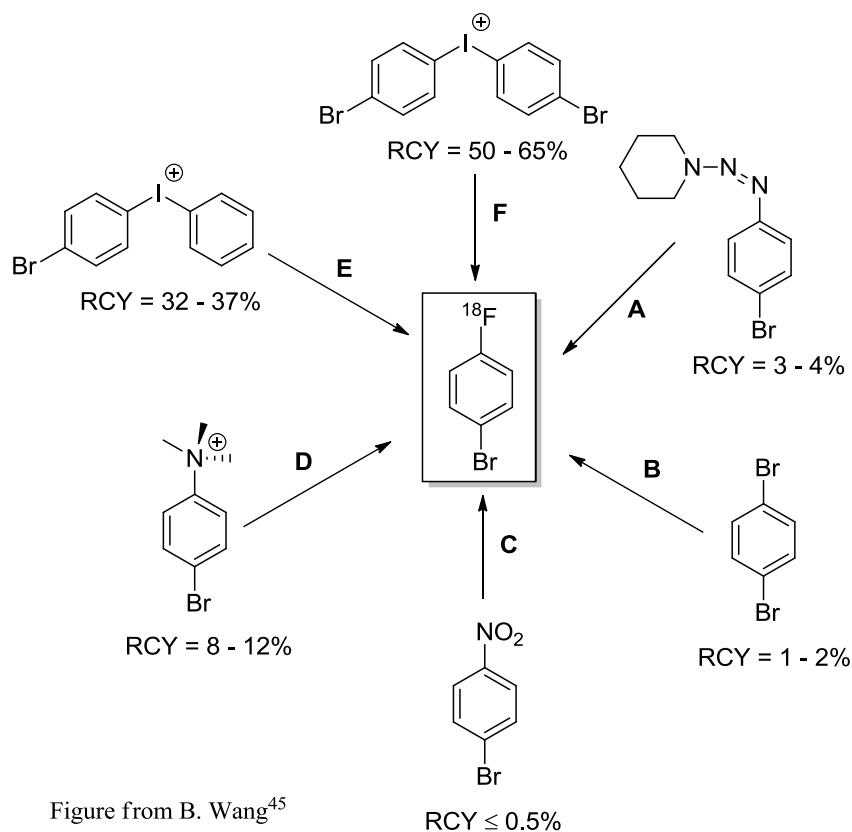
Scheme 2.7. One-step nca Routes to 1-bromo-4-[^{18}F]fluorobenzene[38]

decomposition of symmetrically substituted iodonium precursors maximizes the RCY.

However, the synthesis of such precursors to radiopharmaceuticals with elaborate

structures and oxidatively sensitive functional groups is challenging. Also, the separation

of the resulting fluoro-functionalized and iodo-functionalized arene congeners may not be

trivial for highly functionalized compounds. It is posited that decomposition of diaryliodonium fluoride salts proceeds by the SNAr-type nucleophilic attack of fluoride preferentially on the *ipso* carbon of the more electron poor aryl ring.[39] The electron poor ring should be able to better stabilize the developing negative charge in the ensuing transition state. Hence, extremely electron rich aryl rings such as 4-methoxyphenyl[38] and 2-thienyl[40] are typically installed in iodonium salts as "directing" groups to allow fluorination of relatively electron rich aromatics.

Thermolysis of diaryliodonium fluorides has been employed by a few research groups[40,41] for the [^{18}F]fluorination of model arenes. Since these reactions are run using miniscule amounts (nmol range) of the limiting reagent [^{18}F]F$^-$, not enough fluorinated product is formed for characterization using conventional techniques like NMR. Hence, the products were identified, and their yields determined, by radio TLC and radio HPLC alone. This runs the risk of coeluting isomers or contaminants going undetected.[40,41] Another issue associated with [^{18}F]fluorination is that optimized conditions reported by different research groups[38,42] were sometimes in substantial disagreement, and the fluorination yields resulting from multiple trials of the same procedure were variable. The fluorination methods developed by these groups are fraught with inherent limitations because of an exclusive focus on "hot" [^{18}F]F$^-$ chemistry. The methods do not readily translate to the ^{18}F-radiolabeling of actual radiopharmaceuticals.[42] There are limited reports of investigations with "cold" [^{19}F]F$^-$ in the literature.[43] Since our group had access to highly reactive anhydrous "cold" [^{19}F]fluoride salts[24-26] from previous work, Bijia Wang[45,46] of our group embarked on systematic investigations to optimize the reaction conditions for the thermolysis of simple, model diaryliodonium fluoride salts on the basis

of a mechanism-driven understanding of the reaction. The end goal of the research was to make the method amenable to the efficient synthesis of ^{18}F-labeled radiotracers.

Portions of the rest of this section (2.1.4) are drawn from a journal article – Wang, B.; Qin, L.; Neumann, K, D.; Uppaluri, S.; Cerny, R. L.; DiMagno, S. G., "Improved arene fluorination methodology for I(III) salts", *Org. Lett.* **2010**, *12*, 3352-3355 (reference 46) – on which I am a coauthor, and are shown in quotes. I have clearly attributed individual contributions. "Previously" DiMagno and coworkers "reported the preparation of phenyliodonium difluoride (PhIF$_2$) from anhydrous tetrabutylammonium fluoride (TBAF)[24] and phenyliodonium diacetate [PhI(OAc)$_2$]."[44] "In the course of this work," Bijia Wang[45] "noted that excess fluoride ion led to the eventual reduction of PhIF$_2$ to PhI and bifluoride ion in polar solvents like acetonitrile (CH$_3$CN) and dimethylsulfoxide (DMSO)." "This reaction was largely suppressed in nonpolar solvents like benzene." Bijia Wang[45,46] made similar observations in the arene fluorinations of diphenyliodonium hexafluorophosphate and bis(4-methoxyphenyl)iodonium hexafluorophosphate, **1** (Scheme 2.8) via thermal decomposition. Use of excess fluoride and/or polar solvent (CH$_3$CN) resulted in drastically reduced yields/no yields of fluoroarene. Iodoarene was the predominant/only aryl product with most/all of the fluoride ending up as inorganic bifluoride and tetrafluoroborate, BF$_4^-$ (by reaction with borosilicate glass). Given that fluoride ion is a strong donor for transition metal ions and given its propensity to promote disproportionation of low valent transition metal ions, it was suspected that disproportionation and subsequent redox reactions were responsible for this deleterious decomposition chemistry. Use of low polarity, noncoordinating solvents is a classical method to suppress ionic (disproportionation, ligand exchange,

electron transfer) side reactions of transition metal complexes,[47] and it was reasoned that this strategy could be adopted to promote Ar-F reductive elimination, and thereby improve diaryliodonium fluoride synthetic chemistry.

Bijia Wang[45] did a comparative investigation of the thermolysis of a selection of model diaryliodonium fluorides **1 – 8** (Scheme 2.8) in benzene and acetonitrile.[46] The results are presented in Table 2.3. "In all cases" (especially for iodonium salts that are electron rich and not activated), "the yields of fluorinated arenes were superior for the reactions conducted in benzene." "In acetonitrile, the formation of bifluoride and BF_4^- (from the borosilicate NMR tube) was observed, whereas no inorganic fluoride byproducts were seen when benzene was the reaction solvent. Inspection of the results shows that the 4-methoxyphenyl group strongly directs the fluoride nucleophile to the electron-poor aromatic ring, as is generally observed when diarlyiodonium salts are fluorinated with cyclotron-derived ^{18}F-fluoride ion."

Fluorination regioselectivity (which ring is fluorinated preferentially) is relatively low for salts with two rings that are similarly electron rich. It was also observed that a mixture of regioisomeric fluoroarenes was formed; e.g., thermolysis of **1** generated the expected 4-fluoroanisole, as well as 3-fluoroanisole. Solvent polarity plays a key role in determining the ratio of these regioisomers. Polar solvents minimize the formation of 3-fluoroanisole. Intermediacy of aryne species is regarded as the basis for these outcomes. With the positively charged I(III) center being strongly σ-electron withdrawing, the ortho proton becomes more acidic; it is likely to be abstracted by fluoride to form the aryne and HF. Cage recombination of the aryne and HF results in both the regioisomeric fluoroarenes.
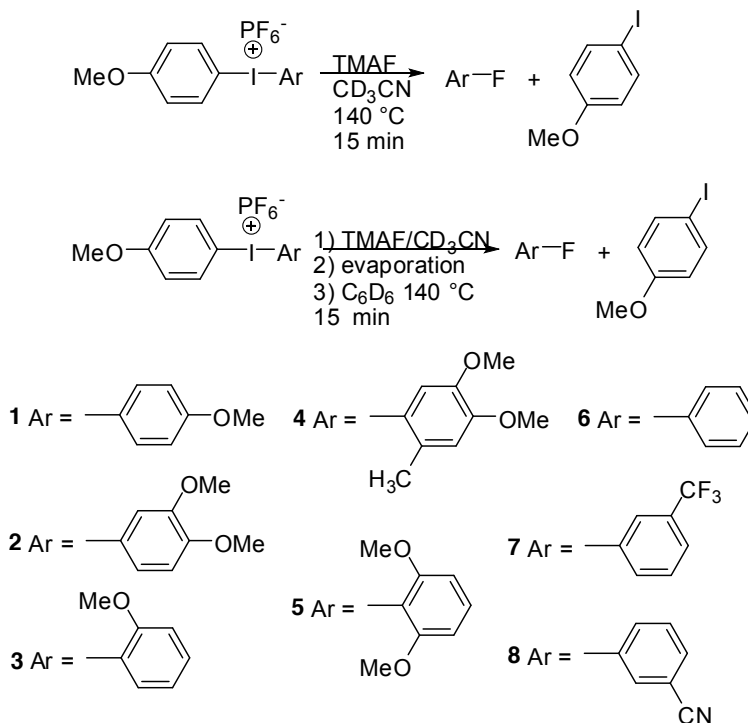
Scheme 2.8. Fluorination of Diaryliodonium Salts. From ref. 46. © 2010 ACS.

Table 2.3. Observed Yields from the Fluorination of Diaryliodonium Salts[45,46]

	No added salt		1 equiv. added TMAPF$_6$	
#	C$_6$D$_6$	CD$_3$CN	C$_6$D$_6$	CD$_3$CN
	(ArF + 4FA)	(ArF + 4FA)	(ArF + 4FA)	(ArF + 4FA)
1	86 (-)	43 (-)	76 (-)	17 (-)
2	91 (77 + 14)	38 (30 + 8)	78 (59 + 19)	3 (2 + 1)
3	72 (49 + 23)	60 (40 + 20)	84 (59 + 25)	3 (2 + 1)
4	90 (78 + 12)	81 (49 + 32)	90 (76 + 14)	3 (2 + 1)
5	70 (32 + 38)	34 (7 + 27)	67 (28 + 39)	3 (1 + 2)
6	77 (57 + 20)	55 (40 + 15)	51 (41 + 10)	4 (3 + 1)
7	95 (85 + 10)	68 (68 + 0)	86 (86 + 0)	33 (33 + 0)
8	89 (89 + 0)	78 (78 + 0)	98 (93 + 5)	0

Table from reference 46. © 2010 ACS.

"In addition to reducing the solvent polarity, the use of benzene as the reaction solvent effectively removes the inorganic spectator ions (tetramethylammonium and hexafluorophosphate) from solution. While these salts are not expected to participate

directly in the thermal decomposition reaction, their presence might facilitate ligand exchange reactions and increase the I-F dissociation rate and dissociation constants." "To probe whether the observed improvement in fluorination yield was a function of solvent polarity or extraneous salt," Kiel Neumann of our group "conducted the thermal decomposition of the diaryliodonium fluorides under "salt-free" conditions in both solvents."[46] "Salt removal was performed by a simple solvent exchange process; compounds **1 – 8** were dissolved in CH_3CN, treated with TMAF, redissolved in benzene and passed through a 0.22 □m PTFE syringe filter" (Scheme 2.8). "Upon evaporation of the benzene, clean samples of the diaryliodonium salts were obtained. ^1H and ^{19}F NMR spectra of the isolated diaryliodonium fluorides showed no residual $TMAPF_6$ in the samples of diaryliodonium fluorides prepared using this solvent exchange method." "The results of thermal decomposition (140 °C, 15 min) of the "salt-free" diaryliodonium fluorides are also summarized in" Table 2.3.[46] "For reactions conducted in benzene, salt-free conditions were associated with a modest enhancement in the yields of fluorinated arenes. In contrast, the yields of reactions conducted in CD_3CN improved dramatically after the salt was removed; in some instances the yields obtained for the thermal decomposition of salt-free diaryliodonium fluorides in acetonitrile approached those seen for reactions conducted in benzene. These results suggest that fluoride ion dissociation may be responsible for some degradation of the arene fluorination efficiency in polar aprotic solvents."

"To more closely mimic the conditions of radiotracer synthesis, the thermal decomposition reactions of **1** at three concentrations (1 mM, 5 μM, and 5 nM)" were examined by Bijia Wang;[45,46] "radiotracer synthesis is typically conducted in the nM-μM

[18]F-fluoride concentration range. Since the studies were conducted exclusively with ^{19}F-fluoride, an appropriate analytical tool was needed to test the impact of dilution upon the yield of fluorinated arenes. GC-TOF-MS was sufficiently sensitive to detect and quantify reproducibly 500 femtograms of injected 4-fluoroanisole. To minimize fluoride losses due to adsorption on glass surfaces during the dilution process, **1** was first treated with TMAF and the bis(4-methoxyphenyl)iodonium fluoride **1(F)** was isolated. Under standard thermal decomposition conditions (140 °C, 15 min, 0.5 mL benzene) the yield of 4-fluoroanisole declined sharply with the concentration of **1(F)**: 1 mM – 90%, 5 □M – 30%, 5 nM – 0%. In contrast, thermal decomposition of a mixture of 5 ng **1(F)** and excess (1 mg) bis(4-methoxyphenyl)iodonium trifluoroacetate under standard conditions gave excellent and reproducible yields of 4-fluoroanisole (80 ± 10% by GC-TOF-MS). Control experiments in which bis(4-methoxyphenyl)iodonium trifluoroacetate was heated in benzene without added **1(F)** produced no detectable fluoroanisole." Hence the new, optimized fluorination methodology for diaryliodonium salts scales down conveniently for PET chemistry. With the conditions for the methodology optimized, the goal of the research was to apply the methodology to the fluorination of clinically relevant radiotracer candidates.

2.1.5   2-[18F]Fluoroestradiol and its Potential Utility as a PET Radiotracer for Breast Cancer[48]

The prognosis and staging of human estrogen receptor (ER) positive breast carcinoma has been shown to be linked to the levels of ER in the tumorous tissue. Formulation of an appropriate therapeutic regimen is based on the prognosis. Conventionally, biopsy of the tumorous tissue, followed by *in vitro* ligand binding assays

or immunoassays were employed to reveal the ER concentration in tissue. These methods are associated with certain limitations, and noninvasive, *in vivo* methods were sought to assess ER concentration. A PET method employing ^{18}F-labeled estrogen radiotracers was a clear option. Efforts in this direction have led to the development of the most promising candidate, 16α-[^{18}F]fluoro-17β-estradiol, designated [^{18}F]FES (Chart 2.1). In human studies, uptake of [^{18}F]FES by breast carcinoma tissue (as evaluated by PET) is consistent with ER concentrations determined by *in vitro* ligand binding assays. Despite the utility and promise of [^{18}F]FES, it does not afford adequately high tumor-to-background-tissue activity ratios (tumor-to-blood uptake ratios). An estrogen-based imaging agent with the utility of [^{18}F]FES coupled with higher tumor-to-blood activity was sought, so that smaller tumors and lower ER levels could be potentially amenable to imaging. The radiolabeled estrogen, 2-[18F]fluoro-17β-estradiol (**9**, 2-FE$_2$)[48], fits the bill. Based on studies that suggested that the serum protein, sex hormone binding globulin (SHGB), binds to estrogens, protects them from metabolism, and delivers them to target ER-rich tissues, an ^{18}F-labeled estrogen radiotracer with high binding affinity for SHGB was desired. 2-FE$_2$ has a high binding affinity for SHGB.
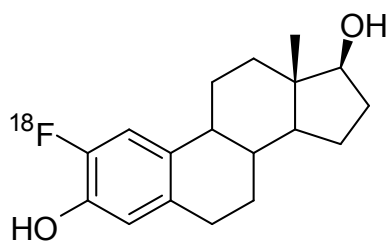
Figure 2.3. 2-[^{18}F]fluoro-17β-estradiol (**9**, 2-FE$_2$)

To evaluate the potentially beneficial role of SHBG binding in the biodistribution of ER-binding radiopharmaceuticals, Katzenellenbogen and coworkers[48] prepared 2-[^{18}F]fluoro-17β-estradiol (**9**, 2-FE$_2$) as an imaging agent that had high binding affinity for

both ER and SHBG. 2-FE$_2$ is 17β-estradiol substituted with ^{18}F on the aromatic A-ring at the 2-position (Figure 2.3). It had a higher affinity for both ER (relative binding affinity, RBA = 87% vs. estradiol = 100%) and SHBG (RBA = 3700%) compared to FES (RBA for ER = 89% vs. estradiol = 100%) and (RBA for SHGB = 9.5% vs. estradiol = 100%).

2.1.6 Previous Synthesis of 2-[^{18}F]Fluoro-17β-estradiol (9, 2-FE$_2$)[48]

Fluorination of 17β-estradiol at the 2-position of the electron rich phenolic A-ring by S$_N$Ar using fluoride ion is a considerable challenge. Katzenellenbogen and coworkers[48] accomplished the nca radiochemical synthesis (Scheme 2.9) of **19** from the suitable precursor, **18** (3.84 μmol), and [^{18}F]TBAF (obtained from 200 mCi or 0.0112 μmol of cyclotron derived [^{18}F]F$^-$). They adopted a conventional strategy of introducing an accessory group (in this case, an electron withdrawing keto group on the steroid B-ring, and *meta* to the methoxy substituent of the aromatic A-ring) and a suitable leaving group (in this case, a trimethylammonium triflate group at the 2-position of the aromatic A-ring) in the precursor to activate it for S$_N$Ar fluorination.
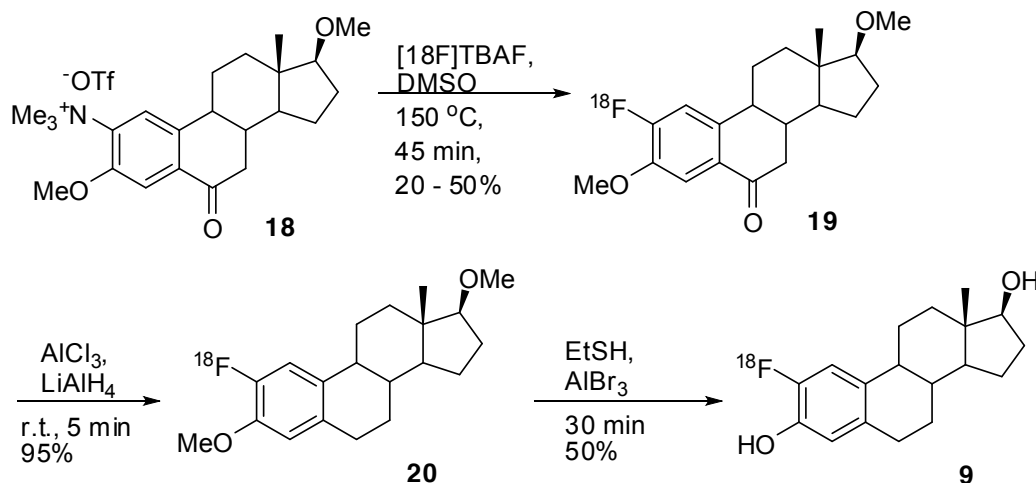
Scheme 2.9. Radiochemical Synthesis of 2-[^{18}F]fluoro-17β-estradiol (**9**, 2-FE$_2$)[48]

The RCY (determined by radio TLC) of **19** was variable between 20 and 50% of initial radioactivity, and the reaction time for the radiolabeling step was 45 min. The radiochemical purity (radio TLC) was 100%. However, the "cold" counterpart of this radiolabeling reaction using a stoichiometric ratio of **18** and unlabeled TBA^{19}F yielded less than 5% of the unlabeled analog of **19**. Stoichiometric fluorination reactions that are inefficient with respect to the organic reactant may still proceed in reasonable RCY when they are performed with radiolabeling levels of the precursor to the radiotracer (superstoichiometric; in this case about 3400-fold excess with respect to [^{18}F]TBAF).

Approximately 10-20% of radioactivity which could not be accounted for was assumed to have been lost as [^{18}F]fluoromethane resulting from the attack of [^{18}F]F$^-$ on one of the methyls of the trimethylammonium group on **18,** or as [^{18}F]fluorobutane from decomposition of [^{18}F]TBAF. A significant portion of the unincorporated radioactivity remained unreacted. Once **19** was obtained, two subsequent deprotection steps afforded the target radiotracer (**9**, 2-FE$_2$), typically in 1 – 2 mCi amounts (starting with 200 mCi of [^{18}F]F$^-$) and in 100% radiochemical purity. The multistep synthetic route to obtain the precursor (**18**) is outlined in Scheme 2.10. Most of the reactions proceeded in good to excellent yields.

The above results from Katzenellenbogen's laboratory clearly show that there is ample scope for improvement in the synthetic methodology for 2-fluoroestradiol. Hence we sought to apply our novel, improved arene fluorination methodology via pyrolysis of diaryliodonium salts to 2-fluoroestradiol synthesis. The results reported here are from my work and have been published by our group.[46]
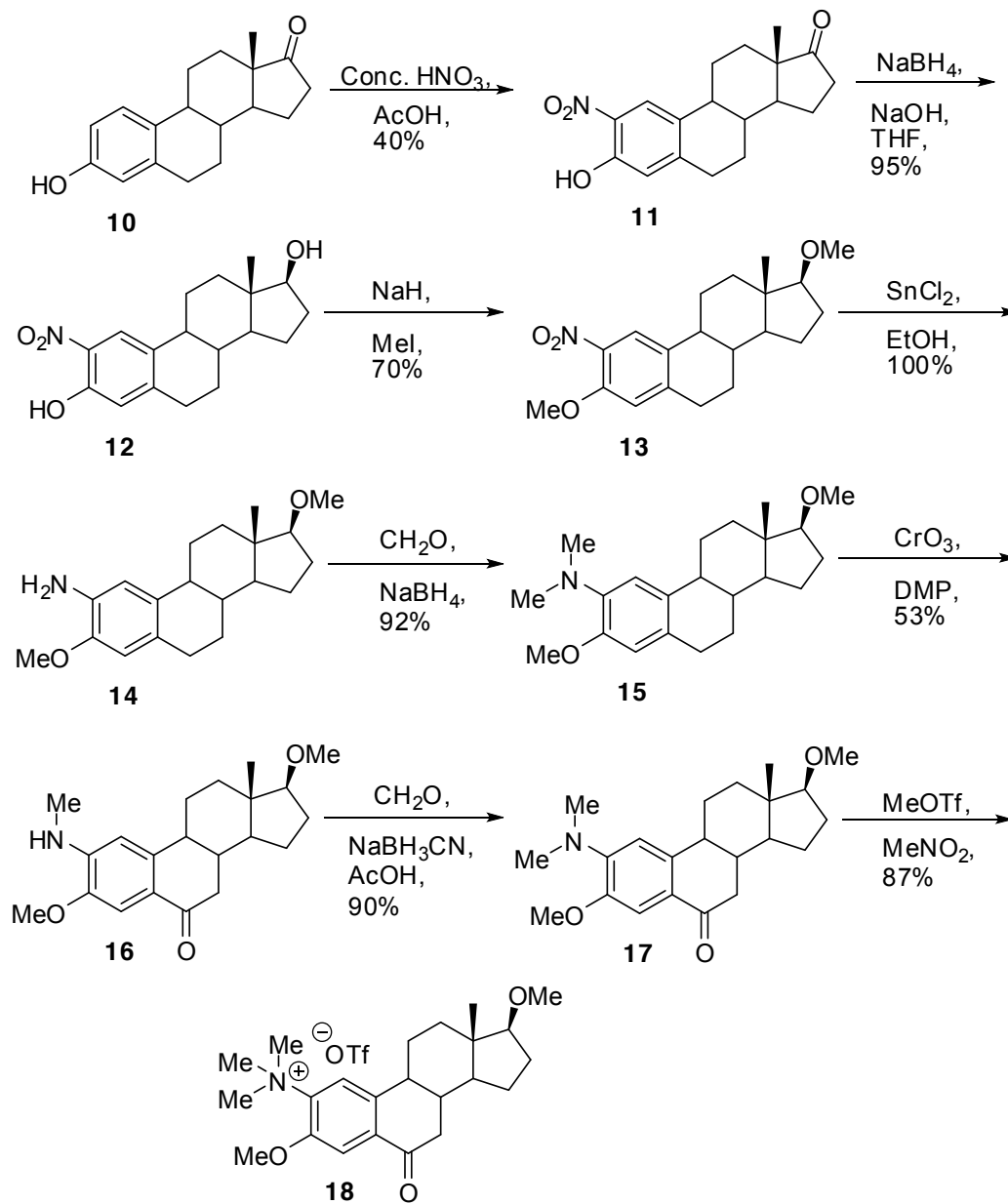
Scheme 2.10. Katzenellenbogen Synthesis of Precursor for 2-[^{18}F]Fluoroestradiol[48]

2.2 Results and Discussion

The results reported here are from my work and have been published by our group.[46] The multistep synthesis that I used for the precursor diaryliodonium hexafluorophosphate (PF$_6$) salt (**26**) featuring 17β-estradioldimethylether as the target

aryl ring for fluorination and 4-methoxyphenyl as the "directing" group is outlined in

Scheme 2.11. Commercially available estrone (**10**) was subjected to sodium borohydride
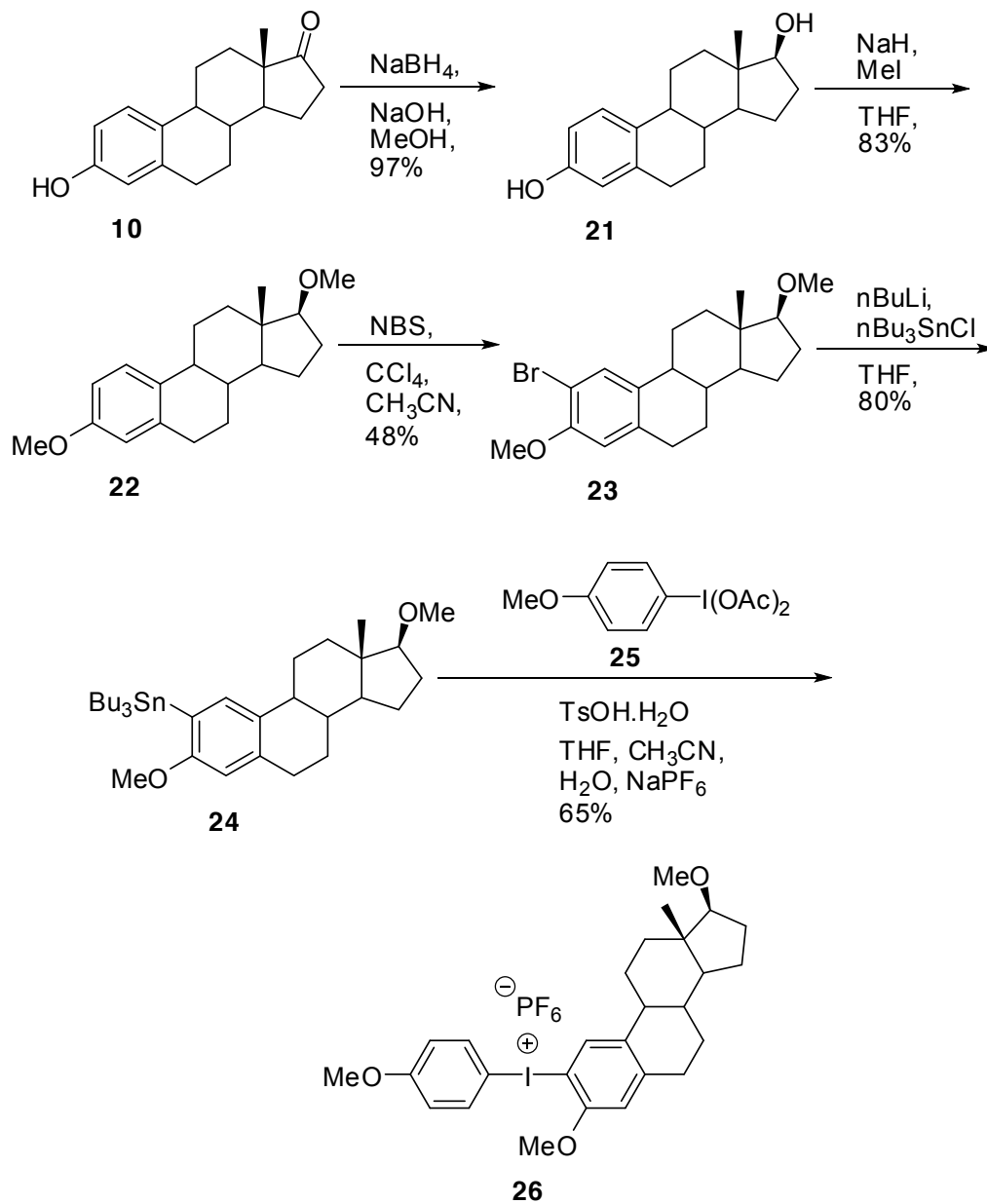
Scheme 2.11. Synthesis of the Precursor Diaryliodonium Hexafluorophosphate Salt

(NaBH$_4$) reduction to provide diastereomerically pure 17β-estradiol (**21**).[51] Methylation

of both the hydroxyl groups on **21** was accomplished using a reagent combination of

sodium hydride (NaH) and methyl iodide (MeI) to afford 17β-estradioldimethylether

(**22**). Bromination of **22** using N-bromosuccinimide (NBS) gave the 2-bromo-17β-estradioldimethylether (**23**). Lithiation of **23** with *n*-BuLi followed by treatment with tetrabutyltin chloride (Bu_3SnCl) provided the 2-stannylated-17β-estradioldimethylether (**24**). Treatment of **24** with 4-methoxyphenyliodonium diacetate [4-MeOPh-I(OAc)$_2$] (**25**) in the presence of *p*-toluene sulfonic acid monohydrate (TsOH·H$_2$O) in a Koser's type procedure yielded the precursor iodonium salt (**26**).[56-58] Yields for the above reactions were fair to excellent. This synthetic route to the tracer precursor represents a considerable improvement in the number of steps as compared to the Katzenellenbogen strategy since it does not involve the use of activating accessory groups.

For the fluorination of the precursor diaryliodonium PF$_6$ salt (**26**), I used a stepwise manner as follows. Treatment of **26** with a slightly substoichiometric tetramethylammonium fluoride (TMAF) in acetonitrile amount resulted in complete PF$_6$/F exchange, with concomitant formation of the corresponding diaryliodonium fluoride and TMAPF$_6$. Evaporation of acetonitrile followed by addition of benzene-d$_6$ and filtration to remove the insoluble TMAPF$_6$ provided a clean C$_6$D$_6$ solution of the diaryliodonium fluoride. Thermolysis (140 °C, 15 min) of this salt afforded 2-fluoro-17β-estradioldimethylether (**27**) in 42% yield (Scheme 2.12). The yield was determined by NMR using *ortho*-difluorobenzene as an internal standard. The yields were reproducible across three runs of the reaction. Both the yield and the reaction time are a considerable improvement compared to the Katzenellenbogen method, which gave a "cold" fluorination yield of less than 5% and the reaction time was 45 min. A small amount of the regioisomeric 1-fluoroestradioldimethylether was also formed. As mentioned previously, we suspect benzyne intermediacy for the pathway that leads to this product.

The other products that were formed were 4-fluoroanisole (38%), a small amount of 3-fluoroanisole, 4-iodoanisole and 2-iodoestradioldimethylether.
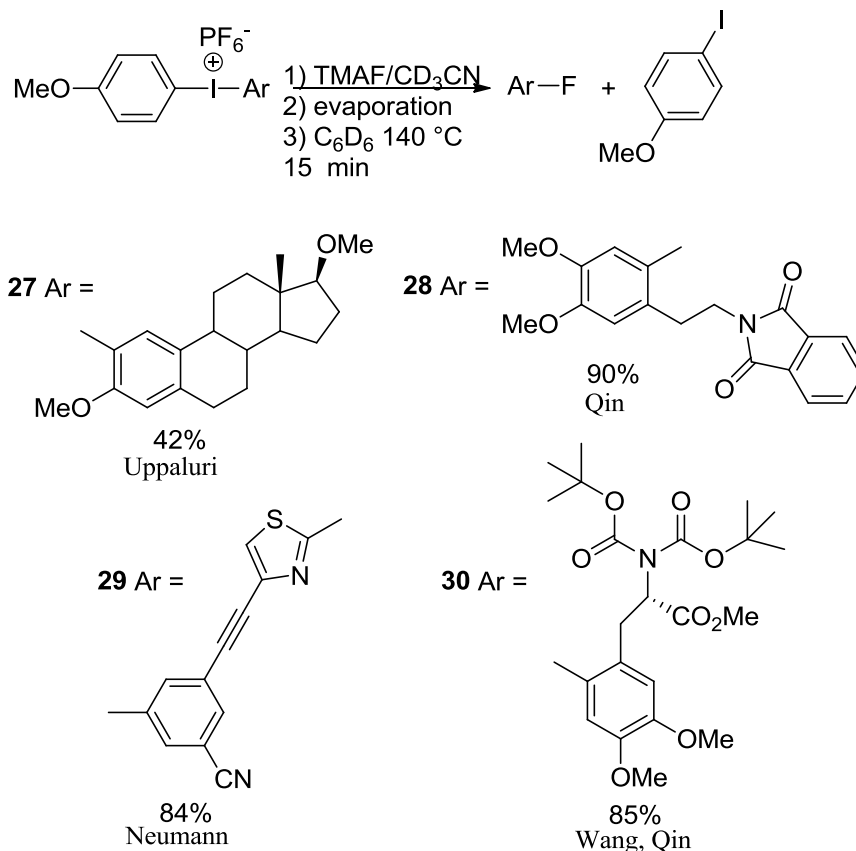
Scheme 2.12. Fluorination of Diaryliodonium Salts Featuring Tracer Candidates

Scheme 2.12 also shows the fluorination yields for the ^{19}F-counterparts of some other significant PET radiotracers that our group has prepared using the new diaryliodonium salt methodology. 6-[^{19}F]fluorodopamine[46] (**28**) (90%) was prepared by Linlin Qin, 3-[^{19}F]fluoro-[(2-methyl-1,3-thiazol-4-yl)ethynyl]benzonitrile ([^{19}F]FMTEB) (**29**) (84%) by Kiel Neumann, and 6-[^{19}F]fluorodihydroxyphenylalanine ([^{19}F]FDOPA) (**30**) (85%) by Bijia Wang[45] and Linlin Qin. Successful fluorination of these arenes indicates that the methodology is sufficiently broad to tolerate suitably protected alcohol

and amine functionalities. In preliminary "hot" chemistry experiments being conducted in collaboration with radiochemistry groups, radiochemical yields for FMTEB were identical to chemical yields, fully surpassing previously established [^{18}F]FMTEB RCY benchmarks (3 – 5%). The [^{18}F]FDOPA RCY was 30% and is still improving in optimization runs. Both the FMTEB and FDOPA reactions are complete in 50 min (including separation and purification), which is optimal for radiotracer synthesis. "Hot" chemistry efforts on 2-fluoroestradiol are currently underway.

In comparison to the excellent fluorination yields obtained for fluorodopamine, FMTEB and FDOPA, the yield for 2-fluoroestradiol was modest. This reduced fluorination yield is accompanied by a concomitant increase in the amount of 4-fluoroanisole produced, consistent with the similar "directing group" abilities of the similarly electron rich 2-methoxy and 4-methoxy substituted aryl rings on the iodonium salt. Recently our group reported a potential solution to this problem.[49,50] Use of an appropriately methoxy-substituted cyclophane as the "directing group" on a diaryliodonium fluoride salt featuring 4-methoxyphenyl as the target aryl ring enabled regiospecific fluorination of the latter ring to afford a mixture of 4-fluoroanisole (major) and 3-fluoroanisole (minor). Another advantage of this method is that benzyne chemistry on the "directing group" is curbed. We hope to exploit this new breakthrough to improve the fluorination yield for 2-fluoroestradiol. We are also currently developing a tin-free methodology to prepare the precursor diaryliodonium salts in a one-pot procedure that uses the "directing group" iodoarene and a suitably borylated species of the target arene to be fluorinated as starting materials, and other appropriate reagents. This methodology would eliminate metal toxicity concerns associated with the current tin methodology.

This methodology could potentially allow the preparation of a symmetrically substituted diaryliodonium fluoride salt for estradiol, whose thermal decomposition should circumvent the regioselectivity problem.

2.3 Summary

Quotes drawn from reference 46 on which I am a coauthor: It has been demonstrated by Bijia Wang of our group that "the perhaps counterintuitive choice of nonpolar media for the pyrolysis of highly polar diaryliodonium fluorides has an important and practical impact on the success of arene fluorination, and that these new conditions give excellent yields of fluorinated arenes." Application of these new conditions to fluorinate tracer candidates (like 17β-estradiol by me) has afforded gratifying results in terms of yields and reaction times that have surpassed the state-of-the-art in "cold" reactions and also in "hot" reactions for FMTEB (Kiel Neumann). Further studies by other group members to optimize these new reaction conditions for ^{18}F-radiotracer synthesis are currently underway.

2.4 Experimental

2.4.1 Materials and Instruments

All chemicals and reagents were used as received from commercial sources unless otherwise noted. Tetramethylammonium fluoride (TMAF) was dried at 60-80 °C in a drying pistol (charged with P_2O_5) under dynamic vacuum for one week. Chlorotributylstannane was distilled in vacuo into flame-dried storage tubes and stored under dry nitrogen. Acetonitrile and acetonitrile-d_3 were heated at reflux over P_2O_5,

distilled into flame-dried storage tubes, transferred to the glove box, and were stored there over CaH_2. Benzene and benzene-d_6 were heated at reflux over CaH_2 overnight and distilled directly into flame-dried storage tubes under dry nitrogen. Diethyl ether was distilled under reduced pressure from sodium/benzophenone. Tetrahydrofuran (THF) was dried over Na/benzophenone and distilled into a flame dried storage flask under dry nitrogen. Iodonium salts were shielded from the light during all operations. All glassware, syringes, and NMR tubes were oven dried (140 °C) for more than 24 h before they were transferred into the glove box for use. NMR spectra were recorded using 400 MHz (QNP probe) and 500 MHz (CP TXI Cryoprobe) Bruker Avance NMR spectrometers in the NMR facility at the University of Nebraska-Lincoln. Mass spectra were acquired at the University of Nebraska Center for Mass Spectrometry.

2.4.2 Synthetic Procedures

17β-Estradiol (21)[51]
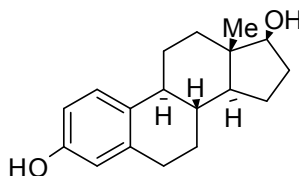
A solution of estrone (**10**) (2.6 g, 9.6 mmol) in 130 mL of methanol was treated with concentrated aqueous NaOH (1.14 g, 28.5 mmol) and added to a stirred solution of $NaBH_4$ (0.97 g, 25.5 mmol) in 130 mL of methanol. H_2 evolution ceased after about 45 min, and the mixture was poured into 200 mL of water and neutralized with 3 M HCl. The precipitate was filtered, washed with water and recrystallized from hot aqueous methanol to give 17β-estradiol (**21**) (2.54 g, 97% from two crops). ^{1}H NMR (DMSO-d_6, 400 MHz, 25 °C): δ 8.983 (s, 1H), 7.044 (d, J = 8.4 Hz, 1H), 6.500 (d, J = 8.4 Hz, 1H),

6.428 (s, 1H), 4.496 (d, J = 4.8 Hz, 1H), 3.52 (m, 1H), 2.697 (m, 2H), 2.229 (m, 1H), 2.065 (m, 1H), 1.94-1.73 (m, 3H), 1.582 (m, 1H), 1.43-1.05 (m, 7H), 0.665 (s, 3H); ^{13}C NMR (DMSO-d_6, 100 MHz, 25 °C): δ 154.89, 137.14, 130.42, 126.05, 114.91, 112.71, 80.06, 49.52, 43.54, 42.82, 38.70, 36.60, 29.90, 29.17, 26.96, 26.09, 22.79, 11.28; HRMS (ESI) calcd. for $C_{18}H_{24}O_2Na$ [M + Na]$^+$ 295.1674 found 295.1668.

3,17-Dimethoxy-β-estra-1,3,5(10)-triene (22)
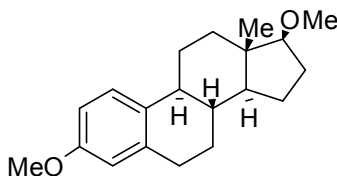
A previously reported procedure[52] was improved slightly. 17β-Estradiol (**21**) (9g) (2.54 g, 9.32 mmol) was dissolved in 125 mL of dry THF under N_2 and cooled to 0 °C. NaH (1.07 g, 44.6 mmol) was added, and the reaction mixture was stirred for 15 min. CH_3I (5.40 mL, 86.5 mmol) was added by syringe, and the turbid reaction mixture was stirred overnight and allowed to warm slowly to room temperature. The reaction mixture was poured carefully into ice-water. After the effervescence ceased, the organic product was extracted into EtOAc (3 x 125 mL), washed with aqueous $NaHCO_3$ (125 mL), and dried over anhydrous $MgSO_4$. The solvent was removed *in vacuo* to afford 3,17-dimethoxy-β-estra-1,3,5(10)-triene (**22**) (2.33 g, 83%) as an off-white solid. ^{1}H NMR (CDCl$_3$, 400 MHz, 25 °C): δ 7.218 (d, J = 8.6 Hz, 1H), 6.722 (dd, J_1 = 8.6 Hz, J_2 = 2.6 Hz, 1H), 6.640 (d, J = 2.6 Hz, 1H), 3.787 (s, 3H), 3.391 (s, 3H), 3.327 (t, J = 8.3 Hz, 1H), 2.861 (m, 2H), 2.297 (m, 1H), 2.200 (m, 1H), 2.15-2.00 (m, 2H), 1.94-1.84 (m, 1H), 1.76-1.64 (m, 1H), 1.58-1.15 (m, 7H), 0.800 (s, 3H); ^{13}C NMR (CDCl$_3$, 100 MHz, 25 °C): δ 157.61, 138.19, 132.89, 126.55, 113.97, 111.66, 91.01, 58.13, 55.41, 50.49, 44.13,

43.43, 38.81, 38.27, 30.04, 27.98, 27.44, 26.67, 23.26, 11.76; HRMS (ESI) calcd. for

$C_{20}H_{28}O_2Na$ [M + Na]$^+$ 323.1987 found 323.1994. (Lit.[51]: ^{1}H NMR (CDCl$_3$): δ 7.18 (d, J

= 8.63 Hz, 1H), 6.68 (d, J = 8.54 Hz, 1H), 6.60 (s, 1H), 3.75 (s, 3H), 3.36 (s, 3H), 3.29 (t,

J = 16.62 Hz, 1H), 2.84 (m, 2H), 2.25 (m, 1H), 2.15 (t, J = 21.87 Hz, 1H), 2.02 (m, 2H),

1.84 (m, 1H), 1.66 (m, 1H), 1.52-1.17 (m, 7H), 0.77 (s, 3H); LRMS (CI): *m/z* (rel

intensity) 301 (MH+, 100).)

2-Bromo-3,17-dimethoxy-β-estra-1,3,5(10)-triene (23)
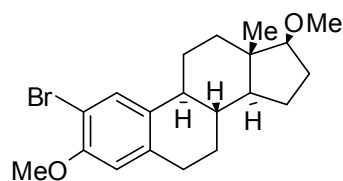
A solution of N-bromosuccinimide (1.5 g, 8.5 mmol) in CH$_3$CN (30 mL) was

added to a CCl$_4$ solution[53] (70 mL) of dimethoxy-β-estra-1,3,5(10)-triene (**22**) (2.3 g, 7.7

mmol), and the resulting mixture was stirred at room temperature protected from light for

2.5 h. The solvent was removed *in vacuo* to obtain a residual mixture with a yellow oil

and a white solid. CCl$_4$ was added and the solution was filtered and evaporated *in vacuo*

to give a yellow oil. The oil was triturated in warm methanol to yield a crude solid, which

was determined by ^{1}H-NMR to be an 80:20 mixture of the 2-bromo and the 4-bromo

estradioldimethylethers (2.30 g, 78.5%). Recrystallization of the crude product mixture

from hot methanol (1st crop) gave 2-bromo-3,17-dimethoxy-β-estra-1,3,5(10)-triene (**23**)

(1.40g, 48%) as a white solid in 95% purity, with the 4-bromo isomer as a trace impurity.

The solid was carried forward to the next step without further purification. ^{1}H NMR

(CDCl$_3$, 400 MHz, 25 °C): δ 7.434 (s, 1H), 6.615 (s, 1H), 3.860 (s, 3H), 3.385 (s, 3H),

3.319 (t, J = 8.4 Hz, 1H), 2.820 (m, 2H), 2.29-2.01 (m, 4H), 1.93-1.85 (m, 1H), 1.75-1.64

(m, 1H), 1.58-1.15 (m, 7H), 0.796 (s, 3H); ^{13}C NMR (CDCl$_3$, 100 MHz, 25 °C): δ 153.70, 137.40, 134.47, 130.44, 112.50, 108.74, 90.89, 58.13, 56.40, 50.38, 43.90, 43.39, 38.53, 38.10, 29.82, 27.96,27.26, 26.63, 23.23, 11.34; HRMS (FAB) calcd. for C$_{20}$H$_{27}$O$_2$Br [M]$^+$ 378.1194, 380.1174 found 378.1149, 380.1174.

2-tributylstannyl-3,17-dimethoxy-β-estra-1,3,5(10)-triene (24)
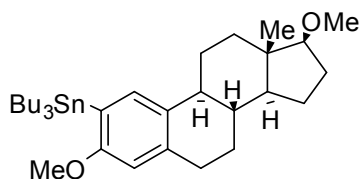
A THF solution of 2-bromo-3,17-dimethoxy-β-estra-1,3,5(10)-triene (**23**) (0.7 g, 1.8 mmol in 20 mL) was cooled to -78 °C under N$_2$. *n*-BuLi (2.47 M in hexanes, 0.78 mL, 1.9 mmol) was added dropwise with stirring, and the resulting solution was stirred at -78 °C for 30 min. Bu$_3$SnCl (0.52 mL, 1.9 mmol) was then added dropwise at -78 °C, and the resultant mixture allowed to warm to room temperature over 12 h.[54] Diethyl ether (50 mL) was added to the reaction mixture and the organic solvents were was washed with water (3 x 50 mL). The organic layer was mixed with KF (0.1 g in 1 mL EtOH) and stirred for a few minutes to remove any residual Bu$_3$SnCl. The mixture was washed with water, and the organic layer was dried over anhydrous MgSO$_4$. The solvent was removed *in vacuo* to obtain 2-tributylstannyl-3,17-dimethoxy-β-estra-1,3,5(10)-triene (**24**) as a colorless, viscous oil (0.87 g, 80%). ^{1}H NMR (CD$_2$Cl$_2$, 400 MHz, 25 °C): δ 7.229 (s, $^3J_{Sn-H}$ = 46.4 Hz, 1H), 6.521 (s, $^4J_{Sn-H}$ = 17.4 Hz, 1H), 3.705 (s, 3H), 3.330 (s, 3H), 3.292 (t, J = 8.3 Hz, 1H), 2.92-2.74 (m, 2H), 2.306 (m, 1H), 2.188 (m, 1H), 2.10-1.96 (m, 2H), 1.93-1.82 (m, 1H), 1.72-1.16 (m, 8H, H$_{alicyclic}$ on steroid overlapping with m centered ~ δ 1.52, 6H, βCH$_2$ and m centered ~ δ 1.32, 6H, γCH$_2$), 1.001 (m, 6H, αCH$_2$), 0.878 (t, J = 7.3 Hz,

9H, CH$_3$), 0.763 (s, 3H); ^{13}C NMR (CD$_2$Cl$_2$, 100 MHz, 25 °C): δ 162.48, 138.91, 134.41, 133.16, 127.03, 109.82, 91.27, 58.07, 55.56, 50.79, 44.69, 43.79, 39.42, 38.68, 30.68, 29.76, 28.25, 27.95, 27.86, 27.14, 23.58, 14.06, 11.95, 10.26; HRMS (FAB) calcd. for C$_{32}$H$_{54}$O$_2$Sn [M]$^+$ 590.3146 found 590.3130.

Bis(acetyloxy)-(4-methoxyphenyl)-λ$_3$ –iodane; 1-(diacetoxyiodo)-4-methoxybenzene (25)
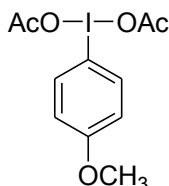
4-Iodoanisole (2.34 g, 10 mmol) was dissolved in 90 mL of glacial acetic acid and the stirred solution was warmed to 40 °C. Sodium perborate tetrahydrate (13.6 g, 110 mmol) was added in portions over the course of one hour.[55] After the addition was complete, the temperature of the reaction mixture was maintained at 40 °C for 8 h before it was allowed to cool to room temperature. Half of the acetic acid (~ 45 mL) was removed by distillation at reduced pressure. The remaining solution was treated with 100 mL of deionized water and the aqueous layer was extracted (3 × 40 mL) with dichloromethane. The combined organic fractions were dried over sodium sulfate, and the solvent was removed by rotary evaporation to give 2.25 g (64%) of 1-(diacetoxyiodo)-4-methoxybenzene, **25**. This compound was dried in vacuo and used without further purification. ^{1}H NMR (CD$_3$CN, 400 MHz, 25 °C): δ 8.055 (d, J = 9.1 Hz, 2H, H2/H6), 7.053 (d, J = 9.1 Hz, 2H, H3/H5), 3.861 (s, 3H, OMe), 1.905 (s, 6H, (OCOCH$_3$)$_2$); ^{13}C NMR (CD$_3$CN, 100 MHz, 25 °C) δ 177.73 (CO), 163.73 (C4), 138.75 (C2/C6), 118.00, (C3/C5), 111.97 (C1), 56.85 (OMe), 20.76 ((OCOCH$_3$)$_2$); HRMS: (HRFAB) calcd. for C$_{14}$H$_{13}$NO$_4$I [M – 2OAc+3-NBA]$^+$ 385.9889 found 385.9885. (lit. [2,3]

^{13}C NMR (CDCl$_3$, 50 MHz, 20 °C) δ 162.0 (C4), 137.0 (C2/C6), 116.5 (C3/C5), 111.4 (C1).); ^{13}C NMR (CDCl$_3$, 75 MHz, 25 °C) δ 176.31 (CO), 111.64 (C1), 20.36 ((OCOCH$_3$)$_2$).)

(3,17-dimethoxy-β-estra-1,3,5(10)-trien-2-yl)-(4'-methoxyphenyl)iodonium hexafluorophosphate (26)
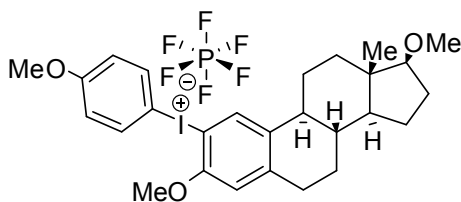
In a glove box under nitrogen, CH$_3$CN solutions of 1-(diacetoxyiodo)-4-methoxybenzene (**25**) (65 mg, 0.19 mmol in 1 mL) and *p*-toluenesulfonic acid monohydrate (35 mg, 0.19 mmol in 1 mL) were mixed together to generate a Koser's type reagent.[56-58] The yellow reagent mixture was added to a THF solution of 2-tributylstannyl-3,17-dimethoxy-β-estra-1,3,5(10)-triene (**24**) (112 mg, 0.19 mmol in 1 mL), and the resultant pale yellow reaction mixture was stirred overnight protected from light. The reaction mixture was brought out of the box, and the solvent was removed *in vacuo* to obtain a white solid residue. The solid was washed with hexanes, redissolved in CH$_3$CN and extracted with hexanes to remove the alkyltin byproducts. Solvent was removed *in vacuo* from the CH$_3$CN layer to obtain a colorless oil. The oil was dissolved in about 5 mL of CH$_3$CN and water (25 mL) and NaPF$_6$ (96 mg, 0.57 mmol) were added; the solution turned into a milky suspension. The mixture was extracted with CH$_2$Cl$_2$ and the organic solvents were removed *in vacuo* to obtain a colorless oil. The oil was triturated twice with hexanes to afford a pale brown solid. The solid was separated and dissolved in CH$_3$CN and filtered. The solvent was removed *in vacuo* and the sticky solid

was triturated again with hexanes to give (3,17-dimethoxy-β-estra-1,3,5(10)-trien-2-yl)-(4'-methoxyphenyl)iodonium hexafluorophosphate (**26**) as a pale brown solid (84 mg, 65%). The solid was collected by filtration and dried under dynamic high vacuum in a P_2O_5 drying pistol (3 d) before fluorination was attempted. ^{1}H NMR (CD$_3$CN, 400 MHz, 25 °C): δ 7.953 (d, J = 8.8 Hz, 2H), 7.826 (s, 1H), 7.018 (d, J = 8.8 Hz, 2H), 6.933 (s, 1H), 3.895 (s, 3H), 3.828 (s, 3H), 3.36-3.23 (s overlapping with t, 4H), 2.918 (m, 2H), 2.28-2.12 (m, 2H), 2.12-1.81 (m overlapping with solvent, 3H), 1.672 (m, 1H), 1.52-1.14 (m, 7H), 0.743 (s, 3H); ^{13}C NMR (CD$_3$CN, 100 MHz, 25 °C): δ 164.52, 155.71, 147.38, 139.13, 138.45, 134.81, 119.23, 114.65, 101.98, 101.67, 91.59, 58.27, 58.23, 57.03, 51.15, 44.94, 44.29, 39.15, 38.81, 30.92, 28.69, 27.60, 27.44, 24.01, 12.35; ^{19}F NMR (CD$_3$CN, 376 MHz, 25 °C): δ -72.876 (d, $^1J_{P-F}$ = 706.9 Hz, PF$_6^-$); ^{31}P NMR (CD$_3$CN, 162 MHz, 25 °C): δ -144.525 (septet, $^1J_{P-F}$ = 706.9 Hz, PF$_6^-$); HRMS (FAB) calcd. for C$_{27}$H$_{34}$IO$_3$ $[M - PF_6]^+$ 533.1553 found 533.1561.

Procedure for Fluorination of (3,17-dimethoxy-β-estra-1,3,5(10)-trien-2-yl)-(4'-methoxyphenyl)iodonium hexafluorophosphate (26)

Inside a N$_2$ charged glove box, 0.5 mL of a dry CH$_3$CN solution of anhydrous tetramethylammonium fluoride, TMAF (3.8 mg, 0.040 mmol) was added to 0.5 mL of a dry CH$_3$CN solution of the diaryliodonium hexafluorophosphate salt (**26**) (28.6 mg, 0.042 mmol). The resulting light yellow solution was transferred into a sealed J Young tube and the solvent was removed *in vacuo* to obtain a yellowish-white solid residue. Dry benzene-d$_6$ (0.7 mL) was added to selectively dissolve the diaryliodonium fluoride salt, and the solution was syringe filtered to remove any traces of insoluble TMAPF$_6$. The resulting light yellow solution was transferred into a sealed J Young NMR tube and heated to

140 °C for 15 min in a constant temperature silicone oil bath. The decomposition products and their yields were determined by diagnostic ^{1}H and/or ^{19}F NMR peaks after adding *ortho*-difluorobenzene as an internal standard. 2-fluoroestradioldimethylether [^{1}H NMR: δ 7.024 (d, $^3J_{F-H}$ = 13.2 Hz, H1), 6.448 (d, $^4J_{F-H}$ = 8.9 Hz, H4); ^{19}F NMR: δ -138.524 (dd, $^3J_{F-H}$ = 13.2 Hz, $^4J_{F-H}$ = 8.9 Hz, F2)]; 1-fluoroestradioldimethylether [^{19}F NMR: δ -108.050 (d, $^3J_{F-H}$ = 13.2 Hz, F1)]; 4-fluoroestradioldimethylether [^{19}F NMR: δ -139.152 (d, $^4J_{F-H}$ = 8.9 Hz, F4)]; 4-fluoroanisole [^{19}F NMR: δ -124.184 (m, F4)]; 3-fluoroanisole [19F NMR: δ -111.492 (m, F3)]; 2-iodoestradioldimethylether [^{1}H NMR: δ 7.753 (s, H1), 6.224 (s, H4)]; 4-iodoanisole [^{1}H NMR: δ 7.354 (d, J = 8.9 Hz, H3), 6.299 (d, J = 8.9 Hz, H2)]. Formation of the 4-fluorosteroid is attributed to the carryover of the 4-bromosteroid (5 % of the 2-bromosteroid sample that was prepared) all the way to the diaryliodonium fluoride stage.

1.5   References

1. Amatamy, S. M.; Honer, M.; Schubiger, P. A., "Molecular Imaging with PET", *Chem. Rev.* **2008**, *108*, 1501-1516.

2. Cai, L.; Lu, S.; Pike, V. W., "Chemistry with [18F]Fluoride Ion", *Eur. J. Org. Chem.* **2008**, 2853-2873. (2a) Alauddin, M. M., "Positron emission tomography (PET) imaging with 18F-based radiotracers", *Am. J. Nucl. Med. Mol. Imaging.* **2012**, 2, 55-76.

3. Biffinger, J. C.; Kim, H. W.; DiMagno, S. G., "The polar hydrophobicity of fluorinated compounds", *ChemBioChem* **2004**, *5*, 622-627.

4. DiMagno, S. G.; Sun, H., "The strength of weak interactions: Aromatic fluorine in drug design", *Curr*. *Top*. *Med*. *Chem*. **2006**, *6*, 1473-1482.

5. O'Hagan, D.; Schaffrath, C.; Cobb, S. L.; Hamilton, J. T. G.; Murphy, C. D., "Biochemistry: Biosynthesis of an organofluorine molecule", *Nature* **2002**, *416*, 279.

6. Hof, F.; Scofield, D. M.; Schweizer, W. B.; Diederich, F., "A weak attractive interaction between organic fluorine and an amide group", *Angew*. *Chem*. *Int*. *Ed*. **2004**, *43*, 5056-5059.

7. Jeschke, P., "The unique role of fluorine in the design of active ingredients for modern crop protection", *ChemBioChem* **2004**, *5*, 570-589.

8. Ojima, I., "Use of fluorine in the medicinal chemistry and chemical biology of bioactive compounds − A case study on fluorinated taxane anticancer agents", *ChemBioChem* **2004**, *5*, 628-635.

9. Schlosser, M., *Enantiocontrolled Synthesis of Fluoroorganic Compounds: Stereochemical Challenges and Biomedicinal Targets*, Ed. Soloshonok, V. A., Wiley, Chichester, **1999**, 613-659.

10. Smart, B. E., "Fluorine substituent effects (on bioactivity)", *J*. *Fluorine Chem*. **2001**, *109*, 3-11.

11. Wu, Y-J.; Davis, C. D.; Dworetzky, S.; Fitzpatrick, W. C.; Harden, D.; He, H.; Knox, R. J.; Newton, A. E.; Philip, T.; Polson, C.; Sivarao, D. V.; Sun, L-Q.; Tertyshnikova, S.; Weaver, D.; Yeola, S.; Zoeckler, M.; Sinz, M. W., "Fluorine substitution can block CYP3A4 metabolism-dependent inhibition: Identification of (S)-N-[1-(4-fluoro-3-morpholin-4-ylphenyl)ethyl]-3-(4-fluorophenyl)

acrylamide as an orally bioavailable KCNQ2 opener devoid of CYP3A4 metabolism-dependent inhibition", *J. Med. Chem.* **2003**, *46*, 3778-3781.

12. Vocadlo, D. J.; Mayer, C.; He, S.; Withers, S. G., "Mechanism of action and identification of Asp242 as the catalytic nucleophile of Vibrio furnisii N-acetyl-β-D-glucosaminidase using 2-acetamido-2-deoxy-5-fluoro-α-L-idopyranosyl fluoride", *Biochemistry* **2000**, *39*, 117-126.

13. Persson, K.; Ly, H. D.; Dieckelmann, M.; Wakarchuk, W. W.; Withers, S. G.; Strynadka, N. C. J., "Crystal structure of the retaining galactosyl transferase LgtC from Neisseria meningitidis in complex with donor and acceptor sugar analogs", *Nat. Struct. Biol.* **2001**, *8*, 166-175.

14. Berkowitz, D. B.; Bose, M., "(α-Monofluoroalkyl)phosphonates: A class of isoacidic and "tunable" mimics of biological phosphates" *J. Fluorine. Chem.* **2001**, *112*, 13-33.

15. McKenna, C. E.; Shen, P-D., "Fluorination of methanediphosphonate esters by perchloryl fluoride. Synthesis of fluoromethanediphosphonic acid and di fluoromethanediphosphonic acid" *J. Org. Chem.* **1981**, *46*, 4573-4576.

16. Nieschalk, J.; O'Hagan, D., "Monofluorophosphonates as phosphate mimics in bioorganic chemistry: A comparative study of CH2, CHF and CF2-phosphonate analogs sn-glycerol-3-phosphate as substrates for sn-glycerol-3-phosphate dehydrogenase" *J. Chem. Soc., Chem. Comm.* **1995**, 719-720.

17. Marquez, V. E.; Tseng, C. K.; Mitsuya H.; Aoki, S.; Kelley, J. A.; Ford, H. Jr.; Roth, J. S.; Broder, S.; Johns, D. G.; Driscoll, J. S., "Acid-stable 2'-fluoropurine

dideoxynucleotides as active agents against HIV", *J. Med. Chem.* **1990**, *33*, 978-985.

18. Leo, A., "The octanol-water partition coefficients of aromatic solutes: The effect of electronic interactions, alkyl chains, hydrogen bonds, and ortho-substitution", *J. Chem. Soc. Perkin Trans. 2* **1983**, 825-838.

19. Menger, F. M.; Venkataram, U. V., "A microscopic hydrophobicity parameter", *J. Am. Chem. Soc.* **1986**, *108*, 2980-2984.

20. Choo, H.; Chong, Y.; Choi, Y.; Mathew, J.; Schinazi, R. F.; Chu, C. K., "Synthesis, anti-HIV activity and molecular mechanism of drug resistance of L-2',3'-didehydro-2',3'-dideoxy-2'-fluoro-4'-thionucleosides", *J. Med. Chem.* **2003**, *46*, 389-398.

21. Ismail, F. M. D., "Important fluorinated drugs in experimental and clinical use", *J. Fluorine Chem.* **2002**, *118*, 27-33.

22. Chong, Y.; Gumina, G.; Mathew, J. S.; Schinazi, R. F.; Chu, C. K., "L-2',3'-didehydro-2',3'-dideoxy-3'-fluoronucleosides: Synthesis, anti-HIV activity, chemical and enzymatic stability, and mechanism of resistance", *J. Med. Chem.* **2003**, *46*, 3245-3256.

23. Boehm, H-J.; Banner, D.; Bendels, S.; Kansy, M.; Kuhn, B.; Mueller, K.; Obst-Sander, U.; Stahl, M., "Fluorine in medicinal chemistry", *ChemBioChem.* **2004**, *5*, 637-643.

24. Sun, H.; DiMagno, S. G., "Anhydrous tetrabutylammonium fluoride", *J. Am. Chem. Soc.* **2005**, *127*, 2050-2051.

25. Sun, H.; DiMagno, S. G., "Room temperature nucleophilic aromatic fluorination: Experimental and theoretical studies", *Angew. Chem. Int. Ed.* **2006**, *45*, 1-6.

26. Sun, H.; DiMagno, S. G., "Fluoride relay: a new concept for the rapid preparation of anhydrous nucleophilic fluoride salts from KF", *Chem. Comm.* **2007**, *5*, 528-529.

27. Argentini, M.; Wiese, C.; Weinreich, R.,"Syntheses of 5-fluoro-D/L-DOPA and [18F]5-fluoro-L-DOPA", *J. Fluorine. Chem.* **1994**, *68*, 141-144.

28. Grushin, V. V., "Organopalladium fluorides", *Chem. Eur. J.* **2002**, *8*, 1006-1014.

29. Yandulov, D. V.; Tran, N. T., "Aryl fluoride reductive elimination from Pd(II): Feasibility assessment from theory and experiment", *J. Am. Chem. Soc.* **2007**, *129*, 1342-1358.

30. Grushin, V. V.; Marshall, W. J., "Ar-F reductive elimination from palladium(II) revisited", *Organometallics* **2007**, *26*, 4997-5002.

31. Ball, N. D.; Sanford, M. S., "Synthesis and reactivity of a mono-sigma-aryl palladium(IV) fluoride complex", *J. Am. Chem. Soc.* **2009**, *131*, 3796-3797.

32. Watson, D. A.; Su, M.; Teveroviskiy, G.; Zhang, Y.; Garcia-Fortanet, J.; Kinzel, T.; Buchwald, S. L., "Formation of Ar-F from LpdAr(F): Catalytic conversion of aryl triflates to aryl fluorides", *Science* **2009**, *325*, 1661-1664.

33. Grushin, V. V.; Tolstaya, T. P.; Lisichkina, I. N., "Phenyl-2-p-carboranyliodonium fluoroborate", *Izv. Akad. Nauk SSSR, Ser. Khim.* **1983**, *9*, 2165-2168.

34. Van der Puy, M., "Conversion of diaryliodonium salts to aryl fluorides", *J. Fluorine Chem.* **1982**, *21*, 385-392.

35. Grushin, V. V.; Kantor, M. M.; Tolstaya, T. P.; Shcherbina, T. M., "Arylation of anions by diarylhalonium tetrafluoroborates under phase transfer catalysis conditions", *Izv. Akad. Nauk SSSR, Ser. Khim.* **1984**, *10*, 2332-2338.

36. Stang, P. J., "Polyvalent iodine in organic chemistry", *J. Org. Chem.* **2003**, *68*, 2997-3008.

37. Pike, V. W.; Aigbirhio, F. I., "Reactions of cyclotron-produced [^{18}F]fluoride with diaryliodonium salts - a novel single-step route to no-carrier-added [18]fluoroarenes", *J. Chem. Soc., Chem. Commun.* **1995**, *21*, 2215-2216.

38. Ermert, J.; Hocke, C.; Ludwig, T.; Gail, R.; Coenen, H. H., "Comparison of pathways to the versatile synthon of no-carrier-added 1-bromo-4-[18F]fluorobenzene", *J. Labelled Compd. Radiopharm.* **2004**, *47*, 429-441.

39. Yamada, Y.; Kashima, K.; Okawara, M., "Substituent effect in the nucleophilic attack by the bromide ion on the p-tolyl-substituted phenyliodonium ions", *Bull. Chem. Soc. Jpn.* **1974**, *47*, 3179-3180.

40. Ross, T. L.; Ermert, J.; Hocke, C.; Coenen, H. H., "Nucleophilic 18F-Fluorination of Heteroaromatic Iodonium Salts with No-Carrier-Added [18F]Fluoride", *J. Am. Chem. Soc.* **2007**, *129*, 8018-8025.

41. Carroll, M. A.; Jones, C.; Tang, S.-L., "Fluoridation of 2-thienyliodonium salts", *J. Labelled Compd. Radiopharm.* **2007**, *50*, 450-451.

42. Zhang, M.-R.; Kumata, K.; Suzuki, K., "A practical route for synthesizing a PET ligand containing [18F]fluorobenzene using reaction of diphenyliodonium salt with [18F]F", *Tetrahedron Lett.* **2007**, *48*, 8632-8635.

43. Carroll, M. A.; Nairne, J.; Smith, G.; Widdowson, D. A., "Radical scavengers: A practical solution to the reproducibility issue in the fluoridation of diaryliodonium salts", *J. Fluorine Chem*. **2007**, *128*, 127-132.

44. Sun, H.; Wang, B.; DiMagno, S. G., "A method for detecting water in organic solvents", *Org. Lett*. **2008**, *10*, 4413-4416.

45. Wang, B., "Functionalization of aromatic organic molecules with anhydrous fluorides and by reductive elimination from iodine(III)", Ph.D. Thesis **2010**, University of Nebraska.

46. Wang, B.; Qin, L.; Neumann, K, D.; Uppaluri, S.; Cerny, R. L.; DiMagno, S. G., "Improved arene fluorination methodology for I(III) salts", *Org. Lett*. **2010**, *12*, 3352-3355.

47. Sun, H.; Xue, F.; Nelson, A. P.; Redepenning, J. G.; DiMagno, S. G., "Reversible electrochemical generation of a rhodium(III) porphyrin: Thwarting disproportionation with weakly coordinating anions", *Inorg. Chem*. **2003**, *42*, 4507-4509.

48. Hostetler, E. D.; Jonson, S. D.; Welch, M. J.; Katzenellenbogen, J. A., "Synthesis of 2-[^{18}F]fluoroestradiol, a potential diagnostic imaging agent for breast cancer: Strategies to achieve nucleophilic substitution of an electron-rich aromatic ring with [^{18}F]F⁻", *J. Org. Chem*. **1999**, *64*, 178-185.

49. Wang, B.; Graskemper, J. W.; Qin, L.; DiMagno, S. G., "Regiospecific reductive elimination from diaryliodonium salts", *Angew. Chem. Int. Ed*. **2010**, *49*, 4079-4083.

50. Graskemper, J. W.; Wang, B.; Qin, L.; Neumann, K. D.; DiMagno, S. G., "Unprecedented directing group ability of cyclophanes in arene fluorinations with diaryliodonium salts", *Org. Lett.* **2011**, *13*, 3158-3161.

51. Biel, J. H., "The reduction of estrone and estrogen esters", *J. Am. Chem. Soc.* **1951**, *73*, 847-848.

52. Edsall, A. B.; Mohanakrishnan, A. K.; Yang, D.; Fanwick, P. E.; Hamel, E.; Hanson, A. D.; Agoston, G. E.; Cushman, M., "Effects of altering the electronics of 2-methoxyestradiol on cell proliferation on cytotoxicity in human cancer cultures, and on tubulin polymerization", *J. Med. Chem.* **2004**, *47*, 5126-5139.

53. Carreno, M. C.; Garcia Ruano, J. L.; Sanz, G.; Toledo, M. A.; Urbano, A., "N-Bromosuccinimide in acetonitrile: A mild and regiospecific nuclear brominating agent for methoxybenzenes and naphthalenes", *J. Org. Chem.* **1995**, *60*, 5328-5331.

54. Kozyrod, R. P.; Morgan, J.; Pinhey, J. T., "Reaction of aryltrialkylstannanes with lead tetraacetate: A convenient route to aryllead triacetates", *Aust. J. Chem.* **1985**, *38*, 1147-1153.

55. Hossain, M. D.; Kitamura, T., "Unexpected, drastic effect of triflic acid on oxidative diacetoxylation of iodoarenes by sodium perborate. A facile and efficient one-pot synthesis of (diacetoxyiodo)arenes", *J. Org. Chem.* **2005**, *70,* 6984-6986.

56. Stang, P. J.; Tykwinski, R.; Zhdankin, V., "Preparation of bis(heteroaryl)iodonium salts via an iodonium transfer reaction between

di(cyano)iodonium triflate and organostannanes", *J. Heterocycl. Chem.* **1992**, *29*, 815-818.

57. Kitamura, T.; Matsuyuki, J.; Nagata, K.; Furuki, R.; Taniguchi, H., "A convenient preparation of diaryliodonium triflates" *Synthesis* **1992**, *10*, 945-946.

58. Koser, G. F.; Wettach, R. H.; Smith, C. S., "New methodology in iodonium salt synthesis. Reactions of [hydroxy(tosyloxy)iodo]arenes with aryltrimethylsilanes" *J. Org. Chem.* **1980**, *45*, 1543-1544.

59. Qaim, S. M., "Nuclear data relevant to the production and application of diagnostic radionuclides", *Radiochim. Acta.* **2001**, 89, 223-232.

60. Qaim, S. M.; Stöcklin, G., "Production of some medically relevant short-lived neutron-deficient radioisotopes of halogens", *Radiochim. Acta.* **1983**, 34, 25-40.

61. Guillaume, M.; Luxen, A.; Nebeling, B.; Argentini, M.; Clark, J. C.; Pike, V. W., "Recommendations for fluorine-18 production", *Radiat. Isot.* **1991**, 42, 749-762.

62. Hess, E.; Takács, S.; Scholten, B.; Tárkányi, F.; Coenen, H, H.; Qaim, S. M., "Excitation function of the $^{18}O(p,n)^{18}F$ nuclear reaction from threshold up to 30 MeV", *Radiochim. Acta.* **2001**, 89, 357-362.

63. Ross, T. L., "Direct no-carrier added ^{18}F-labelling of arenes via nucleophilic substitution on aryl(2-thienyl)iodonium salts", Ph.D. Thesis **2005**, Institut für Nuklearchemie, Forschungszentrum Jülich.

CHAPTER 3

ATTEMPTS AT REDUCTIVE ELIMINATION OF ARYL FLUORIDE

FROM PALLADIUM(II)
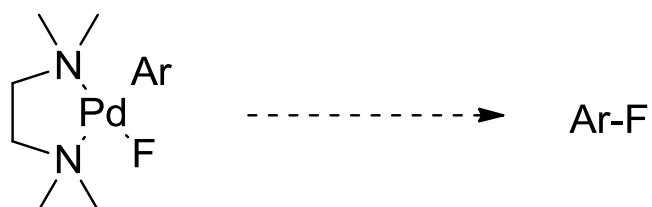
3.1   Introduction

As mentioned in Chapter 2, late transition metal mediated/catalyzed C-F bond formation using a nucleophilic fluoride source is a route that is potentially amenable to the fluorination of electron rich aromatics (Scheme 3.1)[1] for the synthesis of high specific activity ^{18}F PET (positron emission tomography) radiotracers with $[^{18}F]F^-$.
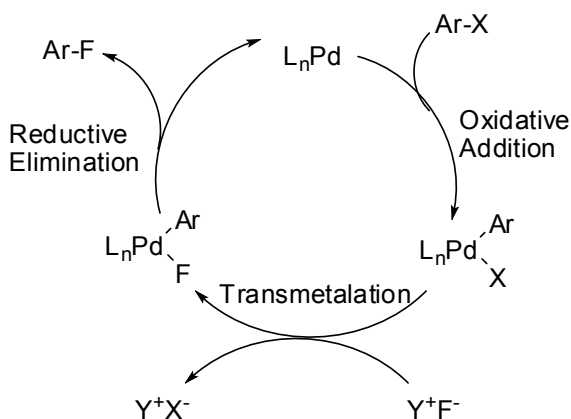
Scheme 3.1. Transition Metal Catalyzed/Mediated Fluorination of Aromatics Using Nucleophilic Fluoride[1]

Since the overall reaction involving the displacement of halide or triflate from an unactivated aromatic halide/triflate by fluoride (Equation 3.1)[1] is thermodynamically favorable, it should be possible to carry out the transformation using catalysis/mediation
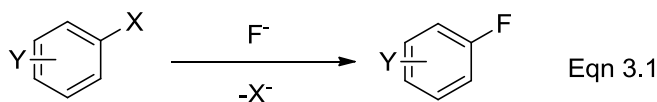
X = I, Br, Cl, OTf
Y = H, electron donor, weak electron acceptor

by a transition metal complex.[1] Attempts to develop such a methodology were first reported by the laboratory of Grushin.[1] The simplified catalytic cycle envisaged in Scheme 3.1 involves oxidative addition of Ar-X to a low valent transition metal complex, followed by metathesis (X/F) to form the aryl fluoro complex of the transition metal, which would subsequently undergo reductive elimination to afford the desired

fluoroarene and regenerate the initial low valent complex. Grushin and coworkers attempted to prepare fluoroarenes from haloarene congeners (halo = chloro, bromo and iodo) and various nucleophilic fluoride sources in the presence of various late transition metal complexes of Ni, Pd, Pt, Ru, Co and Rh. Since these attempts were unsuccessful, they concluded that at least one of the elementary steps in the proposed catalytic cycle was ineffectual, and hindering the overall catalytic transformation. As there was ample precedent for the oxidative addition step, they decided to investigate the feasibility of the latter two steps in detail with a focus on palladium as the metal.[2-30] The choice of Pd was based on its ability to catalyze a wide variety of organic transformations involving C-C, C-N, C-O and C-X bond forming reactions that included nucleophilic aromatic substitution.[2-30] They reported a series of seminal studies[31-47] on the preparation[31-36] and characterization[31-36] of [L_nPd(II)Ar(F)] complexes (L = the monodentate phosphorous based ligand triphenylphosphine, PPh$_3$, and Ar = Ph, 4-MeOC$_6$H$_4$ etc), and the thermal decomposition pathways of these complexes in solution. [(PPh$_3$)$_2$Pd(II)Ar(F)] complexes were prepared via a halide exchange reaction by treating the corresponding iodo complexes, i.e. [(PPh$_3$)$_2$Pd(II)Ar(I)], with AgF in benzene under sonication for 6h at room temperature (Equation 3.2).[1] They determined a *trans* geometry around the Pd atom

$$
\begin{array}{c}
PPh_3 \\
| \\
Ar-Pd-I \\
| \\
PPh_3
\end{array}
\;+\; AgF
\;\xrightarrow[\substack{PhH\ or\ PhMe\\ Ar\text{-}I\ (5\text{-}10\%)}]{ultrasound}\;
\begin{array}{c}
PPh_3 \\
| \\
Ar-Pd-F \\
| \\
PPh_3
\end{array}
\;+\; AgI \qquad Eqn\ 3.2
$$

Ar =
Ph (90-98%)
4-CH$_3$C$_6$H$_4$ (71-92%)
4-CH$_3$OC$_6$H$_4$ (80-96%)
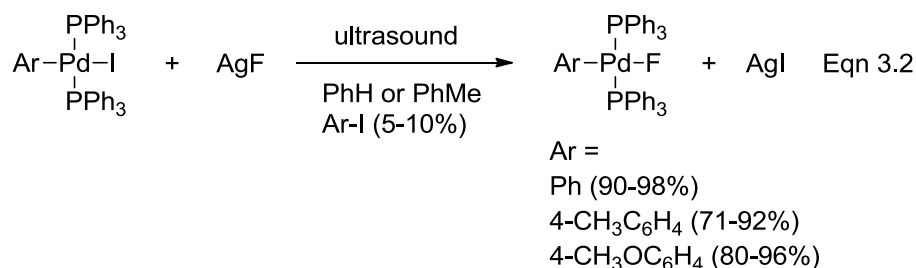
through X-ray structural and solution studies.[36] Thermal decomposition of the [(PPh$_3$)$_2$Pd(II)Ar(F)] complexes in dry toluene at 110 °C resulted in no C-F reductive

elimination products (Ar-F), but rather followed the unproductive P-F and P-C reductive

elimination pathways involving the supporting phosphine ligands to afford a mixture of

products.[32,33] In the specific case of $[(PPh_3)_2Pd(II)Ph(F)]$, thermal decomposition led to a

mixture of Ph_3PF_2, Ph-Ph, $Ph_2P\text{-}PPh_2$, $[(PPh_3)_3Pd]$ and Pd (Equation 3.3).[1] Their attempts

$$[(Ph_3P)_2Pd(II)Ph(F)] \xrightarrow[\substack{110\text{-}120\ ^oC \\ 16\ h}]{toluene,\ N_2} Ph_3PF_2\ +\ Ph\text{-}Ph\ +\ Ph_2P\text{-}PPh_2\ +\ [(Ph_3P)_3Pd]\ +\ Pd \qquad Eqn\ 3.3$$
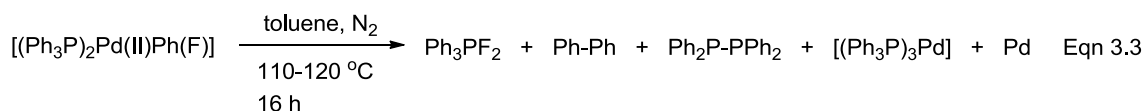
of reductive elimination by conducting the thermal decomposition of

$[(PPh_3)_2Pd(II)Ph(F)]$ in the presence of various bidentate phosphines (in order to enforce

cis geometry around the Pd atom) also did not succeed, and they observed only P-F and

P-C reductive elimination products.[32,39]

We reasoned that using the simple, bidentate, nitrogenous ligand TMEDA

(tetramethylethylenediamine) as a rigid and chelating supporting ligand (L) in the

$[L_nPd(II)Ar(F)]$ complex should preclude the undesirable reductive elimination pathways

involving the supporting ligands, and promote the desired Ar-F reductive elimination.

Besides its commercial availability, our choice of TMEDA was based on the following

considerations: (a) the higher electronegativity of nitrogen and consequently the reduced

donor ability of TMEDA (relative to phosphine ligands) should destabilize the higher

valent Pd(II) state and thereby promote reductive elimination from Pd(II), (b) the higher

electronegativity of nitrogen should preclude N-F reductive elimination, and (c) the

ligand should enforce *cis* coordination of the Ar and F ligands around Pd(II) thereby

bringing them to proximity for Ar-F reductive elimination. Also, we wanted to take

advantage of our highly reactive anhydrous tetraalkylammonium fluoride salts[50] to

improve the preparation of $[L_nPd(II)Ar(F)]$ complexes.

3.2   Results and Discussion

The results discussed here are based on the work that I carried out in the DiMagno

laboratory. The first step was to prepare the precursor iodo complex

[(TMEDA)Pd(II)Ar(I)], **1**, where Ar = 4-MeOC$_6$H$_4$ (an electron rich aryl that is

unactivated toward nucleophilic fluorination). **1** was prepared by adopting a reported

procedure[48,49] that involves oxidative addition of 4-iodoanisole to Pd$_2$(dba)$_3$ (dba =

dibenzylideneacetone) in the presence of TMEDA (Equation 3.4). The reaction was

carried out under nitrogen in benzene as the solvent at 50 °C to afford the complex **1** in

50% yield. The complex was characterized by ^{1}H NMR (Appendix F, Figure F1).
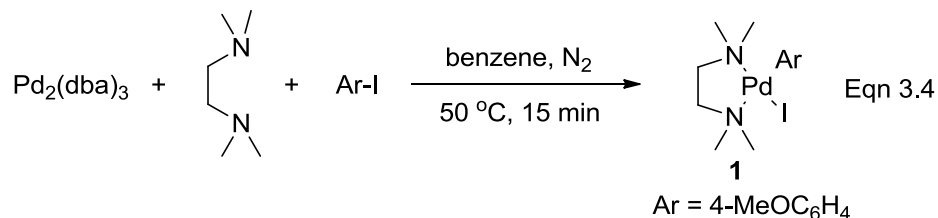
When a C$_6$D$_6$ solution of the iodo complex [(TMEDA)Pd(II)Ar(I)] (**1**) was treated

with 1 equiv. anhydrous TBAF (tetrabutylammonium fluoride)[50] at room temperature, the

equilibrium in Equation 3.5 was established rapidly (< 10 min) leading to the formation

of the corresponding arylfluoro complex [(TMEDA)Pd(II)Ar(F)] (**2**). Complexes **2** and **1**

existed in a 1:2 ratio in this equilibrium mixture. This was evident from the downfield
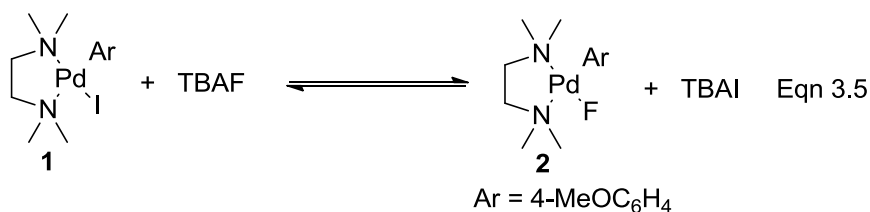
shift of peaks in the ^{1}H NMR of **2** with respect to **1**: aryl protons *ortho* to Pd (δ = 7.398

ppm $\rightarrow$ δ = 7.512 ppm), aryl protons *meta* to Pd (δ = 6.821 ppm $\rightarrow$ δ = 6.849 ppm), and

methoxy protons on aryl ring (δ = 3.463 ppm → δ = 3.518 ppm). There was also a downfield shift of peaks for the protons on the supporting TMEDA ligand (Appendix F, Figure F2). Also, a new peak (singlet) appeared at -347.41 ppm in the ^{19}F NMR, which is characteristic of fluorines bound to a Pd(II) center with bidentate nitrogenous supporting ligands[51-53] (Appendix F, Figure F3). It is significant to note that the fluoro complex is formed very rapidly (< 10 min) upon treatment of the iodo complex with our anhydrous TBAF. As discussed in Chapter 2, this is of particular importance to the synthesis of ^{18}F-labeled radiotracers on a time scale commensurate with [18]F Positron Emission Tomography (PET). Grushin's procedure requires sonicating the iodo complex with AgF for 6 h or more.[31-36,53] Trace amounts of Hoffman elimination products (bifluoride, HF_2^-; 1-butene; tributylamine) were also observed in the ^{1}H and ^{19}F NMR spectra. These resulted from decomposition of TBAF. It was known to us from previous experience that anhydrous TBAF is unstable in benzene.

When the above reaction mixture was heated to 80 °C, the TBAF completely decomposed via Hoffman elimination, and the fluoro complex **2** went back to the the iodo complex **1** (Appendix F, Figures F4 & F5). This suggests that the decomposition of TBAF drove the equilibrium back to the iodo complex. As a result, no Ar-F reductive elimination was observed. Similar observations were reported by Grushin and coworkers. When they treated [(PPh$_3$)$_2$Pd(II)Ph(F)] with [Et$_3$NCH$_2$Ph]Cl in CH$_2$Cl$_2$, the mixture equilibrated with [(PPh$_3$)$_2$Pd(II)Ph(Cl)] and [Et$_3$NCH$_2$Ph]F. The equilibrium was unstable, however, and slowly (5-8 h) drifted to [(PPh$_3$)$_2$Pd(II)Ph(Cl)] at 20 °C suggesting decomposition of the tetraalkylammonium fluoride by Hoffman elimination.[37] We reasoned that using a more robust tetraalkylammonium fluoride should preclude the

above pathway and create a possibility for the desired Ar-F reductive elimination. We decided to use anhydrous trisneopentylmethylammonium fluoride (TNPMAF). This fluoride salt was prepared using procedures that were originally developed by Bijia Wang of our group.[54] Hoffman elimination is precluded for TNPMAF due to the absence of β-hydrogens on the ammonium cation, and the only decomposition mode available for this cation is the higher energy pathway of nucleophilic substitution by fluoride on the methyl substituent to form methyl fluoride and trisneopentylamine. Consequently, TNPMAF is thermally stable in DMSO at 85 °C with only 10% decomposition observed in 12 h.[54]

When a C_6D_6 solution of the iodo complex [(TMEDA)Pd(II)Ar(I)] (**1**) was treated with 0.7 equiv. anhydrous TNPMAF at room temperature, the corresponding fluoro complex [(TMEDA)Pd(II)Ar(F)] (**2**) was formed (Equation 3.6) rapidly (< 10 min) with complete conversion of the TNPMAF as evident from the telltale signs in the ^{1}H and ^{19}F

Ar = 4-MeOC$_6$H$_4$
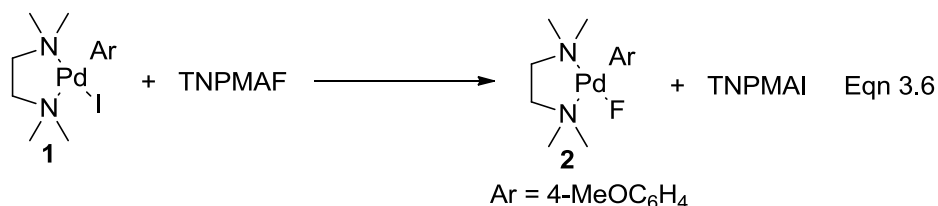
NMR spectra. There was a downfield shift of peaks in the ^{1}H NMR of **2** with respect to **1**: aryl protons *ortho* to Pd (δ = 7.412 ppm → δ = 7.602 ppm), aryl protons *meta* to Pd (δ = 6.831 ppm → δ = 6.849 ppm), and methoxy protons on aryl ring (δ = 3.447 ppm → δ = 3.499 ppm). There was also a downfield shift of peaks for the protons on the supporting TMEDA ligand (Appendix F, Figure F6). Also a new peak (singlet) appeared at -351.35 ppm in the ^{19}F NMR, which is characteristic of fluorines bound to a Pd(II) center with bidentate nitrogenous supporting ligands[51-53] (Appendix F, Figure F7). Also, gratifyingly, the TNPMAI that formed as a byproduct, precipitated out of solution thereby driving the

putative equilibrium forward and removing the TNPMA cation from solution. The solution was syringe filtered to give a clean mixture of complexes **1** and **2**. When this resulting solution was heated to 80 °C for 30 min, the iodo complex **1** stayed intact. However, the fluoro complex **2** disappeared with the concomitant formation of the biaryl species, 4,4'-dimethoxybiphenyl, which was identified by ^{1}H NMR and GC-MS. Related biaryl generating processes have been reported by Sanford and others.[51,52,55] Also some free TMEDA was formed. Besides these two species, no other products were seen in the solution phase, and no Ar-F reductive elimination was observed. No fluorinated products were seen in the ^{19}F NMR, and only a tiny peak at -122.8 ppm was observed, which presumably corresponds to a fluorinated borosilicate species. Results of the NMR experiments are shown in Appendix F; Figures F8, F9 & F10. Also, there was formation of a black precipitate, which was insoluble in $CDCl_3$, CD_3CN and DMSO-d_6. Presumably, the precipitate was palladium black.

A plausible mechanistic explanation of the above results involves a bimolecular transmetalation reaction of [(TMEDA)Pd(II)Ar(F)] (**2**) involving σ-aryl exchange between the Pd centers[51,52, 55-59] to form [(TMEDA)Pd(II)(Ar)$_2$] and [(TMEDA)Pd(II)F$_2$]. Reductive elimination from [(TMEDA)Pd(II)(Ar)$_2$] would generate the biaryl species, 4,4'-dimethoxybiphenyl, with the concomitant formation of Pd(0) and free TMEDA. Since the complex [(TMEDA)Pd(II)F$_2$] was not observed, it is presumed that it must have decomposed and the fluorines must have been transferred to the borosilicate glass. Vigalok and coworkers reported the synthesis of [L$_2$Pd(II)F$_2$] type complexes, where L = a bidentate chelating diphosphine ligand like dippp, dcpp and dppbz. However, these compounds decomposed at room temperature both in solution and the solid state to form

P-F bond containing products and palladium metal.[60,61] Also, Sanford and coworkers reported the preparation of [L$_2$Pd(II)F$_2$] (L = the bidentate, chelating nitrogenous ligand 4,4'-di-*tert*-butylbipyridine). However, the complex completely decomposed after 1 h at 80 °C in nitrobenzene, but the decomposition products were not reported.[51,52] Alternatively, [(TMEDA)Pd(II)F$_2$] could have disproportionated to [(TMEDA)$_2$Pd(0)] and [Pd(IV)F$_4$]. The latter complex would be a potent oxidant, and could have decomposed with fluorine transfer to the borosilicate glass and concomitant precipitation of palladium black. Pertinently, Bartlett and Lohmann have shown that attempts to isolate PtF$_2$ by treatment of PtCl$_2$ with fluoride salts led to disproportionation to PtF$_4$ and Pt metal.[62,63]

3.3 Summary and Recent Developments

The results presented above show that use of the bidentate, chelating, nitrogenous ligand TMEDA as a supporting ligand (L) in the complex [(L)Pd(II)Ar(F)] (Ar = 4-methoxyphenyl), curbs supporting ligand-fluorine reductive elimination in the thermal decomposition of the complex. Ligand-fluorine (P-F) reductive elimination is the preferred pathway in the thermal decomposition of complexes that feature phosphines as supporting ligands. However, for the complex [(TMEDA)Pd(II)Ar(F)] (**2**), the preferred thermal decomposition pathway yields Ar-Ar as the product, and no Ar-F reductive elimination is observed. The studies reported in this chapter were completed in April, 2008. By that time, the research focus in our group shifted to Ar-F reductive elimination by thermolysis of hypervalent iodine (diaryliodonium fluoride) salts for achieving the goal of fluorinating electron rich aromatics using a nucleophilic fluoride source.[64] This

methodology had been optimized by our group for application to the speedy preparation of ^{18}F PET radiotracers.[64] About a year-and-a-half after our studies with the complex [(TMEDA)Pd(II)Ar(F)] (**2**), similar results were reported by Sanford and coworkers on the thermolysis of an arylfluoropalladium(II) complex, [LPd(II)Ar(F)], where L = the bidentate nitrogenous ligand 4,4'-di-*tert*-butylbipyridine. No C-F bond formation was observed, and biaryl was the major organic product.[52]

Starting February, 2009, several breakthroughs in the area of metal-mediated/catalyzed Ar-F bond formation have been reported.[51,65-87] While some of these methods use nucleophilic fluoride, others use electrophilic "F$^+$" sources. A couple of methodologies that use nucleophilic fluoride reported from the laboratories of Sanford[51] and Buchwald[77-79] were mentioned in chapter two. Another remarkable advance was reported by Ritter and coworkers.[76] They accomplished Ar-F reductive elimination from a cationic arylflurorpalladium(IV) complex featuring N-(benzo[*h*]quinolin-10-yl)-arenesulfonamidato and pyridine as ancillary ligands. This complex was generated by oxidative fluorine (F$^+$) transfer to a precursor arylpalladium(II) complex. Oxidative fluorine transfer was accomplished by the use of an electrophilic fluorinating agent featuring a monocationic fluoropalladium(IV) complex with benzo[*h*]quinolyl and tetrapyrazole borate supporting ligands. This electrophilic, oxidative fluorine (F$^+$) transfer reagent was, in turn, accessed from a corresponding dicationic palladium(IV) complex by treatment with fluoride (F$^-$) ion. Short reaction times (10 min) and high yields (67-93%) were reported for the fluorination of electron-rich aromatic molecules akin to those present in ^{18}F PET radiotracers. The ability to generate the critical electrophilic fluorination reagent by capture of a nucleophilic fluoride source makes this methodology

amenable to late-stage fluorination for the synthesis of high specific activity ^{18}F PET radiotracers with [^{18}F]F[-]. Ritter and coworkers also reported the translation of this methodology for the synthesis of potential ^{18}F PET radiotracers in reasonably impressive radiochemical yields (8-40%) and a total synthesis time of about 1 h. Most recently, Ritter and coworkers reported[73] a radical advance for a practical, one-step, nickel-mediated late stage fluorination with aqueous, high specific activity [^{18}F]F[-]. They accomplished the synthesis of an assortment of ^{18}F-labeled small molecule arenes and alkenes (found in potential ^{18}F-radiotracers for PET) by treatment of suitable arylnickel(II) complexes (featuring a pyridyl-sulfonamide and a pyridine as supporting ligands) with aqueous [^{18}F]F[-] in the presence of a hypervalent aryliodine(III) oxidant. The reactions proceeded at room temperature and yielded the products in moderate to good (13-58%) radiochemical yields in less than a minute of reaction time. The precursor nickel complexes were readily synthesized, and were stable and storable. The compatibility of the preparative procedure with aqueous [^{18}F]F[-] renders obsolete the extensive procedures for the drying of [^{18}F]F[-] that are typically associated with radiochemical synthesis using the nucleophilic radionuclide. This allows truncation of the total operational time thereby minimizing unproductive radioactive decay and enhancing radiochemical yield and specific activity of the radiotracer. They also reported other critical advantages that this new methodology confers on the efficiency of radiochemical synthesis.

3.4 Experimental

3.4.1 Materials and Instruments

All chemicals and reagents were obtained from commercial sources and used as received unless otherwise noted. 4-iodoanisole was purified by recrystallization from hot hexanes. TMEDA was dried over NaOH pellets overnight and distilled directly into a flame-dried storage tube. Anhydrous TBAF[50] and TNPMAF[54] were prepared using procedures reported previously from our laboratory. Benzene and benzene-d_6 were heated at reflux over CaH_2 overnight and distilled directly into flame-dried storage tubes under dry nitrogen. All glassware, syringes, and NMR tubes were oven dried (140 °C) for more than 24 h before they were transferred into the glove box for use. NMR spectra were recorded using 400 MHz (QNP probe) and 500 MHz (CP TXI Cryoprobe) Bruker Avance NMR spectrometers in the NMR facility at the University of Nebraska-Lincoln. GC-MS analyses were performed on the Thermo Scientific Focus GC/PolarisQ MS instrument in the Undergraduate Instrumentation Center at the University of Nebraska.

3.4.2 Preparation of [(TMEDA)Pd(II)Ar(I)], 1; Ar = 4-MeOC$_6$H$_4$

A previously reported procedure[48,49] was adopted. To a flame dried 100 mL Schlenk flask in a glove box under nitrogen, Pd$_2$(dba)$_3$ (0.217 g, 0.237 mmol) and 35 mL of dry benzene were added. While stirring the resulting deep purple solution, a 2 mL benzene solution of TMEDA (0.092 mL, 0.61 mmol) and a 2 mL benzene solution of 4-iodoanisole (0.158 g, 0.68 mmol) were added slowly by syringe. The flask was stoppered and brought out of the box, and the reaction mixture was stirred at 50 °C for 15 min. The solution turned a pale yellow during this time and a fine black precipitate was formed. The reaction mixture was syringe filtered and the benzene was removed *in vacuo* to

obtain an orange-yellow solid, which was washed with 5 mL portions of anhydrous ether until the washings were colorless. The solid was dried to give **1** as a yellow solid (0.115 g, 53%). The solid was further dried under dynamic high vacuum in a P_2O_5 drying pistol (1 d) and taken into a N_2 glove box for subsequent use. ^{1}H NMR (C_6D_6, 400 MHz, 25 °C): δ 7.375 (d, J = 7.8 Hz, 2H), 6.825 (d, J = 7.8 Hz, 2H), 3.425 (s, 3H), 2.225 (s, 6H), 1.651 (s, 6H), 1.521 (m, 2H), 1.410 (m, 2H).

3.4.3 Reaction of [(TMEDA)Pd(II)Ar(I)], 1 (Ar = 4-MeOC₆H₄) with TBAF

To a glass vial in a nitrogen glove box, complex **1** (13.3 mg, 0.03 mmol), TBAF[50] (4.2 mg, 0.02 mmol) and 0.7 mL of C_6D_6 were added. The resulting pale yellow solution was transferred to a sealed J Young tube and ^{1}H and ^{19}F NMR spectra were obtained to observe the generation of [(TMEDA)Pd(II)Ar(F)], **2** (Ar = 4-MeOC₆H₄). The reaction mixture was then heated at 80 °C for 1 h during which time a fine black precipitate was formed. The reaction mixture was again analyzed by ^{1}H and ^{19}F NMR. A small syringe-filtered aliquot of the reaction mixture was also analyzed by GC-MS.

3.4.4 Reaction of [(TMEDA)Pd(II)Ar(I)], 1 (Ar = 4-MeOC₆H₄) with TNPMAF

To a glass vial in a nitrogen glove box, complex **1** (8.1 mg, 0.018 mmol), TNPMAF[54] (3.8 mg, 0.014 mmol) and 0.7 mL of C_6D_6 were added. After two minutes of stirring, a pale yellow solution with a white precipitate was formed. The reaction mixture was syringe filtered to remove the white precipitate (TNPMAI). The pale yellow solution was transferred to a sealed J Young tube and ^{1}H and ^{19}F NMR spectra were obtained to observe the generation of [(TMEDA)Pd(II)Ar(F)], **2** (Ar = 4-MeOC₆H₄). The reaction mixture was then heated at 80 °C for 1 h during which time a fine black precipitate was

formed. The reaction mixture was again analyzed by ^{1}H and ^{19}F NMR. A small syringe-filtered aliquot of the reaction mixture was also analyzed by GC-MS.

3.5 References

1. Grushin, V. V., "Palladium fluoride complexes: One more step toward metal-mediated C-F bond formation", *Chem. Eur. J.* **2002**, 8, 1006-1014.

2. Sheppard, T. D., "Metal-catalyzed halogen exchange reactions of aryl halides", *Org. Biomol. Chem.* **2009**, 7, 1043-1052.

3. Hartwig, J. F., "Carbon-heteroatom bond formation catalyzed by organometallic complexes", *Nature* **2008**, 455, 314-322.

4. Hartwig, J. F., "Electronic effects on reductive elimination to form carbon-carbon and carbon-heteroatom bonds from palladium(II) complexes", *Inorg. Chem.* **2007**, 46, 1936-1947.

5. Hartwig, J. F., "Discovery and understanding of transition metal catalyzed aromatic substitution reactions", *Synlett* **2006**, 1283-1294.

6. Schlummer, B.; Scholz, U., "Palladium-catalyzed C-N and C-O coupling: A practical guide from an industrial vantage point", *Adv. Synth. Catal.* **2004**, 346, 1599-1626.

7. Muci, A. R.; Buchwald, S. L., "Practical palladium catalysts for C-N and C-O bond formation", *Top. Curr. Chem.* **2002**, 219, 131-209.

8. Beletskaya, I. P.; Cheprakov, A. V., "The Heck reaction as a sharpening stone of palladium catalysis", *Chem. Rev.* **2000**, 100, 3009-3066.

9. Poli, G.; Giambastiani, G.; Heumann, A., "Palladium in organic synthesis: Fundamental transformations and Domino processes", *Tetrahedron* **2000**, 56, 5959-5989.

10. Yang, B. H.; Buchwald, S. L., "Palladium-catalyzed amination of aryl halides and sulfonates", *J. Organomet. Chem.* **1999**, 576, 125-146.

11. Hartwig, J. F., "Approaches to catalyst discovery. New carbon-heteroatom and carbon-carbon bond formation", *Pure. Appl. Chem.* **1999**, 71, 1417-1423.

12. Grushin, V. V.; Alper, H., "Activation of otherwise unreactive C-Cl bonds", *Top. Organomet. Chem.* **1999**, 3, 193-226.

13. Hartwig, J. F., "Carbon-heteroatom bond-forming reductive eliminations of amines, ethers and sulfides", *Acc. Chem. Res.* **1998**, 31, 852-860.

14. Hartwig, J. F., "Transition metal catalyzed synthesis of arylamines and arylethers from aryl halides and triflates: Scope and mechanism", *Angew. Chem. Int. Ed.* **1998**, 37, 2046-2067.

15. Wolfe, J. P.; Wagaw, S.; Marcoux, J.-F.; Buchwald, S. L., "Rational development of practical catalysts for aromatic C-N bond formation", *Acc. Chem. Res.* **1998**, 31, 805-818.

16. Miyaura, N.; Suzuki, A., "Palladium-catalyzed cross-coupling of organoboron compounds", *Chem. Rev.* **1995**, 95, 2457-2483.

17. Stambuli, J. P.; Weng, Z.; Incarvito, C. D.; Hartwig, J. F., "Reductive elimination of ether from T-shaped, monomeric arylpalladium alkoxides", *Angew. Chem. Int. Ed.* **2007**, 46, 7674-7677.

18. Anderson, K.W.; Ikawa, T.; Tundel, R. E.; Buchwald, S. L., "The selective reaction of aryl halides with KOH: Synthesis of phenols, aromatic ethers, and benzofurans", *J. Am. Chem. Soc.* **2006**, 128, 10694-10695.

19. Vorogushin, A. V.; Huang. X.; Buchwald, S. L., "Use of tunable ligands allows for intermolecular palladium-catalyzed C-O bond formation", *J. Am. Chem. Soc.* **2005**, 127, 8146-8149.

20. Stambuli, J. P.; Incarvito, C. D.; Bühl, M.; Hartwig, J. F., "Synthesis, structure, theoretical studies, and ligand exchange reactions of monomeric, T-shaped arylpalladium(II) halide complexes with an additional, weak agnostic interaction", *J. Am. Chem. Soc.* **2004**, 126, 1184-1194.

21. Roy, A. H.; Hartwig, J. F., "Reductive elimination of aryl halides upon addition of hindered alkylphosphines to dimeric arylpalladium(II) halide complexes", *Organometallics* **2004**, 23, 1533-1541.

22. Mann, G.; Shelby, Q.; Roy, A. H.; Hartwig, J. F., "Electronic and steric effects on the reductive elimination of diaryl ethers from Pd(II)", *Organometallics* **2003**, 22, 2775-2789.

23. Roy, A. H.; Hartwig, J. F., "Directly observed reductive elimination of aryl halides from monomeric arylpalladium(II) halide complexes", *J. Am. Chem. Soc.* **2003**, 125, 13944-13945.

24. Zanon, J.; Klapars, A.; Buchwald, S. L., "Copper-catalyzed Domino halide exchange: Cyanation of aryl bromides", *J. Am. Chem. Soc.* **2003**, 125, 2890-2891.

25. Klapars, A.; Buchwald, S. L., "Copper-catalyzed halogen exchange in aryl halides: An aromatic Finkelstein reaction", *J. Am. Chem. Soc.* **2002**, 124, 14844-14845.

26. Stambuli, J. P.; Bühl, M.; Hartwig, J. F., "Synthesis, characterization, and reactivity of monomeric, arylpalladium halide complexes with a hindered phosphine as the only dative ligand", *J. Am. Chem. Soc.* **2002**, 124, 9346-9347.

27. Roy, A. H.; Hartwig, J. F., "Reductive elimination of aryl halides from palladium(II)", *J. Am. Chem. Soc.* **2001**, 123, 1232-1233.

28. Parrish, C. A.; Buchwald, S. L., "Palladium-catalyzed formation of aryl *tert*-butyl ethers from unactivated aryl halides", *J. Org. Chem.* **2001**, 66, 2498-2500.

29. Mann, G.; Incarvito, C. D.; Rheingold, A. L.; Hartwig, J. F., "Palladium-catalyzed C-O coupling involving unactivated aryl halides. Sterically induced reductive elimination to form the C-O bond in diaryl ethers", *J. Am. Chem. Soc.* **1999**, 121, 3224-3225.

30. Widenhoefer, R. A.; Zhong, H. A.; Buchwald, S. L., "Direct observation of C-O reductive elimination from palladium aryl alkoxide complexes to form aryl ethers", *J. Am. Chem. Soc.* **1997**, 119, 6787-6795.

31. Grushin, V. V., "The organometallic fluorine chemistry of palladium and rhodium: Studies toward aromatic fluorination", *Acc. Chem. Res.* **2010**, 43, 160-171.

32. Grushin, V. V., "Palladium fluoride complexes: One more step toward metal-mediated C-F bond formation", *Chem. Eur. J.* **2002**, 8, 1006-1014.

33. Grushin, V. V., "Thermal stability, decomposition paths, and Ph/Ph exchange reactions of [(Ph$_3$P)$_2$Pd(Ph)X] (X = I, Br, Cl, F, and HF$_2$)", *Organometallics* **2000**, 19, 1888-1900.

34. Pilon, M. C.; Grushin, V. V., "Synthesis and characterization of organopalladium complexes containing a fluoro ligand", *Organometallics* **1998**, 17, 1774-1781.

35. Fraser, S. L.; Antipin, M. Yu.; Khroustalyov, V. N.; Grushin, V. V., "Molecular fluoro palladium complexes", *J. Am. Chem. Soc.* **1997**, 119, 4769-4770.

36. Marshall, W. J.; Thorn, D. L.; Grushin, V. V., "Single-crystal X-ray and solution ^{13}C NMR study of fluoro(*p*-nitrophenyl)bis(triphenylphosphine)palladium(II). Are there effects of through-conjugation?" *Organometallics* **1998**, 17, 5427-5430.

37. Grushin, V. V., "Generation of "naked" fluoride ions in unprecedentedly high concentrations from a fluoropalladium complex", *Angew. Chem. Int. Ed.* **1998**, 37, 994-996.

38. Grushin, V. V.; Marshall, W. J., "Ar-F reductive elimination from palladium(II) revisited", *Organometallics* **2007**, 26, 4997-5002.

39. Marshall, W. J.; Grushin, V. V., "Palladium(II) and palladium(0) complexes of BINAP(O)(2-(diphenylphosphino)-2'-(diphenylphosphinyl)-1,1'-binaphthyl)", *Organometallics* **2003**, 22, 555-562.

40. Flemming, J. P.; Pilon, M. C.; Borbulevitch, O. Ya.; Antipin, M. Yu.; Grushin, V. V., "The trans influence of F, Cl, Br and I ligands in a series of square-planar complexes: Relative affinities of halide anions for the metal center in *trans*-[(Ph$_3$P)$_2$Pd(Ph)X]", *Inorg. Chim. Acta* **1998**, 280, 87-98.

41. Grushin, V. V.; Marshall, W. J., "Is fluoride bound to two palladium acceptors still basic? Three CH_2Cl_2 molecules encapsulating a $Pd_2(\mu\text{-}F)_2$ square and new implications for catalysis", *Angew. Chem. Int. Ed.* **2002**, 41, 4476-4479.

42. Roe, D. C.; Marshall, W. J.; Davidson, F.; Soper, P. D.; Grushin, V. V., "Structure and solution dynamics of $[(Ph_3P)_2Pd(Ph)(FHF)]$", *Organometallics* **2000**, 19, 4575-4582.

43. Macgregor, S. A., "Transition metal-mediated P-C/X exchange at bound phosphine ligands (X = aryl, alkyl, NR_2, OR and F): Scope and mechanisms", *Chem. Soc. Rev.* **2007**, 36, 67-76.

44. Macgregor, S. A.; Roe, D. C.; Marshall, W. J.; Bloch, K. M.; Bakhmutov, V. I.; Grushin, V. V., "The F/Ph rearrangement reaction of $[(Ph_3P)_3RhF]$, the fluoride congener of Wilkinson's catalyst", *J. Am. Chem. Soc.* **2005**, 127, 15304-15321.

45. Grushin, V. V.; Marshall, W. J., "The fluoro analog of Wilkinson's catalyst and unexpected Ph-Cl activation", *J. Am. Chem. Soc.* **2004**, 126, 3068-3069.

46. Marshall, W. J.; Grushin, V. V., "Unexpected outcome of the reaction of $[(COD)_2Rh_2(\mu\text{-}OH)_2]$ with TREAT HF or 50% HF. Peculiar structural features and diminished fluoride basicity of $[(R_3P)_4Rh_2(\mu\text{-}F)_2]$ (R = *i*-Pr, Ph)", *Organometallics* **2004**, 23, 3343-3347.

47. Marshall, W. J.; Grushin, V. V., "Synthesis, structure, and reductive elimination reactions of the first (σ-aryl)palladium complex stabilized by IPr N-heterocyclic carbene", *Organometallics* **2003**, 22, 1591-1593.

48. Kruis, D.; Markies, B. A.; Canty, A. J.; Boersma, J.; van Koten, G., "Selectivity in reductive elimination and organohalide transfer from

methyl(aryl)benzylpalladium(IV) complexes of bidentate nitrogen donor ligands, PdBrMe(Ar)(CH₂Ph)(L₂)", *J. Organomet. Chem.* **1997**, 532, 235-242.

49. Markies, B. A.; Canty, A. J.; de Graaf, W.; Boersma, J.; Janssen, M. D.; Hogerheide, M. P.; Smeets, W. J. J.; Spek, A. L.; van Koten, G., "Synthesis and structural studies of phenyl(iodo)- and methyl(phenyl)palladium(II) complexes of bidentate nitrogen donor ligands", *J. Organomet. Chem.* **1994**, 482, 191-199.

50. Sun, H.; DiMagno, S. G., "Anhydrous tetrabutylammonium fluoride", J. Am. Chem. Soc. **2005**, 127, 2050-2051.

51. Ball, N. D.; Sanford, M. S., "Synthesis and reactivity of a mono-σ-aryl palladium(IV) fluoride complex", *J. Am. Chem. Soc.* **2009**, 131, 3796-3797.

52. Ball, N. D.; Kampf, J. W.; Sanford, M. S., "Synthesis and reactivity of palladium(II) fluoride complexes containing nitrogen-donor ligands", *Dalton Trans.* **2010**, 39, 632-640.

53. Grushin, V. V.; Marshall, W. J., "Fluorination of nonactivated haloarenes via arynes under mild conditions, resulting from further studies toward Ar-F reductive elimination from palladium(II)", *Organometallics* **2008**, 27, 4825-4828.

54. Wang, B., "Functionalization of aromatic organic molecules with anhydrous fluorides and by reductive elimination from Iodine(III)", Ph. D. Thesis **2010**, University of Nebraska.

55. Grushin, V. V.; Marshall, W. J., "*trans*-Difluoro complexes of palladium(II)", *J. Am. Chem. Soc.* **2009**, 131, 918-919.

56. Grushin, V. V.; Marshall, W. J., "Unexpected H₂O-induced Ar-X activation with trifluoromethylplladium(II) aryls", *J. Am. Chem. Soc.* **2006**, 128, 4632-4641.

57. Cardenas, D. J.; Martin-Matute, B.; Echavarren, A. M., "Aryl transfer between Pd(II) centers or Pd(IV) intermediates in Pd-catalyzed Domino reactions", *J. Am. Chem. Soc.* **2006**, 5033-5040.

58. Ozawa, F.; Kurihara, K.; Fujimori, M.; Hidaka, T.; Toyoshima, T.; Yamamoto, A., "Mechanism of the cross-coupling reaction of phenyl iodide and methylmagnesium iodide catalyzed by *trans*-[PdPh(I)(PEt$_2$Ph)$_2$]", *Organometallics* **1989**, 8, 180-188.

59. Negishi, E.; Takahashi, T.; Akiyoshi, K., "Palladium-catalyzed or –promoted reductive C-C coupling. Effects of phosphines and carbon ligands", *J. Organomet. Chem.* **1987**, 334, 181-194.

60. Kaspi, A. W.; Yahav-Levi, A.; Goldberg, I.; Vigalok, A., "Xenon difluoride induced aryl iodide reductive elimination: A simple access to difluoropalladium(II) complexes", *Inorg. Chem.* **2008**, 47, 5-7.

61. Yahav, A.; Golberg, I.; Vigalok, A., "Synthesis of the elusive (R$_3$P)$_2$MF$_2$ (M = Pd, Pt) complexes", *J. Am. Chem. Soc.* **2003**, 125, 13634-13635.

62. Bartlett, N.; Lohmann, D. H., "Fluorides of the noble metals. III. Fluorides of platinum", *J. Chem. Soc.* **1964**, 619-626.

63. Rao, P. R.; Tressaud, A.; Bartlett, N., "The tetrafluorides of iridium, rhodium and palladium", From *Inorg. Nucl. Chem.* -Herbet, H. Hyman Mem. Vol. **1976**, 23-28. Edited by Katz, J. J.; Sheft, I.

64. Chapter 2 of this thesis.

65. Hollingworth, C.; Gouverneur, V., "Transition metal catalysis and nucleophilic fluorination", *Chem. Comm.* **2012**, 48, 2929-2942.

66. Gouverneur, V., "Flipping fluoride's reactivity", *Nat. Chem.* **2012**, 4, 152-154.

67. Furuya, T.; Kamlet, A. S.; Ritter, T., "Catalysis for fluorination and trifluoromethylation", *Nature* **2011**, 473, 470-477.

68. Vigalok, A., "Electrophilic fluorination of Group 10 organometallic complexes. Chemistry beyond oxidative addition", *Organometallics* **2011**, 30, 4802-4810.

69. Furuya, T.; Klein, J. E. M. N.; Ritter, T., "Carbon-fluorine bond formation for the synthesis of aryl fluorides", *Synthesis* **2010**, 11, 1804-1821.

70. Brown, J. M.; Gouverneur, V., "Transition-metal-mediated reactions for C_{sp}^2-F bond construction: The state of play", *Angew. Chem. Int. Ed.* **2009**, 48, 8610-8614.

71. Gouverneur, V., "A new departure in fluorination chemistry", *Science* **2009**, 325, 1630-1631.

72. Furuya, T.; Kutturf, C. A.; Ritter, T., "Carbon-fluorine bond formation", *Curr. Opin. Drug Disc. Dev.* **2008**, 11, 803-819.

73. Lee, E.; Hooker, J. H.; Ritter, T., "Nickel-mediated oxidative fluorination for PET with aqueous [^{18}F] fluoride", *J. Am. Chem. Soc.* **2012**, 134, 17456-17458.

74. Fier, P. S.; Hartwig, J. F., "Copper-mediated fluorination of aryl iodides", *J. Am. Chem. Soc.* **2012**, 134, 10795-10798.

75. Casitas, A.; Canta, M.; Sola, M.; Costas, M.; Ribas, X., "Nucleophilic aryl fluorination and aryl halide exchange mediated by a Cu^I/Cu^{III} catalytic cycle", *J. Am. Chem. Soc.* **2011**, 133, 19386-19392.

76. Lee, E.; Kamlet, A. S.; Powers, D. C.; Neumann, C. N.; Boursalian, G. B.; Furuya, T.; Choi, D. C.; Hooker, J. M.; Ritter, T., "A fluoride-derived

electrophilic late-stage fluorination reagent for PET imaging", *Science* **2011**, 334, 639-642.

77. Maimone, T. J.; Milner, P. J.; Kinzel, T.; Zhang, Y.; Takase, M. K.; Buchwald, S. L., "Evidence for *in situ* catalyst modification during the Pd-catalyzed conversion of aryl triflates to aryl fluorides", *J. Am. Chem. Soc.* **2011**, 133, 18106-18109.

78. Noel, T.; Maimone, T. J.; Buchwald, S. L., "Accelerating palladium-catalyzed C-F bond formation: Use of a microflow packed-bed reactor", *Angew. Chem. Int. Ed.* **2011**, 50, 8900-8903.

79. Watson, D. A.; Su, M.; Teveroviskiy, G.; Zhang, Y.; Garcia-Fortanet, J.; Kinzel, T.; Buchwald, S. L., "Formation of Ar-F from LPdAr(F): Catalytic conversion of aryl triflates to aryl fluorides", *Science* **2009**, 325, 1661-1664.

80. Tang, P. P.; Wang, W. K.; Ritter, T., "Deoxyfluorination of phenols", *J. Am. Chem. Soc.* **2011**, 133, 11482-11484.

81. Tang, P. P.; Ritter, T., "Silver-mediated fluorination of aryl silanes", *Tetrahedron* **2011**, 67, 4449-4454.

82. Tang, P. P.; Furuya, T.; Ritter, T., "Silver-catalyzed late-stage fluorination", *J. Am. Chem. Soc.* **2010**, 132, 12150-12154.

83. Furuya, T.; Benitez, D.; Tkatchouk, E.; Strom, A. E.; Tang, P. P.; Goddard III, W. A.; Ritter, T., "Mechanism of C-F reductive elimination from palladium(IV) fluorides", *J. Am. Chem. Soc.* **2010**, 132, 3793-3807.

84. Furuya, T.; Strom, A. E.; Ritter, T., "Silver-mediated fluorination of functionalized aryl stannanes", *J. Am. Chem. Soc.* **2009**, 131, 1662-1663.

85. Furuya, T.; Ritter, T., "Fluorination of boronic acids mediated by silver(I)triflate", *Org. Lett.* **2009**, 11, 2860-2863.

86. Furuya, T.; Kaiser, H. M.; Ritter, T., "Pd-mediated fluorination of arylboronic acids", *Angew. Chem. Int. Ed.* **2008**, 47, 5993-5996.

87. Furuya, T.; Ritter, T., "Carbon-fluorine reductive elimination from a high-valent palladium fluoride", *J. Am. Chem. Soc.* **2008**, 130, 10060-10061.

APPENDIX A

ADDITIONAL EXPERIMENTAL DATA FOR CHAPTER 1

Contents

Graphic	Pg.

165

Figure A13. Calibration curves for CO and CO2 built using gas chromatography (GC)   176

Figure A1. Changes in the ^{19}F NMR during the reaction of **1[Rh(III)]** with 1 atm CO in a pH 7 D2O solution with phosphate buffer. Spectra a – i were recorded during the course of 18 h of reaction and spectrum j was recorded after 38 h of reaction. Peaks: **1[Rh(III)]** at -140.8 ppm, **1[Rh-H]** at -139.5 ppm, **1[Rh(I)]** at -146.7 ppm, **1[Rh(II)]** dimer at -144.6 ppm and free fluoride at -123.1 ppm. Figure from Biffinger (Ref. 148, Chapter 1).
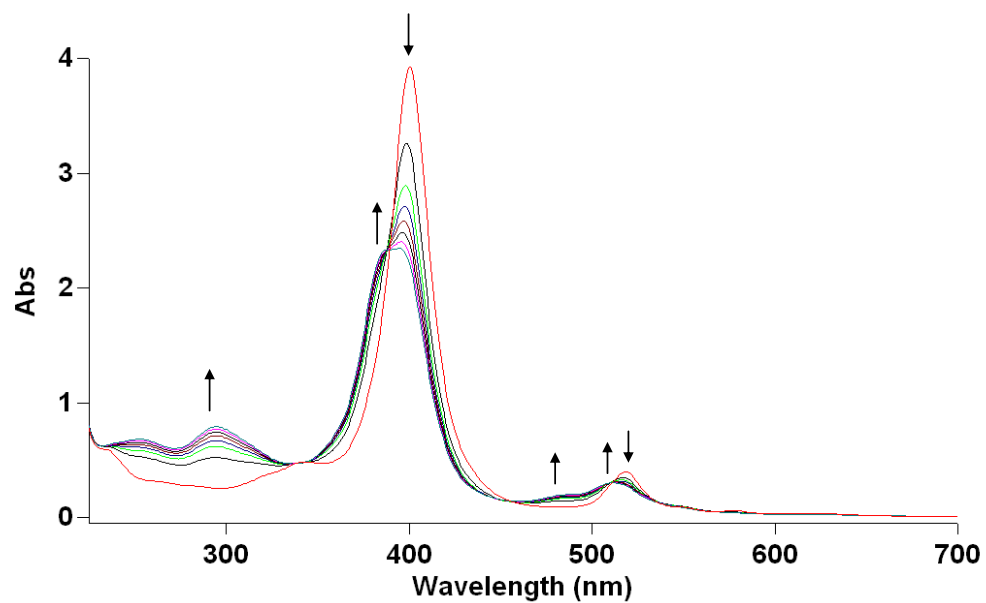
Figure A2. UV-vis profile of the reduction of **2[Rh(III)]** to **2[Rh(I)]** by 1 atm CO in a pH 13, 200 mM aq. phosphate buffer solution at 30 °C.[144] Figure from reference 144 (Chapter 1). Copyright 2011 ACS.

Table A1. Redox mediators tried for the oxidation of CO catalyzed by **2[Rh(III)]**[148]
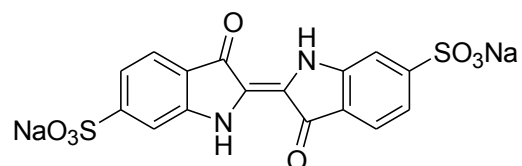
Indigo Carmine	
Methylene Green	
Methylene Blue	
Toluidine Blue O	
Phenazine Methylsulfate	
Methyl Viologen	
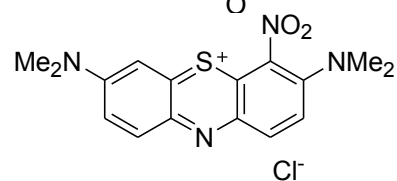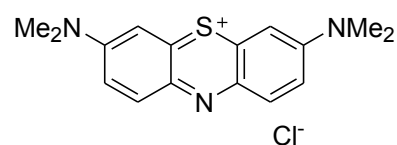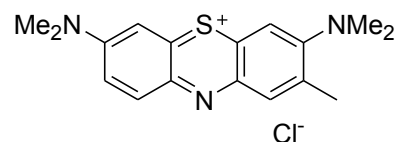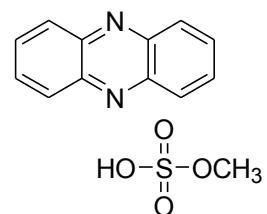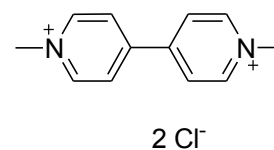
Table from Biffinger (Ref. 148, Chapter 1).

Figure A3. Cyclic Voltammograms (CVs) of the redox mediators in Table A1. Figure from Biffinger (Ref. 148, Chapter 1)
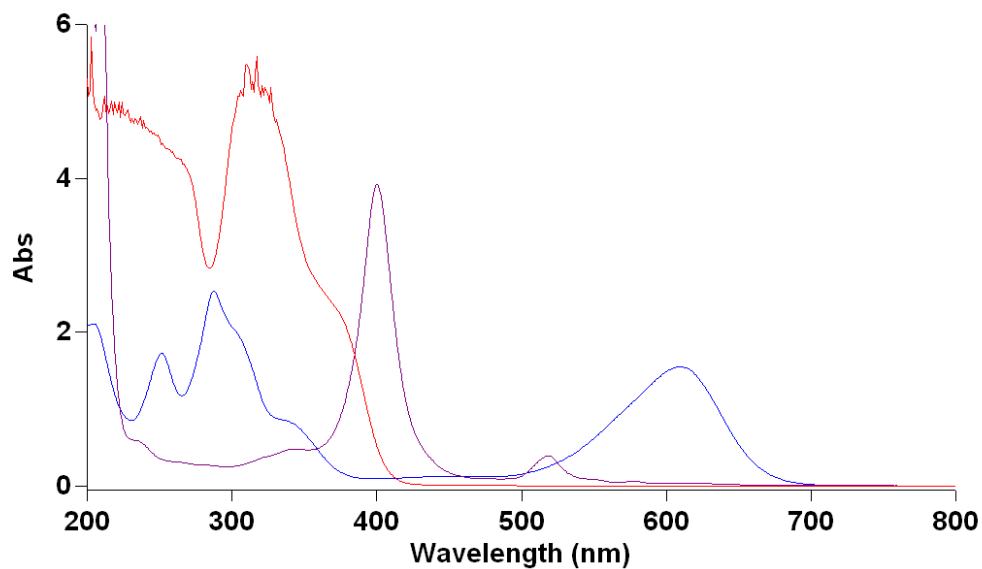
Figure A4. Overlaid UV-vis spectra of 0.064 mM indigo carmine, 0.064 leucoindigo, and 0.032 mM **2[Rh(III)]** in pH 4 phosphate buffer solution at 35 °C.[144] Figure from reference 144 (Chapter 1). Copyright 2011 ACS.
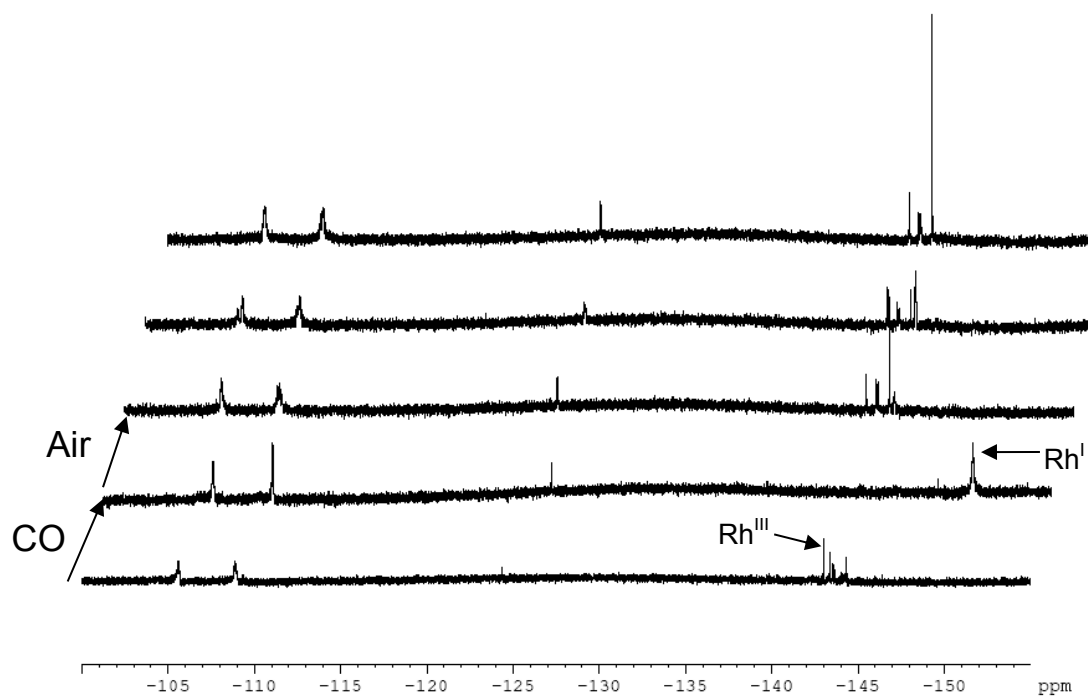
Figure A5. Changes in the ^{19}F NMR during the **2[Rh(III)]** (1 mM) catalyzed oxidation of 1 atm CO by indigo carmine (3 equiv.) at pH 4 (200 mM phosphate buffer) in D_2O. The top two spectra were taken after one and two more degassing/CO/air sequences respectively.
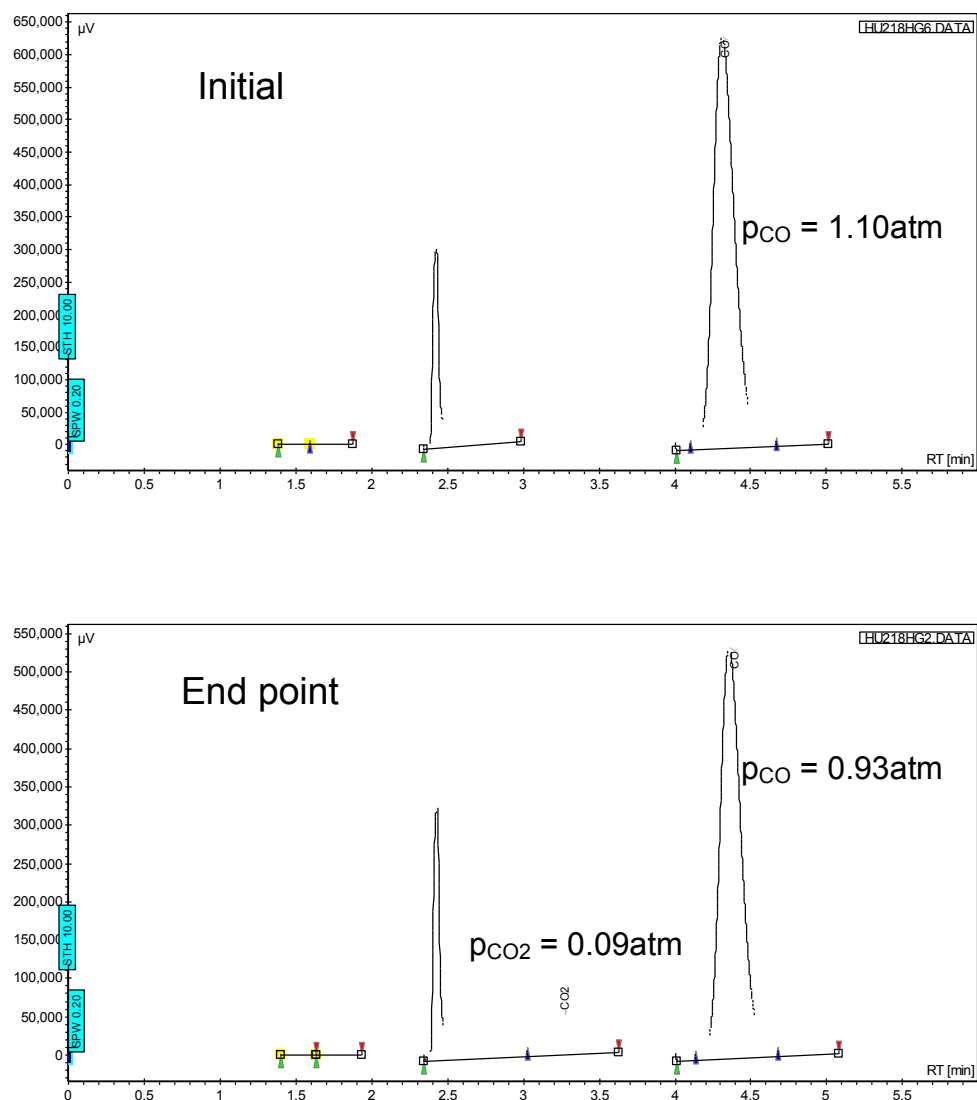
Figure A6. GC (Gas Chromatography) traces of head gas analysis of the **2[Rh(III)]** (1 mM) catalyzed oxidation of 1 atm CO by indigo carmine (10 equiv.) at pH 4 (phosphate buffer). Top trace – initial, immediately after charging the reaction with CO; bottom trace – at the end point indicated by the bleaching of indigo carmine. The peak at 2.45 min represents a pneumatic valve switch associated with instrument operation. The two tiny peaks between 1.4 min and 1.9 min are oxygen and nitrogen (from air) that were introduced during sampling and injection. A part of the CO_2 that is formed remains dissolved in solution and therefore does not show up in the head gas analysis. This is the reason for the decrease in CO partial pressure not being exactly equal to the increase in CO_2 partial pressure.

Table A2. Full data from Turnover Frequency (TOF) measurements at pH = 4 for the **2[Rh(III)]** catalyzed CO oxidation by indigo carmine (IC) at 1 atm pressure and 35 °C. Entries 9 – 22 represent the intermediate concentration range of **2[Rh(III)]** where CO diffusion is not rate limiting. Table adapted from reference 144 (Chapter 1). Copyright 2011 ACS.

Run	2[Rh(III)] (mM)	IC (mM)	Turnover No. TON	End pt. (min)	TOF$_{av}$ (TO min^{-1})	Corrected[a] TOF$_{av}$ (TO min^{-1})
1	1.0	1.0	1.0	3.5	0.28	
2	1.0	2.0	2.0	5.5	0.36	
3	1.0	5.0	5.0	6.5	0.77	
4	1.0	10.0	10.0	12.0	0.83	
5	0.50	1.0	2.0	3.5	0.57	
6	0.50	2.0	4.0	6.5	0.62	
7	0.50	5.0	10.0	13.0	0.77	
8	0.50	10.0	20.0	22.5	0.89	
9	0.25	1.0	4.0	5.0	0.80	
10	0.25	5.0	20.0	13.5	1.48	1.88
11	0.25	10.0	40.0	24.5	1.63	1.85
12	0.10	1.0	10.0	9.5	1.0	
13	0.10	2.0	20.0	15.0	1.33	1.82
14	0.10	5.0	50.0	31.0	1.61	1.86
15[b]	0.10	10.0	100.0	110.0	0.91	
16	0.050	0.50	10.0	11.5	0.87	
17	0.050	1.0	20.0	17.5	1.14	1.67
18	0.050	2.0	40.0	27.0	1.48	1.93
19[b]	0.050	5.0	100.0	110.0	0.91	
20	0.025	0.25	10.0	21.0	0.48	
21	0.025	0.50	20.0	26.0	0.77	2.0
22[b]	0.010	0.10	10.0	60.0	0.17	
23[b]	0.010	0.20	20.0	100.0	0.20	

a. The corrected TOF$_{av}$ is obtained by calculating the difference in TON (ΔTON/Δtime) for consecutive table entries run under the same conditions. This approach corrects for an initial induction period that arises from scrubbing of residual dissolved O_2. For example, the corrected TOF$_{av}$ for run 13 was calculated by using the difference in TON and the difference in end points between run 13 and run 12 [(20-10) / (15.0-9.5)].

b. The abnormally delayed end points observed in these runs are attributed to catalyst decomposition occurring to a significant extent at these low catalyst concentrations.

Table A3. Turnover Frequency (TOF) at pH = 7 for the **2[Rh(III)]** catalyzed CO oxidation by indigo carmine (IC) at 1 atm pressure and 35 °C. Table adapted from reference 144 (Chapter 1). Copyright 2011 ACS.

Run	2[Rh(III)] (mM)	IC (mM)	Turnover No. TON	End point (min)	TOF$_{av}$ (TO min^{-1})	Corrected[a] TOF$_{av}$ (TO min^{-1})
1	0.10	0.50	5	14.5	0.34	
2	0.10	1.0	10	24	0.42	0.52
3	0.10	2.0	20	46	0.43	0.48

a. Defined and calculated in the same way as for the data in Table A2.
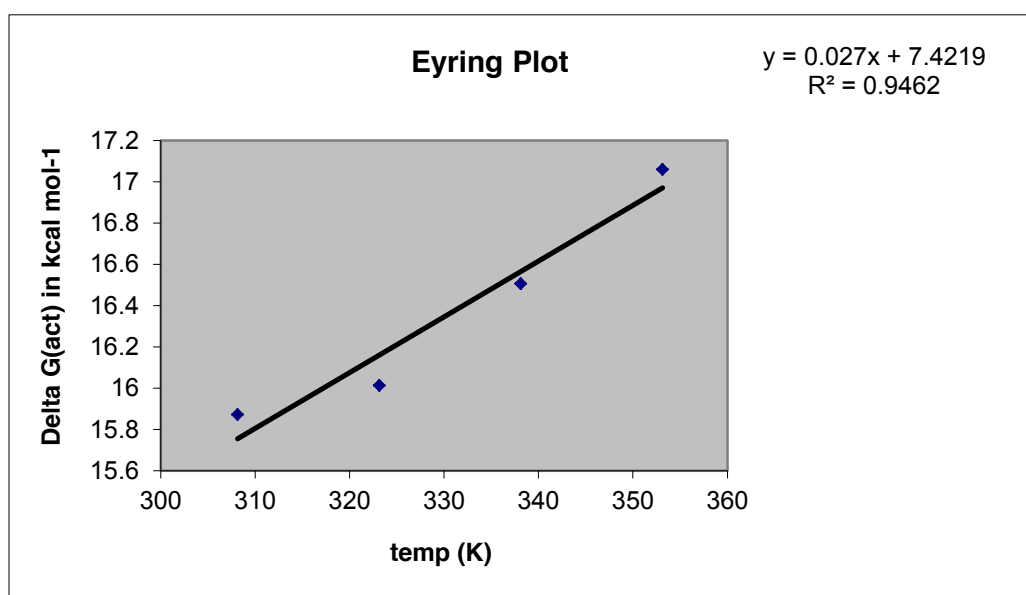
Figure A7. Eyring Plot of Variable Temperature Kinetic Measurements at pH = 4 for the **2[Rh(III)]** Catalyzed Oxidation of CO by Indigo Carmine

Table A4. Data for the Eyring Plot in Figure A7

Entry	Temperature (K)	2nd order rate constant, k (mol^{-1} s^{-1})	ΔG (kcal mol^{-1})
1	308.15	35.5	15.87
2	323.15	99.5	16.01
3	338.15	151.2	16.51
4	353.15	203.6	17.06
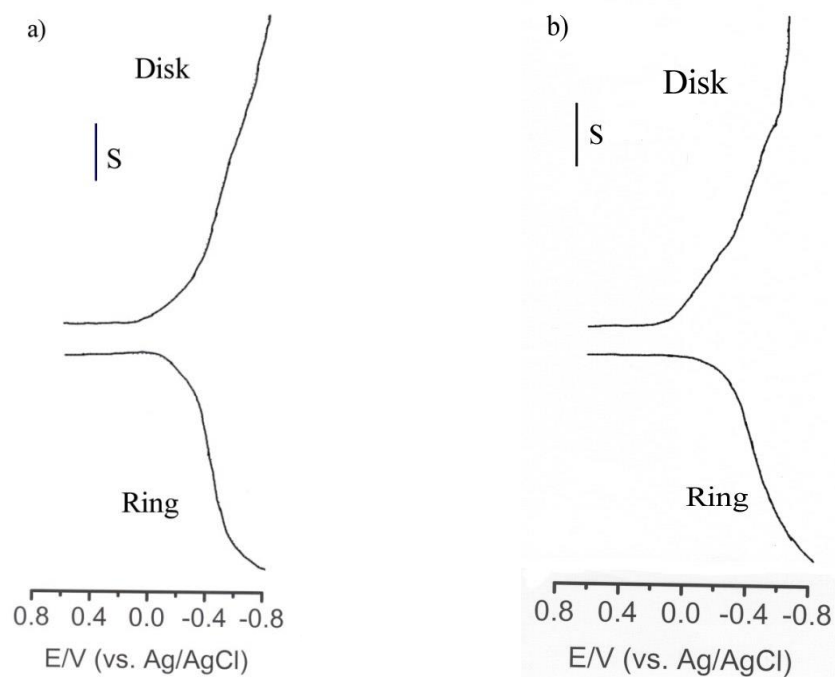
Figure A8. Rotating ring-disk voltammetry of the reduction of O_2 at a graphite disk electrode coated with a) **1[Rh(III)]** and b) **2[Rh(III)]**.[144] Figure from reference 144 (Chapter 1). Copyright 2011 ACS.
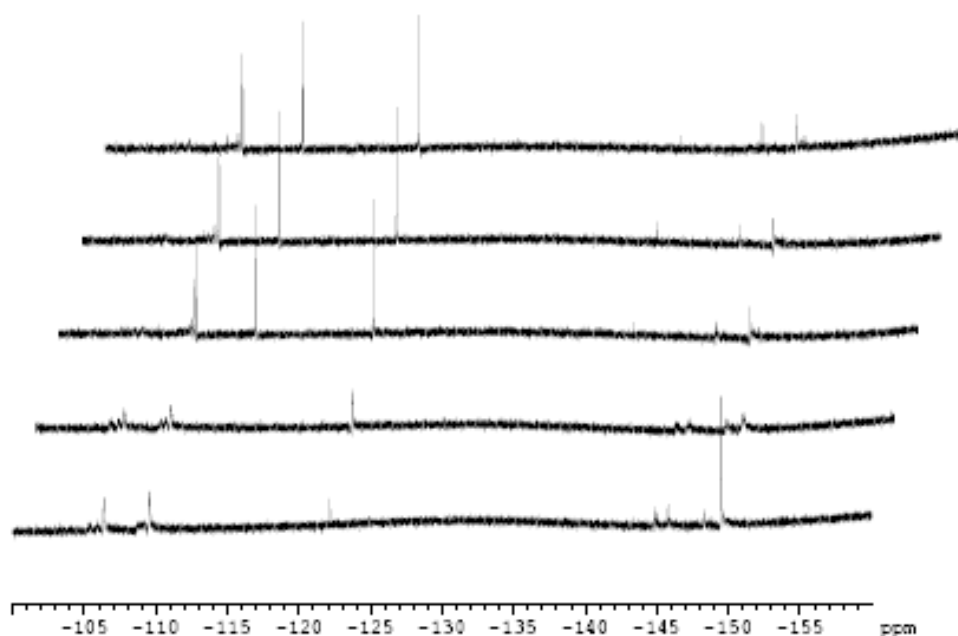
Figure A9. ^{19}F NMR monitoring of a control solution of 1 mM **2[Rh(III)]** + 10 μL of 30% H_2O_2 at pH 13 over two days. The initial spectrum is at the bottom and the final spectrum is at the top of the figure. The growth of the peak at -122 ppm indicates free fluoride liberated from the porphyrin periphery due to catalyst decomposition.[144 (Chapter 1)]
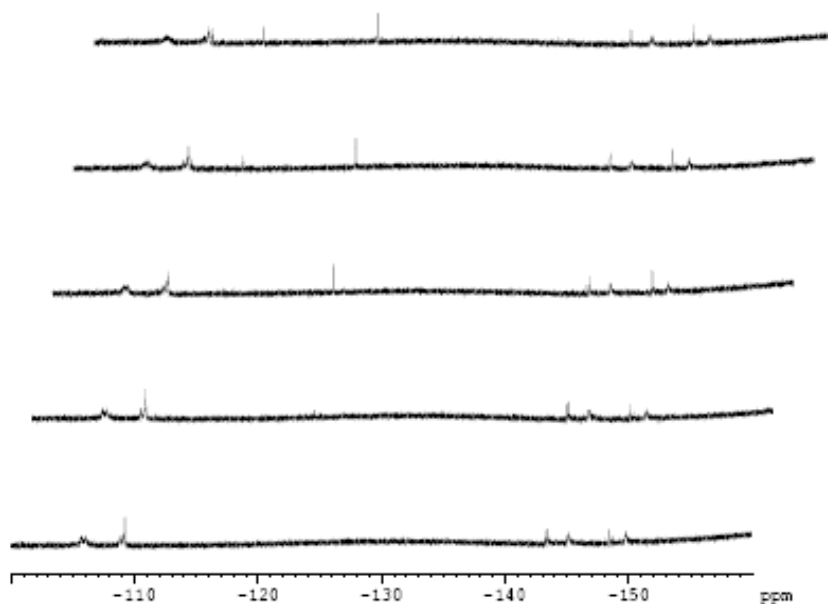
Figure A10. ^{19}F NMR monitoring of a control solution of 1 mM **2[Rh(III)]** + 10 μL of 30% H_2O_2 at pH 4 over two days. The initial spectrum is at the bottom and the final spectrum is at the top of the figure. The growth of the peak at -122 ppm indicates free fluoride liberated from the porphyrin periphery due to catalyst decomposition. It is much less at this pH.[144 (Chapter 1)] Copyright 2011 ACS.
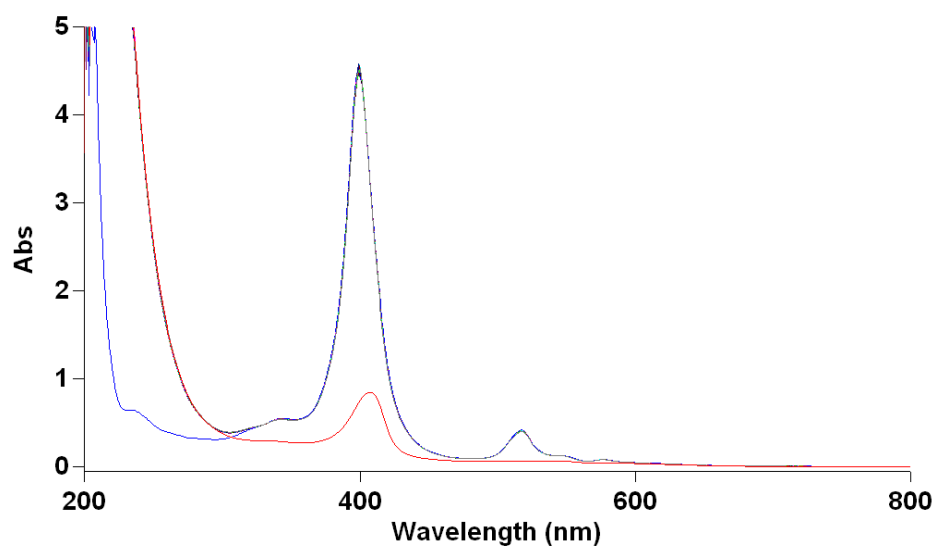
Figure A11. UV-Vis monitoring of a control solution of 0.025 mM **1[Rh(III)]** + 10 µL of 30% H_2O_2 at pH 13 over two days. The initial spectrum is in blue, the second spectrum (black) was recorded immediately after the addition of hydrogen peroxide. The final spectrum, recorded after two days, is shown in red. There is a lot of catalyst decomposition.[144 (Chapter 1)]
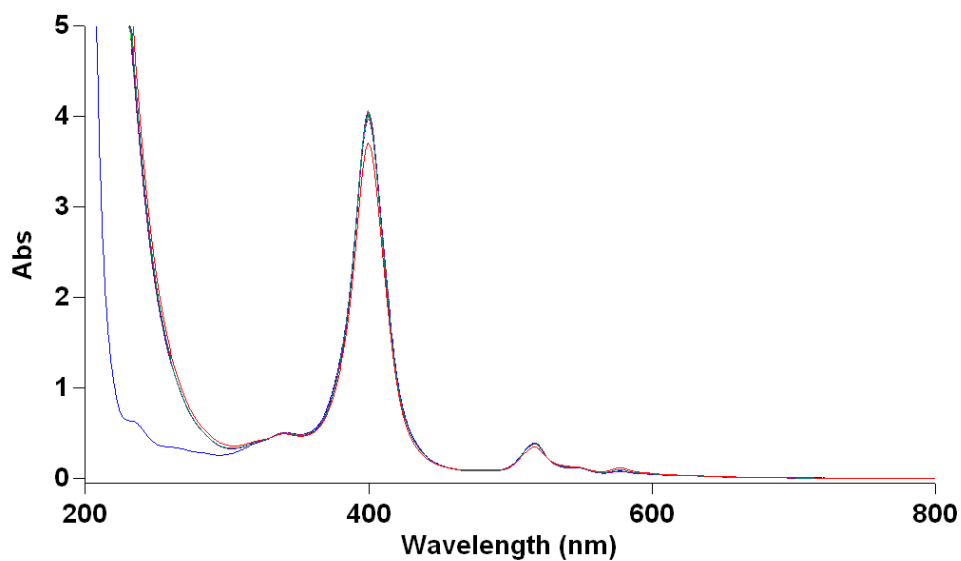
Figure A12. UV-Vis monitoring of a control solution of 0.025 mM **1[Rh(III)]** + 10 µL of 30% H_2O_2 at pH 4 over two days. The initial spectrum is in blue, the second spectrum (black) was recorded immediately after the addition of hydrogen peroxide. The final spectrum, recorded after two days, is shown in red. There is very little catalyst decomposition at this pH.[144 (Chapter 1)] Copyright 2011 ACS.
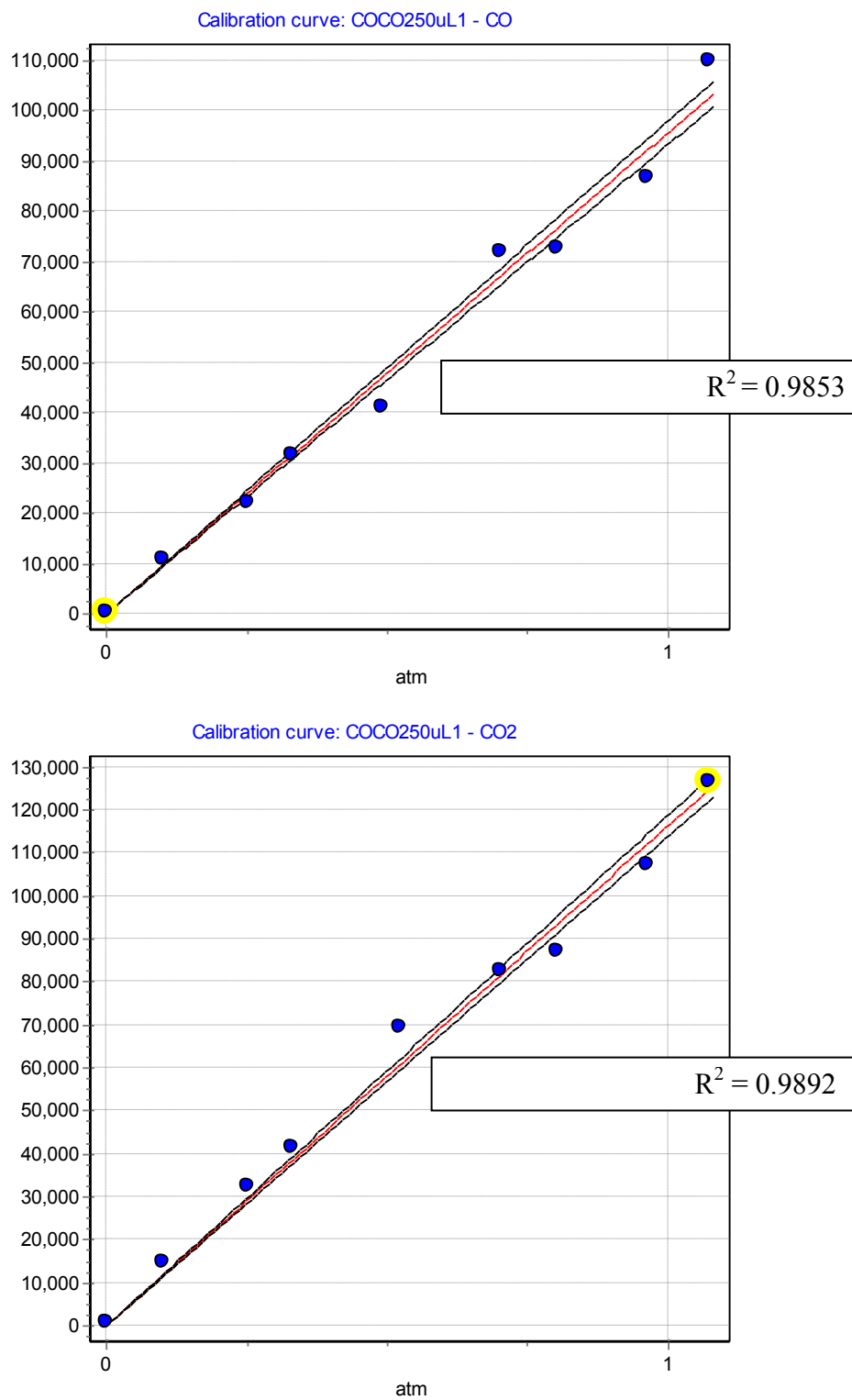
Figure A13. Calibration curves for CO and CO_2 built using gas chromatography (GC)

APPENDIX B

PROBING THE MECHANISM OF THE THERMAL DECOMPOSITION

OF

ARYL IODONIUM DIFLUORIDES

As mentioned in Chapter 2, Bijia Wang of our group examined the stability of phenyliodonium difluoride (PhIF$_2$) at room temperature and elevated temperatures, both in the absence and presence of excess fluoride (Chapter 2; references 24, 45, 46). In polar solvents like d$_3$-acetonitrile (CD$_3$CN), PhIF$_2$ completely decomposes to iodobenzene (phenyliodide, PhI) and bifluoride (DF$_2^-$). The decomposition process is accelerated by elevated temperatures and/or the presence of excess fluoride, but largely suppressed in nonpolar solvents like benzene. I made similar observations with 4-methoxyphenyliodonium difluoride (4-MeOC$_6$H$_4$-IF$_2$). A plausible mechanism for the above reduction of aryliodine(III) species to the corresponding iodoarenes/aryliodides (aryliodine(I)) involves a disproportionation pathway (Scheme B1). The transient aryliodine(V) species, PhIF$_4$, is a potent oxidant, which is rapidly reduced in the reaction mixture. It is known that polar, coordinating solvents and the uniquely hard ligand fluoride can stabilize higher oxidation states of transition metal ions. As mentioned in Chapter 2, Stang and coworkers have noted the similarities between transition metal and iodonium ion chemistries (Chapter 2; reference 36). With the approximation that iodine is a highly electronegative, large transition metal, it can be argued that polar, coordinating solvents like CD$_3$CN, and the strongly coordinating ligand fluoride promote the disproportionation of aryliodoniumdifluorides (ArIF$_2$).
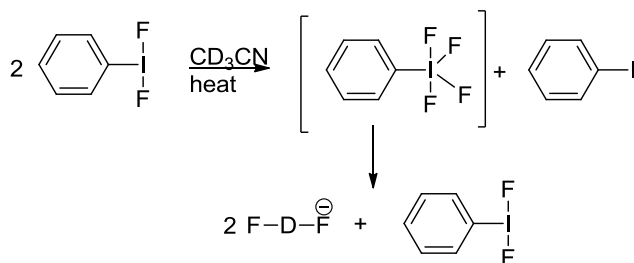
Scheme B1. Disproportionation Mechanism for the Decomposition of PhIF$_2$

Another plausible mechanism for the decomposition of aryliodoniumdifluorides in CD$_3$CN involves deprotonation of coordinated acetonitrile. Coordination of CD$_3$CN to the electronegative I(III) center of the aryliodoniumdifluoride acidifies the methyl proton, which can then be deprotonated by the potent, anhydrous fluoride to form DF$_2^-$. Subsequent reduction of the acetonitrile bound aryliodine(III) species gives the corresponding iodoarene (Scheme B2). If this mechanism is operative, and if deprotonation is the rate limiting step, a primary solvent kinetic isotope effect (KIE) must be observed for reactions performed in CH$_3$CN vs. CD$_3$CN.
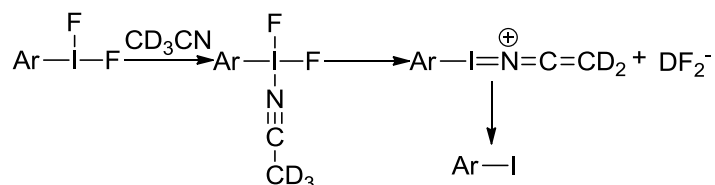
Scheme B2. Solvent Deprotonation Mechanism for the Decomposition of ArIF$_2$ in Acetonitrile

Kinetic studies were performed to test the above hypothesis. Solution samples of 4-methoxyphenyliodonium difluoride (4-MeOC$_6$H$_4$-IF$_2$) were prepared by mixing dry 4-methoxyphenyliodonium diacetate, 4-MeOC$_6$H$_4$-I(OAc)$_2$ (6.1 mg, 0.017 mmol) and anhydrous tetramethylammonium fluoride, TMAF (3.5 mg, 0.038 mmol) in the following dry, degassed solvents: a) 0.6 mL CD$_3$CN, and b) 0.52 mL CH$_3$CN + 0.08 mL CD$_3$CN (Scheme B3). Each sample was loaded into a J Young NMR tube and 1.5 µL of dry
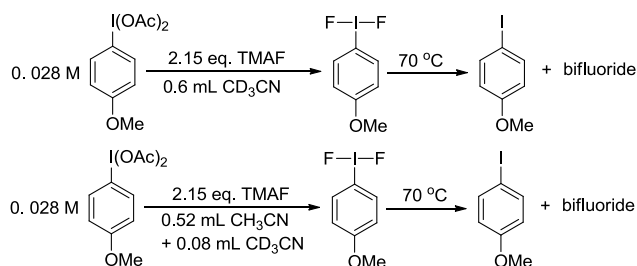
Scheme B3. Preparation and Kinetic Runs of 4-MeOC$_6$H$_4$-IF$_2$

benzene (C_6H_6) was added as an internal standard. The disappearance of 4-MeOC_6H_4-IF$_2$ at 70 °C was monitored by ^{1}H NMR spectroscopy (Figure B1) to generate a concentration vs. time profile (Figure B2). The small amount of CD$_3$CN was added to sample 'b' to lock to the NMR solvent and the CH$_3$CN signal was solvent suppressed. The data was fit to a first order (in 4-MeOC_6H_4-IF$_2$) kinetic model (Figure B3).

Figure B1. ^{1}H NMR of the Decomposition of ArIF$_2$ in CD$_3$CN
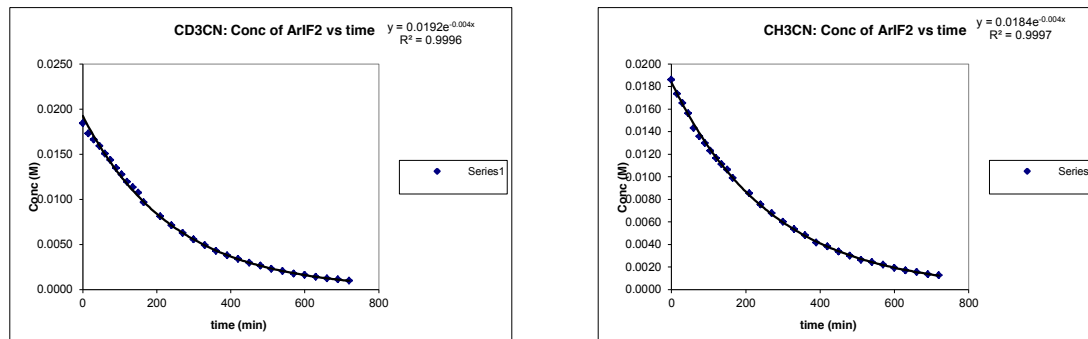
Figure B2. Concentration vs. Time Profiles of ArIF$_2$. Left: CD$_3$CN, Right: CH$_3$CN

Pseudo-first order rate constants (k_1') for kinetic runs 'a' and 'b' were determined to be 0.0041 min^{-1} and 0.0038 min^{-1} respectively. The corresponding first order rate constants (k_1) were $k_D = 0.0041$ min^{-1} and $k_H = 0.0043$ min^{-1}. The k_H/k_D was 1.05, which is not a significant KIE. Hence, deprotonation of coordinated acetonitrile is not the rate limiting step in the mechanism posited in Scheme B2.
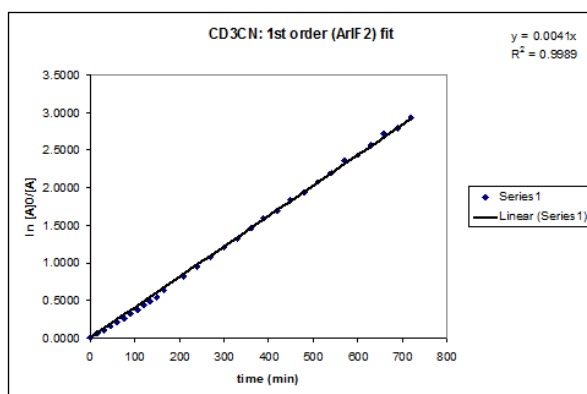
$k_1' = 0.0041$ min^{-1} (CD_3CN)
$k_1 = 0.0041$ min^{-1} (k_D)

$k_H / k_D = 1.05$

$k_1' = 0.0038$ min^{-1} (CH_3CN)
$k_1 = 0.0043$ min^{-1} (k_H)
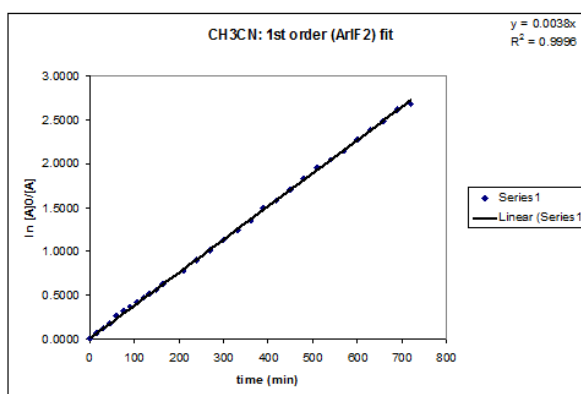
Figure B3. First Order ($ArIF_2$) Fit of Kinetic Data. Top: CD_3CN, Bottom: CH_3CN

APPENDIX C

FLUORIDE-PROMOTED LIGAND EXCHANGE IN

DIARYLIODONIUM SALTS

Portions of the text and certain graphics in this appendix have been reprinted (adapted) from the "Journal of Fluorine Chemistry, Volume 131, Wang, B.; Qin, L.; Neumann, K, D.; Uppaluri, S.; Cerny, R. L.; DiMagno, S. G., "Improved arene fluorination methodology for I(III) salts", Pages 1113-1121, Copyright 2010" (Reference 2), with permission from Elsevier. http://dx.doi.org/10.1016/j.jfluchem.2010.04.004. These items are appropriately cited in the body of the appendix.

Bijia Wang of our group reported[1,2] that diaryliodonium salts undergo rapid, fluoride-promoted aryl exchange reactions at room temperature in acetonitrile, and she studied the kinetics of the process by ^{1}H NMR spectroscopy. Text shown in quotes is drawn from reference 2 on which I am a coauthor. She showed that "treatment of symmetrical diaryliodonium hexafluorophosphate salts ($[Ar_1\text{-}I\text{-}Ar_2]PF_6$; $Ar_1 = Ar_2$) with 1 equiv. of tetramethylammonium fluoride (TMAF) in CD_3CN led to ion exchange and formation of the corresponding fluoride salts. This was evidenced by changes in the ^{19}F NMR spectrum.[1,2] Also, a general upfield shift of the signals in the aromatic region was observed in the ^{1}H NMR spectrum. In contrast, treatment of the unsymmetrically substituted ($Ar_1 \neq Ar_2$) diaryliodonium salt **1(PF$_6$)** (Chart C1) with 1 equiv. of TMAF
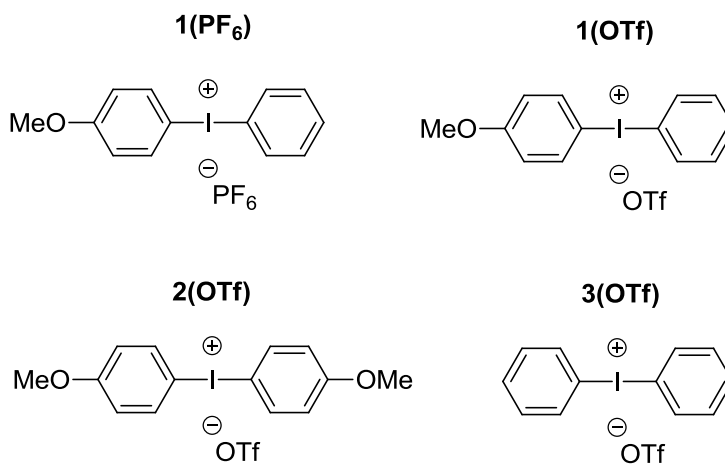
Chart C1. Diaryliodonium salts discussed in the work

under the same conditions led to a complex change in the spectrum and an apparent increase in the number of signals in the aromatic region.[1,2] Several potential explanations for this increase in complexity were considered (Scheme C1), including (a) formation of fluoride-bridged syn and anti dimers, (b) generation of T-shaped diastereomers with different aryl groups occupying the axial position, and (c) fast, fluoride-promoted aryl

ligand exchange resulting in the formation of three distinct diaryliodonium salts." Wang

adduced experimental evidence that ruled out the formation of dimers.[1,2] "The fluoride
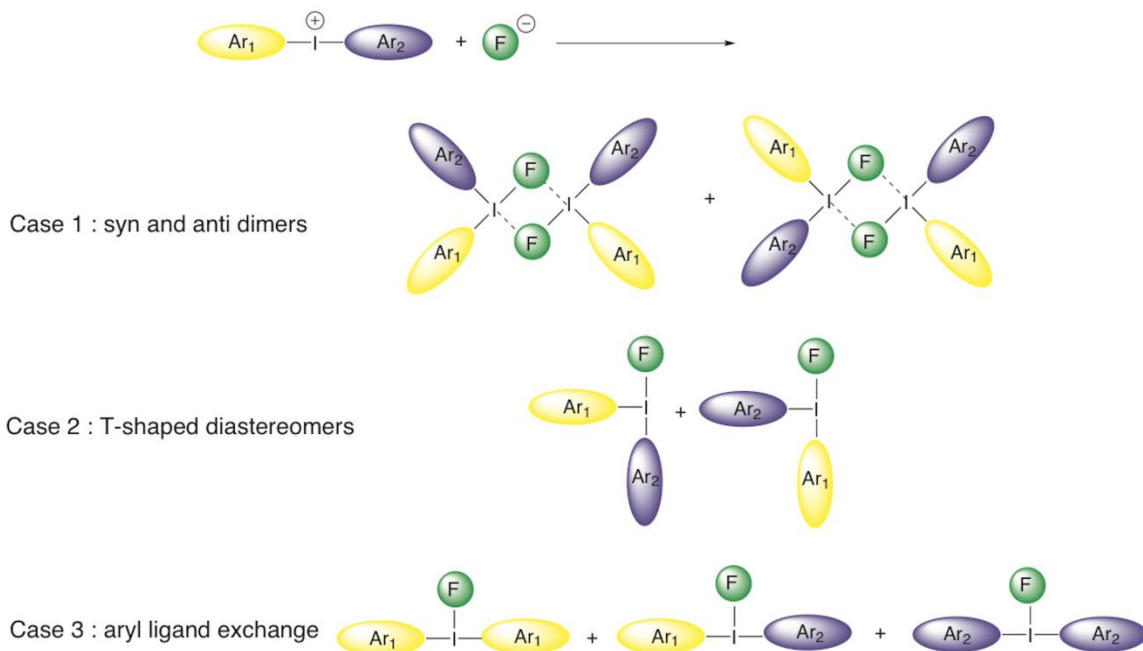
Scheme C1. Possible origins of the additional complexity observed in the ^{1}H NMR spectrum of **1(PF$_6$)** after the addition of fluoride. From reference 2. Copyright Elsevier.

salt obtained by treatment of **1(PF$_6$)** with TMAF was further reacted with TMSOTf

(TMS = trimethylsilyl; OTf = triflate = trifluoromethane sulfonate) to generate the I(III)

triflates and to remove the fluoride in the form of gaseous TMSF. Even after all traces of

fluoride were removed, the ^{1}H NMR spectrum remained complex and distinct from that

of **1(OTf)** (Chart C1), that I prepared using a different synthetic route. Thus the

formation of dimers as a possible origin of the observed spectral complexity could be

excluded."

"To examine whether the addition of fluoride had promoted the formation of two

different T-shaped diastereomers, we independently synthesized **1(OTf)**, **2(OTf)** and

3(OTf) (Chart C1)." While I prepared **1(OTf)** and **2(OTf)**, **3(OTf)** was prepared by

Jayson Kempinger of our group. Dr. Ronald Cerny of the Nebraska Center for Mass
Spectrometry subjected the above triflate salts to ES-MS analysis.[2] "The pure salt **1(OTf)**
gave a single, clean cationic peak of m/z = 310.7 (M$^+$ - OTf). Similarly, **2(OTf)** and
3(OTf) gave cation peaks of m/z = 340.7 and 280.7 respectively, indicating that these
three compounds did not undergo any aryl exchange reactions during the electrospray
ionization process in the mass spectrometer. In contrast, a preparation of the triflate salt
1(OTf) (by B. Wang) that had been previously exposed to fluoride ion (**1(PF₆)** treated
with TMAF, followed by TMSOTf addition) gave three cation peaks of m/z = 280.7,
310.7 and 340.7, indicating the presence of three distinct diaryliodonium salts (Figure
C1)."
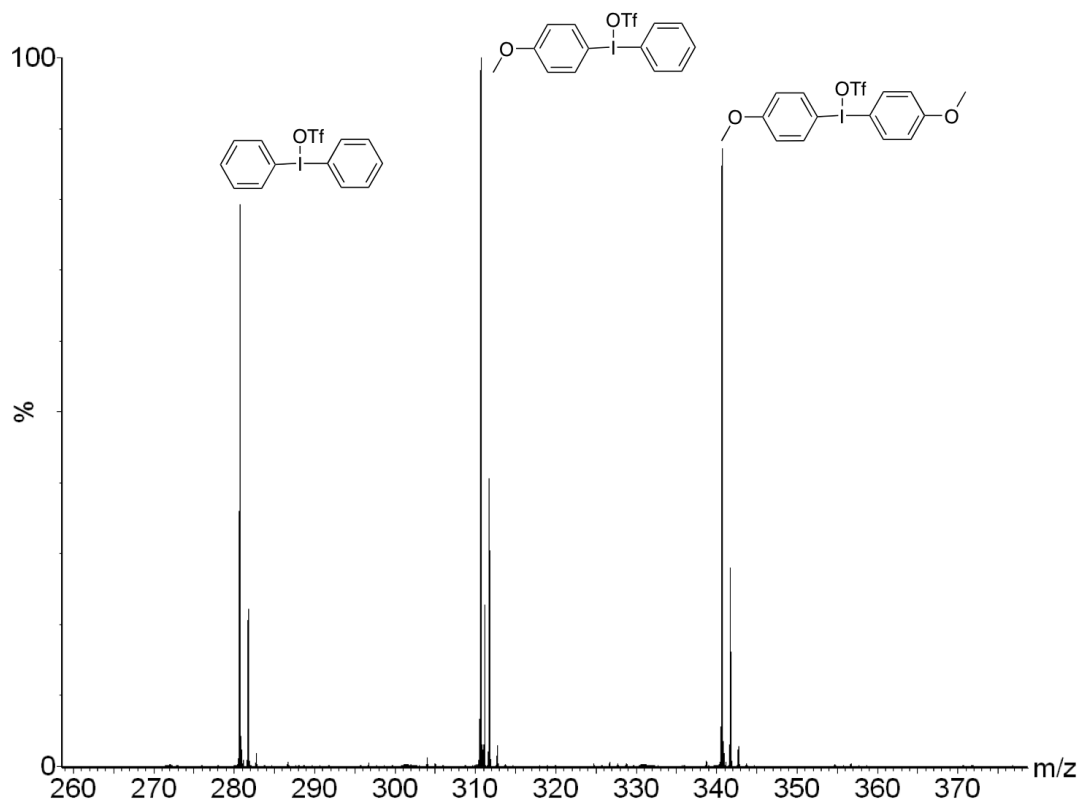
Figure C1. ES-MS of **1(OTf)** obtained by treating **1(PF₆)** with TMAF followed by
TMSOTf. From reference 2. Copyright Elsevier.

"MS-MS analysis of these ions indicated that the principal decomposition product was the corresponding biaryl formed by extrusion of iodine. The ES-MS data are consistent with the formation of three different diaryliodonium salts upon the treatment of unsymmetrical diaryliodonium salts with fluoride in solution, and definitively exclude the formation of different T-shaped diastereomers as a possible origin of the complexity observed by NMR spectroscopy. Treatment of **1(OTf)** with 1 equiv. of TMAF in CD_3CN also led to rapid exchange of aryl ligands, indicating that the weakly coordinating PF_6^- and ⁻OTf anions behave similarly under these conditions. All data support a remarkably rapid, fluoride-promoted aryl exchange reaction for unsymmetrically substituted diaryliodonium salts, and the presence of an equilibrated mixture of three distinct diaryliodonium fluorides in solution."

Preparation of Diaryliodonium triflates

The diacetoxyiodobenzene used here was prepared using the method reported in Chapter 2. The diaryliodonium triflates were prepared using/adapting a reported procedure.[3]

1. Phenyl(4-methoxyphenyl)iodonium triflate, **1(OTf)**:

Prepared by Uppaluri.[2,3] To a stirred suspension of diacetoxyiodobenzene (660 mg, 2.1 mmol) in 10 mL dry methylene chloride at 0 ºC under N_2, trifluoromethane sulfonic acid (triflic acid) (0.36 mL, 4.1 mmol) was added dropwise via syringe. The mixture was stirred at 0 ºC for 5 min and then at room temperature for 1 h. The resulting clear yellow solution was cooled to 0 ºC and anisole (0.25 mL, 2.3 mmol) was added dropwise via syringe. The resulting blue colored solution was stirred at 0 ºC for 5 min

and then at room temperature for 30 min. The volatiles were removed *in vacuo* to obtain a dark brown oil which was triturated with diethyl ether. The solvent was removed *in vacuo* to obtain an off white solid which was triturated with diethyl ether. The solid was collected by filtration and washed with diethyl ether to yield the product **1(OTf)** as a colorless, fine powdery solid. Recrystallization was performed by layering diethyl ether over a solution of **1(OTf)** in methylene chloride to give colorless, needle like crystals (651 mg, 70.7%). ^{1}H NMR (500 MHz, CD$_3$CN, 25 ºC): δ 8.042 (d, J = 8.5 Hz, 2H, H2/H6), 8.017 (d, J = 9.1 Hz, 2H, H2'/H6'), 7.690 (t, J = 7.6 Hz, 1H, H4), 7.524 (t, J = 8.0 Hz, 2H, H3/H5), 7.055 (d, J = 9.1 Hz, 2H, H3'/H5'), 3.835 (s, 3H, OMe). ^{13}C NMR (125 MHz, CD$_3$CN, 25 ºC): δ 164.67 (C4'), 139.02 (C2'/C6'), 136.23 (C2/C6), 134.14 (C4), 133.66 (C3/C5), 122.37 (q, J_{C-F} = 320.9 Hz, CF$_3$SO$_3^-$), 119.47 (C3'/C5'), 115.49 (C1), 102.80 (C1'), 57.06 (OMe). ^{19}F NMR (376 MHz, CD$_3$CN, 25 ºC): δ -79.29 (s, CF$_3$SO$_3^-$).

2. Diphenyliodonium triflate, **3(OTf)**:

Prepared by Uppaluri.[2,3] To a stirred suspension of diacetoxyiodobenzene (660 mg, 2.1 mmol) in 10 mL dry methylene chloride at 0 ºC under N$_2$, triflic acid (0.36 mL, 4.1 mmol) was added dropwise via syringe. The mixture was stirred at 0 ºC for 5 min and then at room temperature for 1 h. The resulting clear yellow solution was cooled to 0 ºC and benzene (0.37 mL, 4.1 mmol) was added dropwise via syringe. The resulting solution was stirred at 0 ºC for 5 min and then at room temperature for 30 min. The volatiles were removed *in vacuo* to obtain a crude brown solid which was triturated with diethyl ether. The solid was collected by filtration and washed with diethyl ether to yield the product **3(OTf)** as a light brown flaky solid. Recrystallization was performed by layering diethyl

ether over a solution of **3(OTf)** in methylene chloride to give colorless, needle like crystals (726 mg, 82.4%). ^{1}H NMR (500 MHz, CD$_3$CN, 25 ºC): δ 8.091 (d, J = 8.2 Hz, 4H, H2/H2'/H6/H6'), 7.710 (t, J = 7.6 Hz, 2H, H4/H4'), 7.540 (t, J = 7.9 Hz, 4H, H3/H3'/H5/H5'). ^{13}C NMR (125 MHz, CD$_3$CN, 25 ºC): δ 136.75 (C2/C2'/C6/C6'), 134.33 (C4/C4'), 133.76 (C3/C3'/C5/C5'), 122.34 (q, J$_{C-F}$ = 321.0 Hz, CF$_3$SO$_3^-$), 114.84 (C1/C1'). ^{19}F NMR (376 MHz, CD$_3$CN, 25 ºC): δ -79.33 (s, CF$_3$SO$_3^-$).

3. Bis(4-methoxyphenyl)iodonium triflate, **2(OTf)**:

Prepared by Jayson Kempinger.[2,3] In a flame-dried 25 mL Schlenk flask charged with N$_2$, 1-(diacetoxyiodo)-4-methoxybenzene (753.0 mg, 2.13 mmol) was dissolved in 7 mL dry methylene chloride. With stirring, anisole (0.93 mL, 8.52 mmol) was added by syringe. The solution was cooled to -10 ˚C in a sodium chloride-ice bath. To this solution, triflic acid (0.21 mL, 2.3 mmol) was added dropwise over the course of 10 minutes by syringe. A deep blue color was immediately observed upon addition. After addition, the solution was allowed to warm slowly to room temperature overnight. The volatiles were removed *in vacuo* to obtain a crude solid. The solid was redissolved in methylene chloride and precipitated with a 10% solution of ether in hexanes to yield bis(4-methoxyphenyl)iodonium triflate as a colorless solid. Recrystallization was performed by layering diethyl ether over a solution of **2(OTf)** in methylene chloride to give colorless, needle like crystals (729.6 mg, 69.5%). ^{1}H NMR (400 MHz, CD$_3$CN, 25 ˚C): δ 7.981 (d, J = 8.8 Hz, 2H, H2/H2'/H6/H6'), 7.038 (d, J = 8.8 Hz, 2H, H3/H3'/H5/H5'), 3.829 (*s*, 3H, OMe). ^{13}C NMR (100 MHz, CD$_3$CN, 25 ˚C): δ 164.258 (C4/C4'), 138.280 (C2/C2'/C6/C6'), 122.148 (q, J = 320.8 Hz, CF$_3$SO$_3^-$), 119.066 (C3/C3'/C5/C5'),

103.383 (C1/C1'), 56.772 (OMe). ^{19}F NMR (376 MHz, CD$_3$CN, 25 ˚C): δ -79.249 (s,

CF$_3$SO$_3^-$).

References

1. Wang, B., "Functionalization of aromatic organic molecules with anhydrous fluorides and by reductive elimination from iodine(III)", Ph.D. Thesis **2010**, University of Nebraska.

2. Wang, B.; Cerny, R. L.; Uppaluri, S.; Kempinger, J. J.; DiMagno, S. G., "Fluoride-promoted ligand exchange in diaryliodonium salts", J. Fluorine Chem. **2010**, 131, 1113-1121.

3. Kitamura, T.; Matsuyuki, J.; Taniguchi, H., "Improved preparation of diaryliodonium triflates", *Synthesis* **1994**, 147-148.

APPENDIX D

THERMOLYSIS OF DIARYLIODONIUM TRIFLATES

I investigated the thermal decomposition of a set of four diaryliodonium triflates (salts **1-4**) in benzene as the solvent. The synthesis of **1**, **3** & **4** was reported in Appendix C. I prepared **2** using a procedure similar to the synthesis of **1** & **3**. The results of the thermolysis reactions are presented in Scheme D1. Product yields/distribution were determined by ^{1}H NMR.
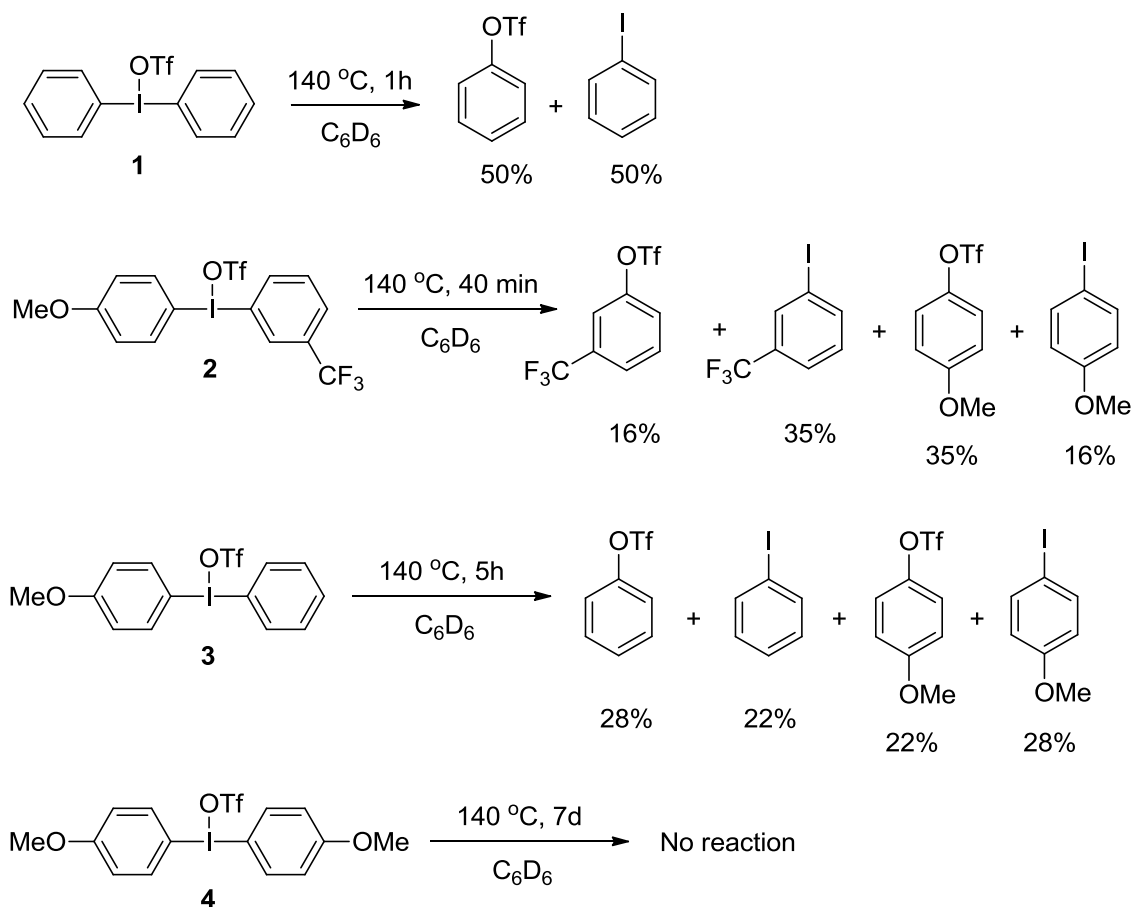
Scheme D1. Thermolysis of diaryliodonium triflates in d_6-benzene

From the results, it is evident that faster reaction times are observed for more electron rich diaryliodonium triflates. Similar trends were observed by Bijia Wang[1] for the decomposition of diaryliodonium salts featuring other counterions/nucleophiles such as halides, azide etc. The exceptional thermal stability of the diaryliodonium triflate, **4**,

which features para-methoxy substituents on the aryl rings is of relevance to the material discussed in Appendix E.

References

1. Wang, B., "Functionalization of aromatic organic molecules with anhydrous fluorides and by reductive elimination from iodine(III)", Ph.D. Thesis **2010**, University of Nebraska.

APPENDIX E

ATTEMPTS AT OXIDATIVE ADDITION OF ARYLIODINE

194

As mentioned in Chapter 2, Stang and coworkers have noted the similarities between iodonium ion and transition metal chemistries (Reference 36, Chapter 2). Iodine resembles the late transition metals in terms of its Pauling electronegativity, atomic radius and variable oxidation states. Hence, iodine can be approximated to be a rather highly electronegative late transition metal. As a consequence, reductive elimination of weakly basic ligands can occur from diaryliodonium salts to form iodoarene and a functionalized arene (as discussed in Chapter 2). 'Transmetalation' (of aryl groups) also occurs with ease at I(III) centers of diaryliodonium salts (Reference 49, Chapter 2). Late transition metals like palladium are known to undergo oxidative addition into Ar-X bonds (X = halogen, OTf). However, oxidative addition of aryliodine into an Ar-X bond has not been reported to date. Hence, we decided to carry out experiments to see if the oxidative addition reaction is possible for aryliodine. Scheme E1 shows the reactions envisaged for a given experiment in which Ar^1-I (an electron rich aryl iodide), Ar^2-X (Ar^2 = electron poor; X = I or OTf), and MY are used as the starting materials. Oxidative addition of the aryliodine in Ar^1-I into Ar^2-X will result in the diaryliodonium salt **1(X)**. Transmetalation of **1(X)** with M^+Y^- will lead to the formation of the diaryliodonium salt **1(Y)**. Reductive elimination can occur from both **1(X)** and **1(Y)** and will result in a scrambling of the aryl groups. Table E1 summarizes the experiments that I carried out.
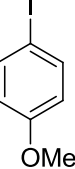
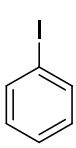**Scheme E1.** Reactions envisaged for a given experiment
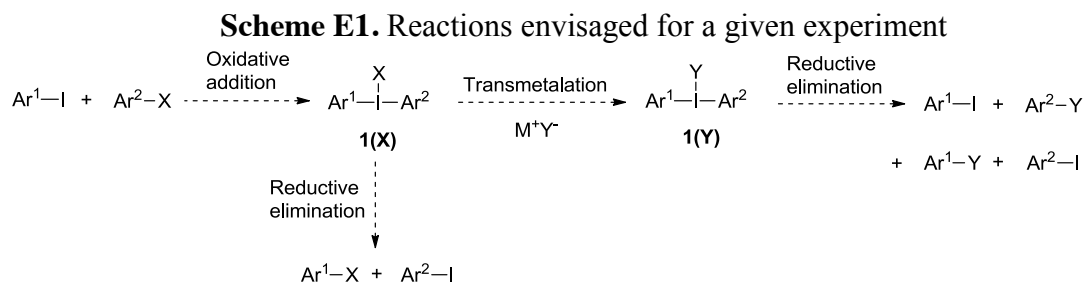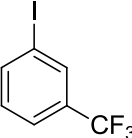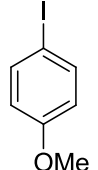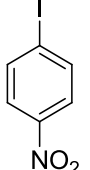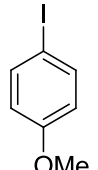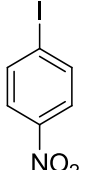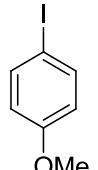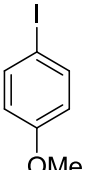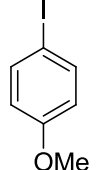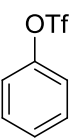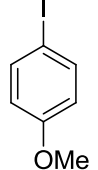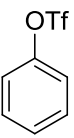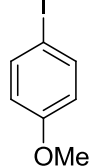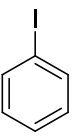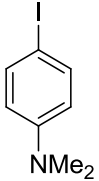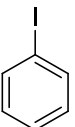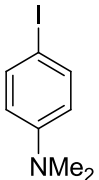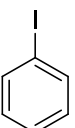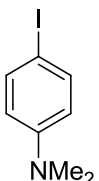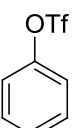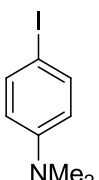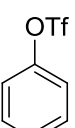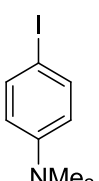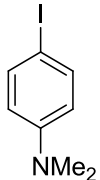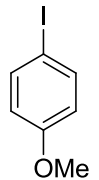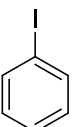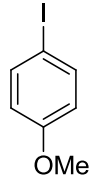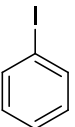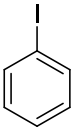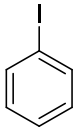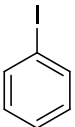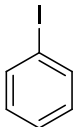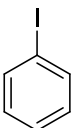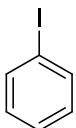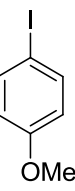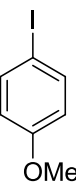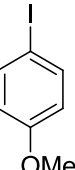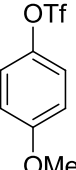
Table E1. Experiments toward oxidative addition of aryliodine

Expt. No.	Ar^1-I	Ar^2-X	MY	Solvent	Temperature
1			TBAOAc	C$_6$D$_6$	rt to 140 °C
2			TBAOAc	C$_6$D$_6$	rt to 140 °C
3			KOAc	DMSO-d$_6$	rt to 180 °C
4			TBAOAc	C$_6$D$_6$	rt to 140 °C
5			TBABr	C$_6$D$_6$	rt to 140 °C
6			TBABr	DMSO-d$_6$	rt to 180 °C
7			CsCl	None	rt to 200 °C

196

#	Aryl halide 1	Aryl halide 2	Additive	Solvent	Temperature
8	4-iodo-N,N-dimethylaniline	iodobenzene	KOTf	None	rt to 200 °C
9	4-iodo-N,N-dimethylaniline	iodobenzene	KOAc	None	rt to 200 °C
10	4-iodo-N,N-dimethylaniline	phenyl OTf	None	C_6D_6	rt to 140 °C
11	4-iodo-N,N-dimethylaniline	phenyl OTf	CF_3COOK	C_6D_6	rt to 140 °C
12	4-iodo-N,N-dimethylaniline	4-iodo-N,N-dimethylaniline	KOTf	C_6D_6	rt to 140 °C
13	4-iodoanisole (OMe)	iodobenzene	CF_3COOK	None	rt to 200 °C
14	4-iodoanisole (OMe)	iodobenzene	CF_3COOK	N-Methyl pyrrolidine	rt to 200 °C

197

15			TMAF	CD$_3$CN	rt to 140 °C
16			TMAF	DMSO-d$_6$	rt to 180 °C
17			CsF	DMSO-d$_6$	rt to 180 °C
18	OMe	OMe	CsF	DMSO-d$_6$	rt to 180 °C
19	OMe		CsF	DMSO-d$_6$	rt to 180 °C
20	OMe	OTf OMe	None	C$_6$D$_6$	rt to 140 °C

The experiments were carried out in sealed NMR tubes under a nitrogen atmosphere, and were monitored by ^{1}H and ^{19}F NMR spectroscopy and GC-MS. In no case was there evidence of the envisaged reactions. In entry number 20, oxidative addition would lead to the diaryliodonium salt, bis(4-methoxyphenyl)iodonium triflate. In Appendix D, I reported that this salt was exceptionally thermally stable, and hence the motivation to prepare this salt. The putative reaction (oxidative addition) involving the

aryl iodide and aryl triflate reactants to go to the diaryliodonium triflate product should be thermodynamically favorable. However, since there was no evidence of product formation, it can be surmised that the reaction has an activation barrier that cannot be surmounted at the experimental temperature. Finally, the reactions shown in Scheme E2 were attempted in C_6D_6 (rt to 140 °C) and DMSO-d_6 (rt to 180 °C). Oxidative addition of iodine of the aryl iodide into the Ar-I bond of the diaryliodonium, followed by elimination of the product aryliodide would lead to the formation of the product diaryliodonium salt. The product aryliodide would function as a "super" leaving group in the mechanism. Once again, there was no evidence of the proposed reactions.
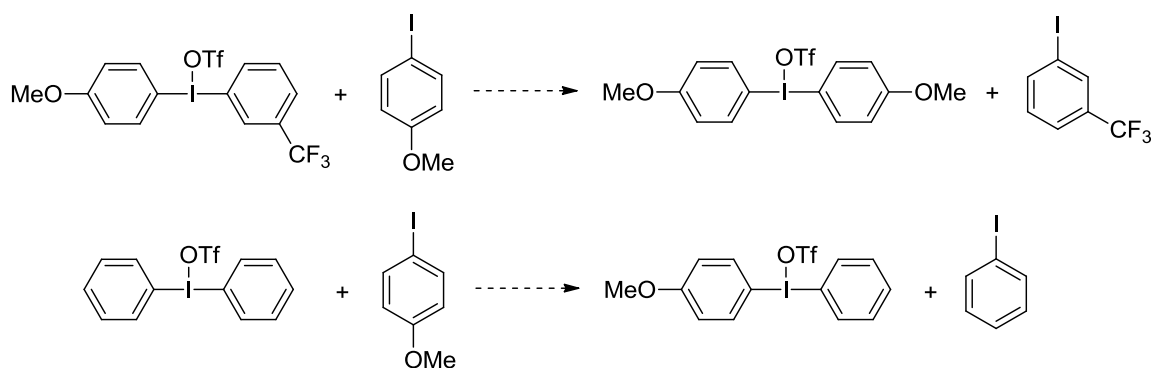
Scheme E2. Attempted oxidative addition reactions

APPENDIX F

ADDITIONAL EXPERIMENTAL DATA FOR CHAPTER 3

Contents

Graphic	Pg.

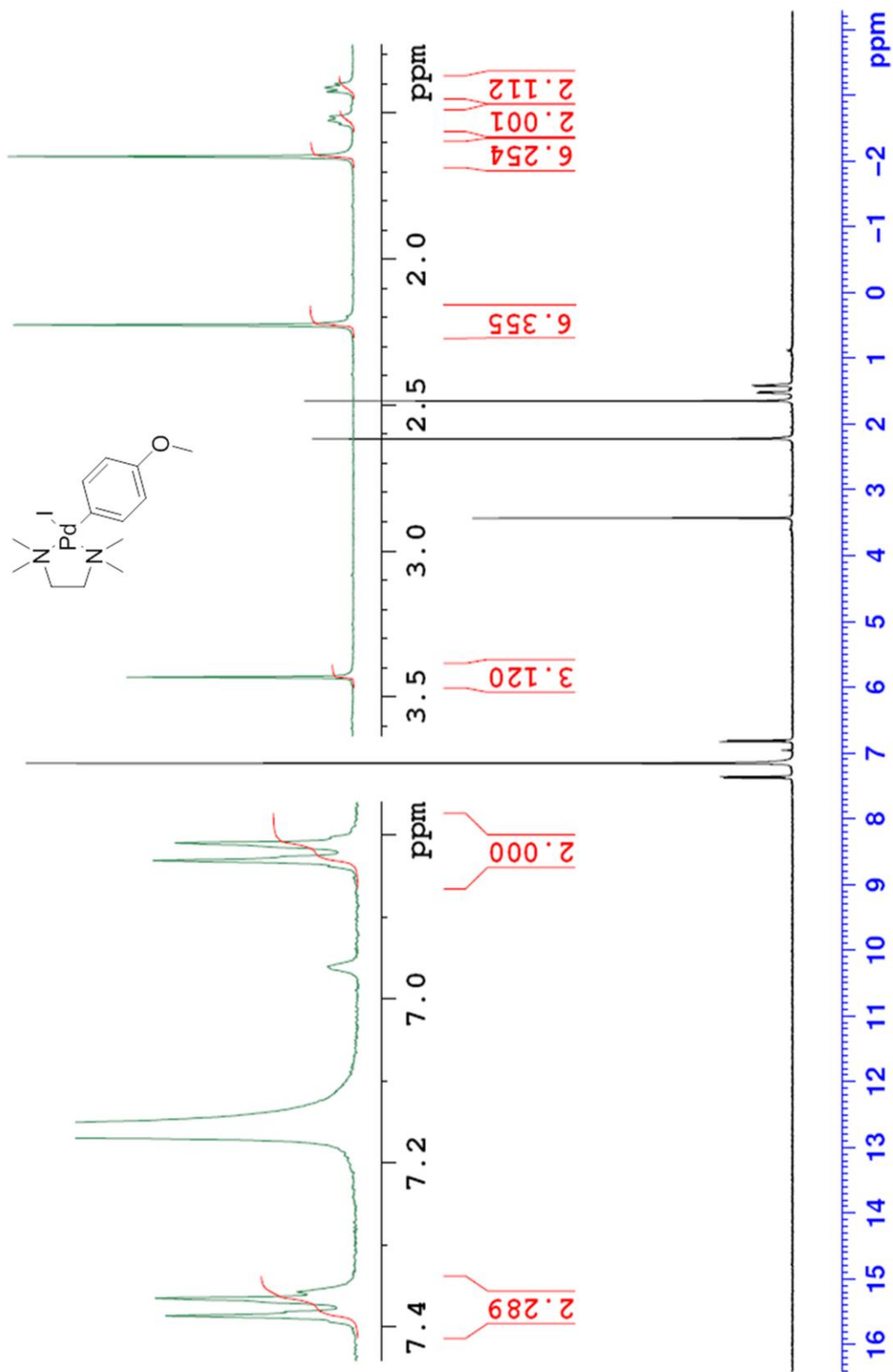**Figure F1.** ^{1}H NMR of [(TMEDA)Pd(II)Ar(I)], **1**

Figure F2. ^{1}H NMR of the I/F exchange reaction of [(TMEDA)Pd(II)Ar(I)], **1**, with TBAF at room temperature
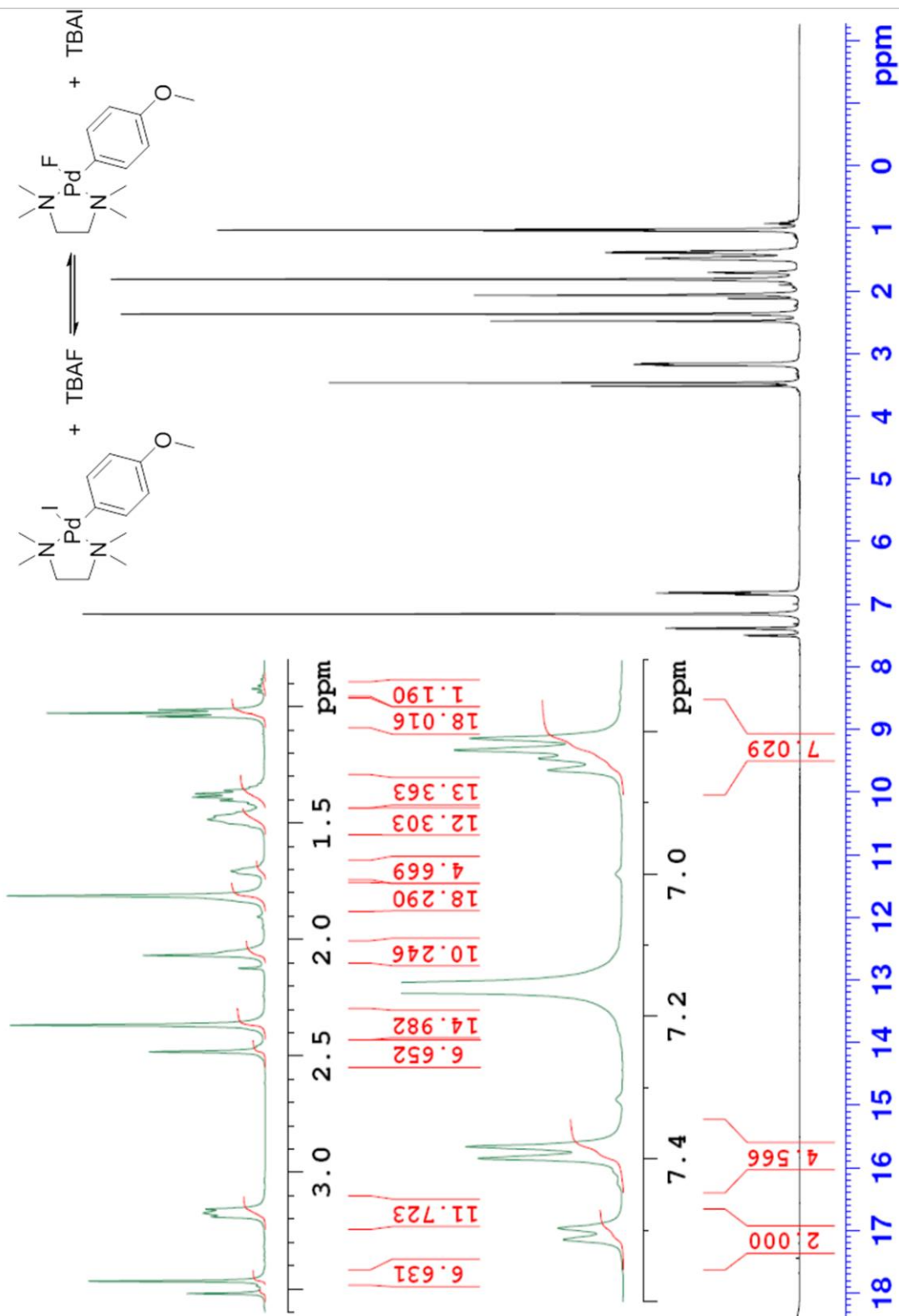
203

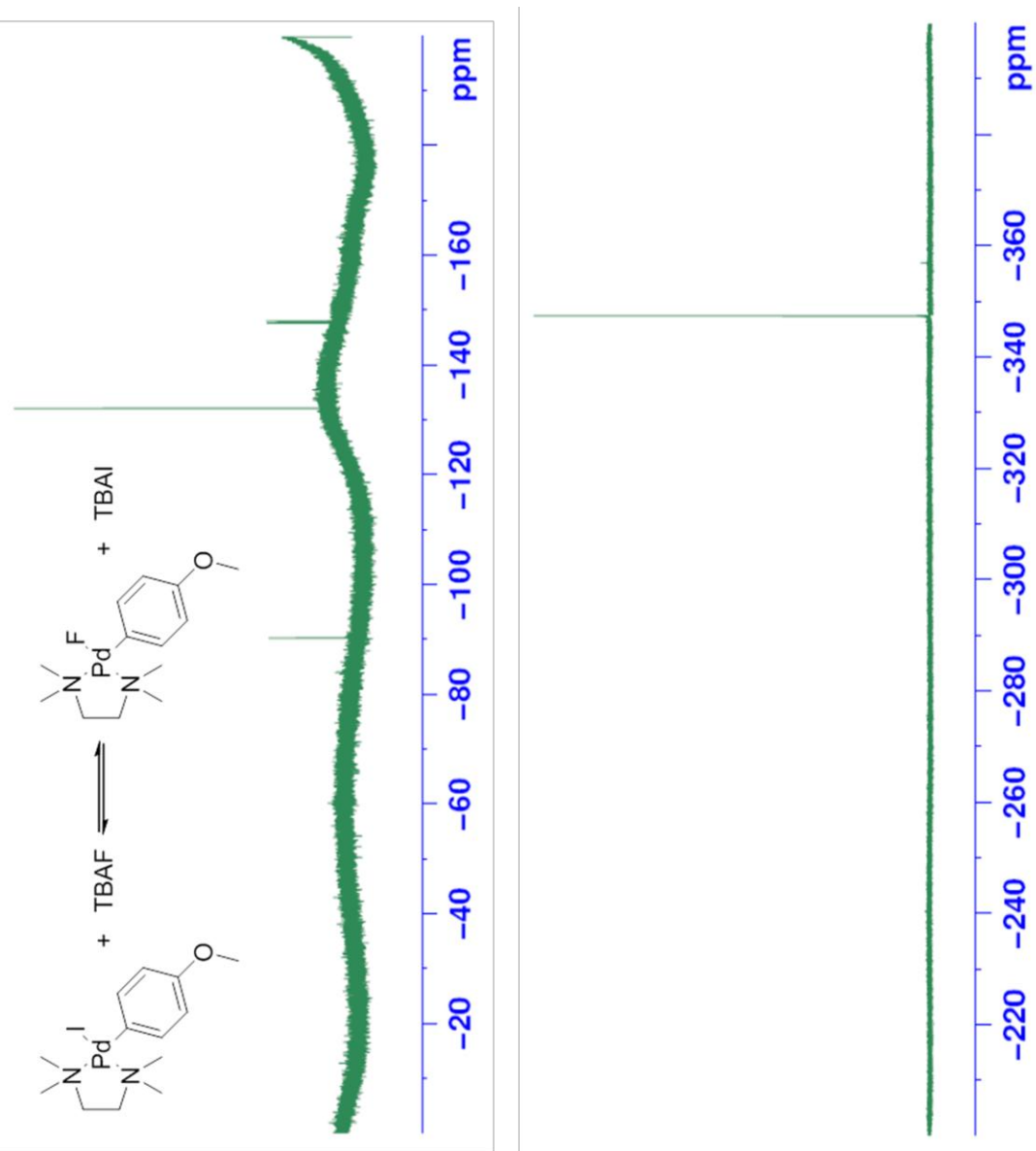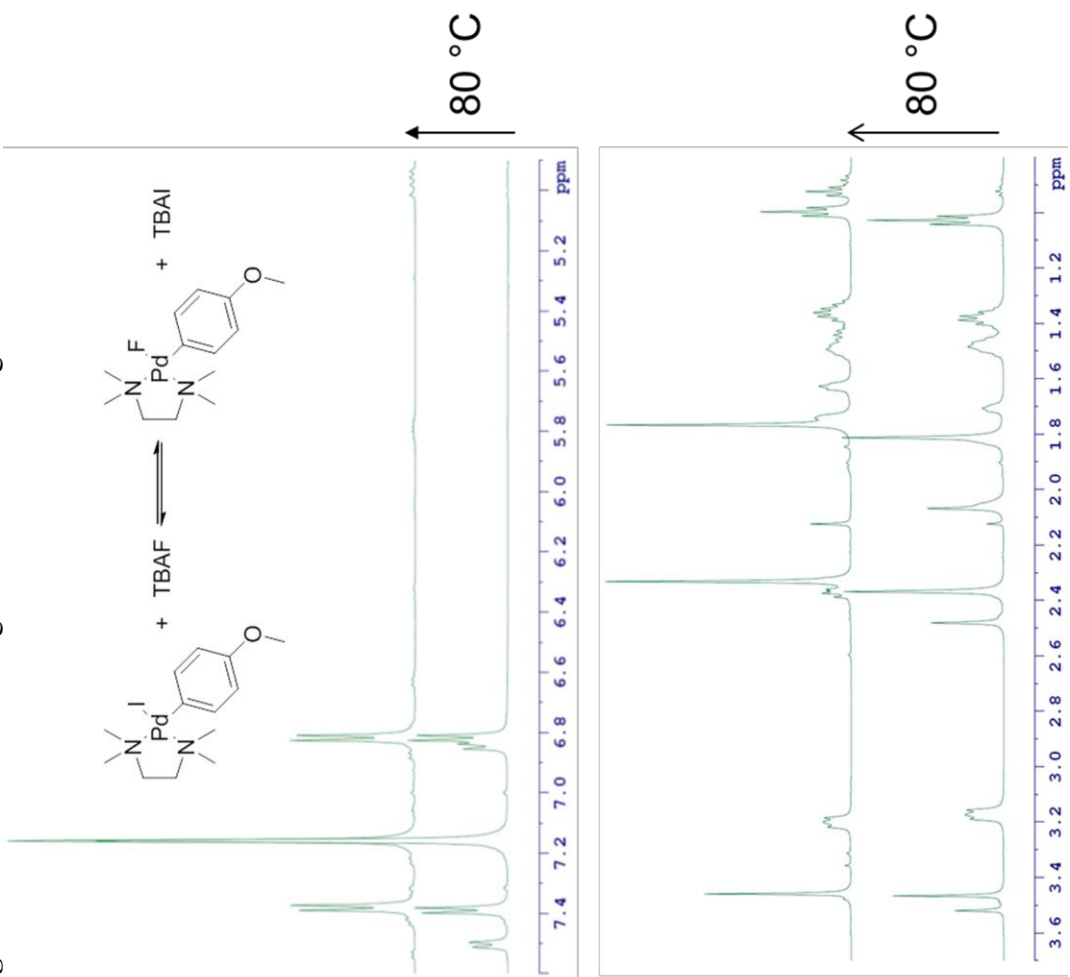**Figure F3.** ^{19}F NMR of the I/F exchange reaction of [(TMEDA)Pd(II)Ar(I)], **1**, with TBAF at room temperature
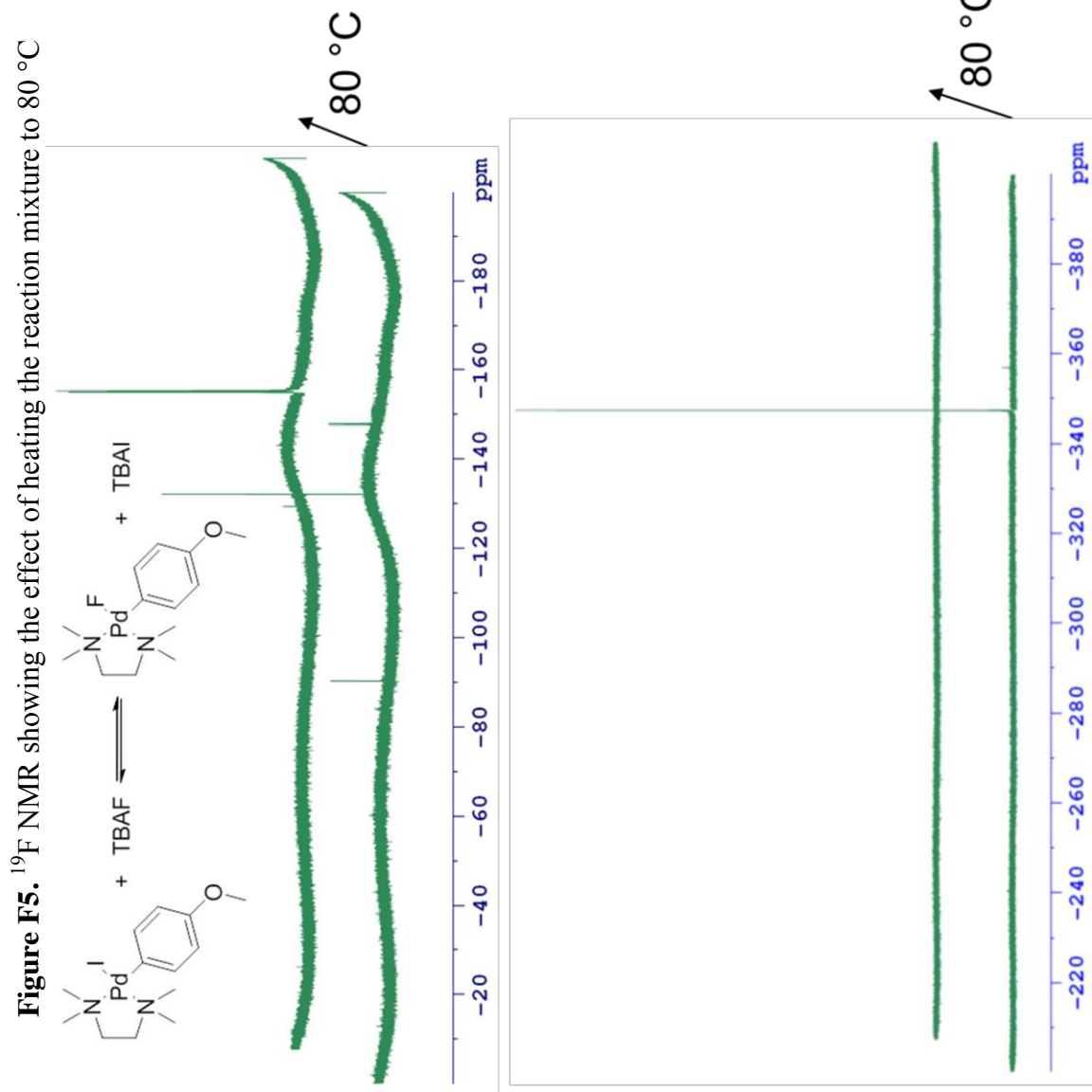
204

Figure F4. ¹H NMR showing the effect of heating the reaction mixture to 80 °C

Figure F5. ^{19}F NMR showing the effect of heating the reaction mixture to 80 °C
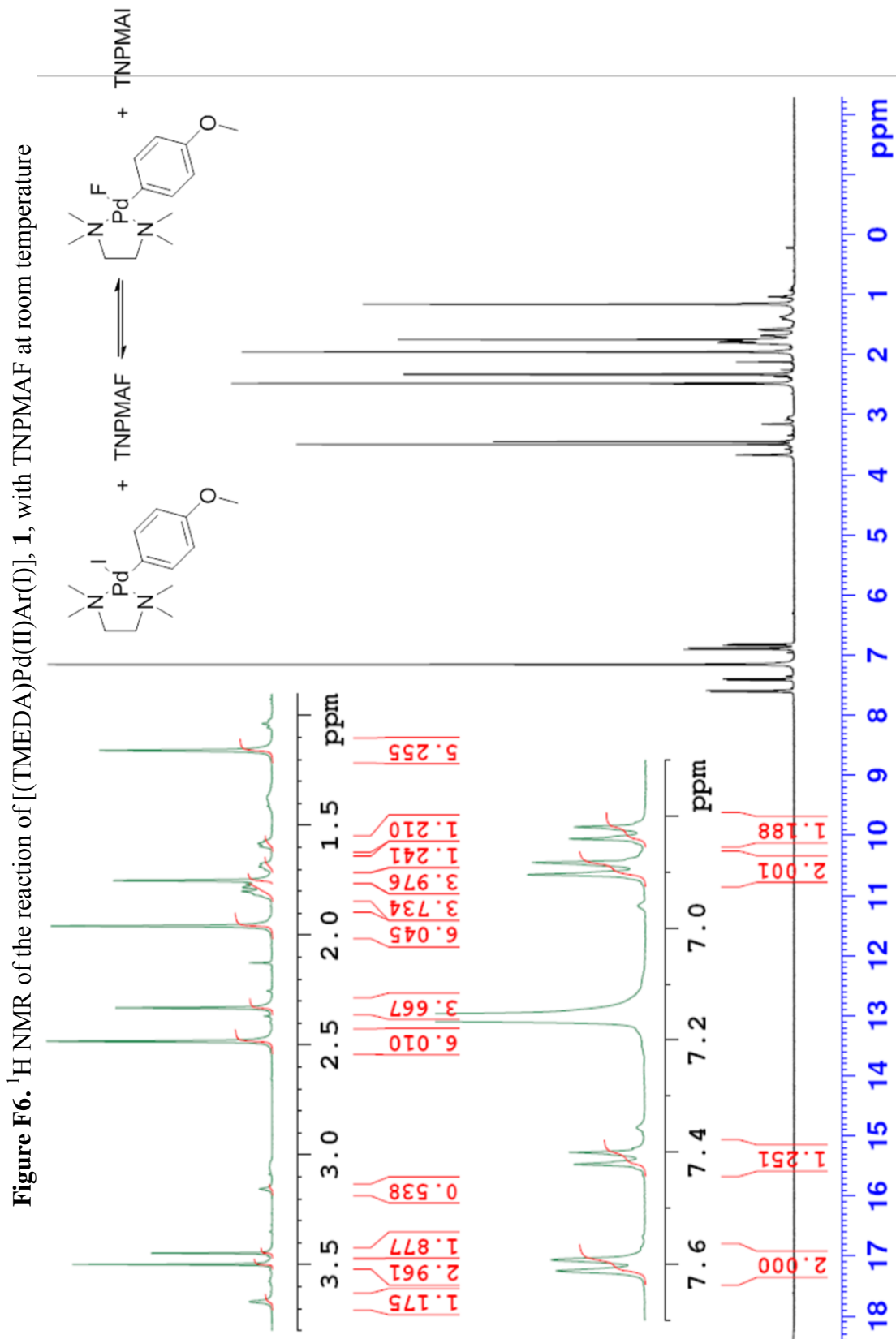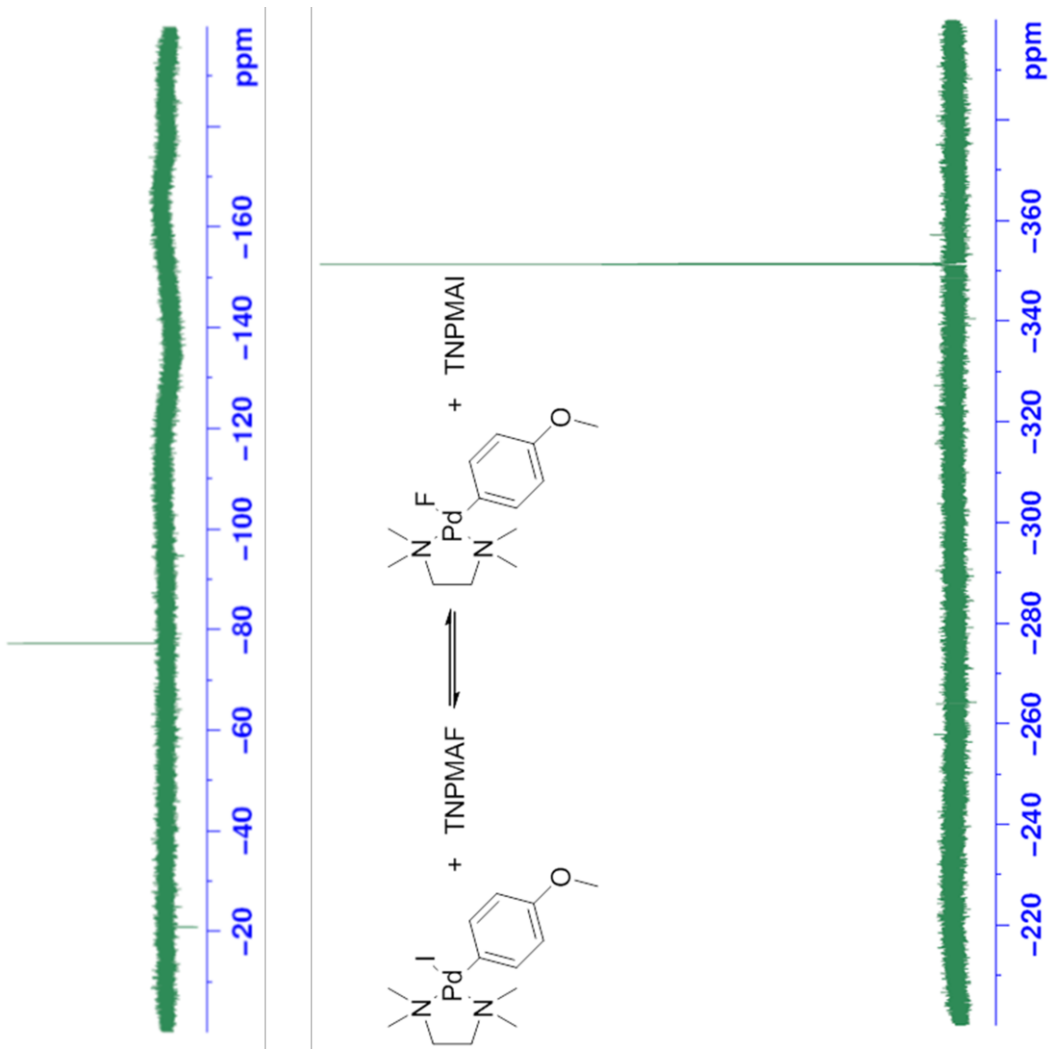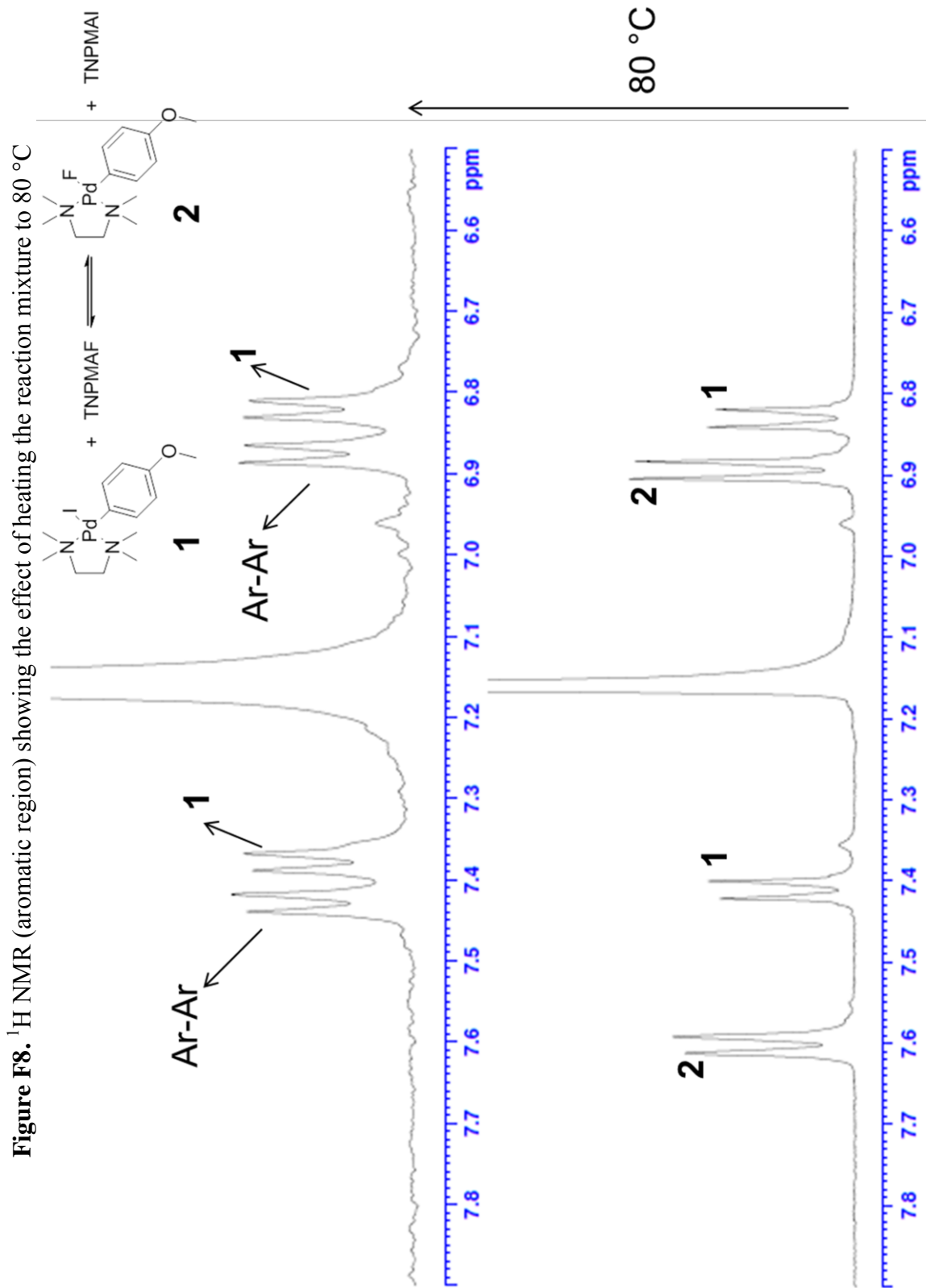
206

Figure F6. ^{1}H NMR of the reaction of [(TMEDA)Pd(II)Ar(I)], **1**, with TNPMAF at room temperature

Figure F7. ^{19}F NMR of the reaction of [(TMEDA)Pd(II)Ar(I)], **1**, with TNPMAF at room temperature

208

Figure F8. ^{1}H NMR (aromatic region) showing the effect of heating the reaction mixture to 80 °C

Figure F9. ^{1}H NMR (aliphatic region) showing the effect of heating the reaction mixture to 80 °C

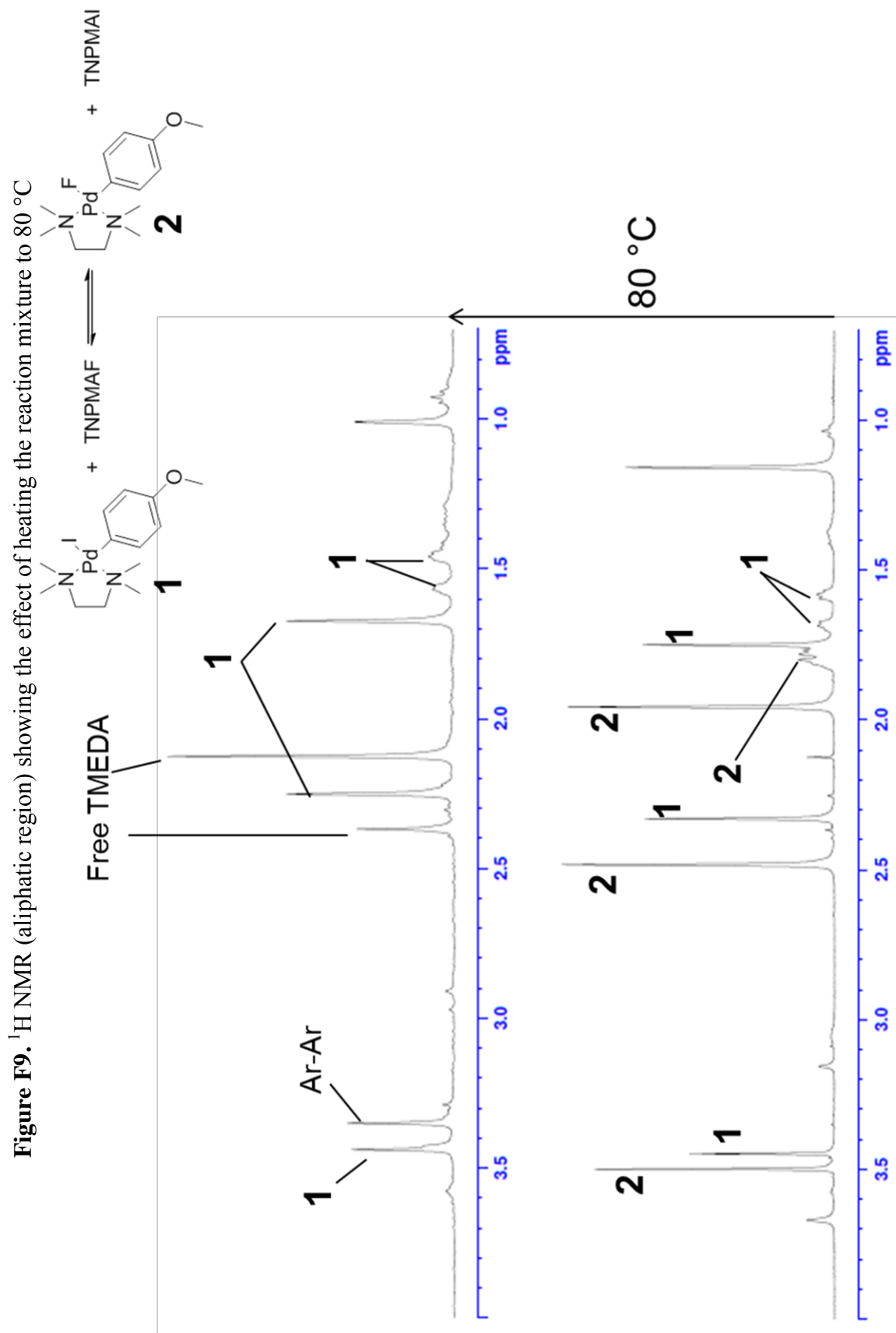**Figure F10.** ^{19}F NMR showing the effect of heating the reaction mixture to 80 °C